Author:
Wood, Deborah Jane

Title:
Pressure-impulse impact problems and plunging wave jet impact.

Pressure-impulse Impact Problems and Plunging Wave Jet Impact

Deborah Jane Wood

School of Mathematics
University of Bristol

Abstract

This thesis looks at two types of problem. The first is that of pressure-impulse modelling of wave impact on structures, following on from work carried out by Cooker and Peregrine (1990 a,b, 1992, 1995). The second is that of the impact of a jet from a plunging breaker on the undisturbed water in front of the wave.

Chapter 1 is a brief summary of the work which will follow. Each chapter has a separate literature review.

Chapter 2 looks at many impact problems using pressure-impulse theory. Models of wave impact on a vertical wall and cylinder are developed in particular looking at more three-dimensional theoretical models than have been previously examined. This work is of importance for the design of coastal structures, especially breakwaters. The effect of having a porous berm in front of the wall and of having an air pocket trapped at the wall are examined. Experimental data from Hattori and Arami (1992 and private communication) and experiments in Edinburgh (Oumeraci, Bruce, Klammer and Easson (1995) and Oumeraci, Partenscky, Klammer and Kortenhaus (1997) and private communication) are used for comparison.

Chapter 3 examines a wave impacting upwards on a deck jutting out from a wall. Pressure-impulse theory is again used, and the effect of depth of water at the wall and length of deck are examined. The implications for the design of coastal structures and off-shore platforms are discussed.

Chapter 4 looks at what happens when a plunging wave jet impacts on the water in front of itself. The impact is considered as the impact of two jets, one of which is infinite in width. Two methods are put forward, the first of which is an extension of a solution presented in Milne-Thompson (1962) which looks at the impact of two finite jets, and we take the limit as one jet becomes infinite (a similar study is carried out in Frankel and Weihs (1990)). The second method produces an exact solution using complex analysis.

Finally, the last chapter draws conclusions from the work in the preceding chapters, and makes some suggestions for future areas of work.

Acknowledgements

Author's Declaration

The work described in this dissertation was carried out in the School of Mathematics, University of Bristol and has not been submitted for any other degree or diploma of any examining body. All the material described herein is the original work of the author, except where otherwise acknowledged.

Deborah Wood

Contents

List of Figures

ix

xii

xiii

List of Tables

Chapter 1

Introduction

This thesis examines two types of water wave impact. The first is that of a water wave impacting on a rigid structure such as a sea wall, oil-rig leg or pier, and the second the impact of a plunging breaker on the undisturbed water in front of itself. The work is divided into three chapters: vertical structure impact, impact under a deck, and jet impact. Each chapter has a separate literature review, but we begin with a brief summary of what will be covered in each chapter and some motivation for carrying out this work. In all the problems we discuss in this thesis we assume that the fluid is inviscid, incompressible and that the motion is irrotational. All the plots shown in this thesis are for non-dimensional quantities, except where units are given for the quantities plotted.

1.1 Impacts on vertical structures.

Research into wave impact on a vertical wall is of particular importance for the design of sea walls and breakwaters. A wave which is breaking or near breaking when it hits a structure can cause large peaks in pressure. These pressures, though often of very short duration (1ms in the laboratory, 10-50ms in prototype), are sometimes substantial enough to shift, or blow holes in, a coastal structure. Hence, structures such as a breakwater are built to reduce these impact pressures as much as possible. Breakwaters come in many forms, shapes and sizes: rubble mound, vertical wall, rubble mound and vertical wall, with perforations, without perforations, rectangular

caissons, cylindrical caissons, and many other variations on these. The choice of which type of breakwater is most suitable is complex, and depends on many factors such as position, tidal range, depth of water, availability of materials, and of course financial restrictions. In this thesis we consider primarily the vertical wall structure, and briefly that of a vertical wall with a berm. A good summary of the design of breakwaters, and how this has changed over the years is given in Takahashi (1996).

Experimental work on impacts on structures has concentrated on the measurement of the evolution in time of the pressures on the structure. If we consider a given wave impacting on a given structure and measure the pressures associated with this particular impact, then the pressures measured from one wave to the next, even with all the wave conditions remaining apparently the same, may vary quite substantially. This makes analysis and prediction of quantities such as maximum pressure and the pressure distribution on the structure difficult. However, Bagnold (1939) noted that if we instead consider the integral of pressure with respect to time, over the impact duration, this is a much more repeatable quantity. The integral of pressure with respect to time over the impact is the quantity pressure impulse, P. Hence, we choose in chapters 2 and 3 to concentrate on the calculation of pressure impulse. A full description of this method, and the assumptions used is given in chapter 2.

Cooker and Peregrine (1990 b, 1992) used pressure-impulse theory to develop a model for the pressure impulse caused by a wave impacting on a vertical wall. In chapter 2 we re-examine and extend this model. The Cooker and Peregrine model considers the impact to be the uppermost part of the water adjacent to the wall at impact, but with the same speed of impact occurring at every position along the wall. i.e. the model is two-dimensional. In both experimental and field work of wave impacts, but probably more noticeably in field studies, it is clear that the wave may only impact on a section along the wall. Hence, the assumption of two-dimensional behaviour may often not be reasonable. We begin by looking at impact on a finite patch of a wall, and later extend this to impact on a semi-infinite patch of a wall.

2

This is of particular value for engineers examining the 'spread' of impact of a wave. If the wave impacts on only the middle portion of a wall it is obviously not reasonable to assume that the pressure impulse has the same distribution down the wall at every position along the wall. However, if the wave impacts over a large region across the wall, it may be reasonable to assume that the impact is two-dimensional towards the centre of the impact region, and we investigate when we can make this assumption.

One method of reducing the loads on a vertical wall breakwater structure is to put a rubble mound/berm in front of it. This can affect the wave reflection and breaking wave force on the vertical wall. We examine the effect of changes in porosity of a rubble berm, on the pressure impulse in the water and on the structure. We find that even varying the porosity quite considerably only changes the pressure impulse in the liquid by at most 20 %. In this case, those models which have an impermeable bed can be used to approximately predict pressure impulse for structures even with a permeable berm.

When a plunging breaker impacts on a vertical wall it often traps an air pocket. This air pocket can take the form of a large trapped bubble. The bubble first contracts in size and then expands. Hence at the surface of the bubble at impact the velocity of the body of water reverses in sign. This is as if the bubble 'bounces' back. We make a simple model of this 'bounce-back' effect, and compare with experimental results from Hattori and Arami, and also PIV (Particle Image Velocimetry) experiments carried out at Edinburgh University. This model can be used to predict pressure impulse down the wall and along the berm. The procedure for comparison with experimental data is far from straight forward and is discussed in this chapter. This model assumes an impermeable berm, but as stated earlier the permeability does not have a great effect on the pressure impulse, so this model could be used even for experiments with a permeable berm. Little research has been done to model the effect of impact with a trapped air bubble, with the exceptions of Bagnold (1939), Oumeraci and Partensky (1991) and Topliss (1994). The model in

3

this chapter, though very crude, goes some way to predict the pressure impulse distribution, usually to within 40 %, with more accurate prediction of the total impulse on the wall.

The second shape of structure we consider is that of a vertical cylinder. This is of particular importance when considering impact on an oil-rig leg or the circular head of a breakwater. We carry out the analysis using pressure-impulse theory (as with the vertical wall) but this time using cylindrical co-ordinates. When a wave impacts on a cylindrical structure the impact region is usually above the main body of the water. However, we consider firstly a wave impacting on a patch, below water level, on a cylinder and secondly of a wedge of water impacting on a cylinder. We discuss how this model can be simply adapted to allow for a more realistic free-surface. It is found, that the convex shape of the cylinder reduces the pressure impulse quite considerably compared with a flat shape. This model is sufficient to make a preliminary analysis of the effect of having a three-dimensional impact, but more realistic/complex model geometries were not considered due to shortage of time.

It should be noted that for many of the situations considered in this chapter and the next there are few previous theoretical formulae for prediction of the pressure impulse, hence even if these models give predictions within 50% of measurement, it is an improvement and useful for engineers.

1.2 Impact under a deck.

If we consider an oil-rig or a pier then it is not only the impact of the waves on the vertical supports or legs of the structure which can cause damage. Violent wave motion can occur when the wave impacts upwards on a horizontal or sloping surface, such as the walkway of a pier or platform of an oil-rig. Often the safest way of designing an oil-rig is to build the platform part of the rig so far out of the reach of predicted violent waves that we can be sure no or little damage will occur.

4

However, every extra centimetre which is added on to the height of a rig costs large amounts of money. Estimates of the magnitudes of pressures which occur when a wave impacts a horizontal surface can lead not only to increased safety but also to decreased building and maintenance costs of a rig.

Impact of waves on a horizontal surface is very closely linked to that of ship-slamming problems. The early work by Von Karman (1929) and Wagner (1932) focused on predicting the stresses involved when a seaplane lands on water. Since then much work has been carried out on the ship-slamming problem, and a full review is given in chapter 3.

In this chapter we discuss a flat deck, jutting out horizontally from a wall, which is very close to the water level. We set up this problem in a similar manner to problems discussed in chapter 2, and solve using pressure-impulse theory. We begin by making some simplifications specific to this problem: that the deck is horizontal, the wall is vertical, and we have a horizontal bed. We also assume that the water surface is flat and level with the deck (though this can be adapted and is discussed further in chapter 3).

Firstly we consider the two extreme cases of infinite depth of water and infinite length of deck. The first case is solved by considering the velocity potential of a plate moving in stationary liquid, and making a change of reference frame. The velocity potential for this fluid flow satisfies the same conditions as we require pressure impulse to satisfy. The infinite deck case can be written down by solving Laplace's equation in the fluid just under the deck.

The most general case is that of finite depth of water at the wall. At the position where the deck meets the free surface we find that there is a square root singularity in P, and hence singular fluid velocity components. Unfortunately this means that many of the usual solution methods are unsuitable so instead we use a series of conformal maps to map the problem to a plane where the singularity is no longer present. We can then use standard solution methods in this plane and then map back

to the original plane. We obtain an explicit Fourier series solution to this problem, which can be used to predict the spatial distribution of the pressure impulse below the deck. In particular we note that the shallower the depth of water, the more confined the motion and hence the the more violent the impact.

This chapter is concluded with a brief analysis of the impact of an elliptic shape on a deck above an infinite depth of water. This is an estimation of a three-dimensional impact.

Throughout chapters 2 and 3 the main method of solution is with Fourier series. This method has the huge advantage that the solutions are quick and easy to evaluate.

1.3 Wave breaking and impinging Jets.

If we were to spend some time watching waves coming in and breaking on a beach, over rocks or near a structure, we would very quickly notice that each wave breaks in a slightly different manner. Some waves appear to almost 'topple over' spilling water down the front of the wave, others break by forming a well developed jet from the top of the wave, and others are somewhere in between. In chapter 4 we consider a 'plunging' breaker where a jet at the top of the wave is well developed and 'plunges' down to impact on the undisturbed water in front of the wave. Chapter 4 begins with a literature review of general wave breaking, and in particular the research which has been carried out on the evolution of the jet from a plunging breaker.

When the jet impacts on the previously undisturbed water in front of the wave a 'splash' occurs, and it is this splash which chapter 4 seeks to model. The undisturbed water can be considered as an infinitely deep jet into which the plunging jet impacts. An important assumption (discussed later) is that we consider the flow to be almost steady. We begin by modelling this impact by extending a model given in Milne-Thompson (1962), for impact of two jets of finite width. This model is also given in Gurevich (1965), which also refers back to many old sources, including Zhukovskii

(1890), Voight (1886) and Cisotti (1921). We take the limit as one of the jets becomes infinitely wide, and find formulae for the free-streamlines of the flow. This model was found to be incomplete as to simplify the mathematics it is necessary to feed into the model the outgoing angle of the jet as it splashes up, as well as the ingoing angle and width of the plunging breaker jet.

We then consider a second solution model, this time where the previously undisturbed water jet is taken to be infinitely deep from the start of the analysis. We use two complex maps, to map the flow to a plane where the flow can be represented by a complex potential made up of a source, sink and uniform flow at infinity. Hence if we know the angle and thickness of both incoming jets we can predict the angle and thickness of the outgoing jets, and the free-streamlines associated with this flow. Some examples of free-streamline plots are given.

Chapter 2

Impacts on vertical structures

2.1 Background.

Much research has been carried out on the impact of waves on structures. The search for improvement in the design of coastal structures such as breakwaters and seawalls has often been the driving force for research in this area.

In the late 1800's and early 1900's much research on impacts was carried out by observational study. Stevenson (1864) made a detailed study of the design of harbours and included surveys of wave impact on structures. Molitor (1935) uses the results of some observational studies to provide formulae to calculate total wave force on a structure. These measurements were important for general conclusions about wave breaking, however, they were inaccurate because electrical recording was not available, hence the rapid changes in the pressure and the peak pressures could not be resolved.

Following on from these papers further experimental and observational studies increased the knowledge of pressures occurring during impact. If a breaking or near-breaking wave hits a structure a high pressure peak in the pressure-time plot occurs. This large pressure is of short duration and throughout this study will be called the impact pressure. Bagnold (1939) made a study of the impact pressures which occur when a wave hits a wall. In particular he noted that for nominally fixed wave conditions the pressures occurring vary from one wave to the next, but examination

of the integral of pressure, with respect to time, over the short duration of impact gives more repeatable results. The integral of pressure over the impact time is called the pressure impulse, and is a much more repeatable quantity from wave to wave than the pressures themselves. Bagnold noted the important role of the air pocket which sometimes occurs between the wave and structure. He developed a theory for the prediction of the maximum pressures occurring, by using a model where the water impacting on a structure is regarded as a piston which compresses a layer of trapped air. Denny (1951) carried out further impact experiments (using Bagnold's equipment) which gave more support to Bagnold's model.

Hayashi and Hattori (1958) also investigated the wave pressures of a breaker impacting on a vertical wall, both theoretically and experimentally. They commented, as Bagnold did, that the initial impact pressures vary from one wave to the next, even with nominally fixed wave conditions, but also noted that the maximum pressure over the rest of the wave period (i.e. the maximum pressure over the impact, excluding the initial impact pressure peak) was much easier to predict. Hence no theoretical prediction of impact pressures could be made but instead predictive methods for maximum pressure, excluding the impact pressure were put forward.

One of the earlier studies of breaking waves on composite type breakwaters (a vertical wall with a rubble mound in front) was Nagai (1960). Formulae were developed to predict both the maximum impact pressures and the maximum resultant pressure per unit length, for use in the design of breakwaters. The formulae were established by looking at the momentum per unit area of a breaking wave to give pressure impulse. A sampling rate of 500Hz for the pressures and high speed video (3000 frames per second) meant the measurements were reasonably good at picking up the impact pressures. For waves which are breaking the empirical formulae derived are much better at predicting the peak pressures and impact duration than Bagnold's piston model.

Richert (1968) looked further at the trapped air cushion. He noted that the

9

maximum pressures always occur below still water level and that the impact pressures never decrease to zero at the bottom. However, this study only looked at breaking waves preceded by non-breaking waves, hence the impact pressures produced are higher than if continual breaking waves were used. This is because if continual breaking waves are used the residual spray and bubbles from the previous breaking wave softens the impact. Many of the theoretical studies of wave impacts at this stage were adaptations of Bagnold's air pocket model. However, Weggel and Maxwell (1970) developed a numerical model for wave pressure distributions for impacts of waves on a wall. They used an approximation to Euler's equation, the continuity equation, and the equation of state, to show that the pressure satisfies the wave equation. They solved this numerically, subject to artificial boundary conditions, to give a model which compared favourably with experimental results.

Accurate field data for impacts on coastal structures is more difficult to obtain than laboratory data. In addition to the work carried out by Stevenson (mentioned earlier), Hiroi (1920) and Sainflou (1928) made measurements in the field. Hiroi and Sainflou each produced formulae for the prediction of wave pressures for breaking and non-breaking waves respectively. However, these studies were so early in research history that the equipment used means the data can not be used for accurate data comparison. More recently Blackmore and Hewson (1984) carried out a series of studies of wave impacts on sea walls in the South and West of England. Using modern measuring and recording techniques, wave impact pressures were considered and an expression to estimate these, related to the percentage of air entrainment, was obtained. In addition an ongoing MAST 3 project on 'Probabilistic design tools for vertical breakwaters' (PROVERBS), is a new source of both laboratory and field data for impacts on vertical walls.

The development of pressure gauges with a very high frequency response allowed Mitsuyasu (1966) to look in detail experimentally at the pressure-time histories of impact pressures. A new air-cushion model for the impact pressures was developed, improving Bagnold's model by allowing for air leakage.

In the late 1980's a series of experimental studies of waves impacting on walls were carried out to improve the predictions of the impact pressures. In particular it was considered important to examine the impact pressure distribution over the structures and to investigate which wave conditions produce the highest pressures. Partensky (1988) commented that in the design of breakwaters the methods used for predicting the peak pressures and resulting forces consistently gave underestimates. This was often due to the lack of comparison of theoretical models with prototype measurements. He put forward a revised predicted pressure-distribution for coastal structures which reduced the inaccuracies of force and peak pressure prediction. Chan and Melville (1988) claimed that in their experiments the trapped air during impact may contribute to both the higher pressures and pressure oscillations. In particular the location of the wall relative to the position of wave-breaking had a significant effect on the distribution of the impact pressures. Witte (1988) also carried out detailed wave impact experiments on a vertical wall and a sloping surface. High peak pressures occurring over short periods were observed. Most earlier investigations considered the local maximums of pressure of the impact, but in contrast Witte also looked at time and space distributions of pressure.

A more theoretical approach in the prediction of the impact pressures was taken by Cooker and Peregrine (1990 a,b). They used the idea of pressure impulse (described later in section 2.2) and they developed a mathematical model for the large short-lived pressures which occur during impacts. They solved a 2D boundary value problem, for a vertical wall being hit by an idealized wave. Using unsteady potential flow computations (Cooker and Peregrine 1990a), to evolve in time an impacting wave, they predicted unexpected, violent motion with very high pressures, accelerations and velocities. This was found to be due to the incident wave meeting the wall with an almost vertical front producing a vertical jet shooting up the wall. Very high pressures were predicted for the 'flip through' case where just before 'impact' the wave face is parallel to the wall. Here the wave surface flips upwards rather than undergoing a direct impact. Cooker (1990) carried out a study on the interaction

11

between steep water waves and coastal structures, using the program based on a boundary-integral method. The pressures predicted in this study were of similar magnitude to those produced in experiment. Topliss (1994) continued these studies by examining impact pressures in containers, the effect of entrained air, and the associated oscillatory pressures which occur.

Cooker and Peregrine (1992) noted that it was not only the high pressures on the structure itself that are important. In particular, bodies close to a structure can be moved away by the significant fluid pressure gradients which occur. The nett impulse is found to be large enough to propel a body in the direction of the pressure gradient, even when fluid drag is accounted for and acts in the opposite direction. A similar effect is described in chapter 3 of this thesis where wave impact under a deck causes a high pressure gradient away from the deck.

Kirkgöz (1991) examined experimentally the impact pressures of regular breaking waves impacting on backward sloping walls. Both the impact pressures and the resulting forces were sometimes higher on the sloping walls than on the vertical walls. A statistical distribution method is used for the prediction of maximum impact pressures. Lundgren (1969, 1991) summarized the developments in the design of structural breakwaters and the methods which are used to reduce or in some cases eliminate impact forces.

Continuing the historical review from 1991 onwards, experimental research now focused more on examination of the effect of the shape of the wave impacting on the resulting pressures, and also as a consequence on the effect of trapped or entrained air. Hattori and Arami (1992) examined the effect of wave shape and the role of the adiabatic processes of trapped air bubbles in the generation of impact pressures. The most severe impact pressures tended to occur when a breaking wave hit, trapping either lots of small air bubbles or a thin lens-shaped pocket of air. These experiments included the use of high speed video as well as pressure measurements on the wall, and are used for comparison with the pressure-impulse model of a 'bounce back'

air pocket described later in this thesis. Schmidt. Oumeraci and Partensky (1992) carried out large scale model tests of impact loads on vertical walls. and classified different types of impact by breaker type. In particular plunging breakers impacting on a vertical wall were examined and the impact pressure distributions, forces and force impulses which came from these were analysed. A statistical approach is taken to aid prediction of these quantities.

Peregrine (1994) and Takahashi, Tanimoto and Shimosako (1994) gave reviews of impacts on structures. Peregrine (1994) gave a summary and discussion of the current theoretical knowledge of waves meeting both vertical and near-vertical walls. He classified the pressures which occur during impact into three categories given by peak, oscillatory and reflecting pressures, and discussed present theoretical methods of predicting them. In contrast Takahashi, Tanimoto and Shimosako (1994) looked at more practical methods to estimate the impulsive pressures on composite breakwaters and reviews these.

Recent experimental studies continue to examine the effect of trapped air. In particular Hattori, Arami and Yui (1994) observed in their experiments that the highest pressures (of very short duration) occurred when the vertical wave front strikes a wall with only a very small amount of air trapped. After the initial peak in the pressure, oscillations may be observed due to the trapping of air. If no air is trapped then 'flip through' (as predicted in Cooker and Peregrine (1990 a,b)) occurs which gives very high impulsive pressures. Hattori, Arami and Yui (1994) observed that the greatest impact pressure occurred where the crest tip impacts near the still water level on the wall. Chan (1994) also looked at a plunging wave impacting on a vertical wall in deep water. Again it was confirmed that the pressures could be decomposed roughly into the primary wave evolution pressures (during the initial period of impact) followed by pressures affected by trapped air dynamics.

More theoretical studies (Cooker and Peregrine (1995)) show that P was insensitive to the shape of the rear part of the incident wave. They also noted that

the more confined the motion the higher the pressure impulse. Losada, Martin and Medina (1995) experimentally investigated a solitary wave incident on a reflecting structure. They computed the velocity field and the pressures along the wall and base using a boundary-integral method, and found that these quantities compared well with the theoretical pressure-impulse approach used by Cooker and Peregrine.

One recent study is that of Zhang, Yue and Tanizawa (1996) who computed a two-dimensional wave impacting on a rigid vertical wall using potential flow theory and a boundary-integral method. They looked at the jet impact on the wall and the pressures occurring due to this with an extension of the work in Cumberbatch (1960) (which modelled an impact of a wedge of water on a wall). Their model gave predictions of both the maximum pressures and the rise time. The maximum pressure from the model predicts a value about three times that of the mean experimental value, and reasons for this are discussed in their paper.

Currently the experiments carried out in connection with the PROVERBS project provide an ongoing source of data to be used as comparison with the theoretical models. In particular the Particle Image Velocimetry (PIV) tests carried out at Edinburgh University in 1994 (data made available through PROVERBS, though experiments carried out prior to the project, see section 2.5.4 and Oumeraci, Bruce, Klammer and Easson (1995) and Oumeraci, Partensky, Klammer and Kortenhaus (1997)) and tests currently being done at Edinburgh University are particularly useful for comparison, as unlike all the previously described experimental investigations, velocity profiles, as well as pressure measurements are available. A summary of these experimental methods is given in section 2.5.4 together with comparisons between the experimental data and the new theoretical models in this thesis.

2.2 Pressure impulse.

Wave pressures on structures occur in three forms, the 'impact' pressures which are high but act over a very short period of time, 'oscillatory' pressures which are

smaller in magnitude but act over a longer period of time, and finally the reflective pressures which occur until the wave crest has been fully reflected away from the wall. An example of a pressure-time curve (from Edinburgh PIV tests. see section 2.5.4) for wave impact on a wall is given in figure 2.1. This particular profile is when
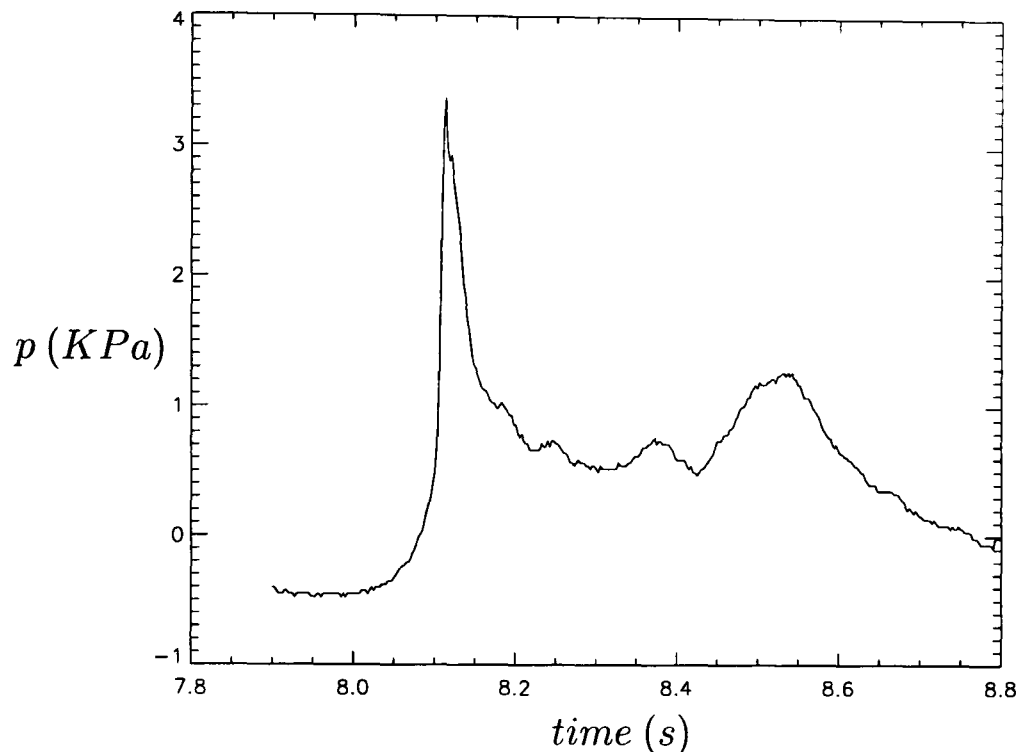
Figure 2.1: A 'typical' pressure-time curve for impact on a wall. (Edinburgh PIV data)

a large air pocket becomes trapped at the wall, and is from a pressure-transducer close to the foot of the vertical wall. Here we can clearly see the three stages, the high peak corresponding to the impact pressure, the oscillations due to the air, and the second peak caused by the reflective pressures. The most severe impacts last only for about 1ms in the laboratory, and around 10-50ms in prototype.

Cooker and Peregrine (1990 b) showed that the effect of the free surface, where the pressure is atmospheric, is to provide lower values than those predicted by a water-hammer pressure model . In creating approximate mathematical models for wave impact Cooker and Peregrine also noted that, except in the case where a thin layer of water undergoes impact, the shape of the wave away from the impact region is relatively unimportant. Hence the shape of a wave impacting on a structure may

often be considered to have a flat free surface for simplicity. As a result of the boundary condition $P = $ constant on the free surface the problem is linear, and hence once the problem is solved, we can choose more realistic free surfaces to be any of the contours of pressure impulse.

2.2.1 Governing equations.

Let p be the excess pressure over atmospheric, and g be the acceleration due to gravity. The pressure impulse P is defined by $P = \int p dt$, as given in Lamb ($\S 11$, 1995) and Batchelor ($\S 6.10$, 1967). In our case the integration is over the short period of time during which the water and the structure collide.

Let $\mathbf{u}$ be the velocity of the liquid. We assume that the liquid is inviscid, that is that the ratio of the magnitude of the inertial forces to the magnitude of the viscous forces is large. We choose a velocity scale U (from experiments later we approximate this as 1.3m/s), a length scale L (again from later we usually choose the depth of water at the wall for which a suitable value is 0.2m) and let μ and ρ be the viscosity and density of the fluid respectively. We can assume the fluid is inviscid if the Reynolds number ($\rho L U / \mu$) is large. We also assume that there is no flow separation (around the body with which the wave impacts), which we may for the short times of impact. The density and viscosity of water are approximately 1000kg/ m^3 and 0.001kg/m s respectively. Hence the Reynolds number is 260000, which is sufficiently large to neglect viscous terms.

We consider the Euler equation of motion:

$$\frac{\partial \mathbf{u}}{\partial t} + \mathbf{u}.\nabla \mathbf{u} = -\frac{1}{\rho}\nabla p - g. \tag{2.1}$$

For simplicity we choose units such that $\rho = 1$ in the following, since only incompressible flow is considered (as our velocity scale is much smaller than the speed of sound, 1500m/s in water, and we assume no sound waves are set up).

The time in which the velocity changes during the impulsive event is very short. The impulsive motion creates large pressure gradients, and a sudden change in the

16

velocity in the fluid. However, the velocity of the fluid itself is not large, except perhaps in a small jet (which for this study we will ignore, but occurs during the case of 'flip through' discussed earlier). Hence g and the nonlinear term involving a spatial derivative of $\mathbf{u}$ (whose ratio with $\partial \mathbf{u}/\partial t$ is $O(\Delta t U/L)$) can be neglected, as they are small compared to the pressure gradient and $\partial \mathbf{u}/\partial t$ (in a similar manner to Cooker (1990)). Note that no assumption about vorticity has been made so we can have arbitrary vorticity. The equation of motion is approximated by:

$$\frac{\partial \mathbf{u}}{\partial t} = -\nabla p. \tag{2.2}$$

Integration with respect to time over the duration of the impact gives:

$$\mathbf{u}_a - \mathbf{u}_b = -\nabla P, \tag{2.3}$$

where $\mathbf{u}_a$ and $\mathbf{u}_b$ are the velocities after and before impact respectively. Now we assume the water is incompressible before and after impact, and so we have $\nabla.\mathbf{u}_a = \nabla.\mathbf{u}_b = 0$. Therefore we need to solve

$$\nabla^2 P = 0 \tag{2.4}$$

in the fluid domain, subject to appropriate boundary conditions. The effects of allowing compressible flow due to dispersed bubbles are discussed in Peregrine and Thais (1996).

2.2.2   Boundary conditions.

The boundary conditions can be grouped into three different types:

1)At the free surface the pressure is taken to be zero, so

$$P = 0, \tag{2.5}$$

since we consider pressures relative to atmospheric pressure.

2)At a section of a rigid boundary where impact occurs the velocity component perpendicular to the boundary is taken to be zero after impact, and some function

17

of position, V, before impact. Using the normal component of equation (2.3) we find:

$$\partial P / \partial n = V, \tag{2.6}$$

where n is in the normal direction to the surface pointing into the fluid. We often choose V to be uniform in space, for want of better information as a reasonable simplifying assumption. We often have $V = -1$, i.e. a velocity with magnitude 1 in the direction towards the wall. Hence, equation (2.6) simplifies to give:

$$\partial P / \partial n = -1. \tag{2.7}$$

3) On a section of the rigid boundary where no impact occurs the velocity normal to the boundary is zero both before and after impact, and so taking the normal component of equation (2.3), we require:

$$\partial P / \partial n = 0. \tag{2.8}$$

We often impose a far-field condition that at an infinite distance away from the impact region, P is zero.

Hence, to find a pressure-impulse model for an impact problem we must solve Laplace's equation subject to these boundary conditions.

2.2.3 Method of solution.

For the impact problems in this thesis the main method of solution is that of obtaining a Fourier series which solves Laplace's equation subject to the appropriate boundary conditions. The great advantage of this method is that providing the Fourier series converges reasonably quickly it is easy to obtain data for the pressure impulse. Even when the Fourier series convergence is not quick, methods such as the use of Lanczos' factors (see section 2.6.2), can be used to improve the convergence. The ease with which the Fourier series can usually be evaluated makes this method of great practical importance. The simpler the formulae for estimates of the

pressure impulse, the more likely it is that they can be put to use by engineers in their calculations.

However, this does not mean that the use of Fourier series is the only way forward. It is thought in particular that methods such as a boundary-integral method would be more adaptable, especially for problems such as the impact on a cylinder.

2.3 Pressure-impulse models for impact on a wall.

Many of the studies of wave impact are for vertical walls or breakwaters. Almost all the theoretical models and experimental studies have assumed that the motion is two-dimensional, i.e. that the motion is the same for every slice taken perpendicular to the wall or structure. Most experimental studies are set up so that the three-dimensional effects are reduced as much as possible. However in the field it is obvious that three-dimensional effects are present. It is possible that using a three-dimensional model may lead to a reduction in the pressures predicted.

2.3.1 Two-dimensional impact on a wall.

Cooker and Peregrine (1990 b, 1992) looked at the pressure-impulse model of two-dimensional impact on a wall. For the study in this section we take L to equal the size of the impact region. All quantities are considered to be dimensionless unless otherwise stated. Using the notation in this thesis we consider impact on a wall which has water of depth D in front of it. We assume the velocity and density of the liquid to be unitary. The impact is assumed to be two-dimensional, and so Laplace's equation was solved in the fluid domain, with the boundary condition $\partial P/\partial n = -1$ on the top depth 1 of the wall below water level, and $\partial P/\partial n = 0$ on the rest of the wall and along the base of the fluid domain. $P = 0$ is required along the free-surface. The origin is taken to be on the wall, at the water level of the wave at impact, with y taken in the direction perpendicular to the wall, and z vertically. The boundary conditions are as shown in figure 2.2.

z

0

$P = 0$

$\partial P/\partial y = -1$

y

-1

$\nabla^2 P = 0$ $P \to 0$

$\partial P/\partial y = 0$

$\partial P/\partial z = 0$

$-D$
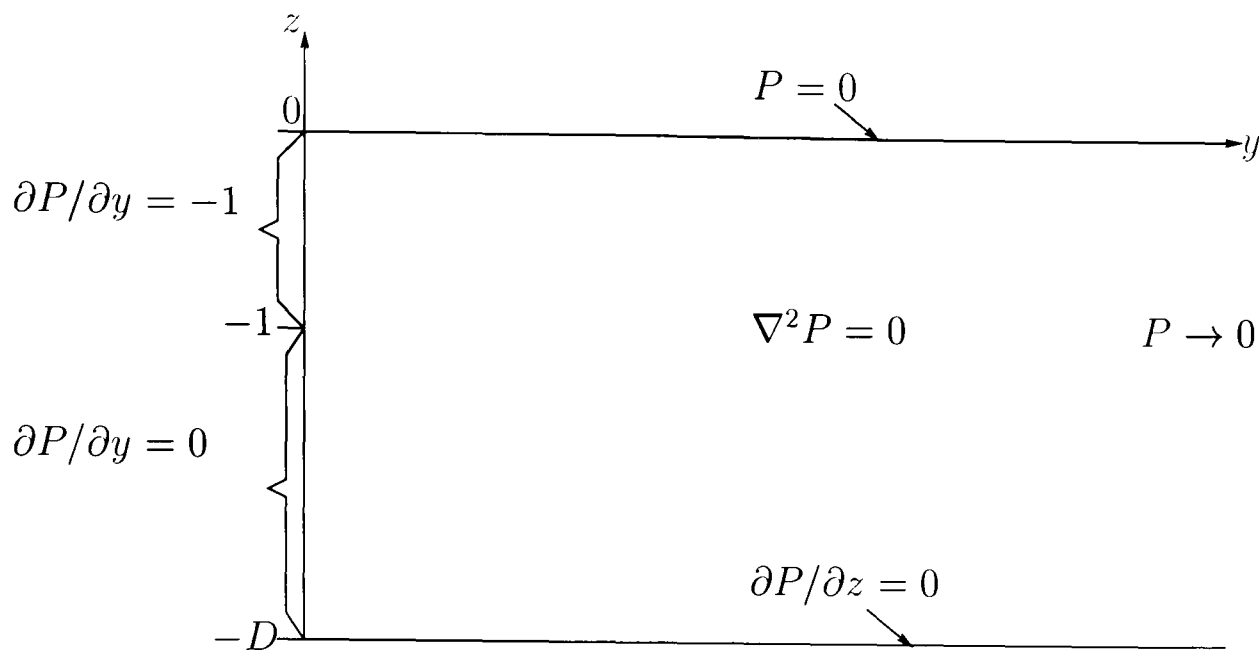
Figure 2.2: Boundary conditions for two-dimensional impact on a wall, as shown in Cooker and Peregrine (1990 b).

Hence the two-dimensional solution, given in Cooker and Peregrine (1990b), is:

$$P_{2D} = - \sum_{n=0}^{\infty} \frac{2}{D\lambda_n{}^2} \left[1 - \cos(\lambda_n)\right] \sin(\lambda_n z) e^{-\lambda_n y}, \tag{2.9}$$

where $\lambda_n = (n + \frac{1}{2})\pi/D$. Note unless otherwise stated the sum in all future expressions is taken to be from 0 to ∞. This Fourier series is obtained using separation of variables and a similar method of solution is described in more detail in section 3.6. The exact sum is from $n = 0$ to ∞, so we must truncate it. For most cases in this thesis inclusion of 50 terms is sufficient to give an accuracy of at least 4 decimal places, but in the case of $1/D$ very small, many more terms are required.

Cooker and Peregrine (1990b, 1992) looked at the effect of varying the impact region height, while keeping the depth of water D constant. We now consider keeping the size of the impact region constant, and looking at the effect of variation of water depth beneath the impact region. Figure 2.3 shows plots of pressure impulse down a wall for different water depth at the wall, but keeping the impact region the same height. (a similar study is carried out in Chan (1994))

As the depth of water increases (i.e. the depth of water below the impact region increases) the pressure-impulse plot has more of a 'tail' which gives a larger total impulse value. Figure 2.4 shows a plot of total impulse against depth of water.
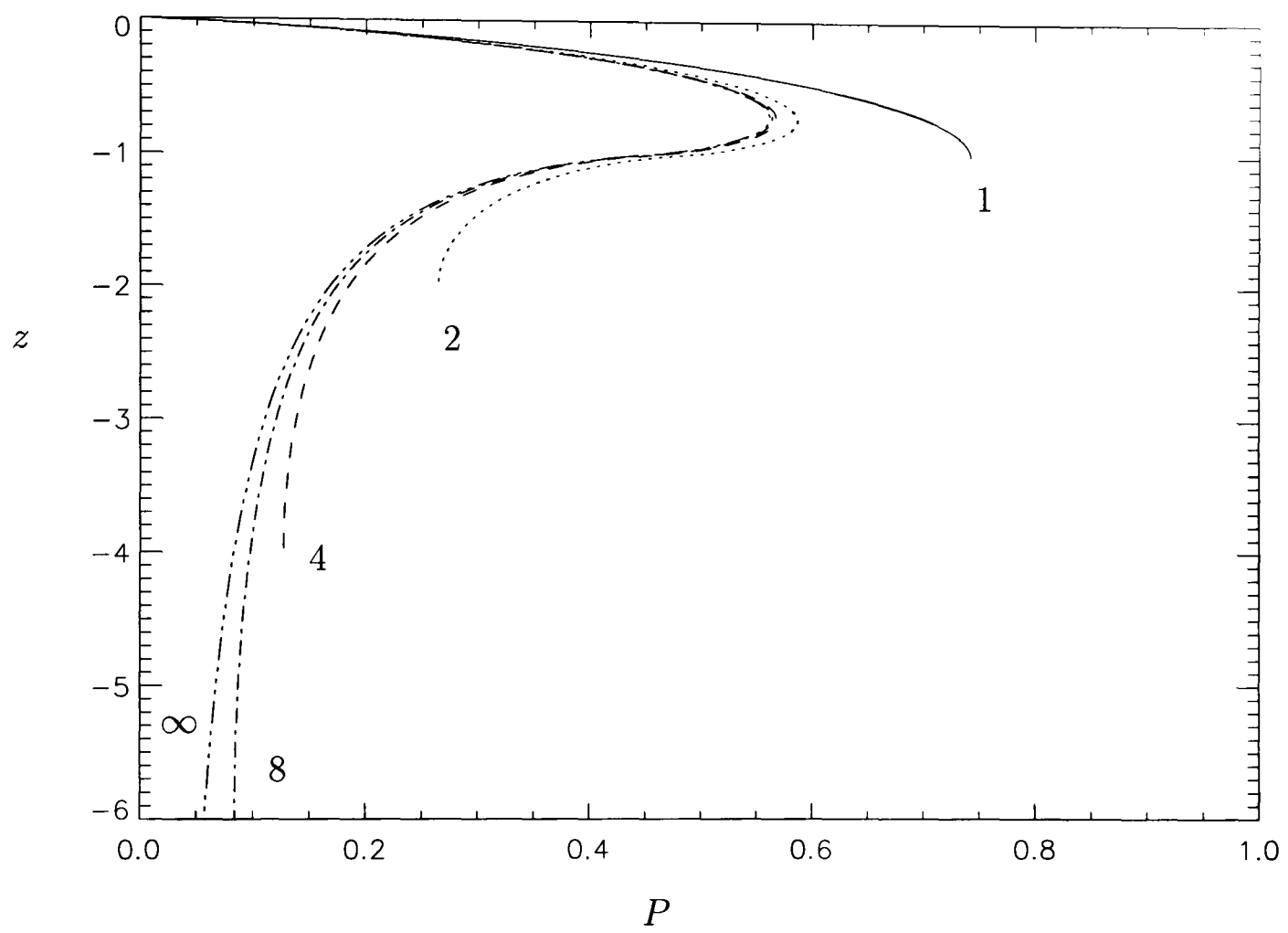
Figure 2.3: Pressure impulse on a wall, keeping the impact region the same height. z is the position on the wall. Each plot is labelled by the total depth of the water.(impact region is $z = -1$ to 0)

(again keeping the height of impact region the same) The total impulse is given by integrating equation (2.9) over the depth of the water:

$$I = \frac{2}{D} \sum_n \frac{1 - \cos(\lambda_n)}{\lambda_n^3}.$$ (2.10)
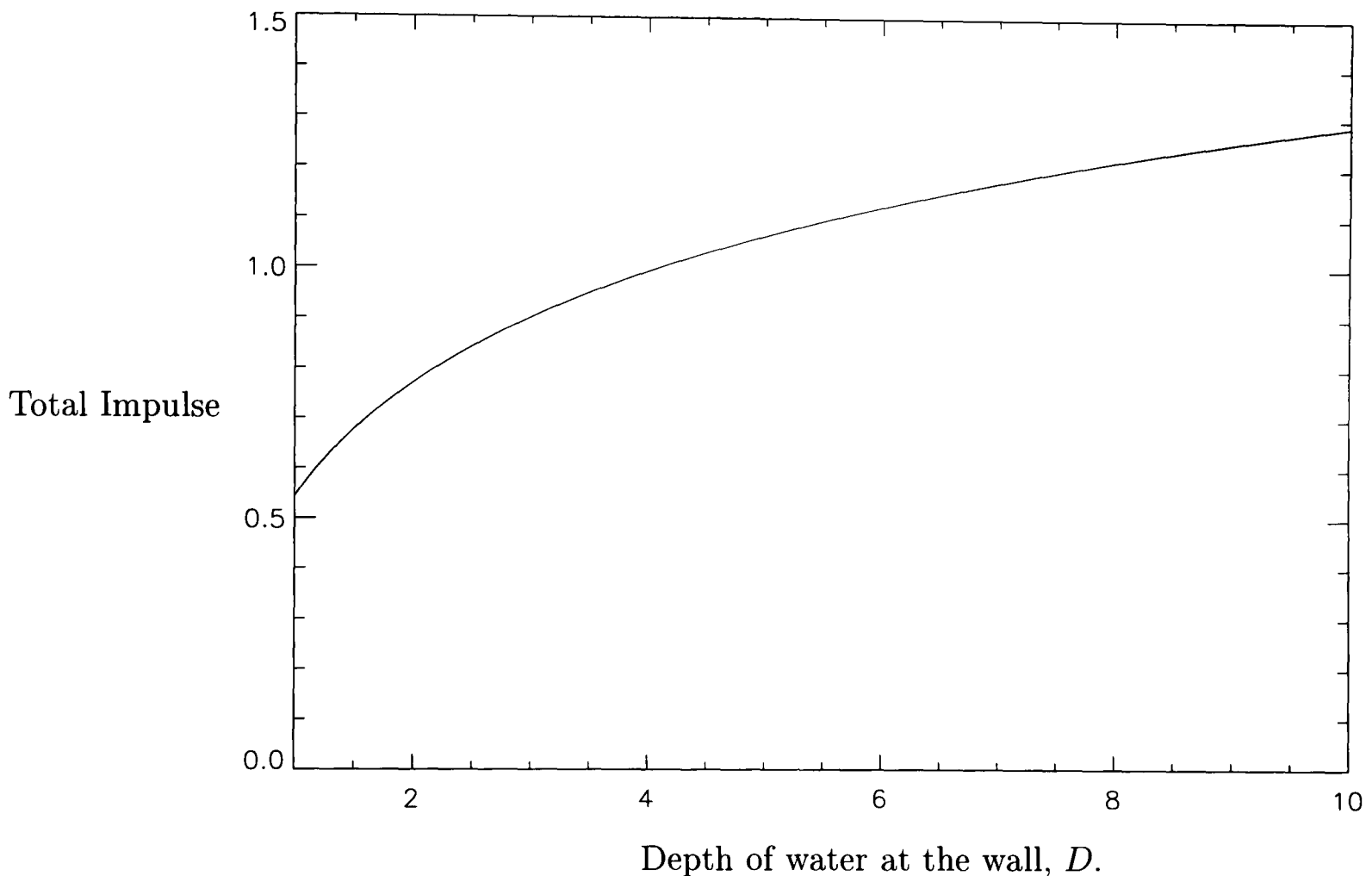
Figure 2.4: Total impulse against depth of water, keeping the impact area constant and varying the depth of water at the wall.

We can see that as the depth of water below the impact region increases the total impulse increases. Of particular note is that the infinite depth solution shows that there is no limit to the increase in total impulse as the water at the wall becomes deeper. Cooker and Peregrine (1995) gives the pressure-impulse distribution on the wall for the infinite depth case, $D \to \infty$:

$$P(0, z) = -\frac{1}{\pi} \left[z \log \left| 1 - \frac{1}{z^2} \right| + \log \left| \frac{1 + z}{1 - z} \right| \right].$$ (2.11)

22

Indefinite integration over z (for $|z| > 1$) gives:

$$\int P(0, z)dz = -\frac{1}{\pi} \left[\frac{z^2}{2} \log \left(1 - \frac{1}{z^2} \right) - \frac{1}{2} \log(z^2 - 1) + (1 + z) \log(1 + z) \right.$$
$$\left. -2 - (z - 1) \log(z - 1) \right]. \quad (2.12)$$

When z is large the dominant term is $\log(z^2)$, which is divergent as $z \to \infty$. Hence the total impulse is infinite. This shows that for deep water cases this model is inadequate. This emphasises the importance of examining either three-dimensional impact (not having the impact the same at every position along the wall) or compressibility effects for impacts on walls in relatively deep water. (as also discussed in Chan (1994))

2.3.2   Three-dimensional impact on a wall.

We now consider the impact of a body of water on a patch of a wall. We let our length scale L equal the depth of water at the wall and again all quantities stated are dimensionless unless otherwise stated. Cooker and Peregrine (1995) noted that unless the width of the impacting water is quite small the actual shape of the wave away from the impact region is relatively unimportant. We take the impact area to be a patch on the wall and the free surface to be simplified to a horizontal surface. Let A denote the area of the patch, and the depth of the wall be 1. We use the boundary conditions described in section 2.2.2. On the free surface the usual condition of $P = 0$ is required. The patch is where impact takes place so we need $\partial P / \partial y = V(x, z)$, where y is the direction normal to the patch, and x and z are as shown in figure 2.5. On the rest of the wall no impact occurs so we require $\partial P / \partial y = 0$. Along the bottom of the region of the fluid we have a solid boundary so $\partial P / \partial z = 0$ is required. We also need $P \to 0$ as we move far away from the impact patch. So a solution to Laplace's equation subject to the boundary conditions shown in figure 2.5 is required.

We can solve this problem in terms of a Fourier series expansion using a Fourier integral. The boundary conditions on the planes $z = 0$ and $z = -1$ enable the

23
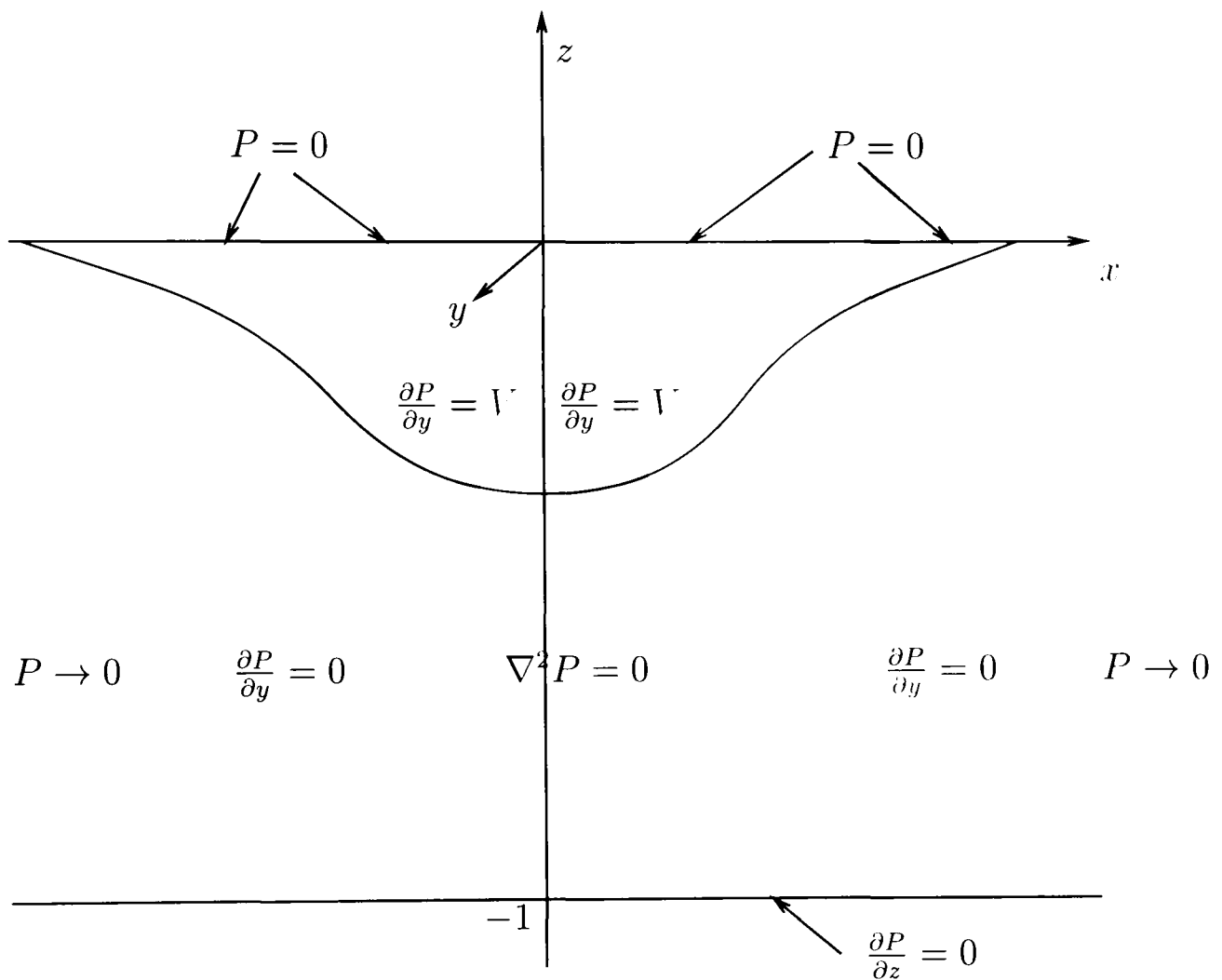
Figure 2.5: Impact on a patch of a wall. View facing wall.

separation of the z dependence giving an expression for P:

$$P(x, y, z) = \sum_n P_n(x, y) \sin(\lambda_n z), \qquad (2.13)$$

where $\lambda_n = (n + 1/2)\pi$. A Fourier transform of the problem in the x direction is taken, where the Fourier cosine transform is given by equation (2.14).

$$\overline{P_n}(k, y) = \int_{-\infty}^{\infty} P_n(x, y) \cos(kx) dx. \qquad (2.14)$$

In using a cosine Fourier transform we must assume that the patch is symmetric about $x = 0$. We consider first the condition on the impact patch, which from equation (2.13) on the patch we have:

$$\sum_n \frac{\partial P_n(x, 0)}{\partial y} \sin(\lambda_n z) = V(x, z). \qquad (2.15)$$

Next we multiply by $\sin(\lambda_r z)$ and integrate with respect to z:

$$\frac{\partial P_r(x, 0)}{\partial y} = 2 \int V(x, z) \sin(\lambda_r z) dz, \qquad (2.16)$$

where the integration in z is, for a given x, over values of z on the patch. Finally we transform this equation in x to give:

$$\frac{\partial \overline{P_n}(k, 0)}{\partial y} = 2 \int_A \int V(x, z) \sin(\lambda_n z) \cos(kx) dz dx, \qquad (2.17)$$

where the integration is done over the patch area A.

We next carry out the transform in x of Laplace's equation:

$$\frac{\partial^2 \overline{P_n}}{\partial y^2} - (k^2 + \lambda_n^2)\overline{P_n} = 0. \qquad (2.18)$$

To make the notation simpler we use $m^2 = (k^2 + \lambda_n^2)$. In future expressions it must be remembered that m is dependent on k and n. We require $P(x, y, z) \to 0$ as $y \to \infty$, which means that we need $\overline{P_n}(k, y) \to 0$ as $y \to \infty$ Solving equation (2.18), and using $\overline{P_n}(k, y) \to 0$ as $y \to \infty$ provides an expression for $\overline{P_n}(k, y)$:

$$\overline{P_n}(k, y) = A_n(k) e^{-my}, \qquad (2.19)$$

where $A_n(k)$ are functions of k, to be found using the boundary condition at the wall. We use equations (2.17) and (2.19) to get:

$$A_n(k) = -\frac{2}{m} \int_A \int V(x,z) \sin(\lambda_n z) \cos(kx) dx dz. \tag{2.20}$$

The final step is to take the inverse transform of equation (2.19) and substitute into equation (2.13) to obtain the Fourier sum for P:

$$P(x,y,z) = \sum_n \frac{1}{\pi} \int_0^\infty A_n(k) e^{-my} \sin(\lambda_n z) \cos(kx) dk, \tag{2.21}$$

with $A_n(k)$ given by equation (2.20).

We next consider the specific case of a rectangular patch of depth and width d and $2a$ respectively (symmetric about $x = 0$). $V(x,z) = -1$ on the patch. Hence, we can carry out the integration in equation (2.20) directly to obtain

$$A_n(k) = -\frac{4}{k\lambda_n m} \sin(ka) \left[1 - \cos(\lambda_n d)\right]. \tag{2.22}$$

Using (2.21), for this specific case, we obtain the Fourier sum for P:

$$P(x,y,z) = -\sum_n \frac{4}{\pi \lambda_n} \left[1 - \cos(\lambda_n d)\right] I(n,x,y) \sin(\lambda_n z), \tag{2.23}$$

where

$$I(n,x,y) = \int_0^\infty \frac{\sin(ka) \cos(kx) e^{-(k^2 + \lambda_n^2)^{1/2} y} dk}{k(k^2 + \lambda_n^2)^{1/2}}. \tag{2.24}$$

To evaluate pressure impulse for this problem the Fourier series must be truncated. For a patch of height 0.1 the difference between taking 20 and 50 terms is only 4% and for a patch of height 1, the difference is substantially less. The integration is carried out using NAG routine D01ASF, which treats the integral as a Fourier cosine transform. This particular integration method splits the integration domain into subintervals and replaces the function to be integrated by a Chebyshev-series approximation. This enables us to plot contours of pressure impulse for this problem. Of particular interest are the contours of pressure impulse on the wall itself, as shown in figures 2.6, 2.7 and 2.8. The patch is of height 0.2, 0.5 and 1.0 for figures 2.6, 2.7 and 2.8 respectively. In all cases the patch has width 2.
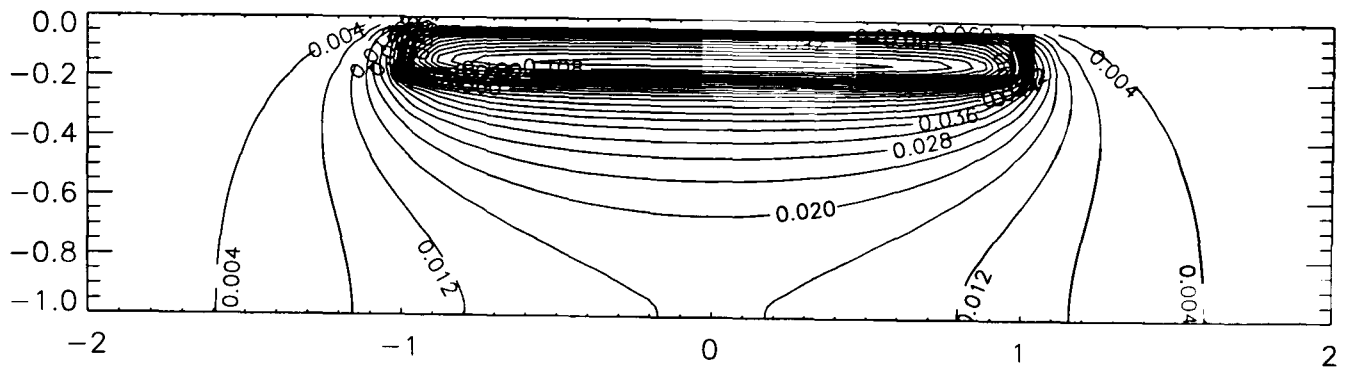
Figure 2.6: Pressure-impulse contours for impact on a patch of a wall where the patch covers the top 20 % of the wall below water level and is width 2.
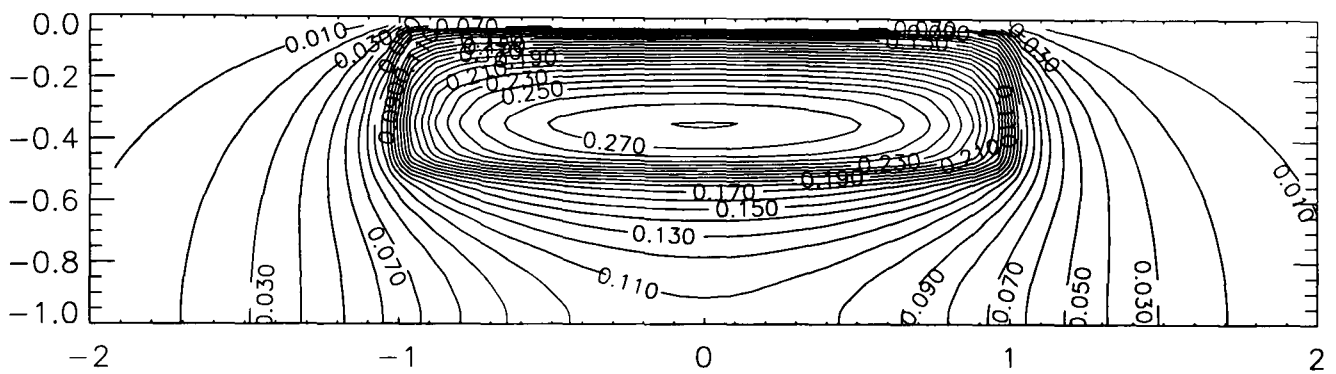
Figure 2.7: Pressure-impulse contours for impact on a patch of a wall where the patch covers the top 50% of the wall below water level and is width 2.
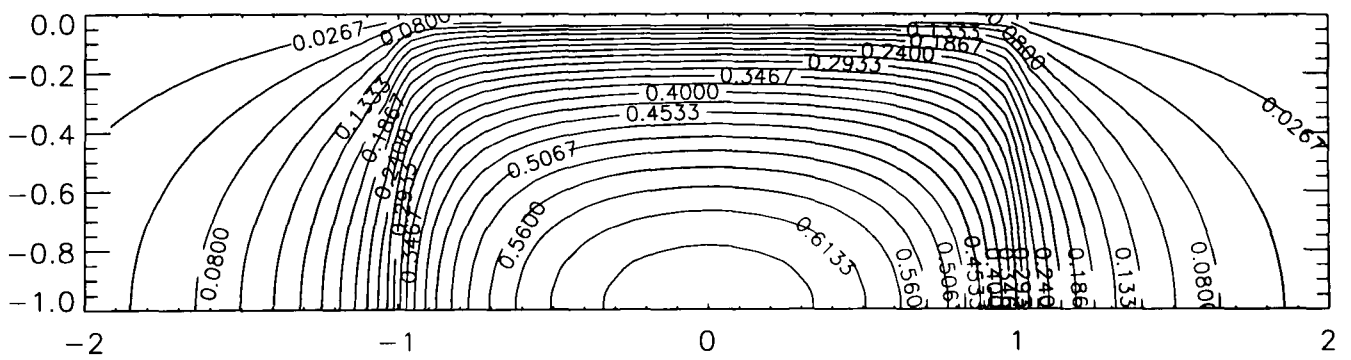
Figure 2.8: Pressure-impulse contours for impact on a patch of a wall where the patch covers the full height of the wall below water level and is width 2.

The total impulse for the full and top 20% impact are 1.085 and 0.085 respectively. If integration is only over the central width $2a$ then the corresponding values are 0.878 and 0.074. As expected the larger the area of impact the larger the total impulse. Figure 2.9 shows a plot of total impulse against depth of water (the total impulse has been temporarily been scaled to have depth of impact 1 as our length scale L), where the integration is over the central width of $2a$, and the impact region is the top distance 1. We note that instead of the total impulse increasing with depth of water below the impact region, as predicted by the 2D Cooker and Peregrine model, it instead predicts that the total impulse tends to a finite value. It is more realistic that as the depth of water at the wall becomes infinitely deep that the total impulse tends to a finite value.

Figure 2.10 shows a comparison of the pressure impulse on the wall for the 2D impact model used in Cooker and Peregrine (1990b, 1992) and down the centre line of the 3D 'patch' model. For the comparison impact on the top 20 % of the depth of water is used for both models, and the length of the patch is taken to be twice the depth of the wall. Even though this patch is quite wide the 'patch' model shows a lower pressure impulse down the centre line than is found using the 2D model. The difference between the pressure impulse down the centre line for the 3D 'patch' and 2D models is only slight but if we move away from the centre line the difference in the models increases rapidly.

Figure 2.11 is a plot of pressure impulse at the base of the wall under the centre of the patch for varying values of d (the depth of the patch). As expected increasing the height of impact increases the pressure impulse at the base of the wall. However, the height of the patch has relatively little effect on the difference between the 2D and 3D model, except when the patch is very small in height. As the height of the patch increases from 0.6 the difference between the two models remains almost the same. Figure 2.12 shows the ratio of the pressure impulse of the 3D 'patch' model and 2D (Cooker and Peregrine) model of impact on a wall, varying the depth of the impact region. The ratio does not vary very much but increases slightly as the
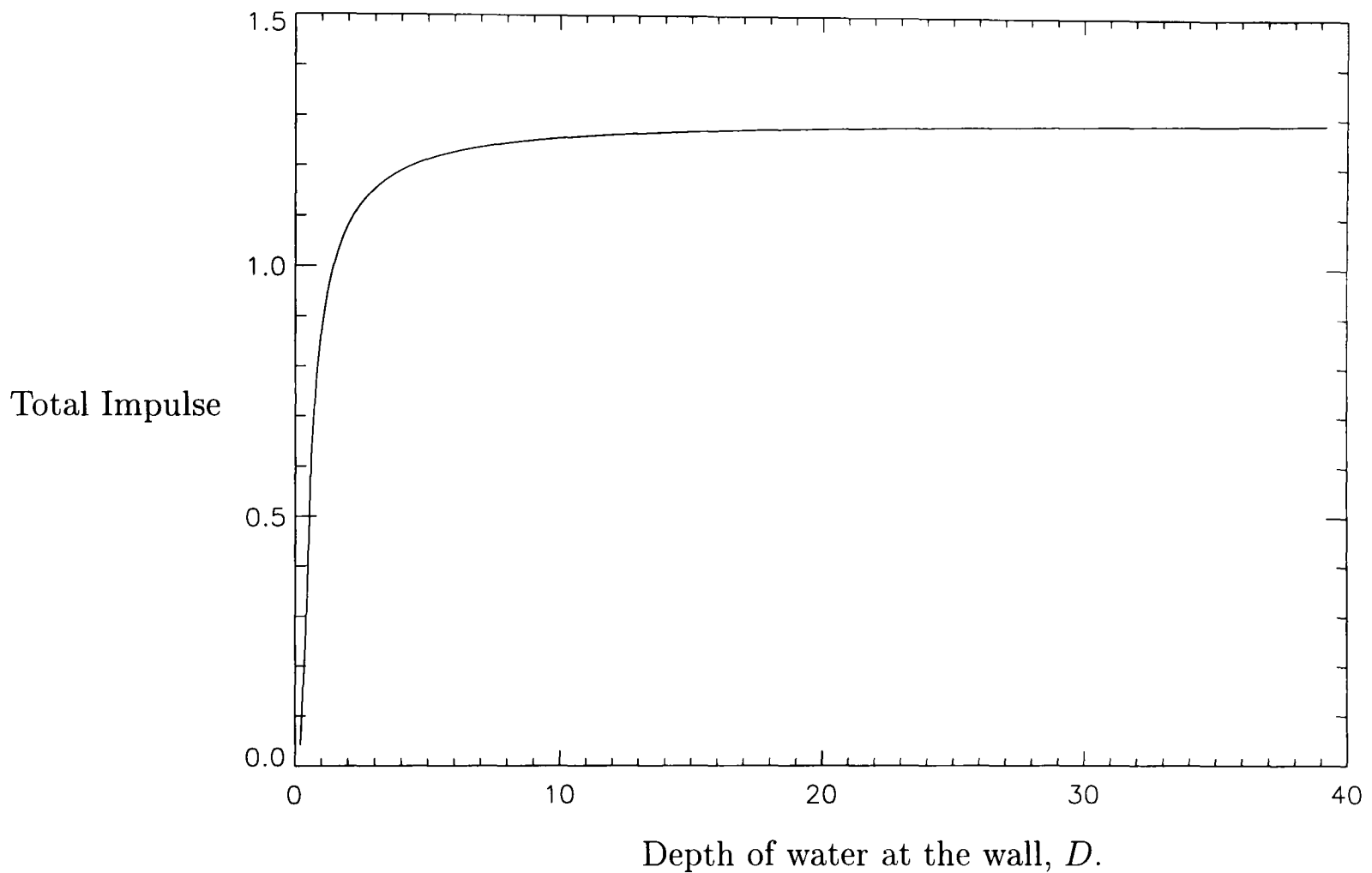
Figure 2.9: Total impulse against depth of water at the wall, for 3D impact on a patch of a wall, where the integration is over the central width of $2a$ ($a = 1$), and the impact region is the top portion of depth 1. The total impulse has been temporarily rescaled (for this diagram only) to have the unit length scale as the depth of impact, and D as the depth of water at the wall.

29
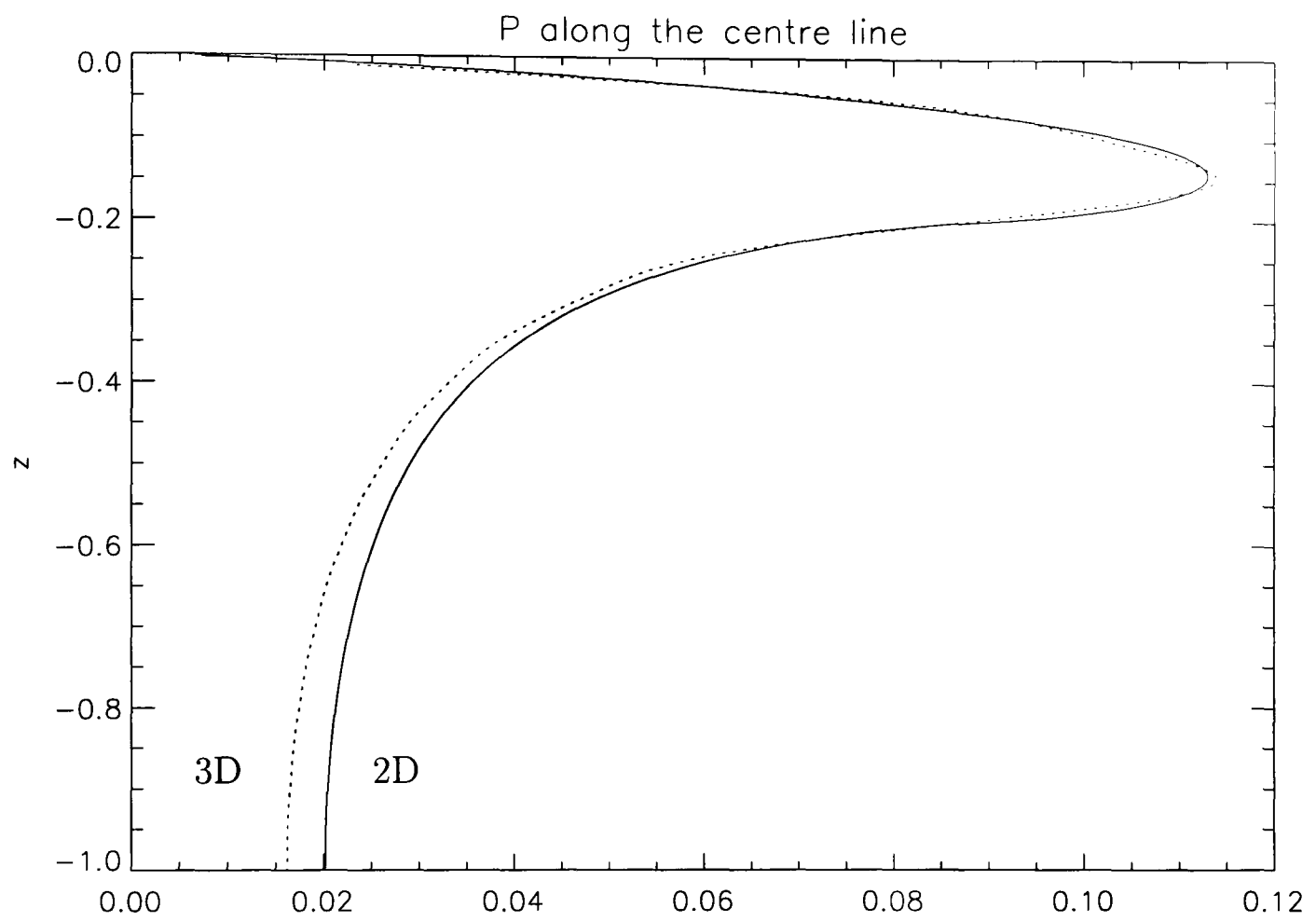
Figure 2.10: Pressure impulse along the centre line for the 2D (Cooker and Peregrine) model and 3D 'patch' models of impact on a wall, with impact on the top 20 %.

depth of impact increases.
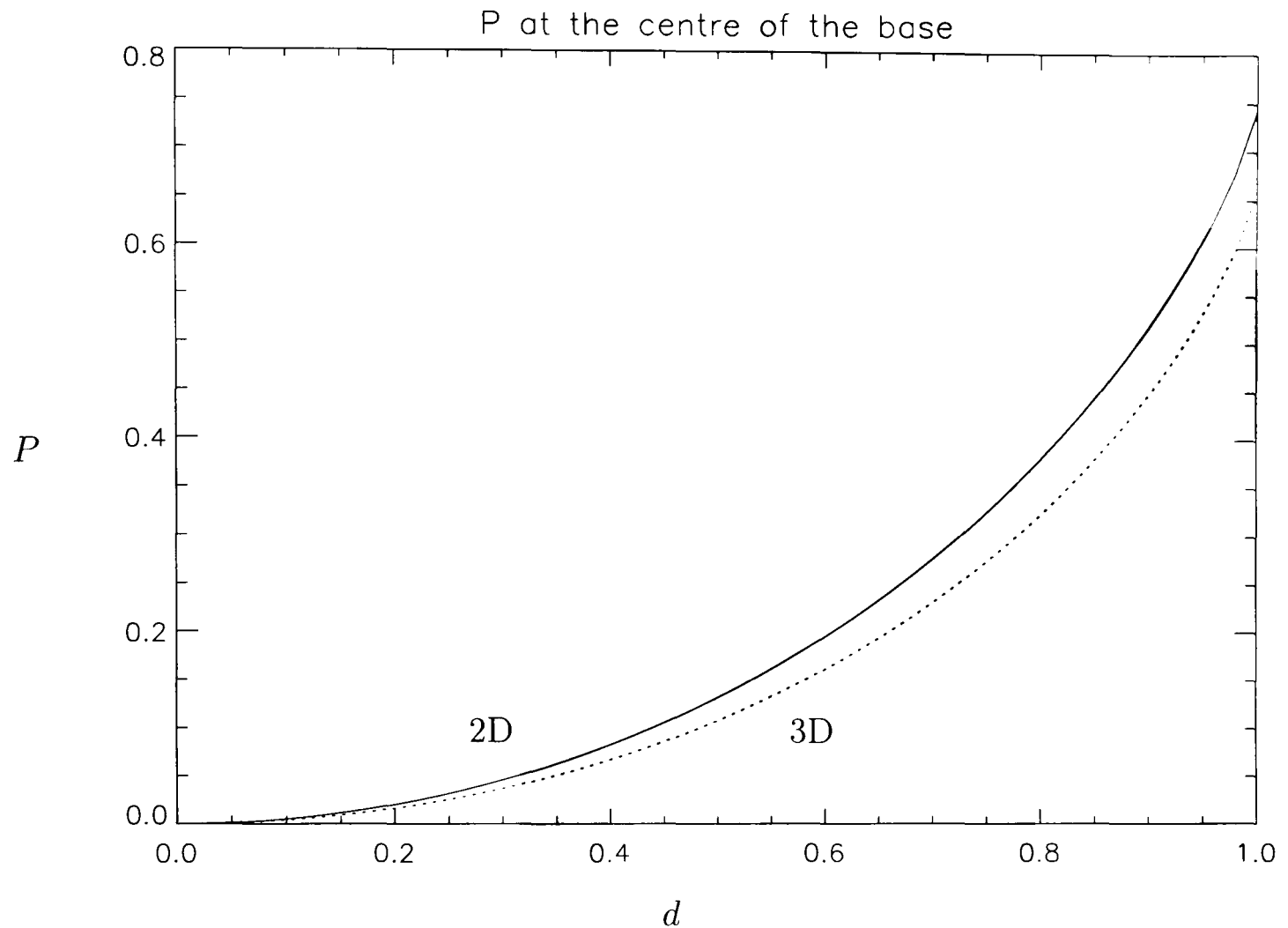
Figure 2.11: Pressure impulse at the base of the wall in line with the centre of the patch for the 2D (Cooker and Peregrine) model and 3D 'patch' models of impact on a wall, varying the depth of the impact region.

Figure 2.13 shows a plot of P/P_m offshore on the bed along the line of symmetry for a comparison of the Cooker and Peregrine 2D model, and the 'patch' model with a patch of length 1 and 2 all for $d = 0.5$ and depth of water 1. P_m is the value of P at the middle bottom of the wall. This shows that once the pressure impulse has been scaled by the value at the wall all the curves are very similar in nature. However, as expected once the patch length is 1 or smaller there is a significant difference between the values predicted by the Cooker and Peregrine model and the 'patch' model.
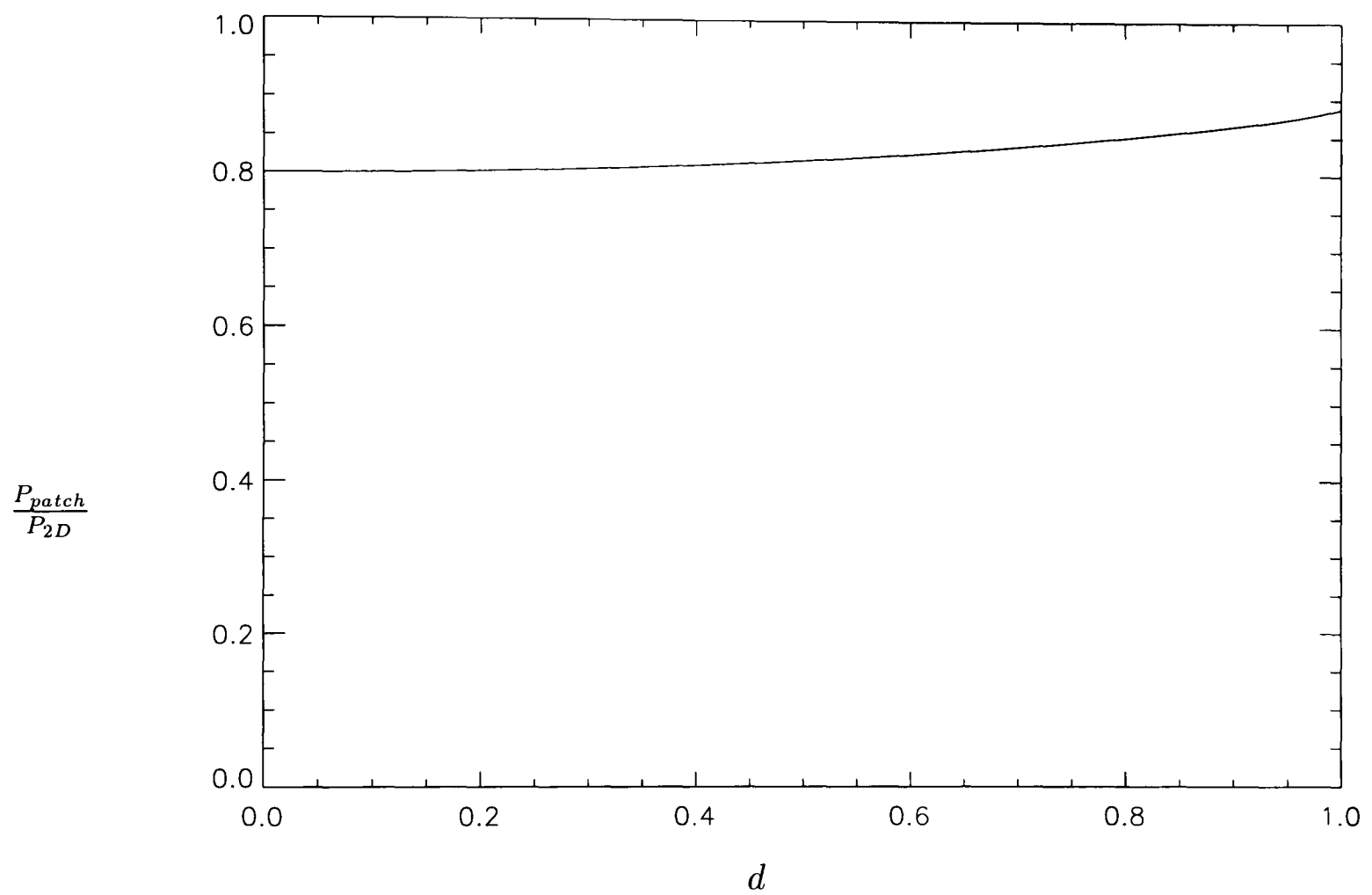
Figure 2.12: Pressure impulse at the base of the wall in line with the centre of the patch for the ratio of the 3D 'patch' model and 2D (Cooker and Peregrine) model of impact on a wall, varying the depth of the impact region, with patch width 2.

32

P along centre line of base
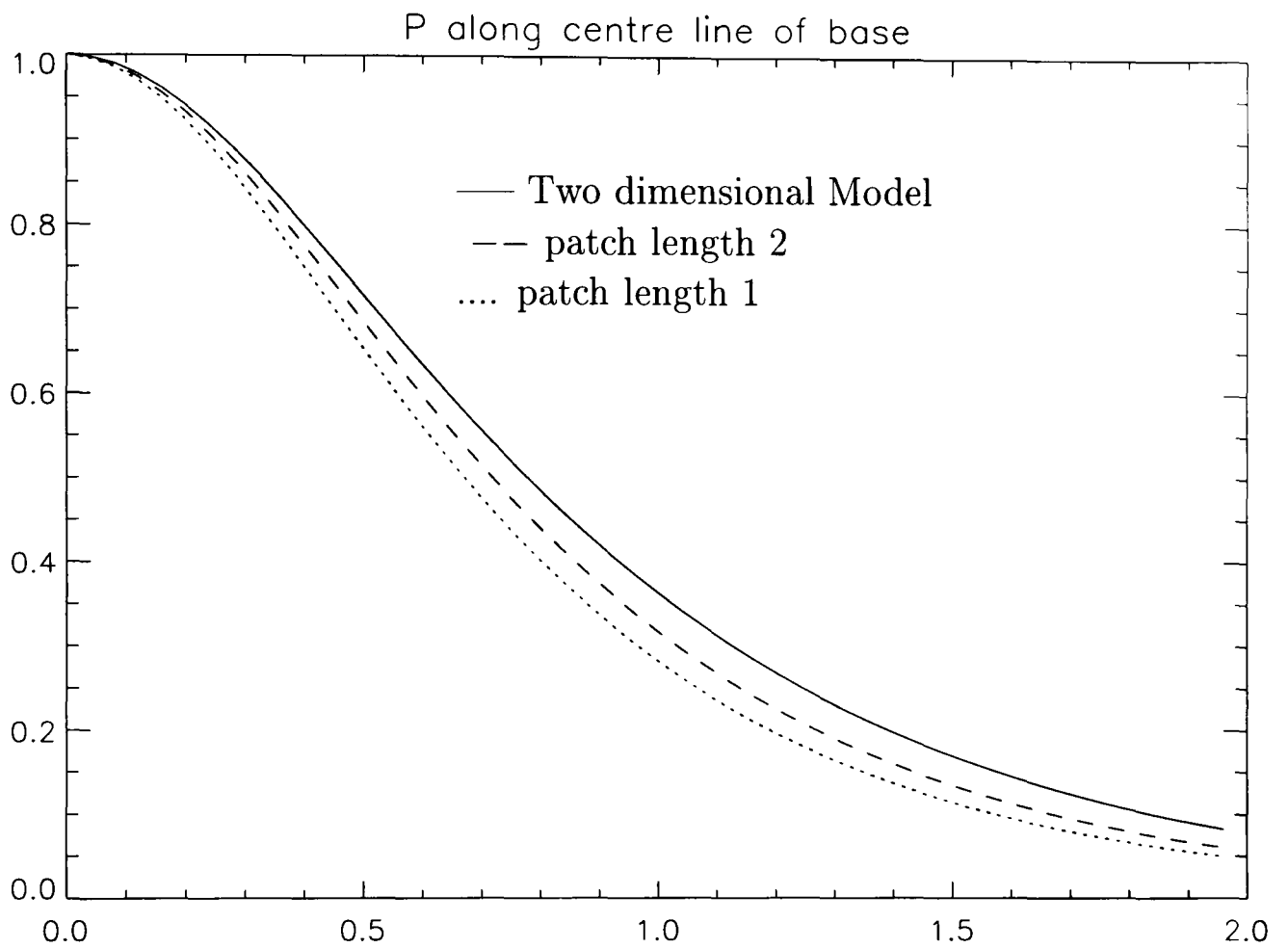
Figure 2.13: Plot of P/P_m offshore on the bed along the centre of the line of symmetry for a comparison of the Cooker and Peregrine 2D model, and the 'patch' model with a patch of length 1 and 2. $d = 0.5$, depth of water 1. P_m is the value of P at the middle bottom of the wall.

2.3.3 Semi-infinite patch of impact.

We need to have a clearer way of comparing the 'patch' model and the two-dimensional Cooker and Peregrine model. If the patch is sufficiently long. at or towards the centre of the patch the solution is the same as for the two-dimensional case. Hence. for a given length of patch, we need to estimate how far into the patch it is reasonable to assume that the solution has become two-dimensional. For a finite patch. this is difficult to assess as both ends of the patch have an effect on the solution. So we next consider a semi-infinite patch.

Figure 2.14 shows the problem we need to solve for impact on a semi-infinite region of the wall. We again take our length scale L as the depth of water at the wall, and work in dimensionless quantities. As we need to impose the forcing

$$P = 0 \qquad P = 0$$

$$\frac{\partial P}{\partial y} = -1$$

$$-d$$

$$\frac{\partial P}{\partial y} = 0 \qquad \nabla^2 P = 0 \qquad \frac{\partial P}{\partial y} = 0 \qquad P \to 0$$

$$\frac{\partial P}{\partial z} = 0$$

$$-1$$
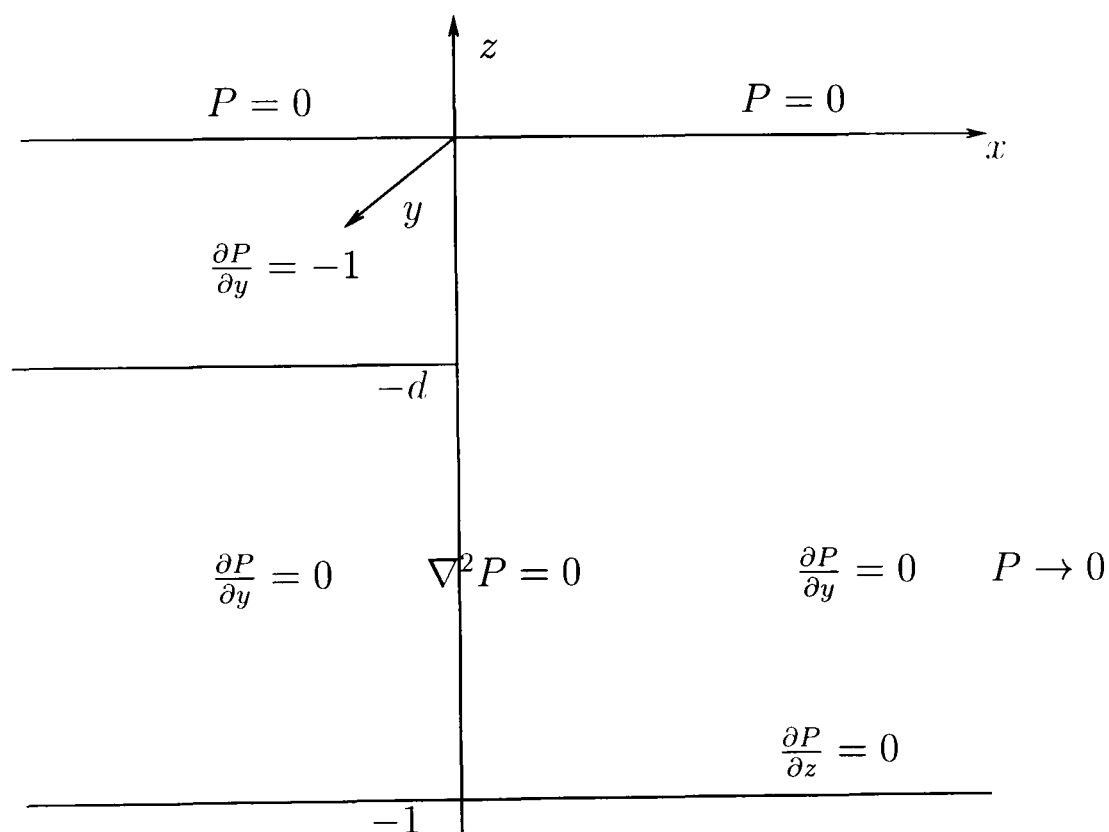
Figure 2.14: Impact on a semi-infinite patch of a wall. View facing wall.

condition on the patch over a semi-infinite region we solve using a slightly different method to that used for the finite patch. We split the problem up into the two regions $x < 0$ and $x > 0$, the solutions to which we will denote as P_l and P_r respectively. We then use continuity of P and $\partial P / \partial x$ along the line $x = y = 0$, to find the

34

solution. We consider first the solution in the left hand region. As $x \to -\infty$ the solution will tend to the two-dimensional Cooker and Peregrine solution for impact on a wall (denoted now by P_{2D}). If we subtract the solution for the 2D problem off P_l then the remaining problem whose solution is P_{re} is the same as in left hand region of figure 2.14 except that the condition over the patch is now $\partial P/\partial y = 0$. So $P_{re} = P_l - P_{2D}$. We can solve this problem for P_{re} and then find P_l using $P_l = P_{re} + P_{2D}$. In a similar manner to the solution of the finite patch model we take a Fourier transform of the problem, to solve for P_{re}, but this time the Fourier transform is a Fourier-cosine transform in the y direction.

$$\overline{P_{re}}(x, k, z) = 2 \int_0^\infty P_{re}(x, y, z) \cos(ky) dy. \tag{2.25}$$

The solution is given by:

$$P_{re} = 2 \int_0^\infty \sum_n A_n(k) e^{mx} \sin(\lambda_n z) \cos(ky) dk, \tag{2.26}$$

where $\lambda_n = (n + \frac{1}{2})\pi$, $m^2 = k^2 + \lambda_n^2$, and the A_n are obtained by the continuity conditions given at $x = 0$.

From equation (2.9) the solution to the two-dimensional problem (rescaled to have the length scale as the depth of water at the wall) is given by

$$P_{2D} = -\sum_n \frac{2}{\lambda_n^2} [1 - \cos(\lambda_n d)] \sin(\lambda_n z) e^{-\lambda_n y}, \tag{2.27}$$

hence

$$P_l = 2 \int_0^\infty \sum_n A_n(k) e^{mx} \sin(\lambda_n z) \cos(ky) dk$$
$$- \sum_n \frac{2}{\lambda_n^2} [1 - \cos(\lambda_n d)] \sin(\lambda_n z) e^{-\lambda_n y}. \tag{2.28}$$

Solution in the right hand region is the very similar to P_{re}. The conditions at $z = 0$, $z = -1$ and on the wall are the same. However we require P_r to be positive, and to decrease to zero as $x \to \infty$ instead of being negative and increasing to zero as $x \to -\infty$ (as P_{re}). The change in sign of in front of the x is to satisfy the conditions at $x = \pm\infty$, and the negative in front of the whole expression is

to ensure continuity of pressure-impulse gradient at $x = 0$. Hence P_r is given by $-P_{re}(-x, y, z)$, hence

$$P_r = -2 \int_0^\infty \sum_n A_n(k) e^{-mx} \sin(\lambda_n z) \cos(ky) dk. \qquad (2.29)$$

From the conditions at $x = 0$ we find that:

$$A_n(k) = \frac{1}{\pi \lambda_n^2} [1 - \cos(\lambda_n d)] \frac{\lambda_n}{k^2 + \lambda_n^2} \qquad k \neq 0$$

$$A_n(0) = \frac{1}{2\pi \lambda_n^3} [1 - \cos(\lambda_n d)] \qquad k = 0. \qquad (2.30)$$

Integration is carried out in a similar manner to that used in the evaluation of the pressure impulse for the finite patch impact. Figures 2.15 (a) and (b) show pressure impulse contours, for the semi-infinite patch, on the wall and base respectively for a patch of depth 0.3. Figures 2.16 (a) and (b) are similar but this time for a patch of depth 1.0.

When the patch is of depth 0.3 and 1.0 the values only approximate the values calculated by the two-dimensional model well at a distance into the patch of two times the depth of the water i.e. the depth of penetration of the boundary conditions outside of the patch is twice the depth of the water. Figure 2.17 is a plot of P along the bottom of the wall for different depths of patch (scaled by the 2D model value). If we examine this then we can see that the depth of impact has little effect on penetration distance of the three-dimensional boundary into the patch. If we look at a distance of 0.5 into the patch (along the bottom of the wall), we can see that the pressure impulse is only approximately 0.775 and 0.850 of the two-dimensional value for patches of depth 0.2 and 1.0 respectively.

2.4 Impact on a wall with a berm.

An important feature of many vertical breakwaters is the berm or rubble mound which sometimes forms the foundation for caissons or is placed in front of the vertical wall to reduce wave reflection and breaking wave force on the vertical wall. We

36

(a)

(b)
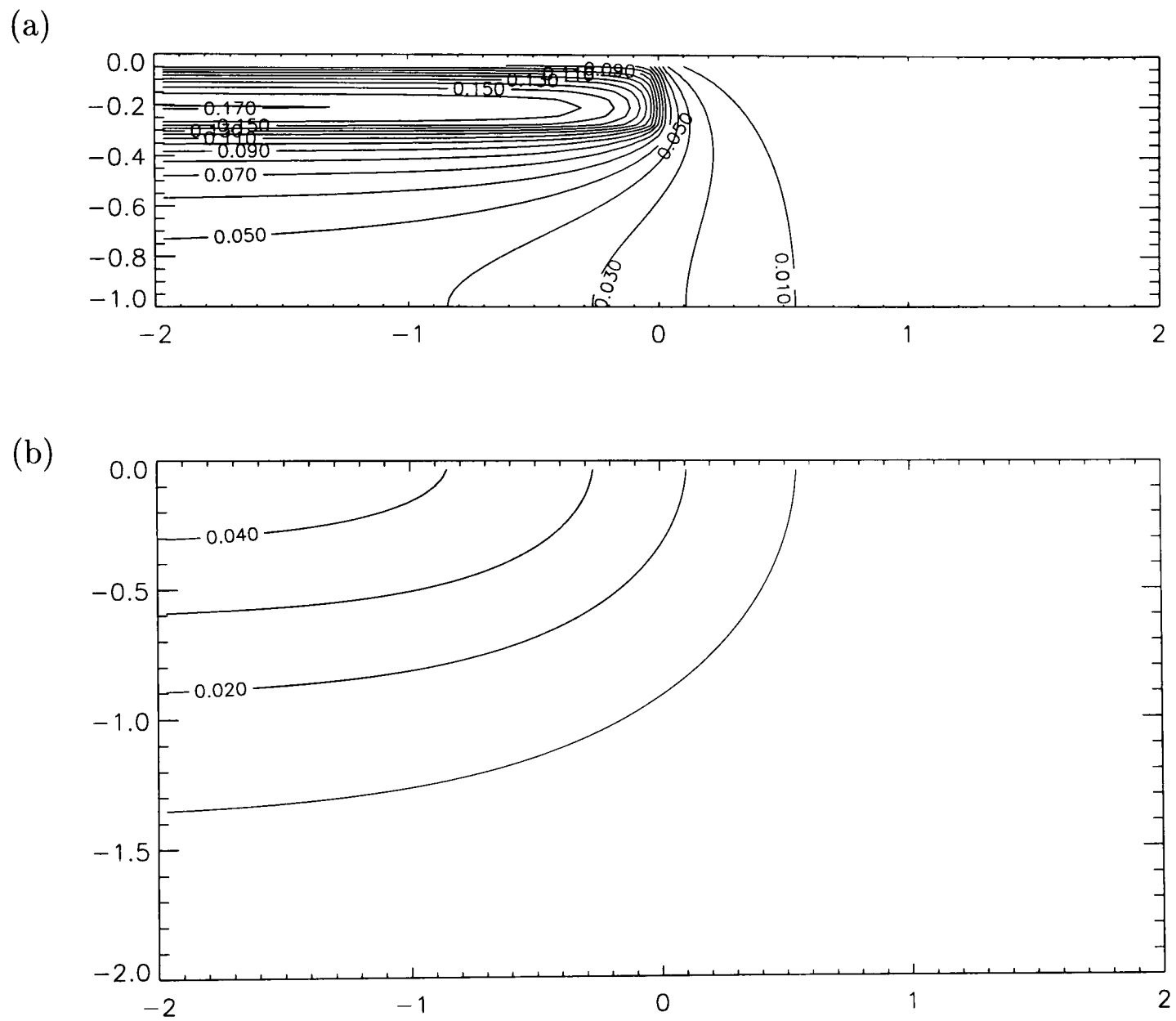
Figure 2.15: (a) Pressure-impulse contours, for the semi-infinite patch, on the wall for a patch of depth 0.3. (b) Pressure-impulse contours, for the semi-infinite patch, on the bed in front of the wall for a patch of depth 0.3.
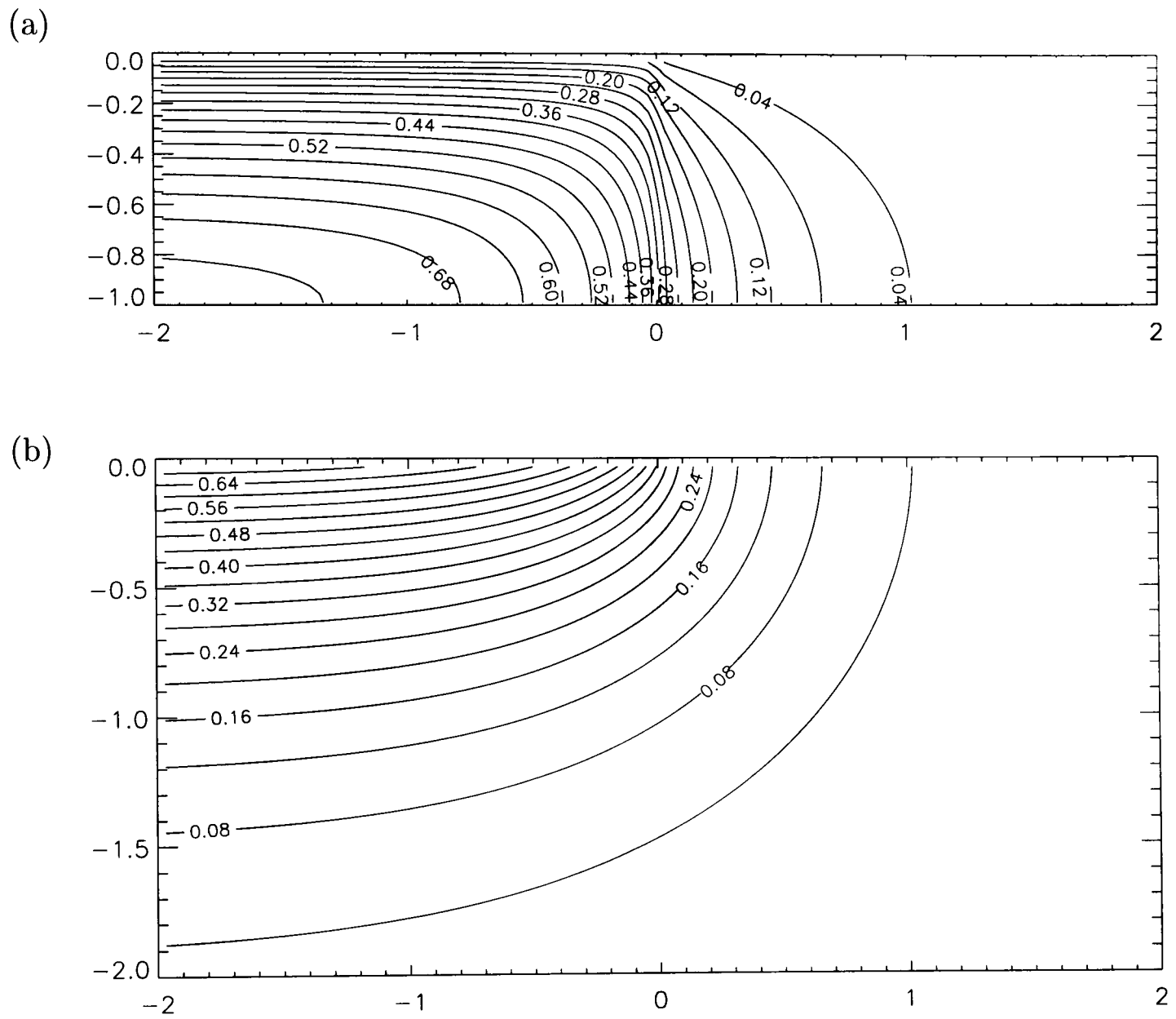
Figure 2.16: (a) Pressure-impulse contours, for the semi-infinite patch, on the wall for a patch of depth 1.0. (b) Pressure-impulse contours, for the semi-infinite patch, on the bed in front of the wall for a patch of depth 1.0.
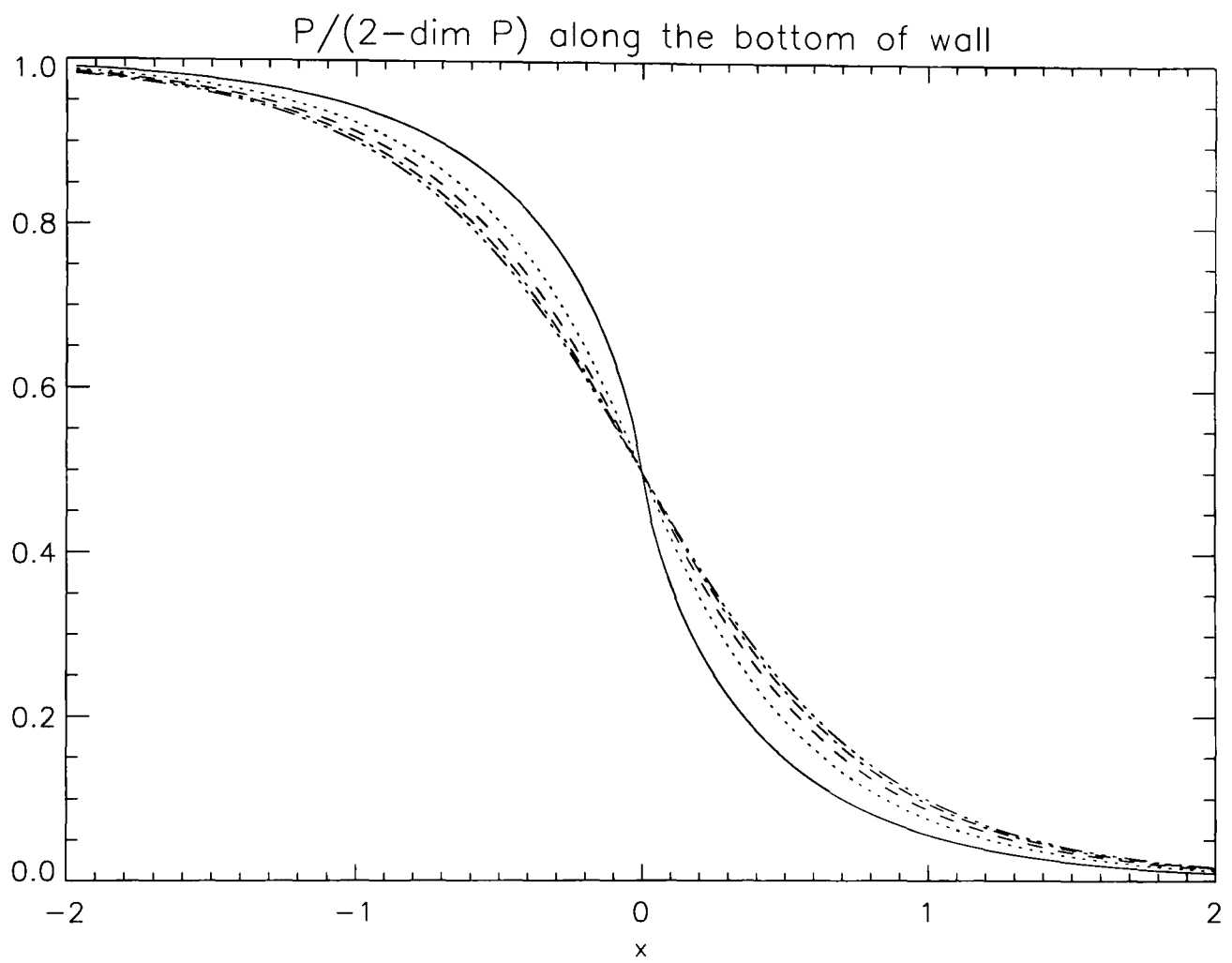
Figure 2.17: P/(2D value) for the semi-infinite patch as a function of position along the base of the wall, for $d = 0.2, 0.4, 0.6, 0.8, 1.0$ (from left to right in the top half of the graph).

39

extend the two-dimensional Cooker and Peregrine (1990 b, 1992, 1995) model for impact on a wall to include a region of porous material in front of the wall. It is assumed to be at a large scale such that all flow is at high Reynolds number, including that in the porous berm. Hence, with allowance for the added mass of the porous structure, the same pressure-impulse approach used for open water can be applied. The berm is represented by a horizontal porous bed in front of a vertical wall.

We split the problem into two regions as shown in figure 2.18 where the top region is simply water and the bottom a rubble berm. We take our length scale L to be the depth of water above the berm and work in dimensionless parameters. $P(x, y)$ is the pressure impulse. Note that for this and the following 'bounce back' model we now take y vertically, and x perpendicular to the wall. A bounded region of water of length c is used to simplify the analysis. A value of $c \geq 2$ is adequate to model the region close to the wall for a semi-infinite region of water. Hence as long as the berm is horizontal for approximately twice the water depth, these results should give a fair indication of the pressure patterns.

$$P = 0$$

$$y = 1$$
$$\mu h$$
$$\partial P / \partial n = -1$$
$$\nabla^2 P = 0$$
$$(1)$$
$$P = 0$$
$$y = 0$$
$$P_1 = P_2 \quad \frac{\partial P_1}{\partial y} = \beta \frac{\partial P_2}{\partial y}$$
$$\partial P / \partial n = 0$$
$$\nabla^2 P = 0$$
$$\text{BERM} \quad (2)$$
$$y = -b \quad x = 0 \quad x = c$$
$$\partial P / \partial n = 0$$
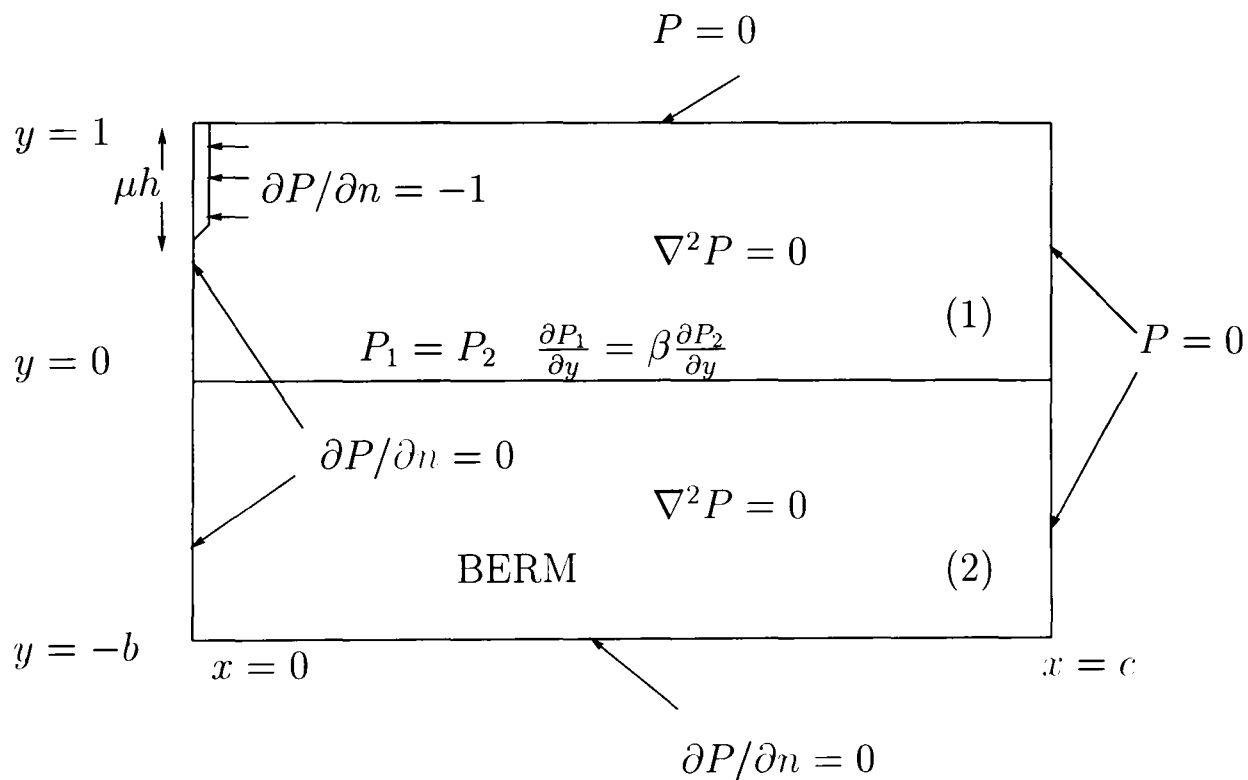
Figure 2.18: Boundary conditions required for wave impact on a vertical wall with a porous berm in front. (vertical section)

For simplicity we use the condition $P = 0$ at a distance $c\,(\geq 2)$ away from the wall. The other boundary conditions are similar to the conditions used before for impact on a wall. Let the top half be region 1, and region 2 the bottom half, and P_1 and P_2 the solutions in the respective regions. In region 1 we have similar conditions to those of impact on the wall, with the exception of the condition between the two regions. In region 2 we have $\partial P/\partial n = 0$ at the wall and base. Let S be the porosity of the berm, assumed to be uniform. Using the same notation as previously used, we have:

$$\nabla P_1 = -\rho(\mathbf{u_a} - \mathbf{u_b}), \tag{2.31}$$

in region 1. In region 2 we not only have the water, but also rubble. Hence it is much harder to accelerate water in region 2 than in region 1 as the water must be given extra acceleration to speed up around the pieces of rubble. To allow for this in region 2 we begin with the same equation as for region 1 (equation (2.31)). However, the fluid passing through a region with obstructions needs a greater velocity to pass the obstacles or restrictions. In general this leads to a greater resistance to the flow so, as equation (2.31) is linear, we have:

$$\nabla P_2 = -\rho\mu_{ij}(u_{ja} - u_{jb}) \tag{2.32}$$

where μ_{ij} is the resisitivity, and u_{ja} and u_{jb} are the jth component of $\mathbf{u_a}$ and $\mathbf{u_b}$ respectively. For simplicity we assume isotropy, so we let $\mu_{ij} = \mu$, where μ is equivalent to the resistivity to the flow of electric current in a metal with insulating intrusions. We take $\rho\mu$ equal to $\rho + \rho_m$, where ρ_m is the added mass. Hence, in region 2 we have:

$$\nabla P_2 = -(\rho + \rho_m)(\mathbf{u_a} - \mathbf{u_b}). \tag{2.33}$$

The divergence of equations (2.31) and (2.33) gives:

$$\nabla^2 P_1 = 0, \tag{2.34}$$

and

$$\nabla^2 P_2 = 0. \tag{2.35}$$

Along the line $y = 0$ we require the pressure, and hence the pressure impulse to be continuous, so along the boundary $y = 0$, we require:

$$P_1 = P_2. \qquad (2.36)$$

Let v_1 and v_2 be the vertical velocities at the interface between the two regions, in region 1 and 2 respectively. At $y = 0$ there is no mass lost, hence the flow of mass is continuous across this boundary, so $v_1 = Sv_2$. S is a measure of porosity and we assume that it is the fraction of the interface which has holes. The volume measure of porosity (percentage of holes) is equivalent to the surface porosity. This can be seen if we consider taking lots of thin slices to make up a volume, each slice has porosity S, so the total volume must have porosity S. It is worth noting that the equivalent velocity, mass flow per unit area $= S\mathbf{u}$ is often used for porous media. Combining this with equations (2.31) and (2.33) we obtain the condition that $\partial P_1/\partial y = \beta \partial P_2/\partial y$, where $\beta = \rho S/(\rho + \rho_m)$. So along $y = 0$ we also need:

$$\frac{\partial P_1}{\partial y} = \beta \frac{\partial P_2}{\partial y}. \qquad (2.37)$$

We need to solve equations (2.34) and (2.35) with equations (2.36) and (2.37) holding along line $y = 0$ subject to the boundary conditions shown in figure 2.18.

Let $P_1 = P_0 + Q$ where Q satisfies the problem in region 1 except with $\partial Q/\partial n = 0$ along the left hand wall, and where P_0 is the solution in region 1, with an impermeable bed, i.e. $\partial P_0/\partial y = 0$ on $y = 0$. P_0 and Q both satisfy Laplace's equation.

The solution to the impermeable bed problem (originally Cooker and Peregrine 1990b), is given by:

$$P_0 = \sum_m E_m \frac{\sinh \lambda_m (c - x) \cos(\lambda_m y)}{\cosh(\lambda_m c)}, \qquad (2.38)$$

with $\lambda_m = (m + \frac{1}{2})\pi$ and

$$E_m = \frac{2}{\lambda_m{}^2}(-1)^m \left[1 - \cos(m + \frac{1}{2})\pi\mu \right]. \qquad (2.39)$$

42

By satisfying the appropriate boundary conditions, Q and P_2 are found to be of the form:

$$Q = \sum_n B_n \sin k_n(c - x) \frac{\sinh k_n(1 - y)}{\sinh(k_n)}, \tag{2.40}$$

with $k_n = (n + 0.5)\pi/c$ and

$$P_2 = \sum_n A_n \sin k_n(c - x) \frac{\cosh k_n(y + b)}{\cosh(k_n b)}. \tag{2.41}$$

We now impose the conditions given in equations (2.36) and (2.37) so that we have P continuous:

$$\sum_n A_n \sin k_n(c - x) = P_0(x, 0) + \sum_n B_n \sin k_n(c - x), \tag{2.42}$$

and the flux continuous:

$$-\sum_n k_n \coth(k_n) B_n \sin k_n(c - x) = \beta \sum_n k_n \tanh(k_n b) A_n \sin k_n(c - x) \tag{2.43}$$

respectively.

Multiplying equation (2.42) by $\sin k_r(c - x)$ and integrating with respect to x gives:

$$A_r - B_r = \frac{2}{c} \int_0^c P_0(x, 0) \sin k_r(c - x) dx = D_r, \text{say}. \tag{2.44}$$

Next we substitute for $P_0(x, 0)$ and carry out the integration to obtain an expression for D_n:

$$D_n = \sum_m \frac{4(-1)^m}{c\lambda_m} \frac{\left[1 - \cos(m + \frac{1}{2})\pi\mu\right]}{\lambda_m^2 + k_n^2} (-1)^n. \tag{2.45}$$

From equation (2.43) we have

$$B_n = -\beta A_n \tanh(k_n) \tanh(k_n b), \tag{2.46}$$

hence

$$A_n = D_n/(1 + \beta \tanh(k_n) \tanh(k_n b)). \tag{2.47}$$

We can find expressions for A_n and B_n by using equations (2.44), (2.45) and (2.47). Thus pressure impulse can be calculated by evaluating the Fourier series (after truncation). Figure 2.19 shows a plot of pressure-impulse contours for $\mu =$
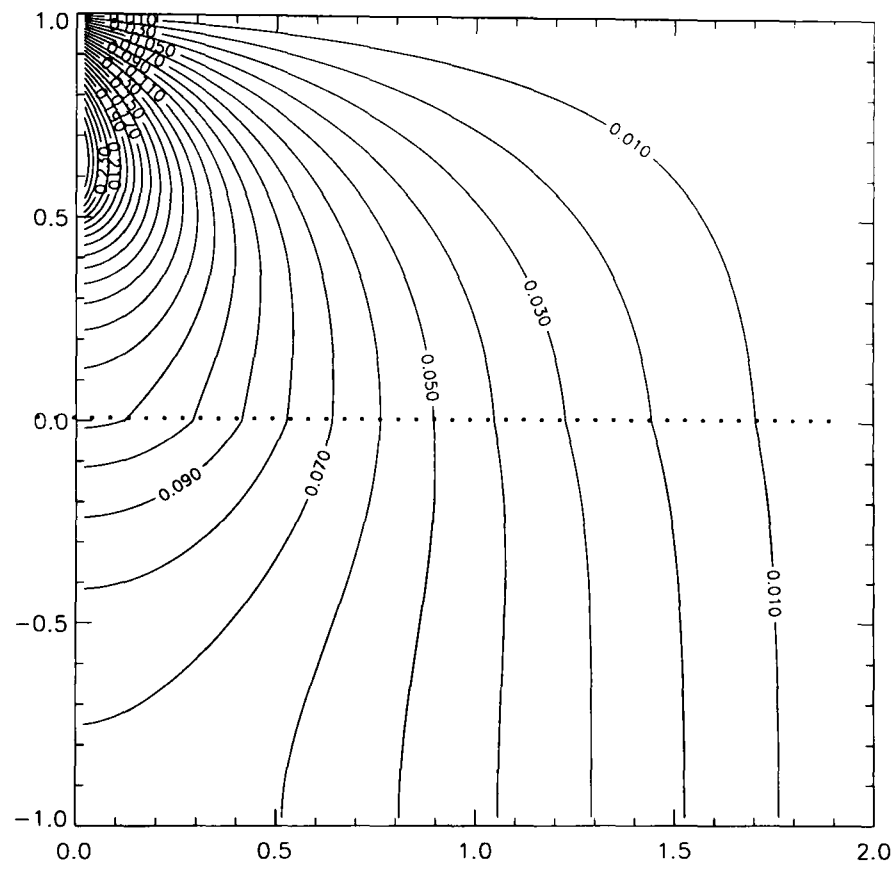
Figure 2.19: Pressure-impulse contours for impact on a wall with a porous berm in front. $\mu = 0.5, \beta = 0.3, b = 1.0, c = 2$

$0.5, \beta = 0.3$, $b = 1.0, c = 2$. The top half of the graph is above the berm and the bottom half is the berm. Note the bending of the contours along the line $y = 0$ caused by the discontinuity of the pressure-impulse gradient where the water and the water containing rubble meet.

Let P_m be the value of pressure impulse at the bottom of the wall. Figures 2.20 and 2.21 are plots of P and P/P_m respectively with $\mu = 0.2, b = 1.0, c = 2.0$. and $\beta = 0.0, 0.1, 0.3$. Figure 2.22 is a plot of P with $\mu = 1.0, b = 1.0, c = 2.0$, and $\beta = 0.0, 0.1, 0.3$
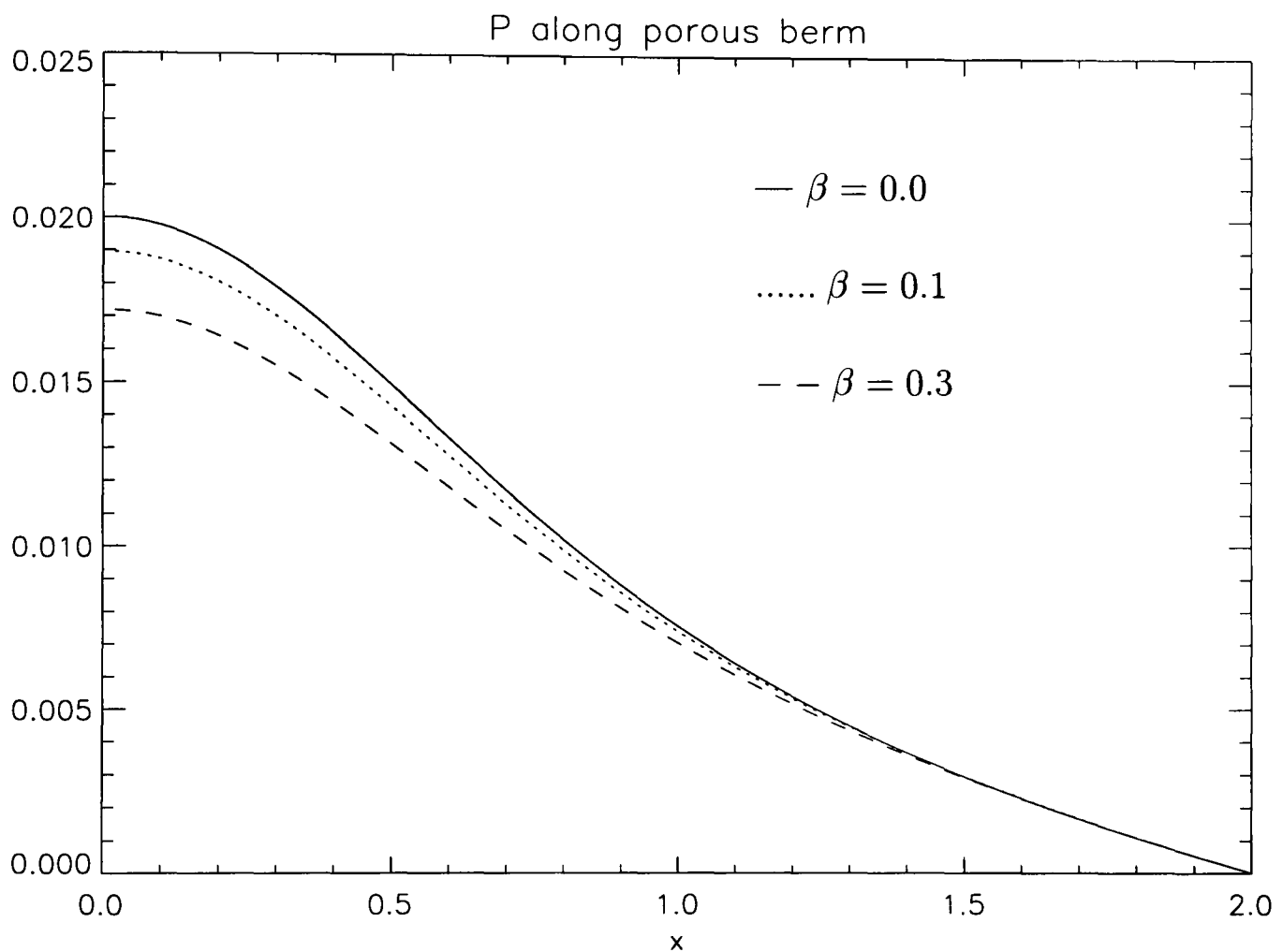
Figure 2.20: Pressure impulse along the berm for impact on a wall with a porous berm in front. $\mu = 0.2, b = 1.0, c = 2, \beta = 0.0, 0.1, 0.3$

Figures 2.20 and 2.22 show that the magnitude of the pressure impulse is reduced for a berm with higher porosity. The greatest difference in the predicted pressure impulse, from the models with differing porosity is closest to the wall. The larger the value of μ, the greater the effect. However, even for $\mu = 1.0$, the effect is still

45
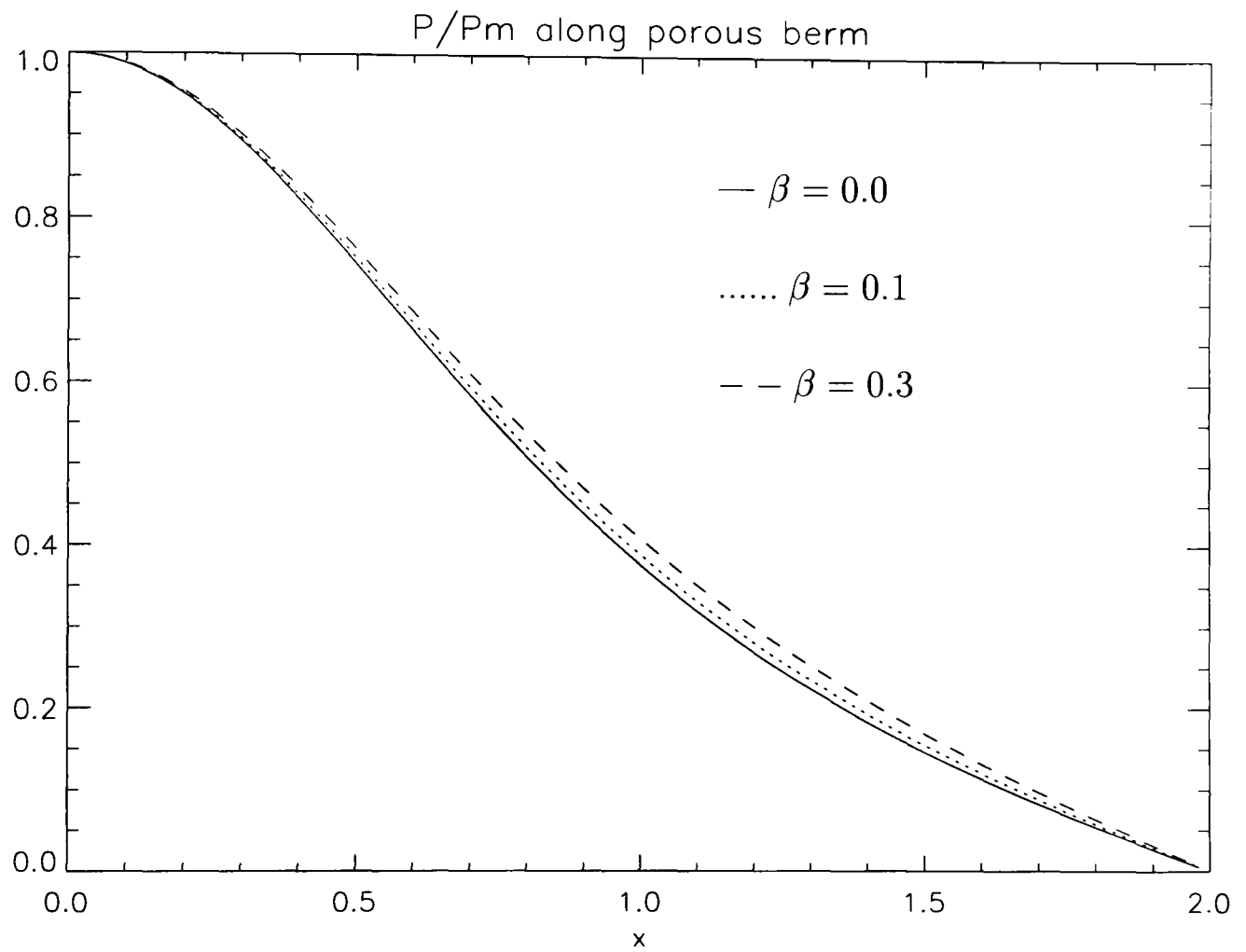
Figure 2.21: Pressure impulse/P_m along the berm for impact on a wall with a porous berm in front. $\mu = 0.2, b = 1.0, c = 2, \beta = 0.0, 0.1, 0.3$
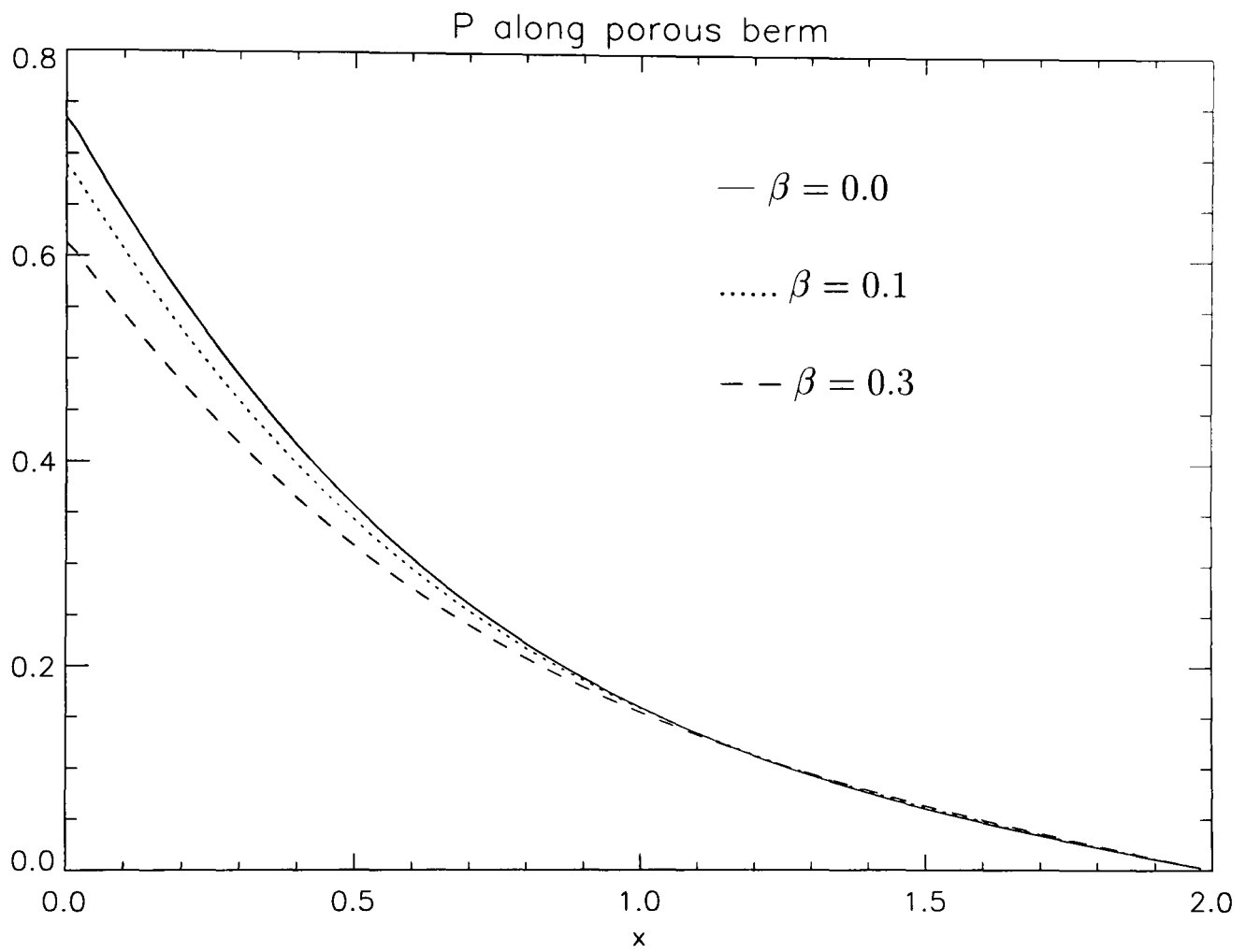
Figure 2.22: Pressure impulse along the berm for impact on a wall with a porous berm in front. $\mu = 1.0, b = 1.0, c = 2, \beta = 0.0, 0.1, 0.3$

quite small. So we examine the first of these plots but scaled by the value at the wall. Figure 2.21 shows that the distribution of pressure impulse over the berm for this particular set of values (and similarly for other values) is not affected greatly by the porosity. If μ is larger then the effect of changing the porosity was found to be greater. The reduction in pressure impulse on the wall is at most 20% and usually much less. Thus for practical purposes impact pressures in the free water above the berm are little affected by the berm's porosity. Thus impact pressures above the berm may be estimated by taking the pressure at the berm's surface to be the same as if the berm were impermeable.

Of course for shallow water above a berm the propagation of waves onto the wall is strongly affected by the berm. The above study only applies to the violent impact of a wave at the wall.

2.5   Wave 'bounce back'.

2.5.1   Theory.

In experiments of waves impacting on vertical walls, in addition to the three-dimensional effects being important, the effect of dispersed bubbles or trapped air is also important. In addition to the studies described in section 2.1 some recent studies have been carried out in this area. If a wave is breaking, or near breaking, when it hits a wall often a large amount of air becomes trapped. The air can be in one of two forms: as a trapped bubble or as dispersed air, or most likely as a combination of both. In particular Topliss (1994) looked at a theoretical model of a trapped air pocket. In this study the trapped air was taken to be an oscillating circular air bubble. The oscillations were modelled by the flow due to an oscillating line source, and the oscillations of the radius of the bubble were taken to be small, hence an equation for the complex potential of the flow could be calculated. Topliss also developed a model for the bubbly mixture in the fluid that a plunging wave leaves behind after it has impacted on a structure. Peregrine (1994) gives a review of some

of the methods used to model air entrainment/trapping during impact. Peregrine and Thais (1996) model scaling for entrained air in violent water wave impacts by using a 'filling flow' model (where a region is rapidly filled with liquid), following on from Peregrine and Kalliadasis (1996). This model has many similarities to the 'flip through' flow. Peregrine and Thais give an estimate of the reduction in pressure caused by the presence of the air.

In this section we consider a large air bubble trapped at the wall, which produces oscillatory pressures. The impulse due to the first oscillation instead of bringing the water to rest, may bounce the water backwards. So the velocity of the part of the wave impacting may reverse in sign. Cooker and Peregrine (1990 b) looked at a pressure impulse model for the 'flip through' conditions which corresponds to water motion normal to the wall ceasing on impact. If the compressed air causes the water to be pushed back, then boundary conditions corresponding to a reversal of the normal component of velocity, may be more appropriate.

We consider a plunging breaker impacting on a vertical wall, with our length scale L the water depth at the wall. As before we solve Laplace's equation subject to appropriate boundary conditions. In a similar way to the model of impact on a wall we take the free surface to be horizontal and take $P = 0$ along it. Along the rigid bottom of the liquid region we have the usual boundary condition of $\partial P/\partial n = 0$, where n is in the normal direction to the boundary. Section 2.4 showed that this assumption is reasonable even if a porous berm is present in front of the wall, providing we have a reasonably large depth of water at the wall below the impact region. We assume the wave is moving towards the wall with a horizontal velocity component of $-U$. The conditions on the wall can be split into three separate regions. At the top of the wall we have a region where the jet part of the breaking wave impacts with the wall, here there is a velocity component perpendicular to the wall before impact but none after impact (similar to the 'flip through' approach). Using equation (2.3) we find we need $\partial P/\partial n = -U$ on the jet impact region ($b < y \leq 1$). At the other extreme, at the bottom of the wall is a region where there

is no impact $(0 \leq y < a)$ so the velocity is zero perpendicular to the wall both before and after impact so using equation (2.3) again we require $\partial P/\partial n = 0$ on the no impact region. In between these two regions $(a \leq y \leq b)$ we can have a region where there is a bubble. If there is no bounce back the boundary condition is the same as at the top section of the wall. However if we have a region of 'bounce back' then the velocity perpendicular to the wall in this region is assumed for simplicity just to undergo a change in sign. Again we use the component of equation (2.3) normal to the wall and have $\partial P/\partial n = -2U$ in this region. We assume that U is uniform and hence take $U = 1$. The boundary conditions for the 'no bounce back' and 'bounce back' cases are shown in figures 2.23 and 2.24 respectively. We
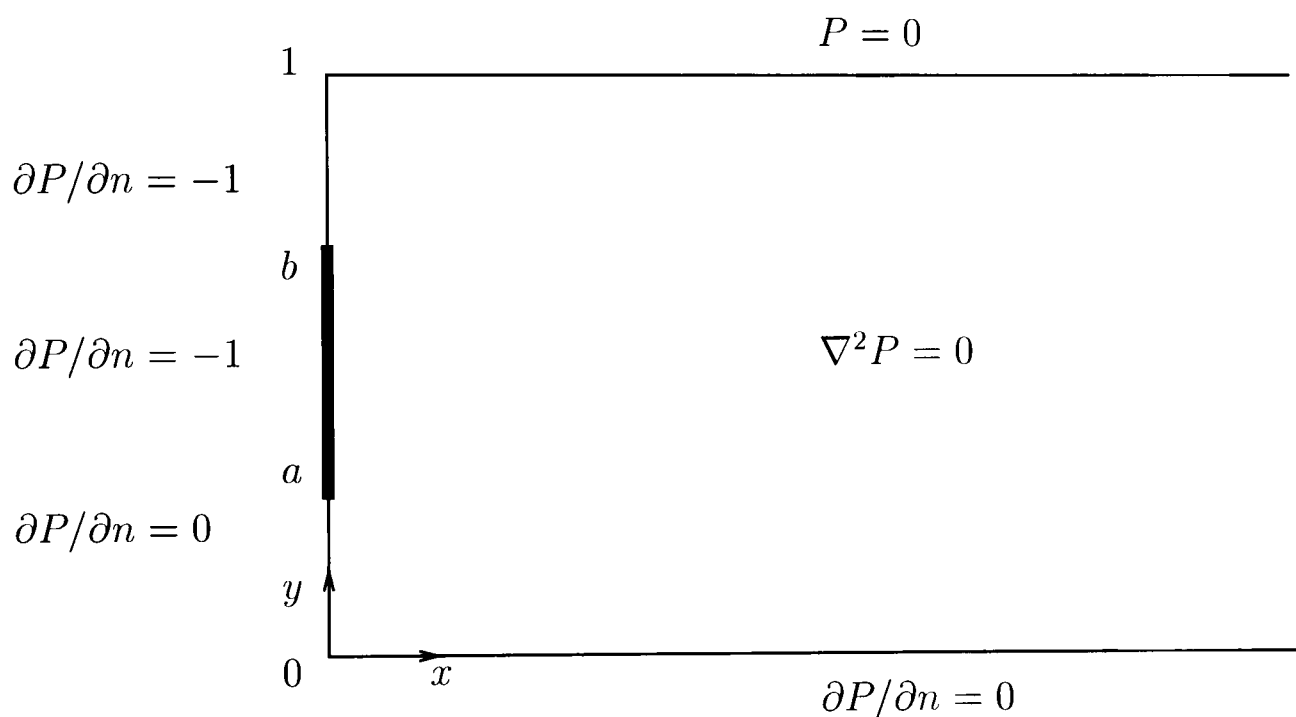
Figure 2.23: Boundary conditions required for wave impact with 'no bounce back'.(vertical section)

solve Laplace's equation using separation of variables to get a Fourier series solution given in equation (2.48) where $\alpha_n = (n + \frac{1}{2})\pi$. The expressions for A_n are given in equations (2.49) and (2.50) for 'no bounce back' and 'bounce back' respectively.

$$P = \sum_n A_n e^{-\alpha_n x} \cos(\alpha_n y) \tag{2.48}$$

$$\text{No bounce back}: A_n = \frac{2}{(n + \frac{1}{2})^2 \pi^2} [(-1)^n - \sin(\alpha_n a)] \tag{2.49}$$

50
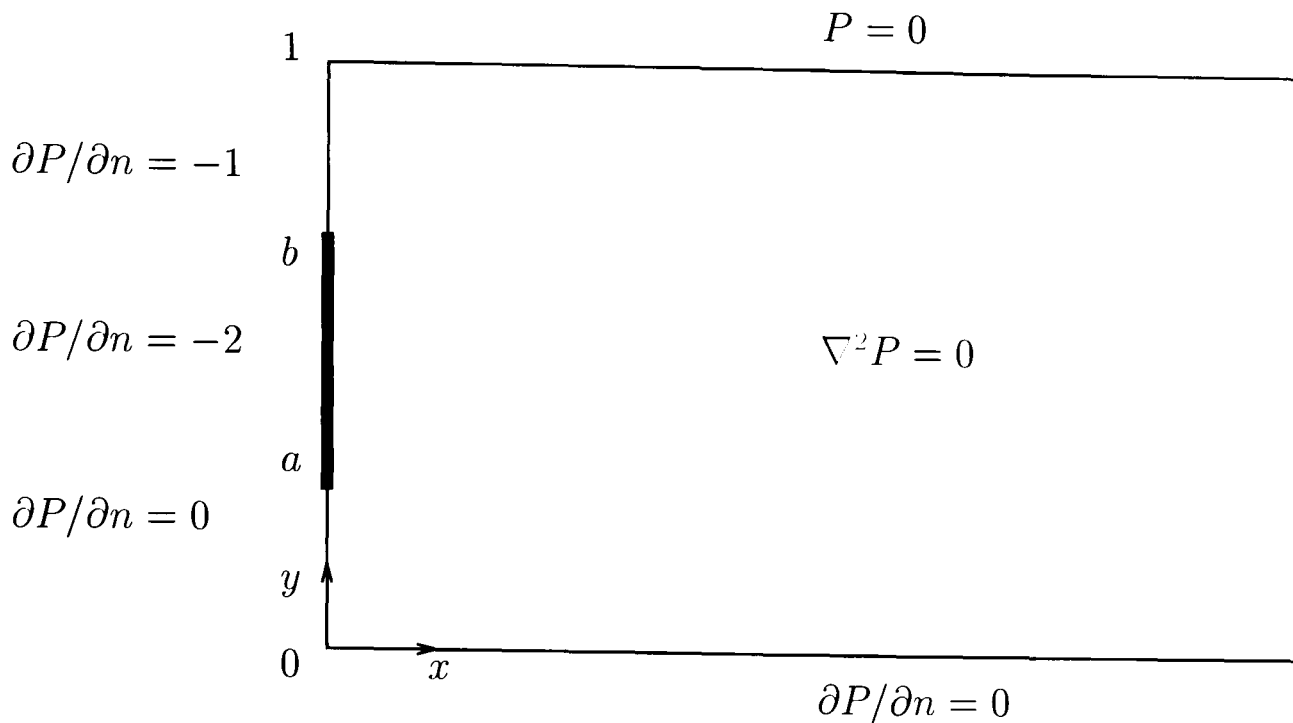
Figure 2.24: Boundary conditions required for wave impact with 'bounce back'.(vertical section)

With bounce back : $A_n = \dfrac{2}{(n + \frac{1}{2})^2 \pi^2} [\sin(\alpha_n b) + (-1)^n - 2\sin(\alpha_n a)]$.   (2.50)

Figures 2.25 and 2.26 show the pressure impulse contours for 'no bounce back' and 'bounce back' respectively. The dark solid line shows the position of the middle region (bounce back/no bounce back).

Clearly a much bigger impulse arises from bounce back. If we examine figure 2.27, which is a plot for pressure impulse down the wall, we can see that the peak P is almost twice as big for the bounce back situation as for the no bounce back case.

Pressure-impulse contours give a fair approximation to maximum pressure contours if a good estimate of impact duration is available. However in the case of bounce back, the time scale is dependent on the compression of the air, and hence is longer. Since bounce back gives a longer duration the estimated maximum pressures are generally smaller. If the duration is too long the pressure-impulse approximation becomes less appropriate.
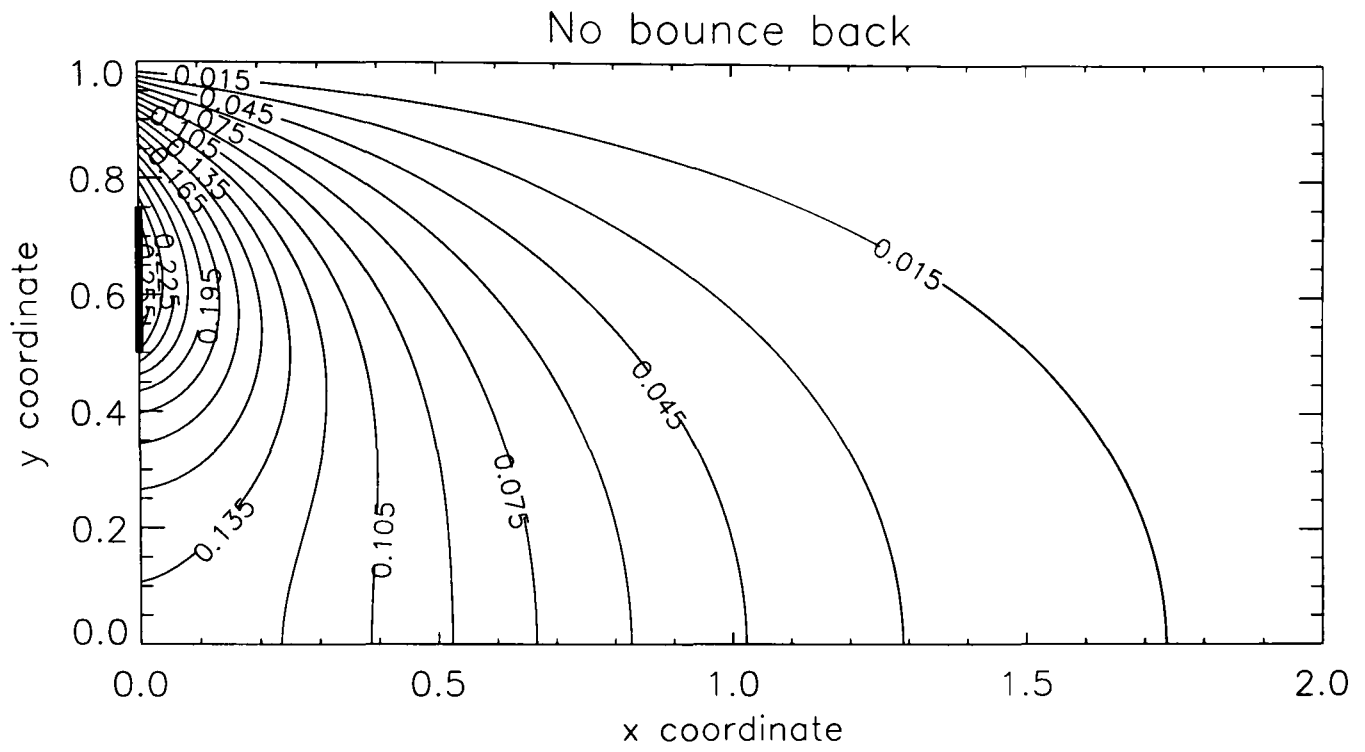
Figure 2.25: Pressure-impulse contours without bounce back.
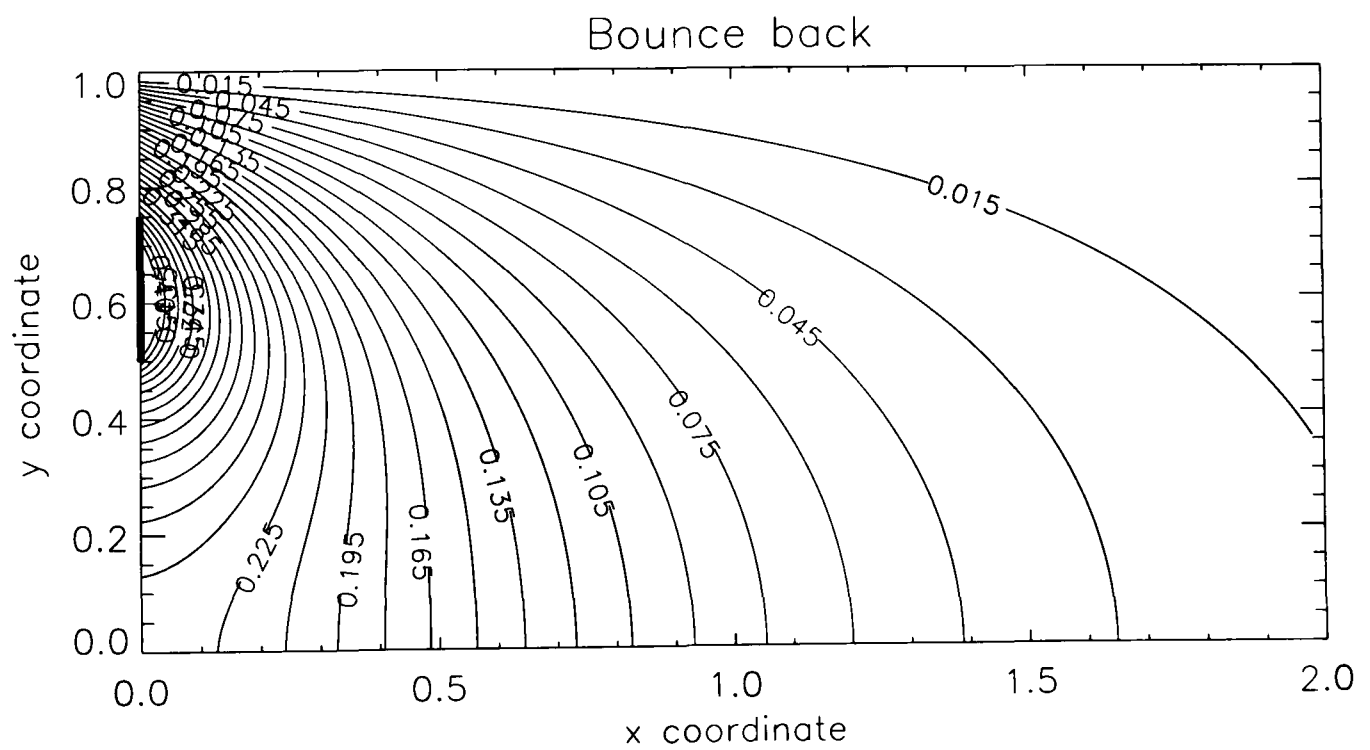
Figure 2.26: Pressure-impulse contours with bounce back.
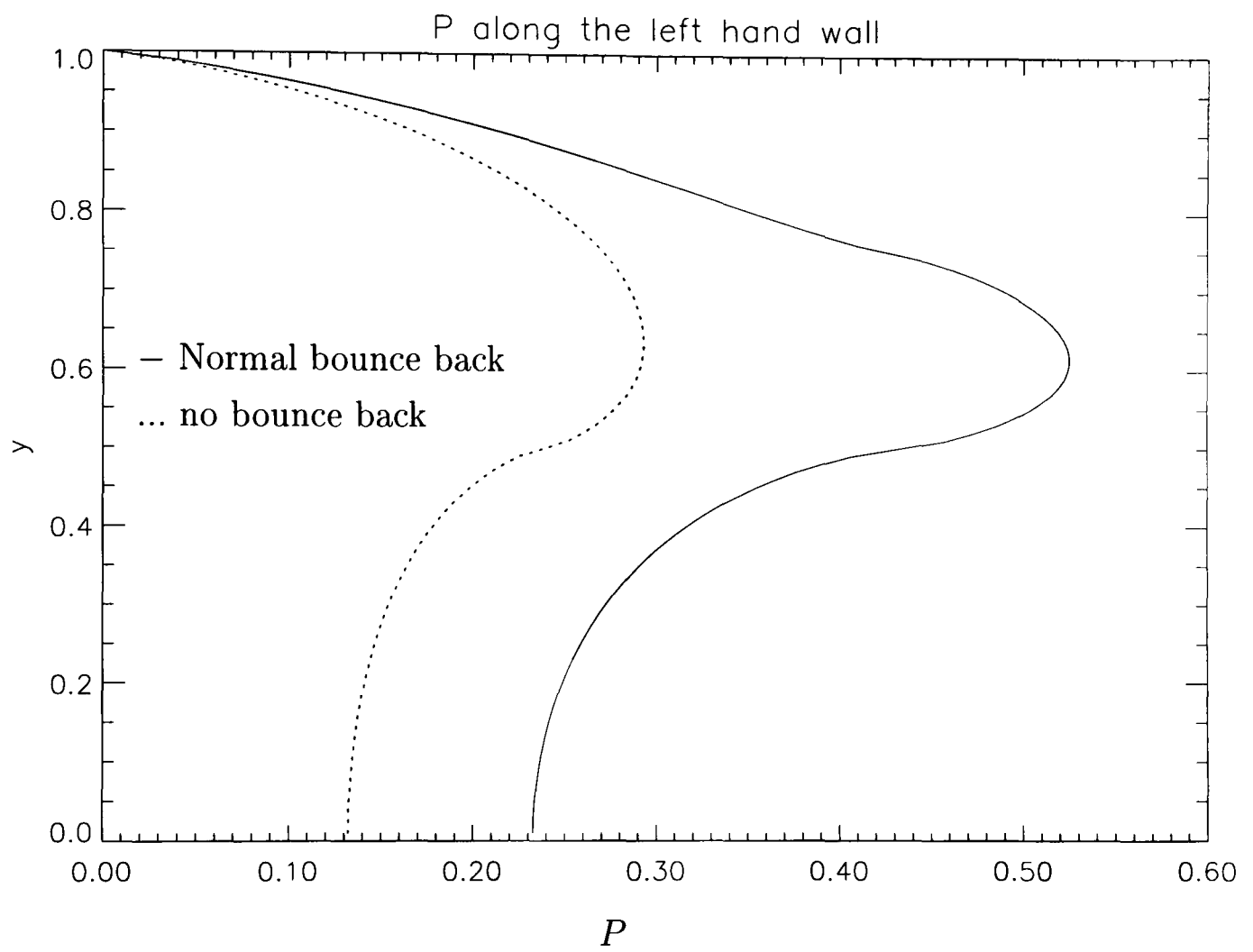
Figure 2.27: Pressure impulse down the left hand wall.

2.5.2 Experimental comparison.

In the next two sections we discuss the comparison of the 'bounce-back' model with experiments. One problem which is discussed in more detail in section 2.5.4, is that of the definition of pressure impulse when analysing experimental results. In particular it is difficult to know which interval of time we should integrate the pressure over to obtain an estimate of the pressure impulse from experiments.

To analyse the data from Hattori and Arami (1992 and private communication) a very simple analysis procedure was used. A simple isoceles triangular distribution of pressure against time was chosen. Hence the pressure impulse was calculated by multiplying the rise time (the time taken for the pressure to rise from zero to its first peak value) by the first peak in pressure.

For the Edinburgh PIV data, the measurements are available, and so a more detailed analysis procedure could be applied and is described in detail in section 2.5.4.

2.5.3 Comparison with Hattori experiments.

Hattori and Arami (1992 and private communication) carried out experiments to analyse the effect of entrained air. An estimate of the position of the bubble (values of a and b) and the velocity of the wave was obtained from 'snapshots' from a video taken of the experiments. Figure 2.28 shows a comparison of the pressure impulse down the wall obtained in these experiments with the pressure impulse predicted by the Cooker and Peregrine 2D wall impact model and the 'bounce back' model. The bubble position is denoted by a dark line. The 'bounce back' and 'no bounce back' are over and under predictions in comparison with some of the experimental data. The magnitude of the pressure impulse is predicted reasonably well, but the shape of the pressure-impulse distribution is not reflected in the theoretical values. Total impulse for the 'bounce back', no bounce back and Hattori data are 1.746Ns/m, 1.078Ns/m and 1.742Ns/m respectively. So the 'bounce back' model is better. The

value of total impulse is predicted well by using the 'bounce back' method. whereas the 'no bounce back' method under predicts.

The distribution of the pressure impulse down the wall for the experimental data is quite an evenly spread distribution with a peak pressure lower than that predicted by the 'bounce back' model. Both these inadequacies of the model can probably be explained by not having a very realistic boundary condition at the position of the bubble. The boundary condition is inadequate in at least two respects. The first is the assumption that the water is bounced back with the same velocity with which it began. It is likely that the velocity of bounce back is less than the incoming velocity, which would make the peak in pressure smaller. Secondly in taking the boundary condition as being $\partial P/\partial n = -2$ at the position of the bubble, we have taken no account of the shape of the bubble. We have assumed a uniform velocity distribution and imposed the corresponding boundary condition flat on the wall. A more realistic boundary condition could be obtained by considering the velocity distribution around the bubble after the impact to be normal to, for mathematical simplicity, a semi-circle. This would soften the boundary condition and lead to a more widely spread pressure-impulse distribution. However, in most experiments the velocity distribution is not measured, so it is difficult to obtain a good approximation of a non-uniform velocity distribution from experiment, though a boundary-integral method as used in section 3.8 could be used. We also note that in these experiments the size of the transducers are approximately 1cm in diameter and the wave height is only about 8cm, so one source of error could be that the transducers are not localized enough. This together with the crude method of analysing the data means that we could be as much as 30 % out when evaluating the pressure impulse from the experimental data.

2.5.4 Comparison with Edinburgh PIV experiments.

One of the major problems with comparing experimental data with theoretical models, is that often the information required for the theoretical model is difficult to
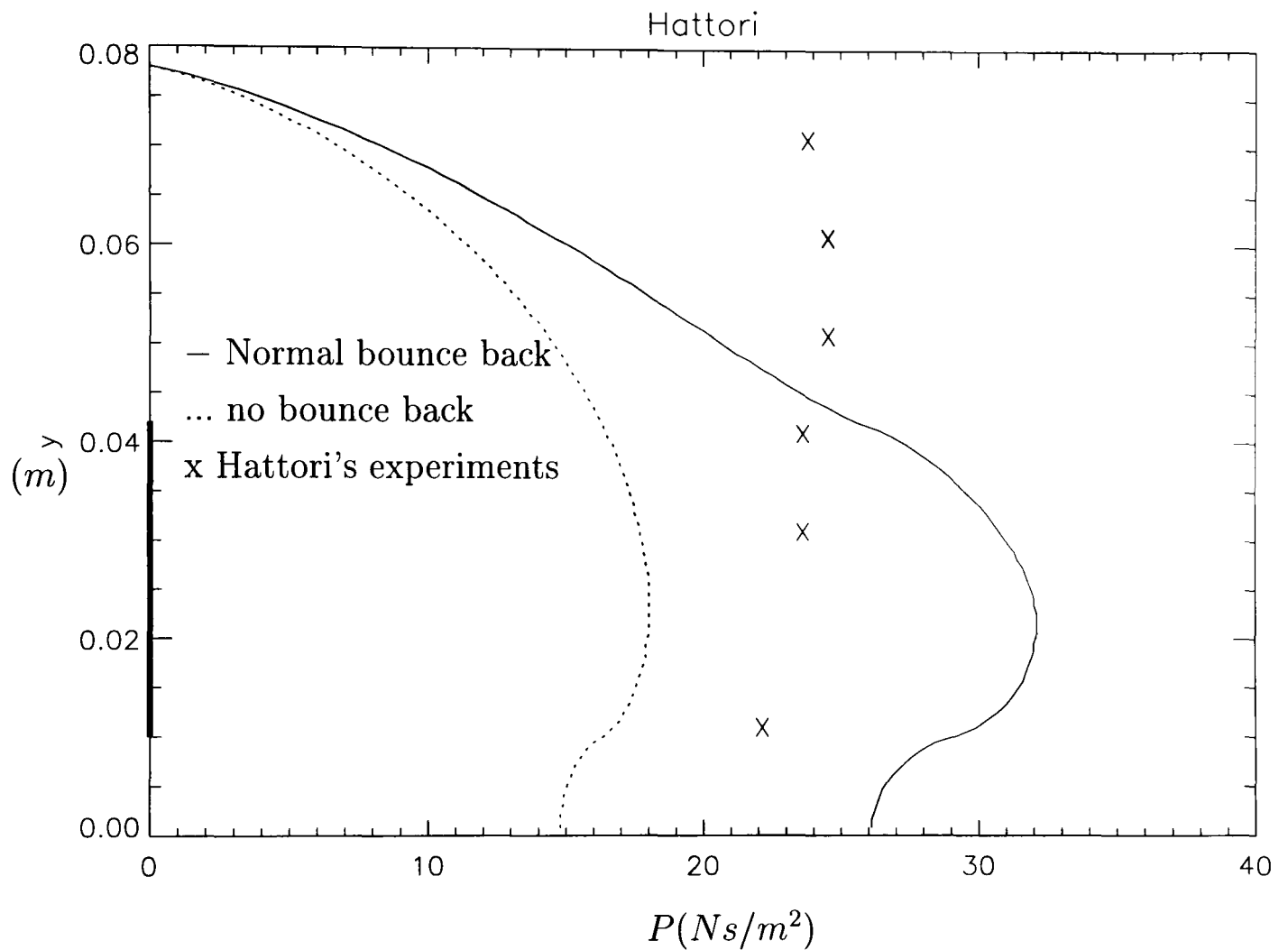
Figure 2.28: Pressure impulse along the left hand wall, for 'bounce back', 'no bounce back' and Hattori's experiments (1992). Error in the evaluation of pressure impulse from the experimental data could be as much as 30 %.

measure experimentally. In these theoretical models we need to feed in not only the height of the wave, and position of the air pocket at impact but also a measure of velocity at impact. Most experiments concentrate on the measurement of pressures. but no measurements of velocity are made. It is sometimes possible to make estimates of the velocity of the wave if high speed video is available as we did for the Hattori and Arami experiments.

A relatively new method of experimentally obtaining a velocity profile for an impact is Particle Image Velocimetry (PIV). Oumeraci, Bruce, Klammer and Easson (1995) and Oumeraci, Partenscky, Klammer and Kortenhaus (1997) describe PIV measurements made at the University of Edinburgh. The measurements in these papers together with further data and an analysis program from Bruce (Private communication) and Kortenhaus (Private communication) respectively are used in this chapter to further compare the 'bounce back'/ no 'bounce back' models with experimental data. PIV works by seeding the wave with tiny reflective particles which are then stroboscopically illuminated, i.e. subjecting the wave to flashes of light, interspersed with dark periods at a known frequency. At a particular time when the velocity profile is required a photograph with a long shutter speed is taken which includes at least two times when the wave is illuminated. Hence the velocity at a local point can be determined by looking at the sets of images. A velocity map can then be built up.

We examine the data from a test where an impacting plunging breaker is well developed, and which traps a large pocket of air and an air-water mixture. From Figure B-5 of Oumeraci, Partenscky, Klammer and Kortenhaus (1997) (reproduced in figure 2.29 by using the analysis program), a plot of horizontal force against time. we make a choice of the period of integration for the calculation of the pressure impulse. The choice of start time is when the force graph cuts the axis: $t_b = 8.07$ seconds (the start of the rise in force). The choice of where to integrate up to is complex. Firstly, we must consider for what length of time pressure-impulse calculations are valid for. We can use pressure-impulse calculations only if $u_t \gg$

uu_x, u is the velocity. That is the ratio of the nonlinear term to the $\partial u/\partial t$ term. ($O(\Delta t U/L)$)), is small. So we require $\Delta t \ll L/U$. In this particular experiment we have a velocity (U) of 1.3m/s (see later), and a length (height of the water at the wall at impact, L) of 0.2m (see later), hence the time scale must be much less than 0.15s. So we choose to integrate up to $t_a = 8.16$ s, which is the point where the plot starts to flatten off a bit. This makes the duration of the impact to be 0.09s, which is about as large as we can make it before our assumptions become really questionable.

From Figure B-1 (c) of Oumeraci, Partenscky, Klammer and Kortenhaus (1997), reproduced in figure 2.30, which is a profile of the wave a short time before impact, we estimate that the height of the wave is 0.235m, and the position of the top and bottom of the bubble are 0.194m, and 0.073m respectively (the height of the wall is 0.316m).

We also need an estimate of the velocity of the wave. Using figures 6 and 7 from Oumeraci, Bruce, Klammer and Easson, we see that (height)/(water depth at the wall) of the underside of the jet from the plunging breaker is approximately 1.4. Here the horizontal velocity does not change much in time and can be estimated as 1.3m/s. Feeding these into the 'bounce back' and Cooker and Peregrine model we obtain the plots shown in figure 2.31.

Here it is clear that the profile is reasonably the same shape, but the theoretical predictions have the maximum pressure impulse too far down the wall. The Cooker and Peregrine model under predicts the pressure impulse and the 'bounce back' over predicts it. As mentioned in the analysis of Hattori's experimental values, the 'bounce back' model produces values of pressure impulse which are too high because we assume that the bubble bounces back with the opposite of the incident velocity component normal to the wall. A more realistic approach is to consider the bubble bouncing back with a cosine velocity profile, i.e. that there is no 'bounce back' at the edges of the bubble and the maximum 'bounce back' is at the centre of
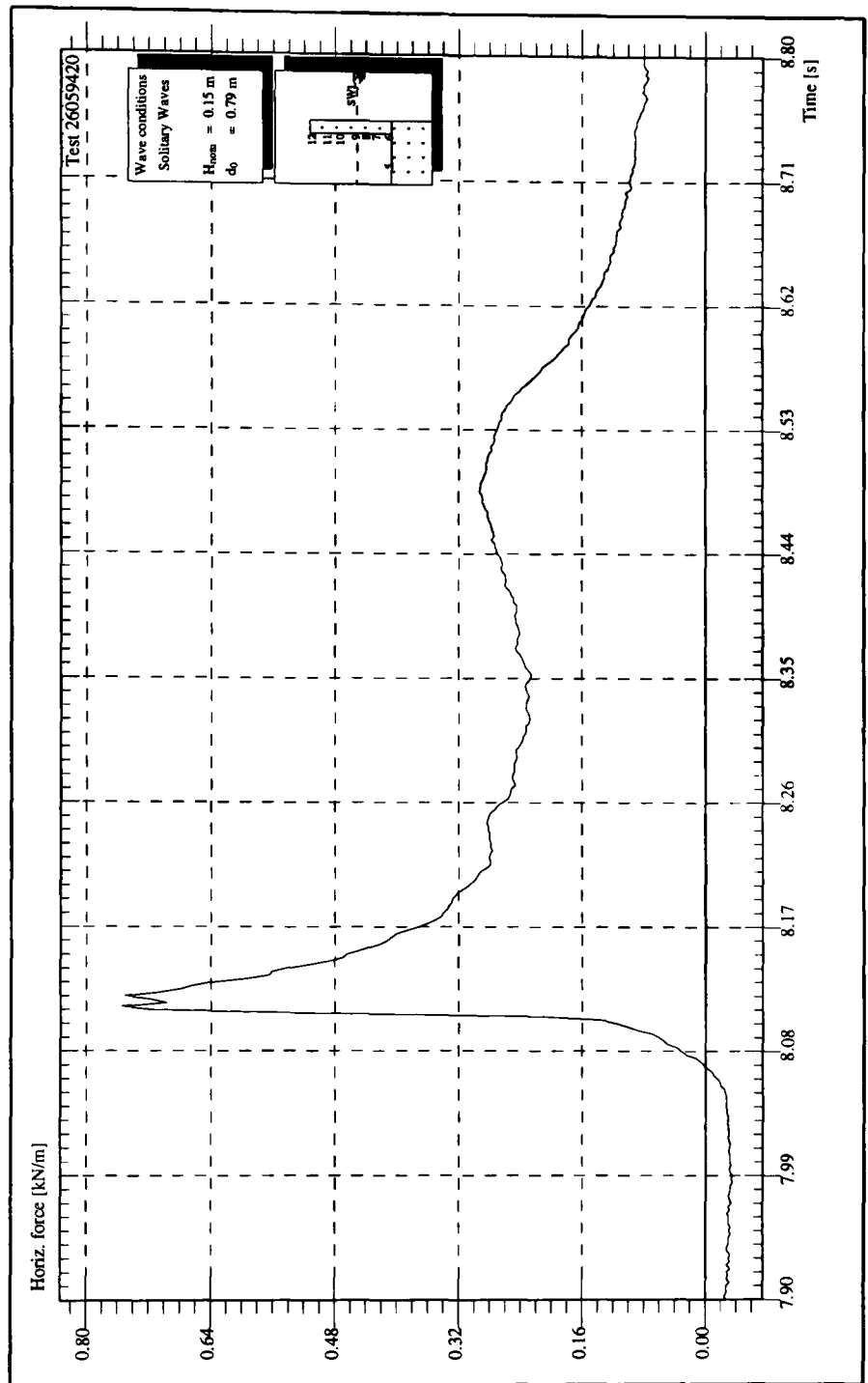
Figure 2.29: Horizontal force on the wall, for impact of a plunging breaker trapping a large air pocket. Edinburgh PIV data. (Plotted using analysis program Kortenhaus (private communication))

Figure 2.30: Profile of a wave used in Edinburgh PIV tests, trapping a large air bubble at a time just before impact, from Oumeraci, Partenscky, Klammer and Kortenhaus (1997).
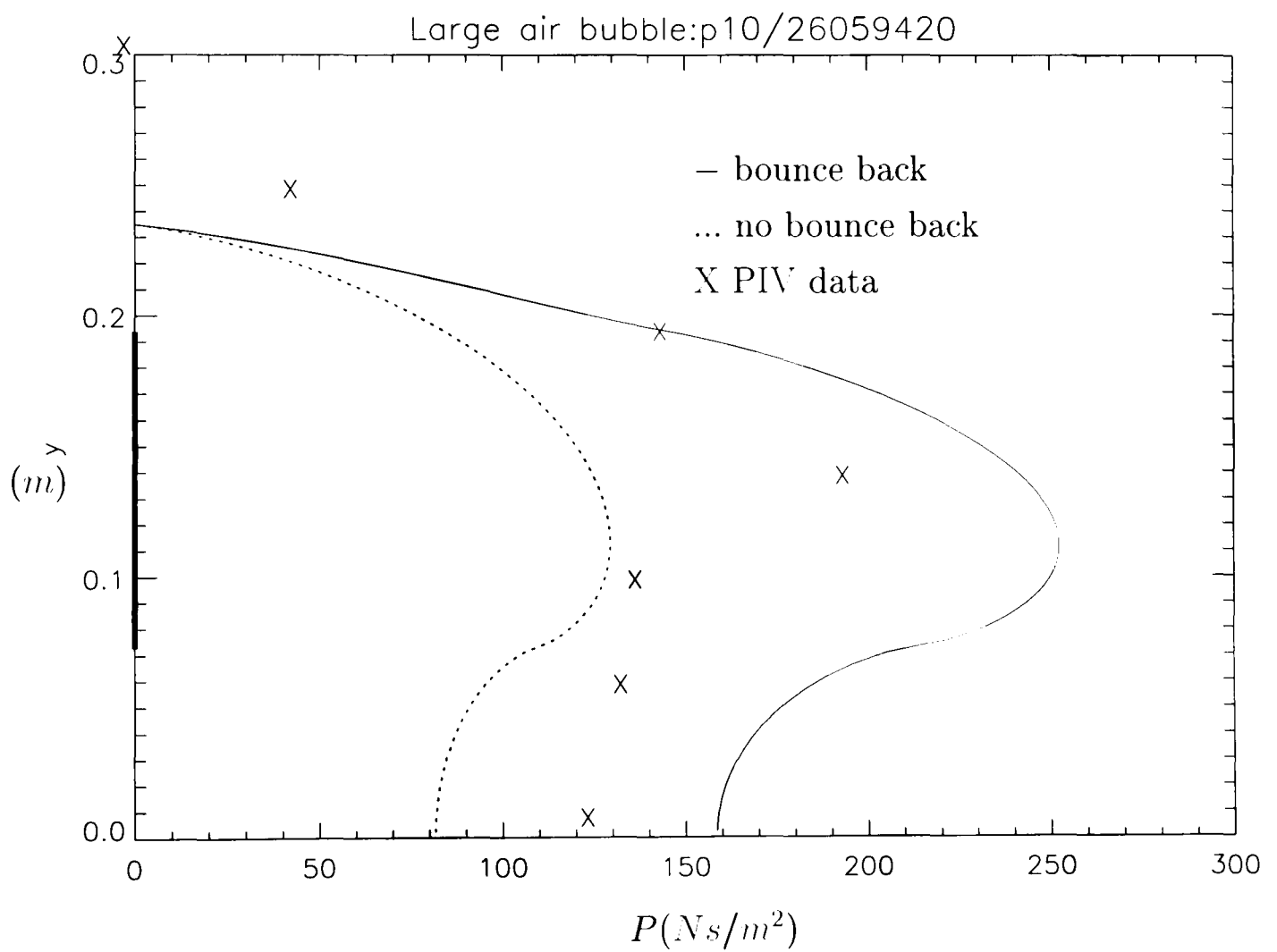
Figure 2.31: Pressure impulse on the wall, for impact of a plunging breaker trapping a large air pocket

the bubble. This is similar to considering the bubble as being cylindrical and just 'bouncing back' with the component of the radial velocity (of the bubble) in the direction normal to the wall. This gives a slightly better prediction of the pressure impulse as shown in figure 2.32.
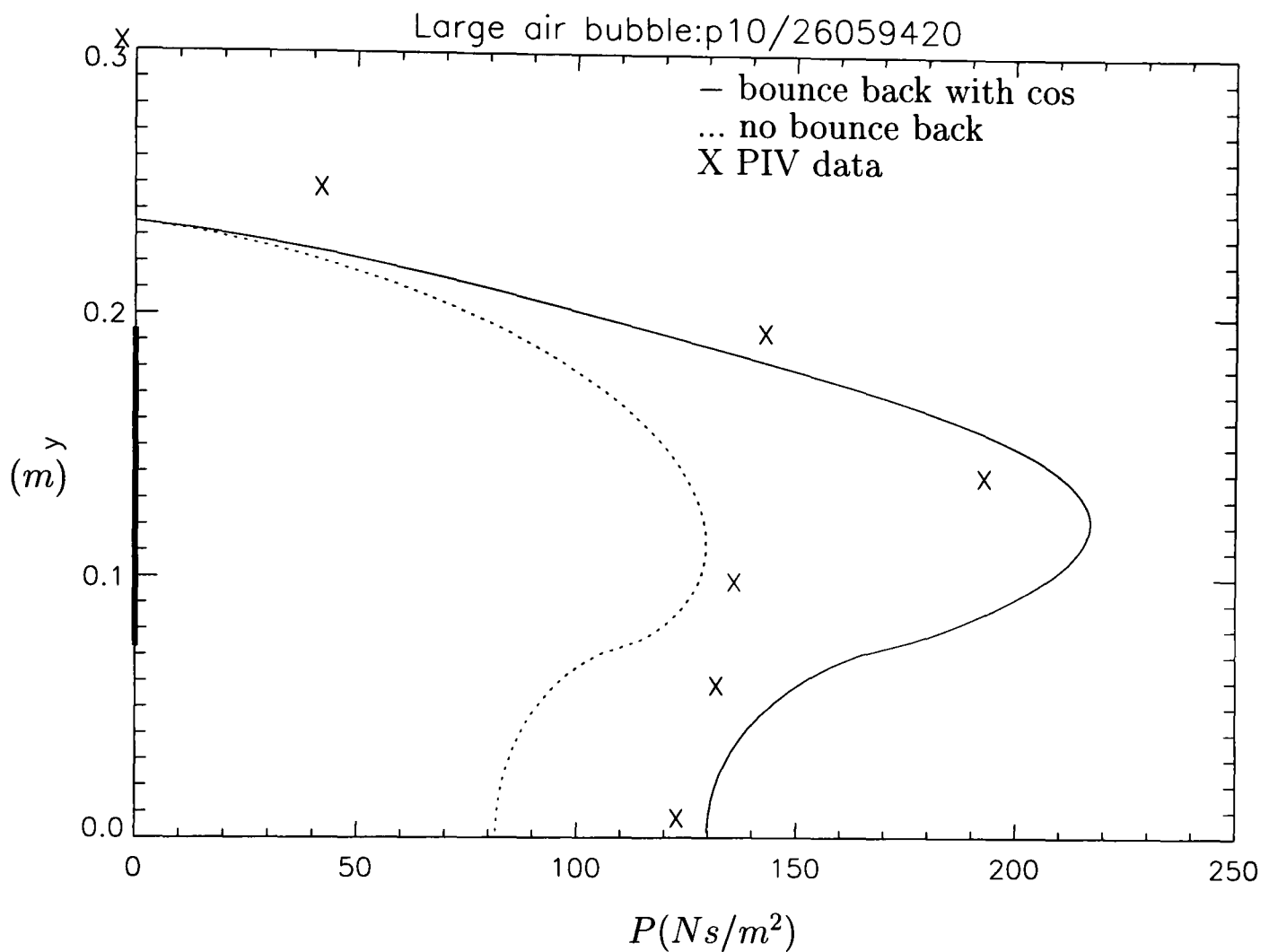
Figure 2.32: Pressure impulse on the wall, for impact of a plunging breaker trapping a large air pocket

However, we still have two further adjustments to our model. Firstly, the 'snap shot' picture from which we estimated the position of the bubble and height of the wave is at a time before the actual impact, on examination of a video of the experiments it is clear that the top of the wave drops a few centimetres, and the bubble moves up and decreases in size slightly before it impacts. Hence a better estimation for the height of the wave, bottom and top of the bubble are 0.195m, 0.08m and 0.17m respectively. Using these values we obtain figure 2.33. However, the pressure impulse from the experimental data is much larger than both theoretical
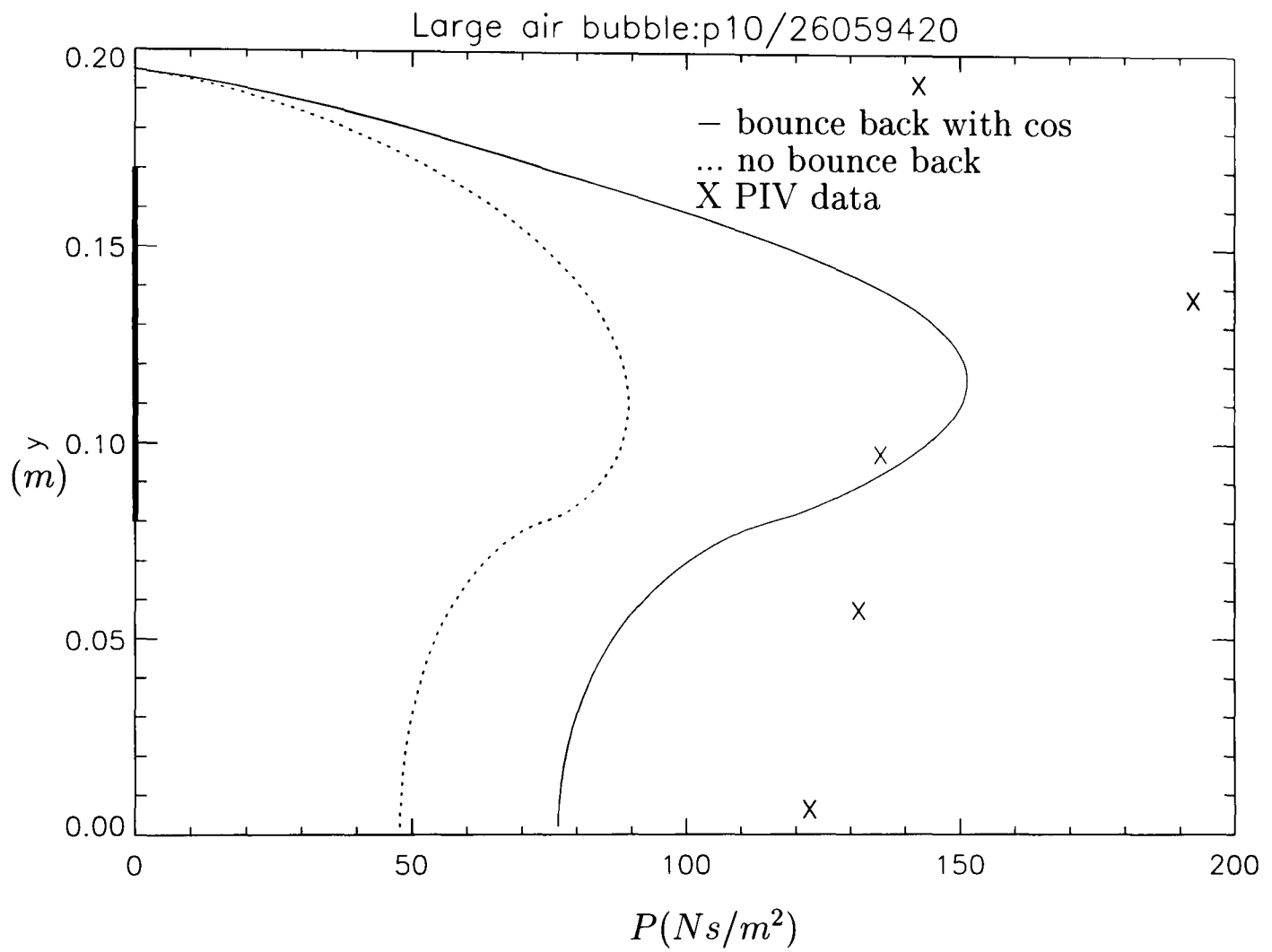
Figure 2.33: Pressure impulse on the wall, for impact of a plunging breaker trapping a large air pocket

predictions. This means we require one more stage of analysis. Figure 2.34 is a plot of the pressure from the transducers on the berm in front of the vertical structure. Here channel 6 is the reading of the pressure transducer almost at the level of the berm, at the wall, and channel 1 is at the edge of the berm furthest away fom the wall. Channels 2-5 are on the berm in between 1 and 6. The distance of the transducers 6 to 1, from the wall, are 0.000m, 0.120m, 0.240m, 0.350m, 0.516m and 0.662m respectively. If we look at the pressure plots we can see that often the impact pressure peak occurs on top of a background pressure. We now examine figure 2.1 specifically to look at the reflective pressures. The pressure-impulse model we use in this chapter takes no account of gravity. The second peak in the profile, the reflective pressure, is caused by the wave motion of the water being accelerated/decelerated by the wall. So, when we compare our theoretical model with experimental results we should subtract off a profile that the reflective pressures would have if there were no high peak impact pressure distribution on top of this. The most accurate way of doing this would be to reflect the shape of the reflective pressure peak in the local minimum at about 8.325s to give the reflective pressure distribution below the high pressure peak caused by impact. However this is complex, and would be difficult to do for large amounts of data. Hence we approximate this 'background' pressure caused by gravity as a triangular or trapezoidal distribution and subtract this off our calculation of pressure impulse. If at t=8.07s the pressure plot is below zero then a triangular shape is subtracted off, as shown in figure 2.35. If the pressure plot is above zero at t=8.07s, then we subtract off a trapezoidal shape as shown in figure 2.36. This makes the procedure for calculating the 'background pressure' simple and therefore could be applied to large amounts of data. This is based on a suggestion in Walkden, Hewson and Bullock (1997).

Figure 2.37 shows the pressure impulse on the wall for the impact of a plunging breaker trapping a large air pocket, for the two theoretical models and the PIV data, where the PIV data has had the background pressure removed.

The distribution prediction is far from perfect but adequate. The pressures on
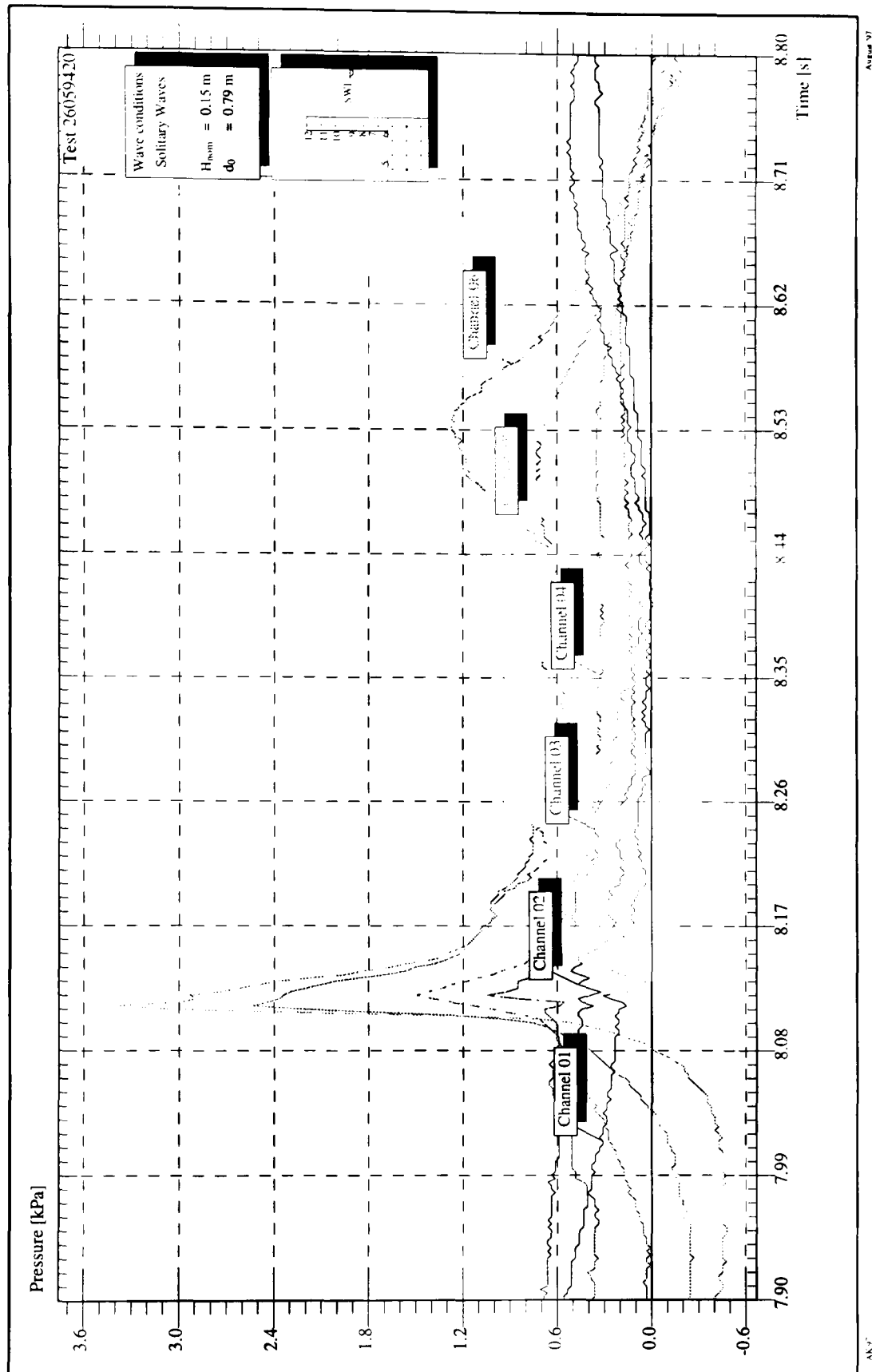
Figure 2.34: Pressure against time for transducers on the berm with impact of a plunging breaker trapping a large air pocket. Edinburgh PIV data. (Plotted using analysis program Kortenhaus (private communication))
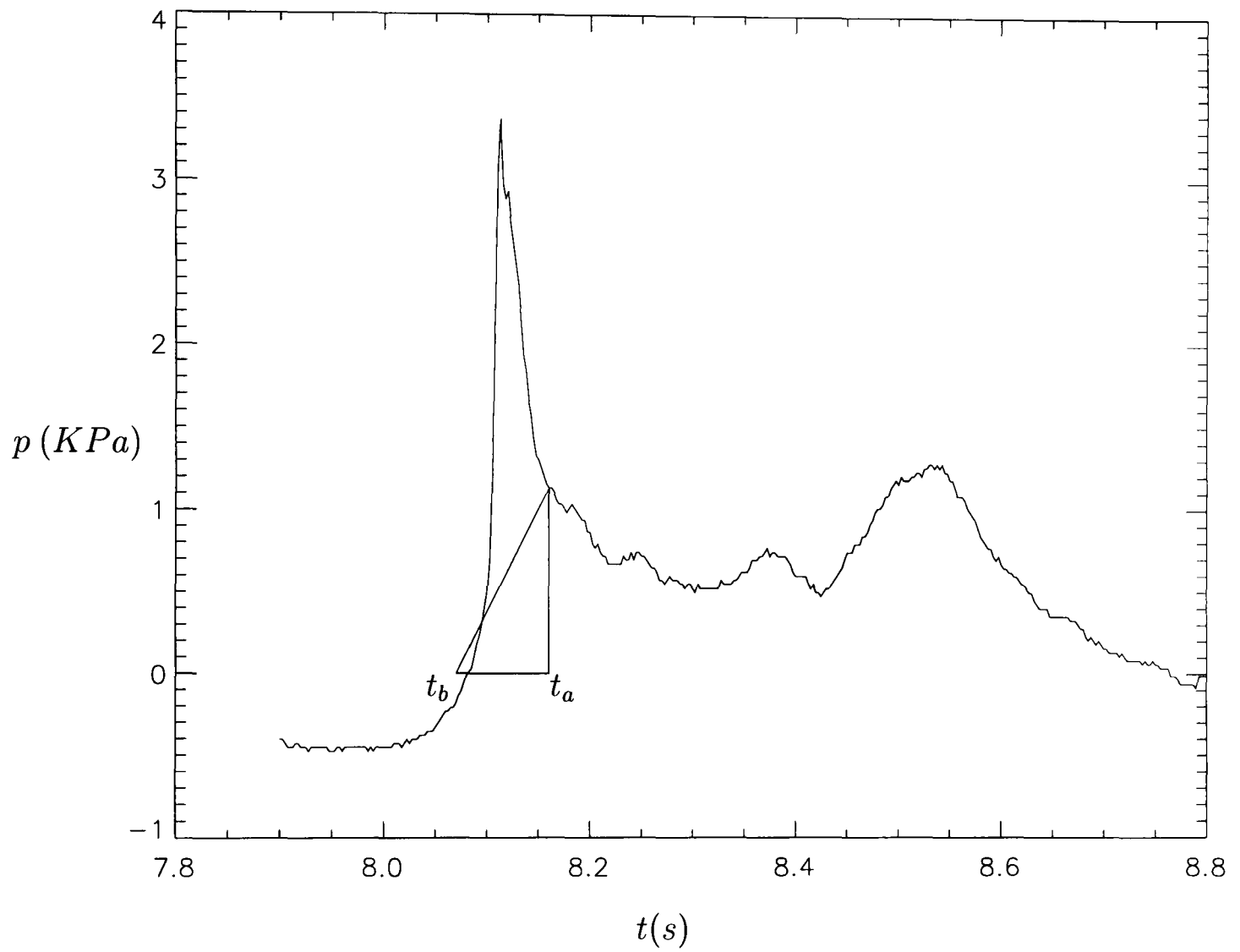
Figure 2.35: Pressure against time for transducer 6 (almost at the base of the wall), showing the triangular background pressure to be removed. (Edinburgh PIV data)
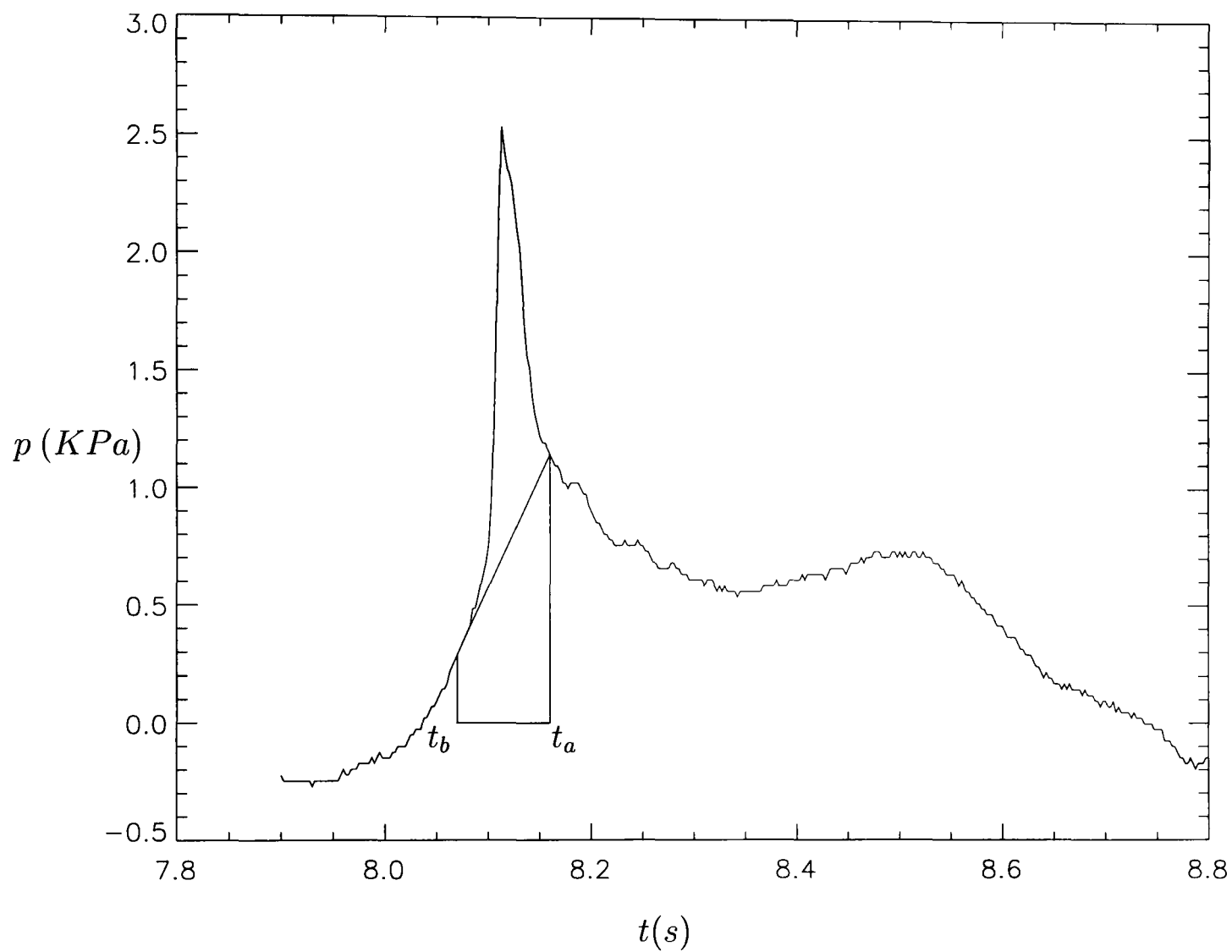
Figure 2.36: Pressure against time for transducer 5 (on the berm), showing the trapezoidal background pressure to be removed. (Edinburgh PIV data)
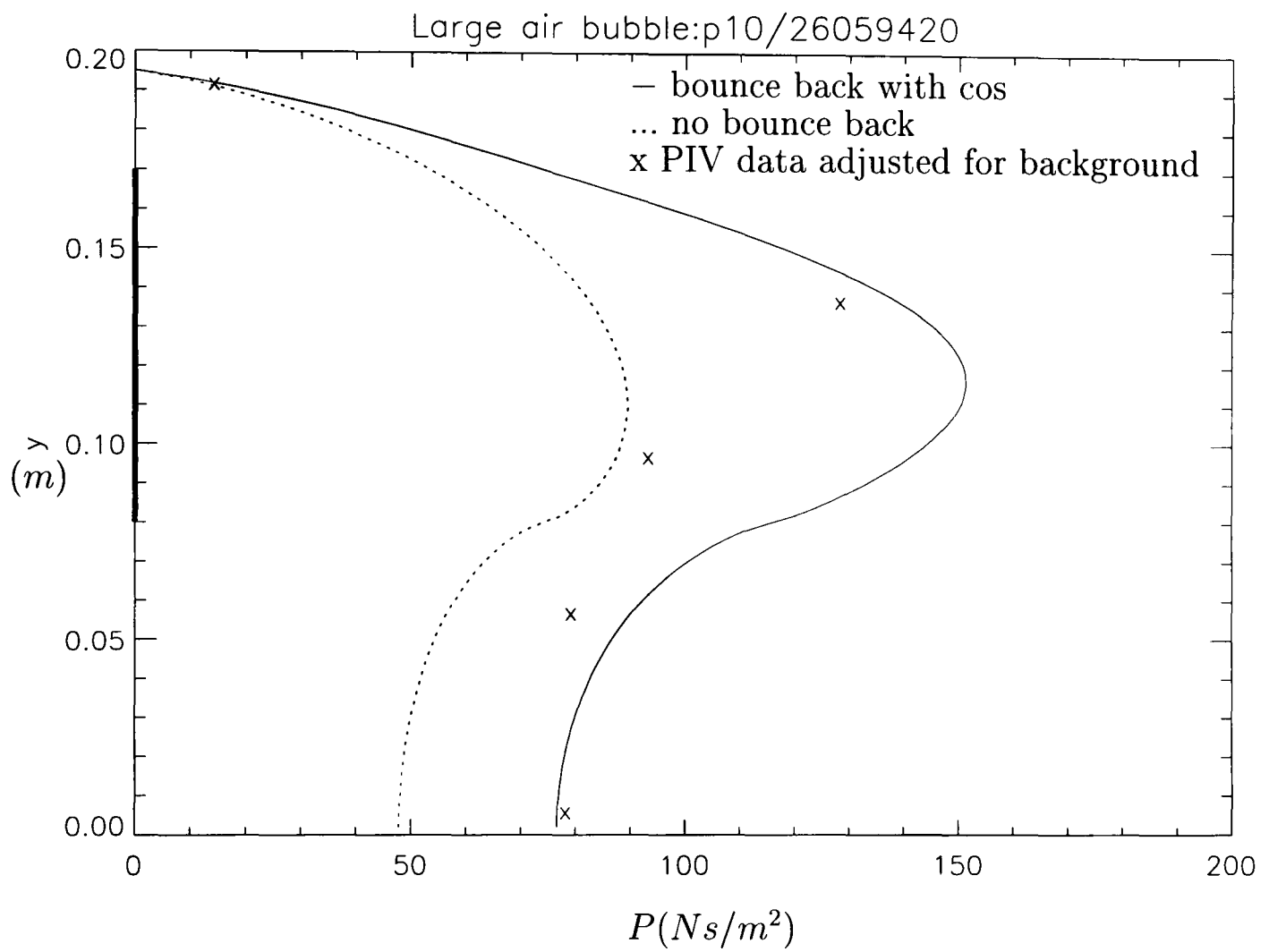
Figure 2.37: Pressure impulse on the wall, for impact of a plunging breaker trapping a large air pocket

the berm are reasonably predicted using this model, as shown in figure 2.38.
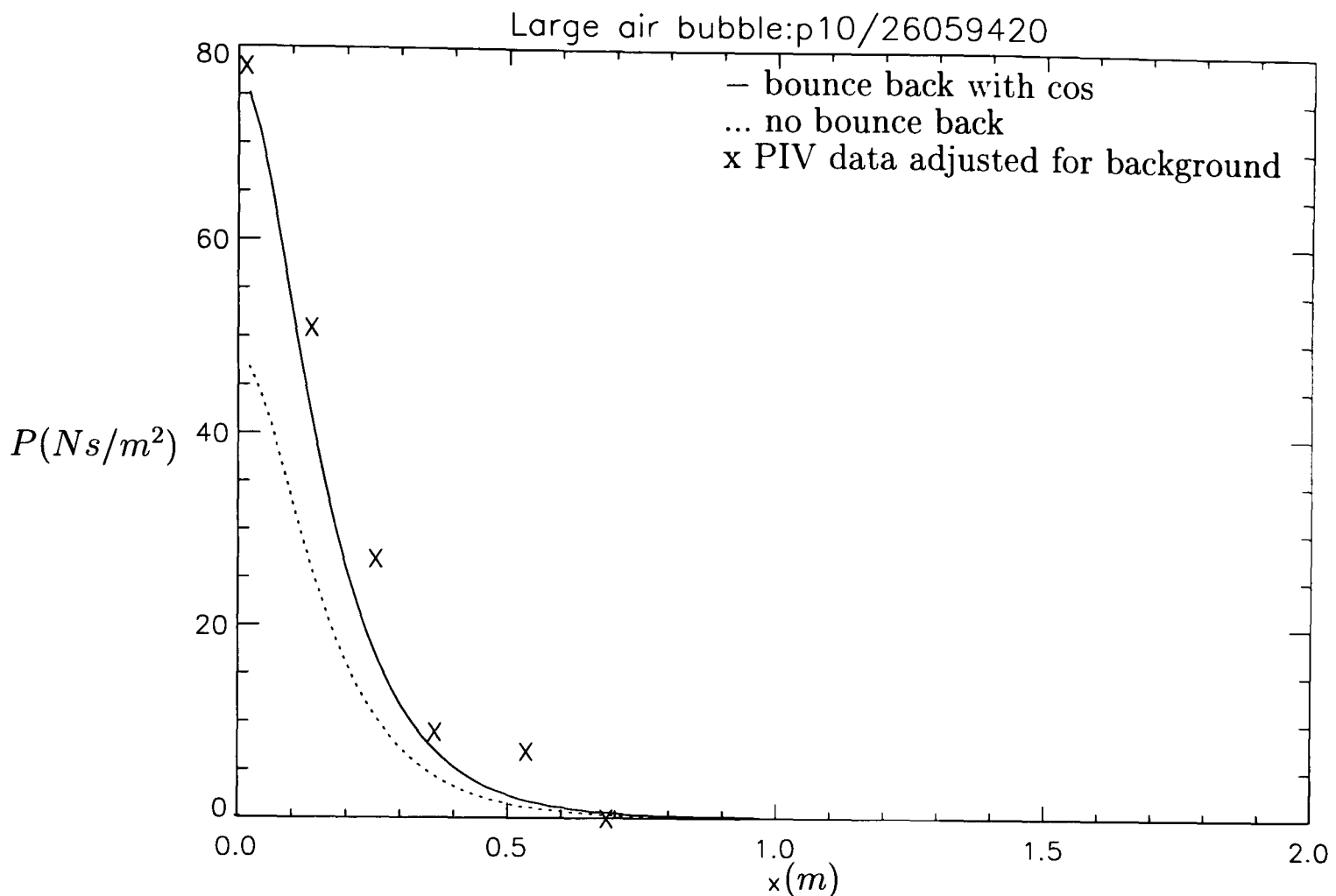
Figure 2.38: Pressure impulse along the berm, for impact of a plunging breaker trapping a large air pocket

2.5.5 Experimental conclusions.

The 'bounce back' model could not predict the distribution of the pressure impulse down the wall for the Hattori and Arami experiments. However the total impulse could be quite accurately predicted. Two reasons for the inadequacy of the prediction of the pressure-impulse distribution could be the simple way in which the pressure impulse was calculated from the experimental data, and also the difficulties in estimating the velocity of the wave and the position and size of the air bubble.

The Edinburgh PIV data compared well with the 'bounce back' model which also predicted the distribution of pressure impulse along the berm well. In particular the cosine distribution for the velocity seemed most appropriate. The pressure

impulse was calculated by integrating from the start in the rise in force, to the first 'flat' part of the force graph after the peak, keeping within the time limit within which pressure-impulse theory is valid. A triangular (or trapezoidal) distribution of pressure was subtracted off the pressure impulse so as to remove the effect of a background pressure.

Theoretical work on the prediction of pressures, forces or pressure impulse for impacts with large air pockets, where the air bubble is taken account of is very scarce. With the exception of the work carried out by Topliss (1994), Ramkema (1978) and Bagnold (1939), virtually no theoretical work exists for the prediction of pressure impulse for impact on a wall with any sort of model for the trapped air. Our model, predicts the distribution of the pressure impulse to within about 40%. Although far from perfect these predictions are at least a start. The prediction of the total impulse (as demonstrated with the Hattori and Arami data, section 2.5.3) is much better.

There are many difficulties in building into a model of impact the effect of the pocket of air. The biggest is that of the choice of boundary condition at the position of the air pocket. Ideally the shape of the bubble should be taken into account. We only made a very simple approximation to this by using a cosine distribution for the 'bounce back' velocity. If we imposed boundary conditions on the surface of the bubble (assuming the bubble has the same shape before and after bounce-back) then the problem solution domain becomes more complicated. This model may be extended to allow for this, using for example, boundary-integral methods. Another problem is that even if we can allow for the shape of the bubble, it is difficult to know what boundary condition we should impose on it. The pressure on the bubble boundary must be one constant before and another after impact but it is not clear what the change in this constant should be, or how to estimate it. This problem needs further investigation.

Inaccuracies in our ability to estimate parameters such as the velocity, wave

height and bubble position (PIV 'snapshots' are not taken at impact but a short time before) are also a source of error. This is because PIV analysis is difficult at the time of impact due to the air entrainment which occurs.

2.6 Impact on cylinders.

Although the study of wave impact has mainly concentrated on vertical wall or breakwater structures it is also useful to study impacts on other geometrical shapes. In particular we consider impact on a circular cylinder, representing an oil rig leg, a pile, or the circular head of a breakwater.

Many experimental and theoretical studies have been carried out for impacts on cylinders. In particular most have focused on non-breaking waves. However, Honda and Mitsuyasu (1974) carried out an experimental investigation into wave forces of breaking waves impacting on a vertical cylinder on a sloping beach. The effect of varying the position of the cylinder on the wave forces was examined. Relations between the wave force and the relative depth of the water at the cylinder, the deep water steepness of the wave and the beach slope were found. Good predictions of the wave forces for the cylinder in deep water were found, but not for shallow water. Further experimental investigations were carried out including Dalton and Nash (1976), Wiegel (1982) and Apelt and Piorewiz (1987). Dalton and Nash concluded that further study of elements in offshore platforms which are in the splash zone was necessary, as the forces/pressures which were involved were significant enough to cause damage. Wiegel presents a method for analysing the forces exerted by breaking waves on a circular pile. They comment on the difficulties of predicting the forces on the cylinder as Morison's equation is often used which is for prediction of wave forces due to non-breaking waves whereas, for example, plunging breakers are known to give much larger forces. Improvements on this model were thought to be difficult to achieve due to the impact forces being of such short duration that the equipment of the time was not sufficiently good to deal with this. Apelt and

Piorewicz, using their own and previous experiments, found that the maximum force for a breaking wave on a cylinder is dependent on the bottom slope, diameter to height ratio of the cylinder, and the wave steepness. They summarized the existing papers on impact forces on cylinders and comment that very little research has been carried out for breaking waves on cylinders.

Experimentalists have focused recently on looking at breaking waves, rather than non-breaking waves, impacting on vertical cylinders. Zhou, Chan and Melville (1991) undertook laboratory measurements to obtain pressure distributions on surface piercing vertical cylinders. They looked at ensemble averages of the pressure-time histories and also looked at pressure plots round the cylinder. They comment that the extrapolation from present laboratory scale to prototype for the structural response to wave impact may be achieved by using pressure-impulse theory.

The problem of scaling was further examined by Chaplin, Greated, Flintam and Skyner (1992). Three widely different scales were used for the loading experienced by a vertical cylinder in breaking and steep non-breaking waves. The results obtained for the loading on the cylinders were found to be reasonably consistent with the use of Froude Scaling (see Goda (1985) for details). The usual method for predicting loads (Morison's equation) was found to be inadequate in the splash zone of breaking waves. Extreme loading associated with severe particle velocities and accelerations were experienced by structural members in the splash zone of breaking waves. High impact pressures of short duration were again experienced when a member underwent rapid submergence by fast flowing water showing that it is appropriate to use pressure-impulse theory for this impact problem.

2.6.1 Pressure-impulse method.

We now consider the pressure impulse of a wave impacting on a cylindrical structure in a similar manner to the method used for impacts on vertical walls. Ideally we would consider a wave rising up out of the main body of the water and impacting on a cylinder, or a breaking wave jet front impacting on the cylinder. However, for

simplicity we consider a cylinder with water surrounding it. and impact occurring on a patch of the cylinder just below water level as shown in figure 2.39.

As previously mentioned, we can simplify the shape of the free surface without too much effect on the solution of the impact problem. Hence, we take the shape of water surface impact on a cylinder to be a horizontal free surface. Once the contours of pressure impulse are plotted for the impact a more realistic free surface may be taken by using any of the lines of constant pressure impulse.

2.6.2   Impact on a cylinder just below water level.

Using boundary conditions described in section 2.2.2. we begin by examining the case of an infinite body of water with the impact on a patch of the cylinder just below the water level . This is similar to the 3D patch on a wall example of section 2.3.2. So we need to solve Laplace's equation in cylindrical co-ordinates, (given by (r, ψ, z), where r is in the radial direction, ψ is the angle round the cylinder and z is the vertical position) in the body of water. We take our length scale L to be the radius of the cylinder. The patch is taken to be the area $-\beta \leq \psi \leq \beta$, $-l \leq z \leq 0$ on the cylinder at radius $r = 1$. On this patch of the cylinder the impact occurs and we require $\partial P / \partial r = -\cos \psi$, corresponding to unit velocity in the $-x$ direction. On the rest of the cylinder no impact occurs so $\partial P / \partial r = 0$. At the free surface $P = 0$, and along the bottom rigid boundary $\partial P / \partial z = 0$. We must also have that $P \to 0$ away from the cylinder. The boundary conditions are summarized in figure 2.39.

Laplace's equation in cylindrical co-ordinates is given by:

$$\frac{1}{R}\frac{\partial}{\partial R}\left(R\frac{\partial P}{\partial R}\right) + \frac{1}{R^2}\frac{\partial^2 P}{\partial \psi^2} + \frac{\partial^2 P}{\partial z^2} = 0. \tag{2.51}$$

We solve this by using separation of variables. Let $P(r, \psi, z) = Z(z)\Psi(\psi)R(r)$. The problem we are solving has finite depth so we require a periodic condition in the z direction. Hence the equations we need to solve are:
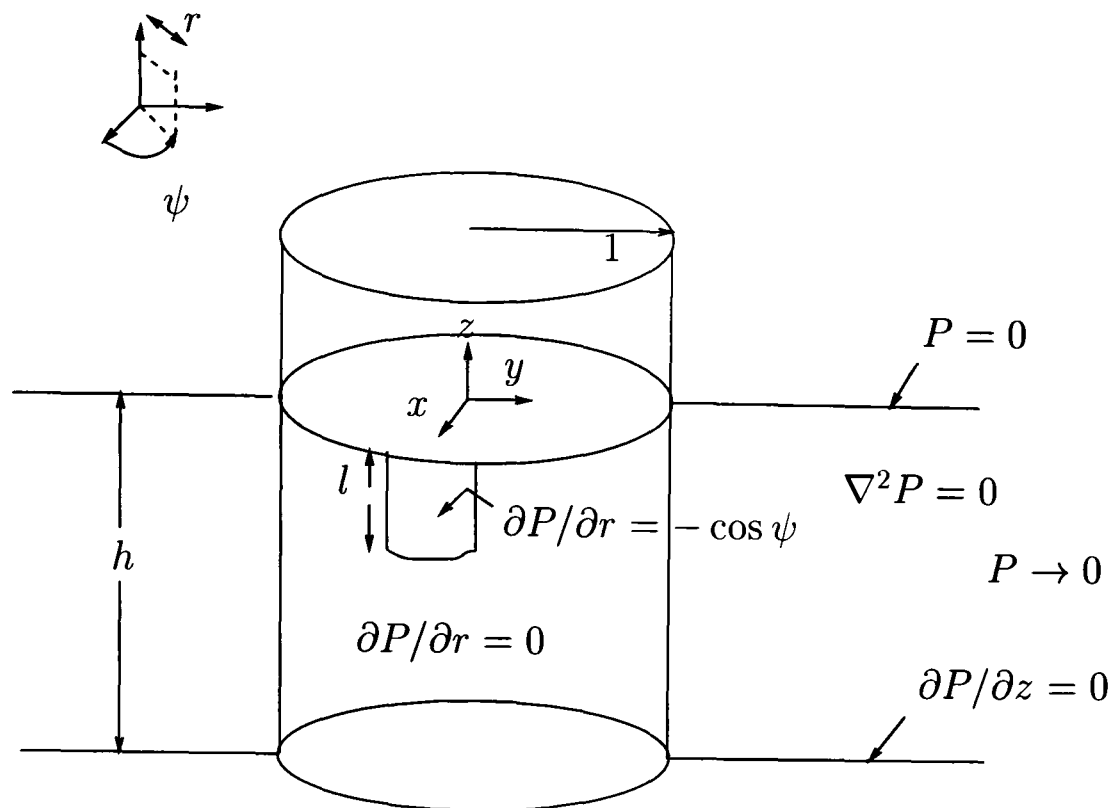
Figure 2.39: Impact on a cylinder below water level.

$$\frac{\partial^2 Z}{\partial z^2} + q^2 Z = 0, \qquad (2.52)$$

$$\frac{\partial^2 \Psi}{\partial \psi^2} + p^2 \Psi = 0, \qquad (2.53)$$

$$\frac{\partial^2 R}{\partial r^2} + \frac{1}{r}\frac{\partial R}{\partial r} - \left(q^2 + \frac{p^2}{r^2}\right) R = 0, \qquad (2.54)$$

where p and q are to be found by imposing the boundary conditions. The boundary conditions at the base and free surface imply that solutions to equation (2.52) are given by $Z = A\sin(qz)$ where A is a constant and $q = (n + 1/2)\pi/h$. We wish our solution to be symmetric about $\psi = 0$ so solving equation (2.53) gives $\Psi = B\cos(p\psi)$ where p is an integer (as we require P to be periodic in ψ), and B is a constant. Finally solution of equation (2.54) gives $R = CK_p(qr) + DI_p(qr)$ where K_p and I_p are modified Bessel functions. Using the condition that $P \to 0$ as we move away from the impact patch we obtain $R = CK_p(qr)$, where again C is a

73

constant.

So the Fourier-Bessel series is found to be :

$$P = \sum_{m,n} A_{mn} K_m(q_n r) \sin(q_n z) \cos(m\psi). \tag{2.55}$$

Imposing the boundary condition on the cylinder, $r = 1$, we obtain expressions for the A_{mn} :

$$A_{mn} = \frac{2[1 - \cos(q_n l)]}{q_n{}^2 K'_m(q_n) h\pi} \left[\frac{\sin(m + 1)\beta}{m + 1} + \frac{\sin(1 - m)\beta}{1 - m} \right]. \tag{2.56}$$

unless $m = 0$ when A_{mn} is half the above expression.

However, great care is needed when evaluating the sum as convergence is poor. We truncate the series at $n = N$ and $m = M$. As q_n gets large, $K'_m(q_n) \to 0$, so $1/K'_m(q_n) \to \infty$, whereas $K_m(q_n) \to 0$. This makes the terms in the sum difficult to evaluate. If we take a Fourier series, $f(t)$, and truncate it to N terms to give $f_N(t)$, and average it over the interval $(t - \pi/N, t + \pi/N)$ then extra factors appear. Convergence is aided by using these factors called Lanczos' factors. i.e. multiplying each term in the series in equation (2.55) by $\sin(q_n\pi/q_N)/(q_n\pi/q_N)$ and $\sin(m\pi/M)/(m\pi/M)$ (except when $m = 0$, when only the first factor is needed) (see Hamming 1973).

Figures 2.40 and 2.41 show the distribution of pressure impulse on a cylinder (unwrapped) with the impact on half (i.e. $\beta = \pi/2$) of the top 10 % and half of the full water depth respectively. Total impulse for figures 2.40 and 2.41 are 1.010 and 23.370 respectively. Increasing the impact region greatly increases the pressure impulse and hence the total impulse on the cylinder.

The maximum pressure for this impact occurs at roughly the same place as for impact on a wall. If we examine pressure impulse along the line $\psi = 0$ for this case and for the two-dimensional impact on a wall (Cooker and Peregrine 1990 b), we can see from figure 2.42 that the pressure impulse is less for the cylinder than for the wall. This is due to the convex three-dimensional nature of the cylinder.

The pressure-impulse contours, as we would expect, take the form of squashed el-lipses, with the highest pressures on the impact region itself. The pressure impulse

74
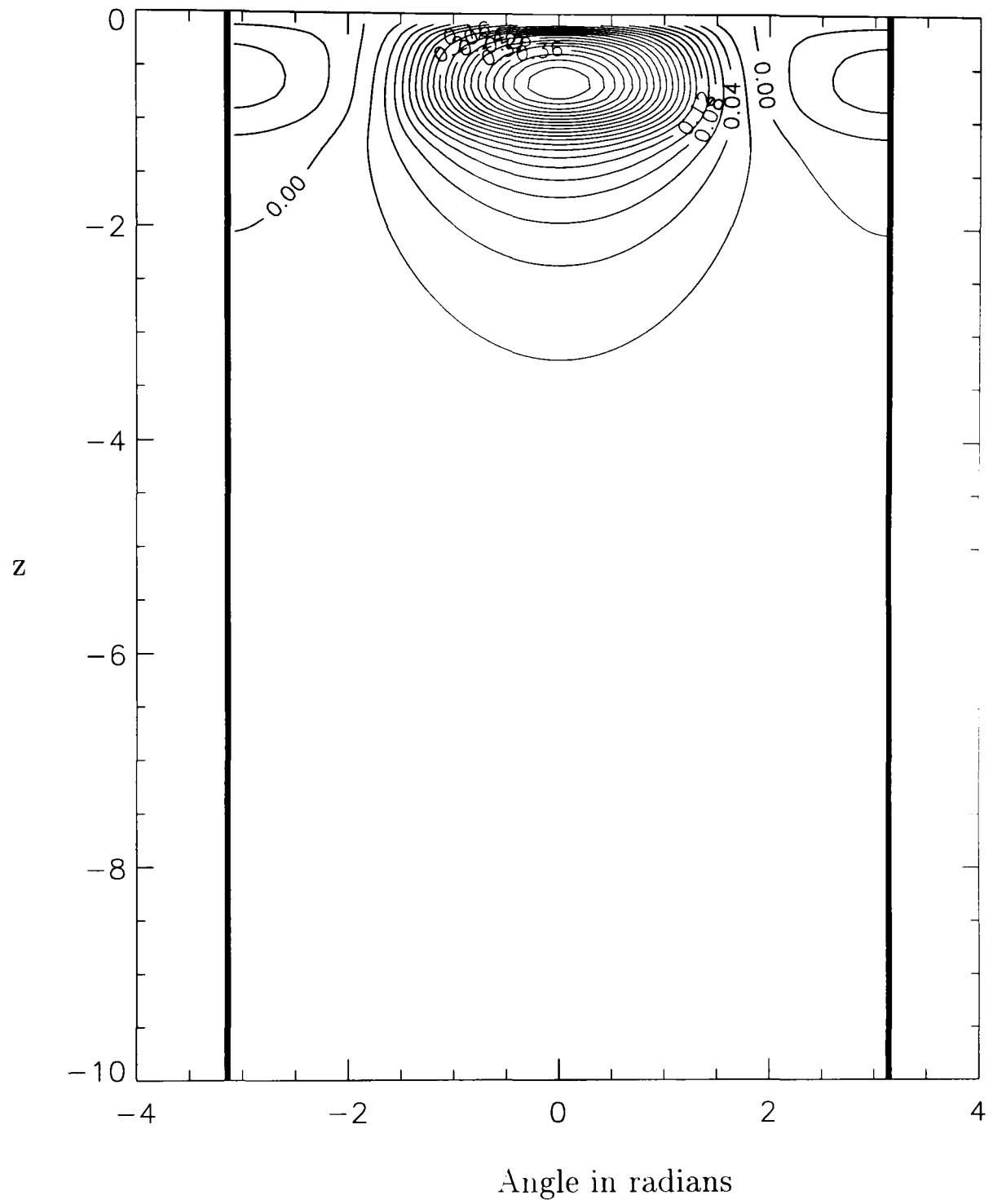
Figure 2.40: Distribution of pressure impulse on a cylinder (unwrapped) with the wave impact on half (i.e. $\beta = \pi/2$) of the top 10 % of the water depth. Total impulse 1.010.
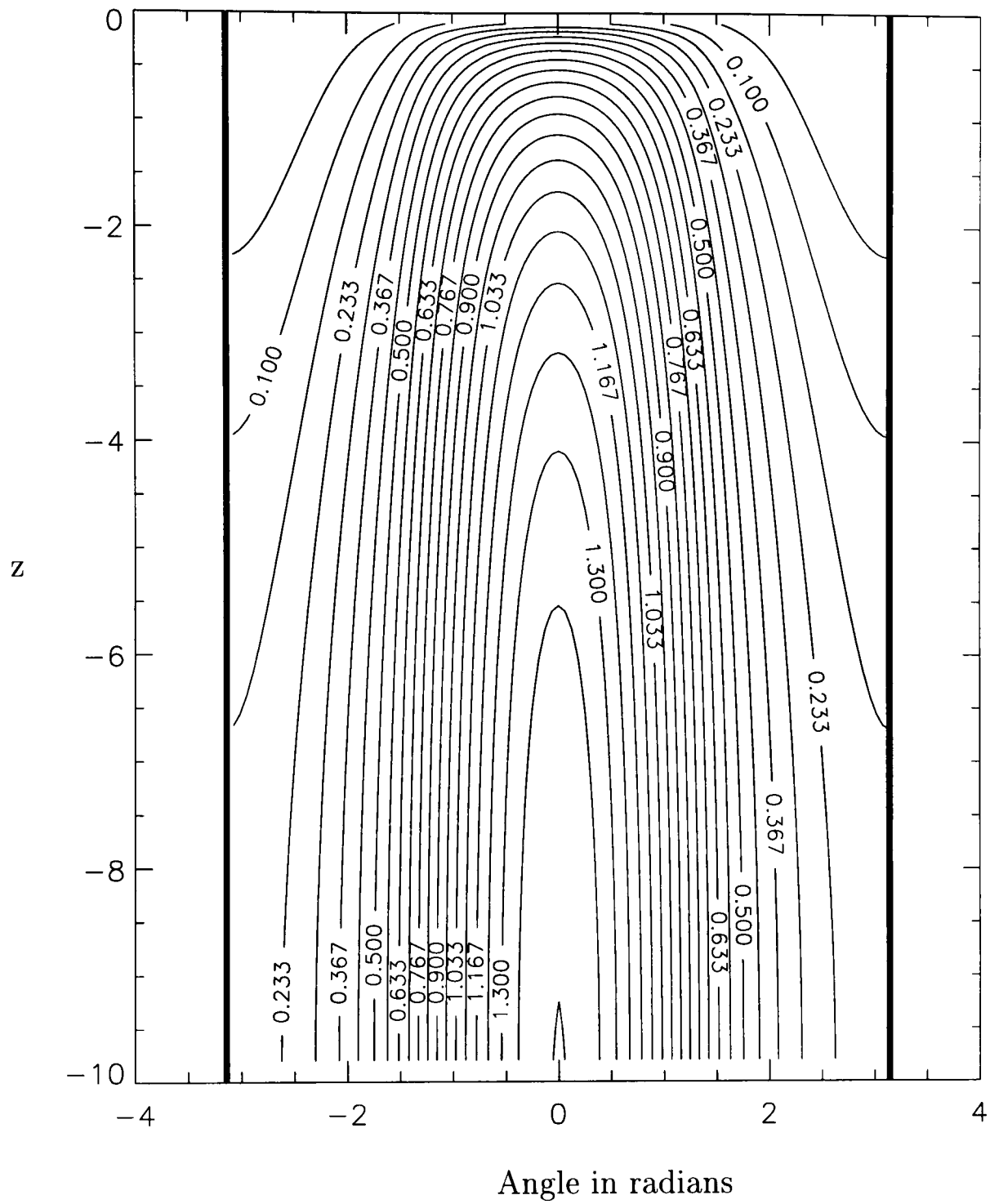
Figure 2.41: Distribution of pressure impulse on a cylinder (unwrapped) with the wave impact on the front half (i.e. $\beta = \pi/2$) of the cylinder. Total impulse 23.370

reduces in value very rapidly going down the cylinder. At a distance of approximately 3 down a cylinder of depth 10, with impact on the top 10%, the pressure impulse is less than 5% of its peak value. Note that the impact region is only on the front 50% of the cylinder and in the region at the back of the cylinder where no impact takes place there is a region of negative pressure impulse. This seems to happen regardless of the percentage of impact area, however the negative pressures are substantially bigger for the case of 10% impact when compared to 100% impact. If we examine figure 2.40 we can see that the pressure-impulse contours are very close together, hence we deduce there is a high pressure-impulse gradient. The negative values at $z = -0.5$ at the back of the cylinder for the top 10% and full impact case are -0.048 and -0.033 respectively. Hence in the 10% impact case the pressure impulse drops through zero quite quickly as we go round the cylinder and continues to drop to significant negative values. For the full impact case the drop off in pressure impulse is much more gentle hence only very small negative values are present.

It is not thought that these negative values are caused by not taking enough terms in the Fourier-Bessel series. If we consider, as in table 2.1, the case with impact on the top 10%, the maximum negative value of P at position $z = -0.59, \psi = -\pi$, increases in magnitude as more terms are taken. In addition, the difference in the terms is very small and reduces as the number of terms taken increases. The negative values may be a symptom of the particular mathematical model used.

	$n = 45$	$n = 50$	$n = 55$	$n = 60$
$m = 16$	-0.0487228	-0.0489856	-0.0492012	-0.0493464
$m = 17$	-0.0487713	-0.0490343	-0.0492501	-0.0493955
$m = 18$	-0.0488126	-0.0490757	-0.0492917	-0.0494372

Table 2.1: Values of P, at $\psi = -\pi, z = -0.59$ (position of largest negative value of P) for impact on a patch of a cylinder with the wave impact on half (i.e. $\beta = \pi/2$) of the top 10 % of the water depth. Values of m and n used for truncation are given.

To begin with we assumed that the free surface was horizontal. The solution for the problem with the contour of constant pressure impulse taken as the free surface can be found by subtracting off that constant from the original solution. We also note that we could take the zero pressure-impulse contour (particularly shown in figure 2.40) as a more realistic wave free-surface. By taking a different contour as the free surface the change in load can be found by multiplying the value of the pressure-impulse contour by the cylinder surface area.
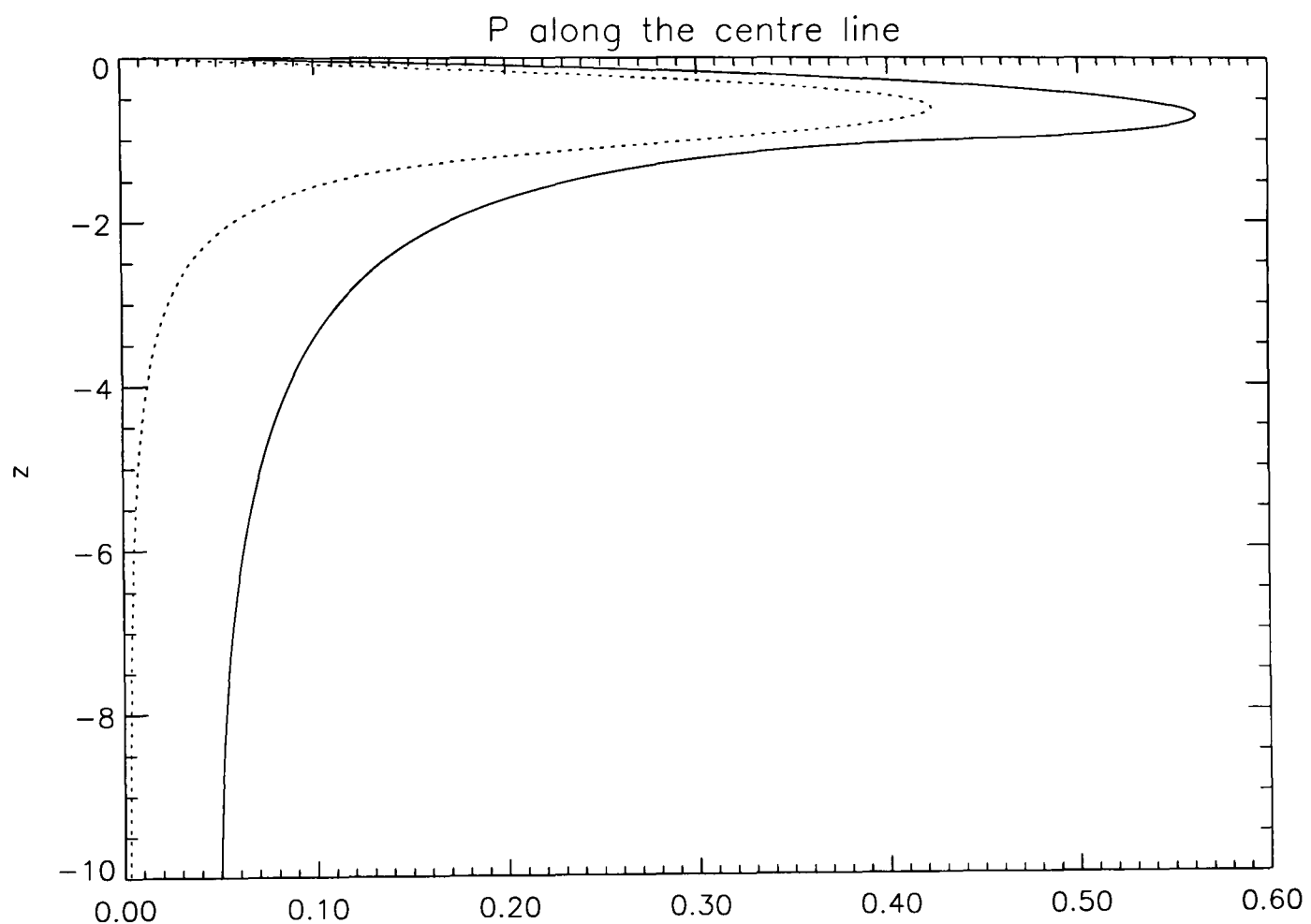
Figure 2.42: P along the centre line $\psi = 0$, against z. $-$ down the wall (Cooker and Peregrine (1990b) model) ,...down the cylinder. The impact is on the top 10% of the water depth.

2.6.3 Impact on a cylinder by a wedge of water.

When considering wave impact on a cylinder the impact region is often above the level of the main body of the water where the wave has risen up to impact on the cylinder. We begin by looking at a wedge (height a, impact between $\psi = \pm\beta$) of water impacting on the cylinder with a rigid boundary at the base. The length scale L is again the radius of the cylinder. The rigid boundary is required, for the present, to make the mathematical model simpler. The water is trapped in the wedge. It is hoped that eventually this model could be extended to have a body of water beneath the wedge rather than the rigid boundary, to make the model similar to a wave rising up and hitting the cylinder. We take cylindrical co-ordinates similarly to the previous cylinder model. The wedge of water must have a free surface along the top and edges of the wedge, where we take $P = 0$. Where the impact region occurs we require $\partial P/\partial r = -\cos\psi$, where no impact occurs $\partial P/\partial r = 0$, and along the base we take $\partial P/\partial n = 0$, where n is the direction normal to the base. Again we solve Laplace's equation to obtain a Fourier-Bessel series for the pressure impulse. The problem to be solved is shown in figure 2.43. We need to solve equations (2.52), (2.53) and (2.54) with the boundary conditions for this new problem.

Again in the z direction the solution must be periodic. Imposing the conditions from the base and the free surface gives $Z = A\cos(qz)$, where $q = (n + 1/2)\pi/a$. In the radial direction, as before, $R = BK_p(qr)$ because $P \to 0$ as $r \to \infty$. We require the solution to be periodic in ψ and that $P = 0$ at $\psi = \pm\beta$. Hence $\Psi = C\cos(p\psi)$, where $p = (n + 1/2)\pi/\beta$. So the solution to the impact of a wedge of water on a cylinder is:

$$P = \sum_{m,n} B_{mn} K_{p_m}(q_n r) \cos(q_n z) \cos(p_m \psi) \tag{2.57}$$

with the B_{mn} given by:

$$B_{mn} = \frac{2(-1)^{n+1}}{q_n{}^2 K'_{p_m}(q_n r) a\beta} \left[\frac{\sin(p_m + 1)\beta}{p_m + 1} + \frac{\sin(p_m - 1)\beta}{p_m - 1} \right] \tag{2.58}$$

except in the case when $p_m = 1$, then the square bracket in the above expression is

79
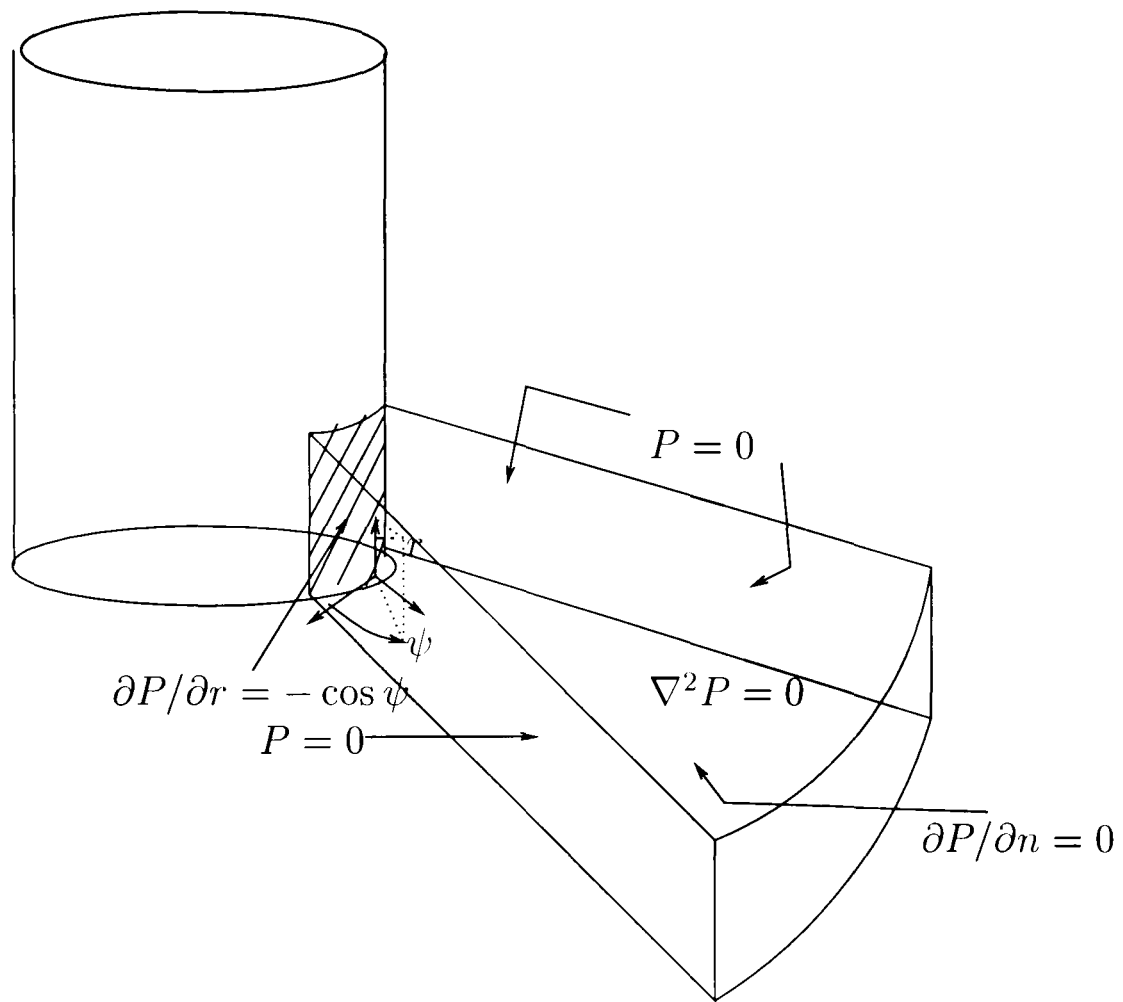
Figure 2.43: Impact on a cylinder of a wedge of water.

$\left\lfloor \frac{1}{2} \sin 2\beta + \beta \right\rfloor$ instead.

Figure 2.44 shows the distribution of pressure impulse on a cylinder (unwrapped) with the wave impact from a plane wave's front for a wedge of semi-infinite extent ($a = 1$). However, this model has a solid boundary at the base. If we were to take
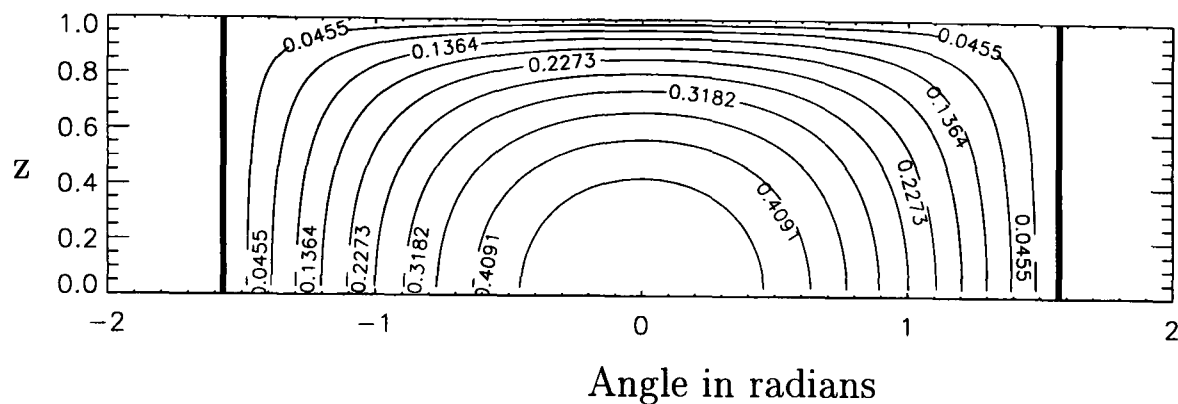
Figure 2.44: Distribution of pressure impulse on a cylinder (unwrapped) with the wave impact from a wedge of water. The impact region is between the two dark lines. $\beta = \pi/2$

the more realistic case of deep water the pressures would be somewhat lower than in this example. Figure 2.45 is a plot of the pressure impulse down the centre line on the cylinder for the 'wedge' of water impact and patch impact on a cylinder. The 'wedge' impact as expected has a lower pressure impulse, this is due to the imposition of $P = 0$ along the edges of the wedge. The difference is most noticeable towards the bottom of the cylinder where the difference between the two cases is about 15 %.

2.6.4 Comparisons.

These results can be compared in two ways. The width of the patch on which the impact occurs as seen by the approaching wave equals the diameter of the cylinder. If we consider the 2D model of impact on a wall we can compare this with the two cases described above if we let the impact on the wall be over the same length. The total impulse then for impact on a wall (2D impact on a wall of length 2, height 10, impact on the top 10 %) is 2.574, on a cylinder (of diameter 2, again height 10,

81
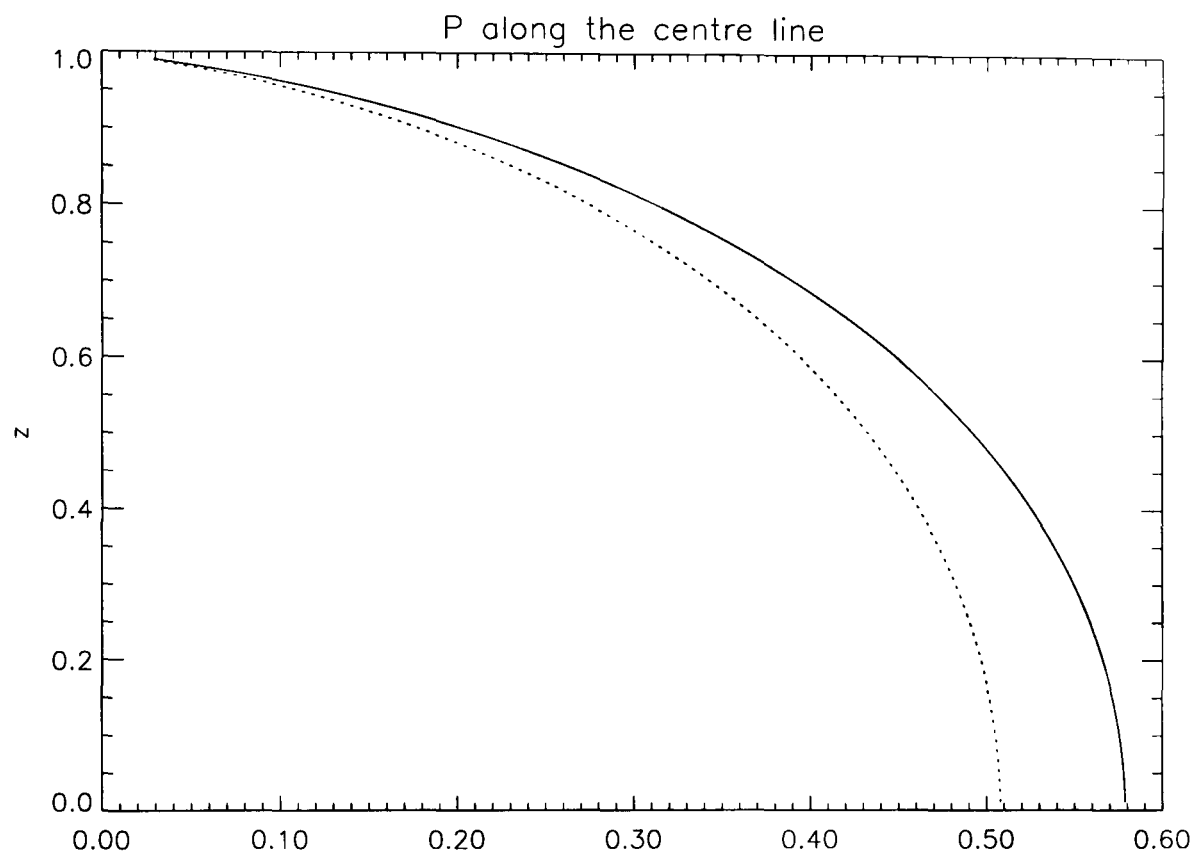
Figure 2.45: P along the centre line $\psi = 0$, against z. — for impact on a patch below water level of a cylinder ,...for impact of a wedge of water on a cylinder. The impact is on the full depth of the water.

and impact on the top 10%) it is 1.010 when the impact is surrounded by water and 0.604 for the 'wedge' of angle π (of diameter 2, height 1, impact over the full depth) bounded below by a fixed bed. As expected the total impulse is largest for a wall as there are no three-dimensional effects to attenuate the high pressures. The impact of the 'wedge' of water has the least total impulse due to enforcing $P = 0$ down the edges of the wedge. Finally we consider the 'patch' impact on a wall, the total impulse for this for a patch of width 2, height 1, on a wall of height 10 (where we sum the pressure impulse over width 2) is 1.242. As again we expected the total impulse is not as much as for the 2D impact on a wall as the pressure impulse on the patch model only reaches the peak 2D values at the centre of the patch. The patch model, however, has a greater total impulse when compared with both the cylinder impacts, showing that the effect of having a cylindrical shape for the impact is very strong.

Most of the horizontal component of the momentum is lost from a region close to the wall during impact. The significant thickness of the fluid (i.e. the depth over which the momentum is lost) can be calculated by equating the total impulse on the impact region with the momentum lost from the volume of water of thickness L_m with the impact velocity. The momentum length for 2D impact on a wall is 2.574, substantially larger than the value of 1.242 for impact on just a patch of wall and 0.980 for the impact on a patch of cylinder. (These examples are all having depth of water 10, impact on the top 10%, and width 2, so that the projected area of impact is the same for each.) As expected the cylinder is affected by less of the fluid since most of the momentum is related to oblique impact.

2.6.5 Conclusions.

Wave impact on a vertical cylinder has been analysed for two simple cases. As expected the model shows that the resulting pressure impulse is lower for impact on a cylinder than on a wall. The peak pressure on the cylinder occurs at approximately the same distance (relative to the height of the patch) below the free surface as for

impact on a wall.

For impact on a patch on the cylinder a negative pressure impulse is experienced at the opposite side of the cylinder to the impact. It is a possibility that it is a fault in the mathematical model chosen for the problem.

Chapter 3

Impact under a deck.

3.1 Introduction.

Many coastal structures and natural coasts have openings, overhangs and projections which are open to impact by incident water waves. The sudden impact of a wave on a rigid surface leads to a rapid rise of pressure and consequent violent water motions. We consider the wave impact on the underside of a projecting surface. The example discussed is that of a flat deck close to the mean water level. A pressure-impulse approach is used, which has the advantage that given a solution for one problem it is possible to select pressure-impulse contours which give the solution to related problems. The pressure gradient on the underside of the deck is especially strong near the seaward edge of the impact region, so this is a region where any projections on the structure's surface may be subject to strong forces. On the other hand the maximum pressure impulse is at the landward end of the impact zone, it is here that the deck is most likely to be 'blown' upward.

There are a number of circumstances in which the effect of the upward impact of a wave beneath a rigid horizontal surface needs to be estimated. For offshore oil-rigs the lack of good estimates of such upward impacts leads to designs where the main platform of rigs is built to be out of reach of 'green water'. This may not be an option for some coastal structures, including piers and jetties, and temporary works in inter-tidal zones. Here we present pressure-impulse calculations for an impact on a horizontal surface in finite depth. For convenience we refer to the rigid surface as

a deck.

3.2 Background.

The study of a wave impacting on the underside of a deck is mathematically very similar to the slamming of a body into a liquid. In the first case it is the solid that is fixed and the liquid which is in motion and in the second case the other way round. Hence it is only the frame of reference which differs.

Improvements in the design of sea-planes inspired much research in the area of ship-slamming, with early simple models given by Von Karman (1929) and Wagner (1932). Von Karman analysed the stresses which occur when a seaplane float impacts with the sea. He developed an impact formula for a wedge penetrating a liquid surface, by looking at conservation of momentum. The liquid is assumed to be incompressible. For the limiting case of a flat plate, Von Karman predicts pressures of infinite magnitude. Wagner adapted Von Karman's formulae to allow for a 'piling' up of the liquid along the sloping edges of the wedge. However, both of these approaches take no account of the initial air cushion which is present.

Keldysh (1935) developed expressions for the total impulse for a plate dropping on finite depth. However no expression for the pressure-impulse distribution on or below the plate was given. Similarly an expression for the total impulse on a deck. with only a very shallow body of water below it, was given in Veklich and Malykh (1984), but again no distribution was given.

Further experiments in the area of slamming were carried out by Verhagen (1967), who also introduced a more theoretical approach. When a plate impacts on a body of water a layer of air becomes trapped. Verhagen assumed that this layer of trapped air is released sideways as the impact occurs. and an equation for the release of the air was developed. The model treats the water as incompressibe and uses the method of characteristics to solve the equations. The model predicts the shape and magnitude of the pressure-time history of the impact quite successfully

and focuses on prediction of maximum impact pressures instead of the distribution of the pressure along the plate. A model for a flat plate dropping vertically onto a body of water, dealing mainly with the trapped air, was presented in Whitman and Pancione (1973). They built up a model of a plate falling within a 'leaky' cylinder, and considered this as a piston. Plots of pressure change in terms of size of plate are shown, which compare well with experimental data. However, both Verhagen (1967) and Whitman and Pancione (1973) only looked at the plate dropping onto infinite depth of water.

Extensions of Von Karman's and Wagner's formulae have been developed, in particular by Cointe and Armand (1987) and Cointe (1989). The former being for vertical entry of a rigid cylinder (where the direction of motion is radial) into an incompressible inviscid fluid, with the formula differing from Von Karman's by just a wetting corrective term (similar to Wagner's). The second paper uses asymptotic expansions to extend the formulae for non-normal impact and initially curved free surfaces. Again these studies are for infinite depth of water. Korobkin and Puknachov (1988) give a good review of the numerical and analytical methods which have been used to look at the initial stage of impact of solid bodies with water.

When two equal progressive waves travel in opposite directions they can produce a standing wave, and the wave height of this standing wave is, according to linear theory, twice the height of each progressive wave. Hence standing waves can occur at a wall where the original wave and its reflection interact. The peak in the standing wave can only be sustained if the depth of water is twice the height of the original progressive wave. So if this condition is satisfied then it is possible to have a standing wave which occurs at a wall which impacts upwards onto an overhang. Furudoi and Murota (1966) and the later study of Ramkema (1978) both examined the uplift forces caused by standing waves impacting upwards on protrusions. Furudoi and Murota developed empirical formulae for the uplift forces in terms of the water depth and the standing wave properties. Ramkema extended Bagnold's piston model for impacts (as discussed in chapter 2), to include adiabatic and isothermal compression

87

of the air cushion. The model allowed for the compression of the liquid and predicted the spatial pressure distribution. He also reviewed wave impact and ship-slamming literature.

French (1969) performed experiments to investigate uplift pressures on a platform. This was carried out by having a platform fixed a short distance above the still water level, and sending waves along to impact first on the edge of the plate and then to continue to travel under the plate. The peak pressures and the reflective pressures were found to be related to the wave celerity under the platform, and a simple theoretical formula was developed. Negative pressures were also observed as the wave became detached from the platform. French gives a review of previous similar experimental investigations. Following on from French's and other experimental studies, Lai and Lee (1989) developed a Galerkin finite element method, for this problem, the predictions of which compare well with experiment. However, these studies are for a wave travelling horizontally, with the top of the wave above the height of the deck, and hence are not comparable with our theoretical results.

When designing marine structures, they are often built out of reach of potentially destructive waves, however this is expensive, especially if the structure could be built to withstand some wave impacts more cheaply than to build it high enough to be away from the wave impact region. A study by Dalton and Nash (1976) looked at impacts on a cylindrical member and concluded that it is possible to scale model tests to give predictions for full scale impacts. Massel, Oleskiewicz, and Trapp(1978) studied the impact wave forces on a horizontal plate, but give no pressure-time plots. They suggested that both the peak and slowly varying pressures are functions of the Ursell number. These experimental studies all treat the impact as though it were two-dimensional, ignoring end effects due to the finite width of the plate. Shih and Anastasiou (1992) looked experimentally at the vertical loading on a platform, and in particular examined the effect of the width of the plate, and scale effects. They concluded that the platform width has no effect on the impact pressures. They also concluded that Froude's scaling law was inappropriate. However the distribution

of duration and impulse characteristics could be well described by Rayleigh and exponential distributions respectively. Again though this was for a horizontal wave similar to those studied in French (1969).

Howison, Ockendon and Wilson (1991) carried out a theoretical examination of wave impact of an impacting body nearly parallel to the undisturbed liquid surface. They obtained explicit solutions for the two-dimensional case and a numerical algorithm for the three-dimensional case.

Another theoretical method for estimating forces on the underside of a marine structure is given in Peregrine and Kalliadasis (1996). They looked at the filling up of a container or a confined region. The solution is found by looking at mass and momentum conservation, and free-streamline theory. The flow involved is very similar in nature to that described in some of the more experimental papers such as French (1969), where the wave impacts on the edge of a horizontal plate and then travels under the plate.

Takagi (1997) used a matched asymptotic expansion method to look at a three dimensional plate impacting on a body of water. The impact force is stronger when air becomes trapped between the plate and the water. This study is again for the infinite depth case.

Finally, some recent experimental work described in Smith and Stansby (1997) looks at the vertical force on a plate in free flight impacting on a wave. They obtain a formula for the general slam coefficient by dimensional analysis and physical reasoning. This experimental investigation is very similar to the model described in this thesis. However, in this thesis we assume that the deck is hit by a wave whose motion is primarily vertical at impact, but in the experimental study the plate drops at an angle on to the top of the wave, making comparison difficult. Hence, for the experimental work the plate has both a horizontal and vertical component of velocity, whereas in the model considered later the plate has only a vertical velocity. It may be possible to treat the two velocity components independently as the model

is for inviscid fluid. Further experiments are being undertaken by Stansby and it may be reasonable to use these as a comparison.

3.3 Mathematical model.

We now consider the specific case of impact of a body of water upwards on to a deck. The geometrical simplifications we make may be seen in figure 3.1. The water is taken to be of finite depth $CD = a$, and to impact the horizontal deck BC of length L with an upward velocity V. The free surface not hitting the deck is taken to be flat, as BA, and to stretch to infinity. However, as indicated below alternative surface shapes are easily found by choosing different contours of pressure impulse. The boundary conditions on CD given in figure 3.1 indicate that the problem can be reflected in the vertical plane of CD, corresponding to impact on a horizontal surface of length $2L$ with a central plane of symmetry.
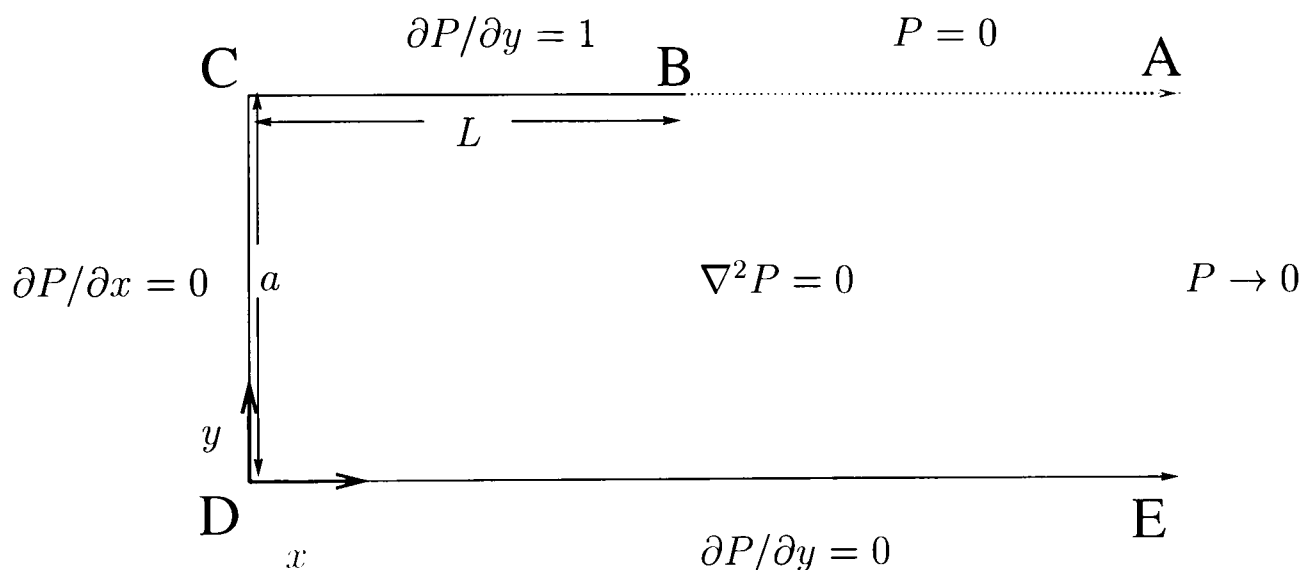
Figure 3.1: Impact under a deck: the problem to be solved.

The boundary condition at the free surface is that the pressure must be constant and continuous therefore $P = 0$. At the walls and on the bed, the normal velocity must be zero before and after impact, therefore using equation (2.3), $\partial P/\partial n = 0$, where n is the normal direction. As the water meets the deck BC, the water has vertical velocity V, which could be any function of x, and after impact the water has zero vertical velocity. Therefore, again using equation (2.3), we have

$\partial P/\partial n = V$. For simplicity, we again choose V to be constant. We make the problem dimensionless by choosing units for which $V = 1$ and $L = 1$.

We begin by considering the two extreme cases first. where the ratio of deck length to water depth is firstly very small and secondly very large. We then discuss and solve the more general case.

3.4 Infinite depth solution.

The problem of a wave hitting upwards under a deck jutting out from a wall, is mathematically equivalent to a plate dropping onto a body of water and setting the water in motion. Also when considering solving Laplace's equation we can use the direct analogy with the velocity potential of irrotational flow. We temporarily take the origin to be at the centre of the plate, with x along the plate, and y downwards perpendicular to the plate. If we consider the complex potential for a flow past a plate then we just need a change of reference frame to find the complex potential of a moving plate in a stationary fluid. With a complex potential $w = \phi + i\psi$, then $\partial\phi/\partial x = 0$ on $x = 0$, and $\partial\phi/\partial y = -1$ along the plate. These are the conditions that are required by P, and so the lines of constant pressure impulse are given by lines of constant ϕ. The solution may be found in Lamb (1932, section 71), and in Milne-Thompson (1962, section 6.3), for a fluid flowing past an ellipse. If we allow one of the semi-axes to shrink to zero then we have a plate instead of an ellipse in the flow. Finally choosing the plate to be perpendicular to the flow, the length of the plate to be 2, and the velocity -1, we get an expression for the complex potential of a uniform stream flowing past a plate:

$$w = \sqrt{1 - z^2}. \tag{3.1}$$

where the origin is taken to be the centre of the plate.

If we subtract the complex potential for a stream from this expression we have the potential for a moving plate. As the velocity of the stream is $(0. -1. 0)$, we

91

must therefore subtract $-iz$ to get:

$$w = iz + \sqrt{1 - z^2}. \tag{3.2}$$

This solution is symmetric about the centre of the plate. This means that we can consider a line drawn perpendicular to the plate from the centre of the plate, to be a wall, bringing us back to the original problem of the water hitting a deck jutting out from a wall. Hence we have an expression for the pressure impulse:

$$P = \text{Re}(iz + \sqrt{1 - z^2}). \tag{3.3}$$

This is the infinite depth solution. Figure 3.2 shows contours of pressure impulse. The total impulse on the deck is $\pi/4$, in dimensional terms $\pi \rho V L / 4$.
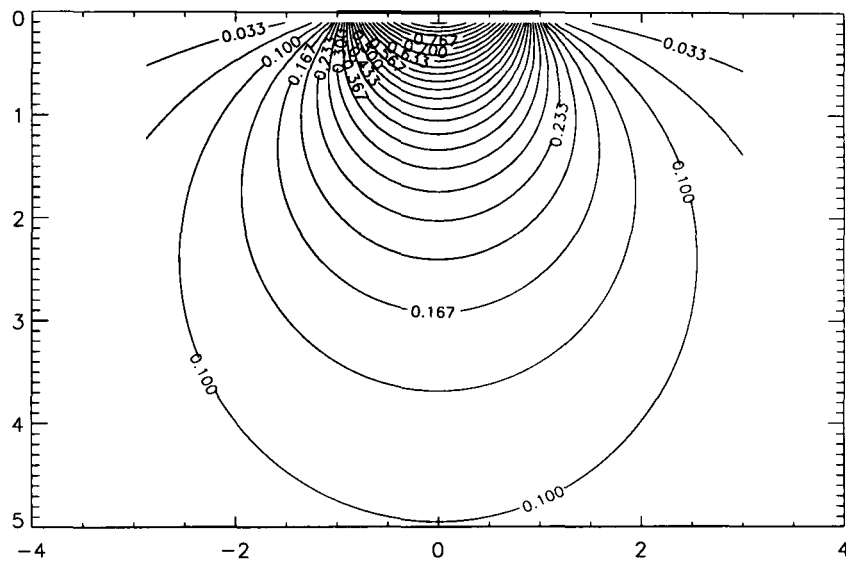
Figure 3.2: Infinite depth solution. Total impulse on deck (0,1) is $\pi/4$.

3.5 Infinitely long deck.

We next consider the other limiting case where the deck is infinite in length, or in our units a becomes small. As a becomes small the effect of the free surface on the solution under the deck becomes small. This means it is possible to solve in that region by neglecting the condition at the free surface. We now return to the

co-ordinates used in figure 3.1. Hence we solve Laplace's equation on a strip where $\partial P/\partial y = 1$ along the top, $\partial P/\partial n = 0$, where n is the normal direction, along the left-hand edge and bottom.

The solution is given by:

$$P = \frac{1}{2a}\left[y^2 - x^2\right] + K, \tag{3.4}$$

where K is a constant which depends on the behaviour of P near $x = 1.0$, where this approximation fails. Figure 3.3 shows the case when $a = 0.1$, and $K = (1/2a) - (a/2)$. This choice of K forces the pressure impulse to be zero at the edge of the deck. This is is probably too harsh a condition, leading to the prediction of the pressure impulse being too low. In practice the 'filling flow' solution of Peregrine
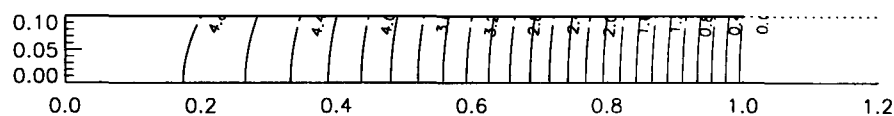
Figure 3.3: Analytic solution when a is small.($a = 0.1$, K=4.95)

and Kalliadasis (1996) may be more relevant to this case.

3.6 More general solution.

Consideration of the boundary conditions in Figure 3.1, or the solution (3.3) shows that at B there is a square root singularity. This singularity causes problems for many numerical solution methods. The singularity is due to the abrupt change in the boundary conditions due to the particular mathematical model chosen. However, one way to eliminate the problem of the singularity is to map the original problem using conformal maps as follows. First map to a half-space, then use another conformal map to perform a shift and stretch so that by using a final conformal map we can bend the problem back to a semi-infinite strip but with the boundary conditions shifted round to a convenient position, i.e. shift the boundary conditions

on the deck round to the vertical wall. The singularity is no longer a problem as it is contained within the complex map, and so no longer exists in the solution plane. That is, that the problem in the final plane which we actually solve has the change in boundary conditions at the corner and so is no problem to solve.

Let the original plane in which the problem is posed be the z plane. The first map we need is $w = u + iv = \cosh(\pi z/a)$. This gives the problem shown in figure 3.4. As we only use conformal maps P continues to satisfy Laplace's equation throughout.

$$\nabla^2 P = 0$$
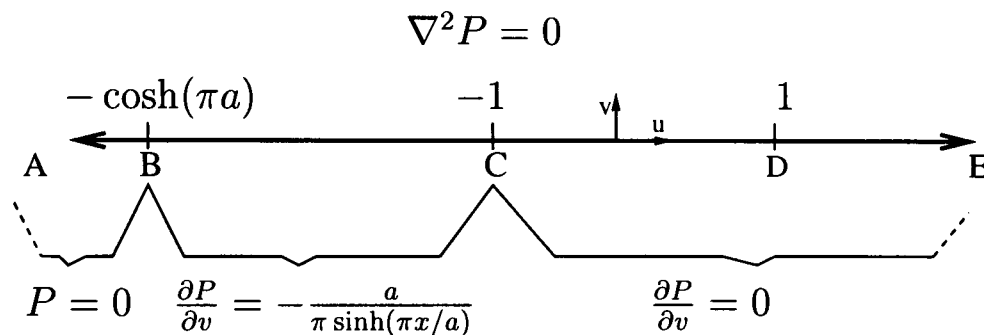
Figure 3.4: The problem in the w-plane after the first complex map.
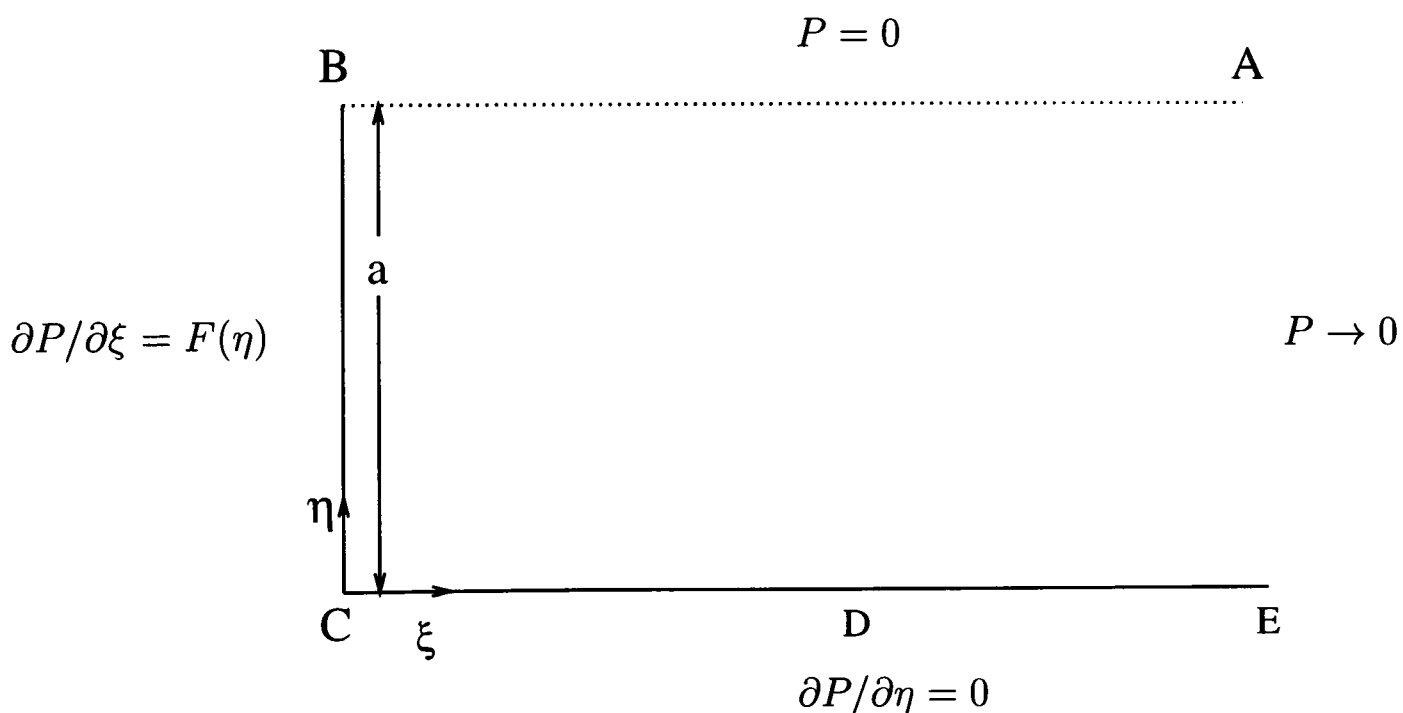
Figure 3.5: The final problem to be solved in the ζ-plane, where $F(\eta) = -\sin(\pi\eta/a)/(M\sqrt{b^2-1})$ with $b = [\cos(\pi\eta) - N]/M$.

We then use a translation and magnification to shift B to -1, and C to 1.

94

The map required is $h = f + ig = Mw + N$ where $M = 2/(\cosh(\pi/a) - 1)$ and $N = M + 1$. The last step is to map this problem back to the strip. The final map required is $\zeta = \xi + i\eta = a\cosh^{-1}(h)/\pi$. This gives the problem as shown in figure 3.5. We note here that $F(\eta)$ is zero at the two corners of the box so the square root singularity is eliminated.

We solve Laplace's equation in this region by separation of variables. Let $P = f(\eta)g(\xi)$, giving $f'' = -\alpha^2 f$ and $g'' = \alpha^2 g$, where α is a constant. Solving for f, using the boundary condition that $f = 0$ at $\eta = a$, and $\partial f/\partial \eta = 0$ at $\eta = 0$, gives $f = A\cos(\alpha_n \eta)$ where $\alpha_n = (n + 1/2)\pi/a$. We now solve for g, using the condition that $P \to 0$ as $\xi \to \infty$. This gives $g = Re^{-\alpha_n \xi}$. Hence we have an expression for the pressure impulse:

$$P = \sum_n A_n e^{-\alpha_n \xi} \cos(\alpha_n \eta). \qquad (3.5)$$

Finally we use the condition that $\partial P/\partial \xi = -\sin(\pi\eta/a)/(M\sqrt{b^2 - 1})$, where $b = [\cos(\pi\eta) - N]/M$ along $\xi = 0$ to get expressions for the A_n. Using this condition we get:

$$-\sum_n A_n \alpha_n \cos(\alpha_n \eta) = -\frac{\sin(\pi\eta/a)}{M\sqrt{b^2 - 1}}. \qquad (3.6)$$

The final step is to multiply both sides by $\cos(\alpha_m \eta)$, and integrate along the line $\xi = 0$ to get:

$$A_m = \frac{2}{\alpha_m a} \int_0^a \frac{1}{M} \frac{\sin(\pi\eta/a)\cos(\alpha_m \eta)}{\sqrt{b^2 - 1}} d\eta. \qquad (3.7)$$

Similar results can be found for any velocity distribution $V = V(x)$.

3.7 Results and discussion.

The integral in (3.7) is evaluated by using a NAG numerical routine, D01ARF. The positioning of the division by α_m in the expression for A_m was found to be

important. For $a < 0.5$ the division by α_m was included in the integrand, but not for $\alpha \geq 0.5$. This 'cutoff' was chosen purely so that the numerical routine was able to evaluate the integral to an accuracy of 10^{-10}. For the cases of $a = 0.5$ and $a = 2.0$ taking thirty terms in the sum, gives an accuracy of 4 and 12 decimal places respectively in P. The distribution of pressure impulse in the water beneath the deck is shown for water depth to deck length ratios of 2.0, 1.0 and 0.5 in figures 3.6, 3.7 and 3.8 respectively. The values of the total impulse on the deck and on the wall beneath each deck are given in each caption.
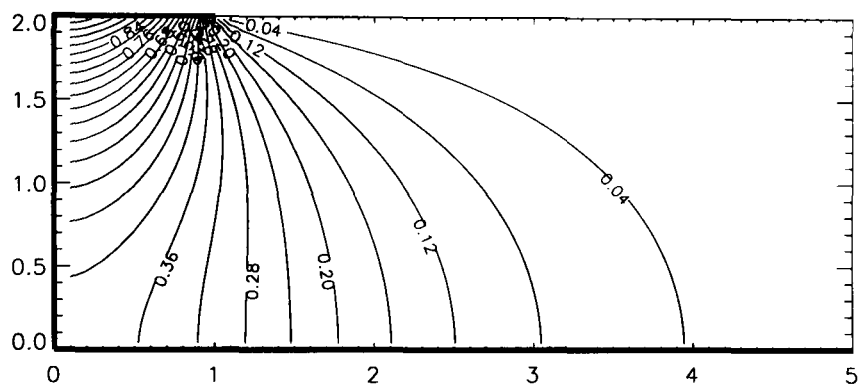
Figure 3.6: Pressure-impulse contours with $a = 2.0$. Total pressure impulse on the deck and wall respectively are 0.81 and 1.12
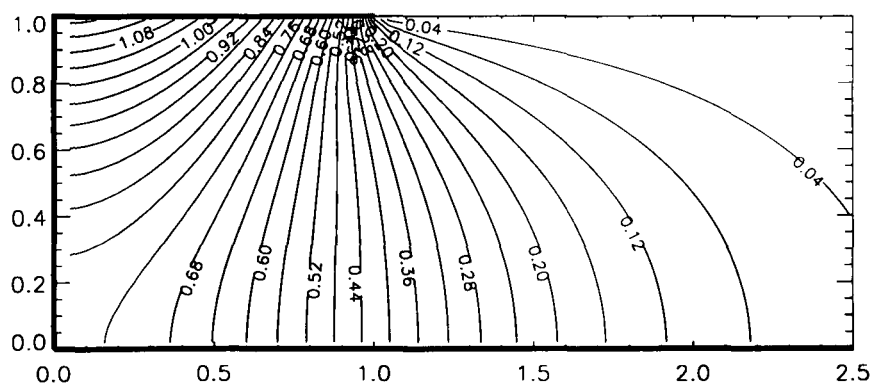
Figure 3.7: Pressure-impulse contours with $a = 1.0$. Total pressure impulse on the deck and wall respectively are 0.92 and 0.87.

In figures 3.6, 3.7, and 3.8 note the differing contour intervals, and the increasing impulse on the deck as the water depth a is decreased. The value of total impulse
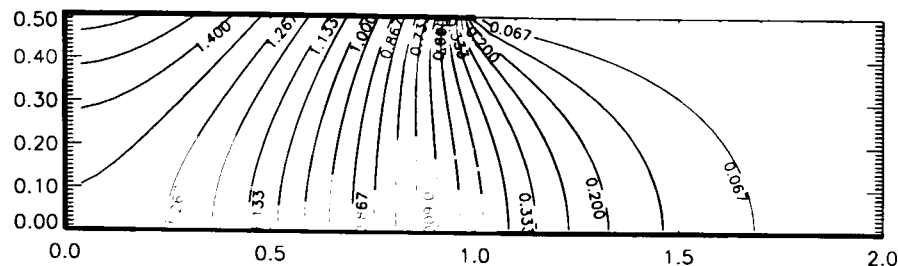
Figure 3.8: Pressure-impulse contours with $a = 0.5$. Total pressure impulse on the deck and wall respectively are 1.193 and 0.7.

on the deck is given as a function of a in figure 3.9. This trend is for the impulse from impact of a given velocity and area to increase as the body of impacting water becomes more confined. The same trend is described by Cooker and Peregrine (1995) for impact on an interior wall of a rectangular box and by Topliss (1994) for impact within a circular cylinder. Consideration of flow in the most confined circumstances, as a becomes small, leads us to the 'filling flows' (Peregrine and Kalliadasis, 1996). Further, an estimate of how the compressibility of dispersed air bubbles, such as those entrained in waves during breaking, may soften wave impact is given in Peregrine and Thais (1996).

The results are in dimensionless units, for practical use the dimensional pressure impulse is needed; that is

$$P^*(x^*, y^*) = \rho V LP(Lx, Ly), \tag{3.8}$$

where * denotes only some dimensional quantities. Whilst ρ and L will generally be known, V the vertical velocity of impact needs to be estimated. A simple method of estimating V is first to estimate how high a wave would be in the absence of the deck. Suppose it would have a height ΔH above the deck level. In simple projection of a particle this would require a velocity of $\sqrt{2g\Delta H}$. This is a reasonable, somewhat conservative, estimate for V.

It is useful to think of the same problem but fixing the depth of water at 1
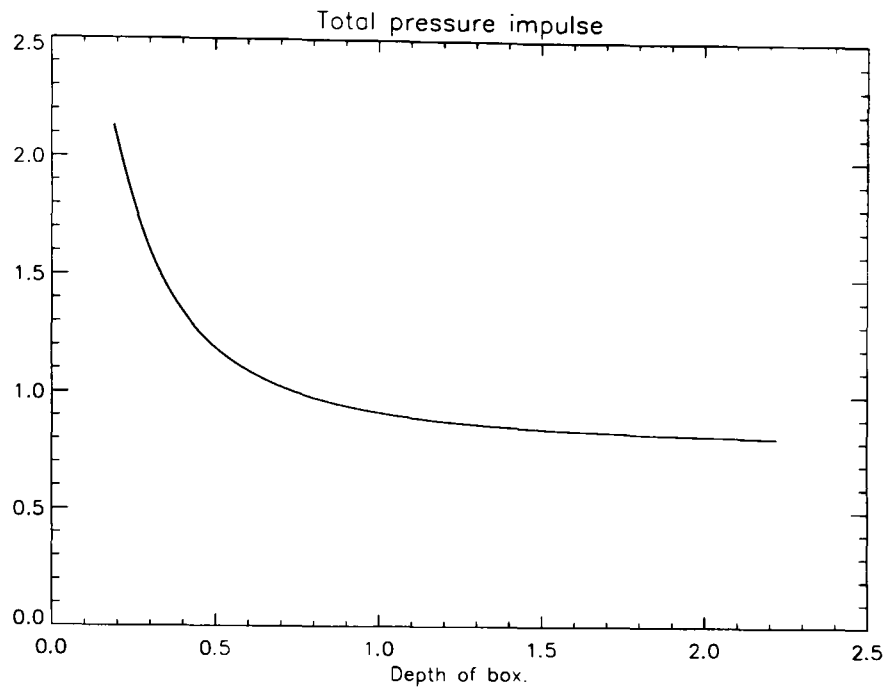
Figure 3.9: Total impulse on deck against depth a.

and calculating quantities such as total impulse as we increase the length of the deck. This is obtained by simply scaling the previous results. We present plots of maximum pressure impulse (figure 3.10), total impulse on the left hand wall (figure 3.11), total moment on the left hand wall (figure 3.12) and total impulse on the deck (figure 3.13).

First we consider figure 3.10. We note that increasing the length of the deck increases the maximum pressure impulse. Similarly in examining figures 3.11 and 3.12, increasing the length of the the deck increases the total impulse and impulsive moment along the left hand wall.

Note, the above solutions are not appropriate for impact from jets, e.g. see Cooker and Peregrine (1995), where the semi-infinite rectangular impact on a wall is equivalent to half of a plane jet and section 3.5 gives the solution for a circular jet. However, the solutions can be used for waves which are not nearly level with the deck as follows. By subtracting the appropriate constant from P, any of the contours of P can be chosen as an alternative free surface. Although such a surface tends downward rather than towards a horizontal level, this is not of great significance as long as the shape reasonably close to the impact region is appropriate. See Cooker
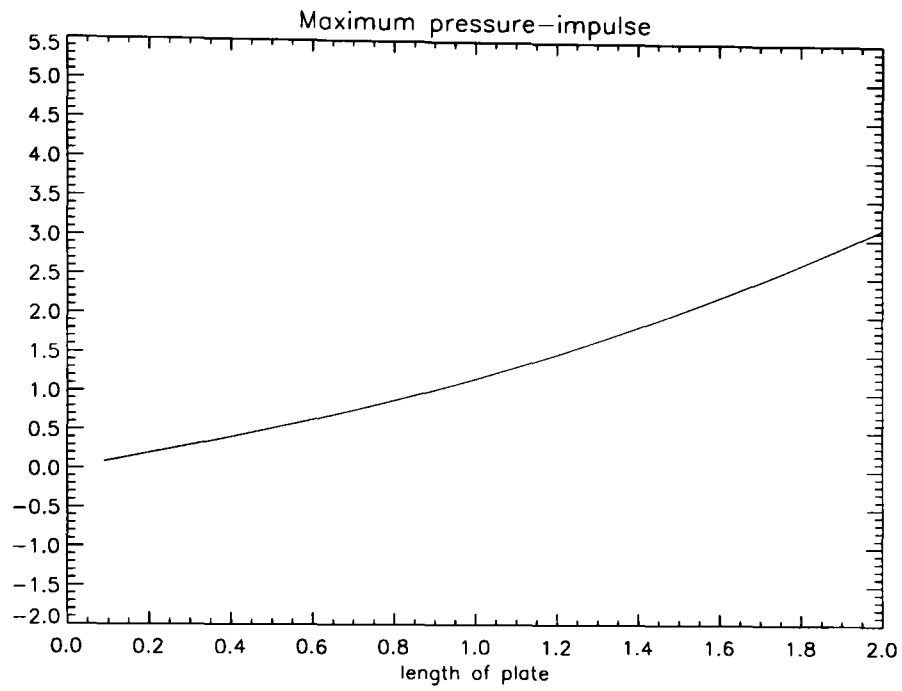
Figure 3.10: Maximum pressure impulse against length of deck.
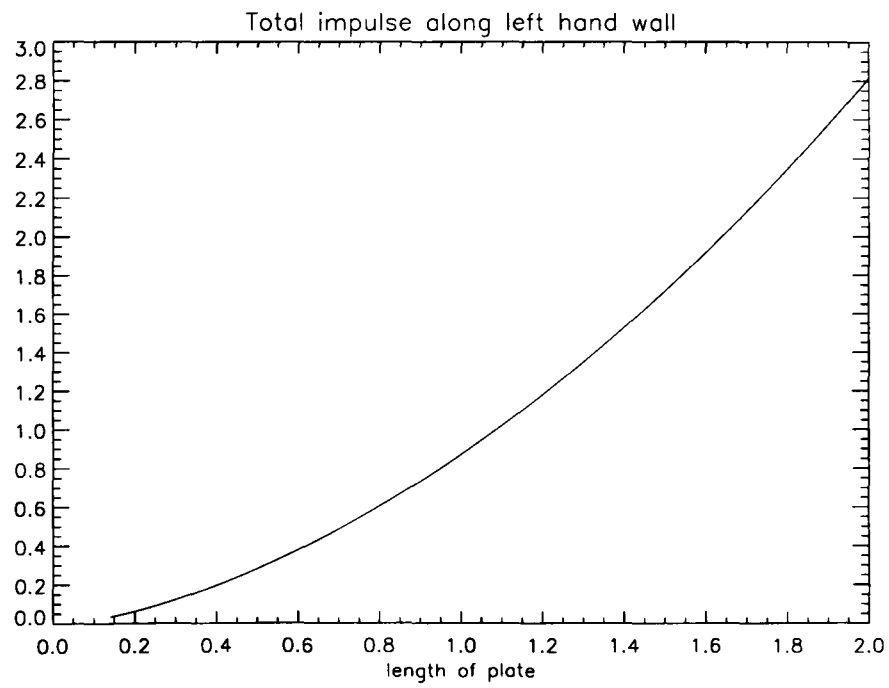
Figure 3.11: Total impulse on the wall due to impact of given length on the free-surface.

99
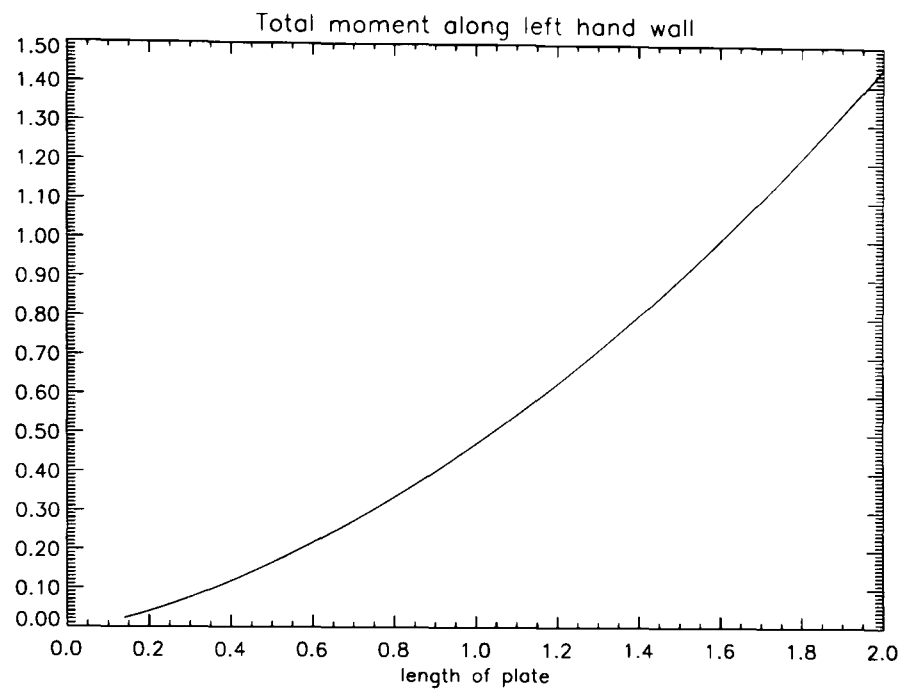
Figure 3.12: The impulsive moment on a wall as a function of impact length.
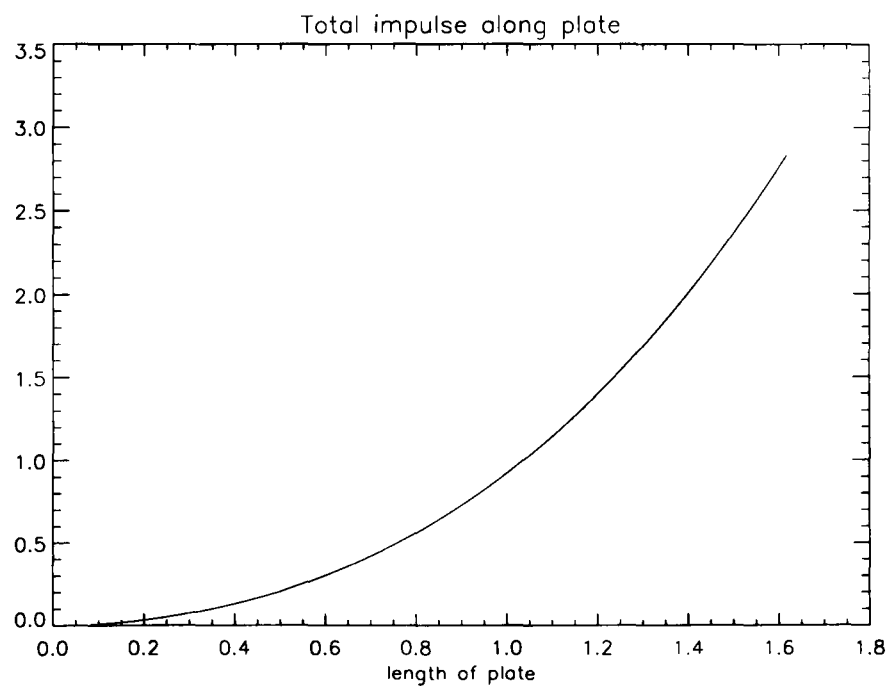
Figure 3.13: The total impulse on the deck as a function of impact length.

100
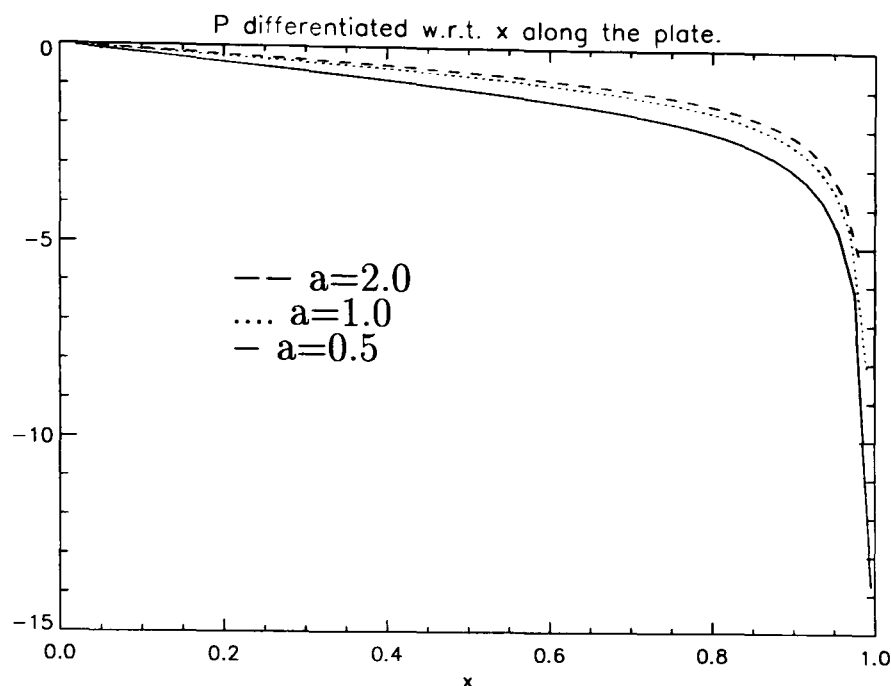
Figure 3.14: $\frac{\partial P}{\partial x}$ along the deck.

and Peregrine (1995) for some examples.

Clearly the results presented here can be used to estimate the impulse and the spatial distribution of a wave impact. In addition, as shown by Cooker and Peregrine (1992) it is possible to estimate the impulse on bodies (which are small compared with the water depth) on and near the wave impact area. The impulse on the body may be estimated from the local pressure-impulse gradient and a boundary-value problem posed in the vicinity of the body. Figure 3.14 shows the local gradient along the surface of the deck, and figures 3.15 and 3.16 show the gradient down the wall and along the bed respectively for a selection of values of a. On the wall and the bed the pressure gradient is tangential since $\partial P/\partial n = 0$. However, on the deck where the impact occurs $\partial P/\partial n \neq 0$ so that there is also a component of impulse perpendicular to the deck and downward. This could be particularly dangerous for a fixture on the lower surface of the deck, for example a pipe. The upward impact on the pipe due to direct impact from the wave is accompanied by a downward impulse when the wave hits the deck above. The direction of pressure-impulse gradient can be found from the contour diagrams since it is perpendicular to the contours in the direction of decreasing pressure impulse.

101
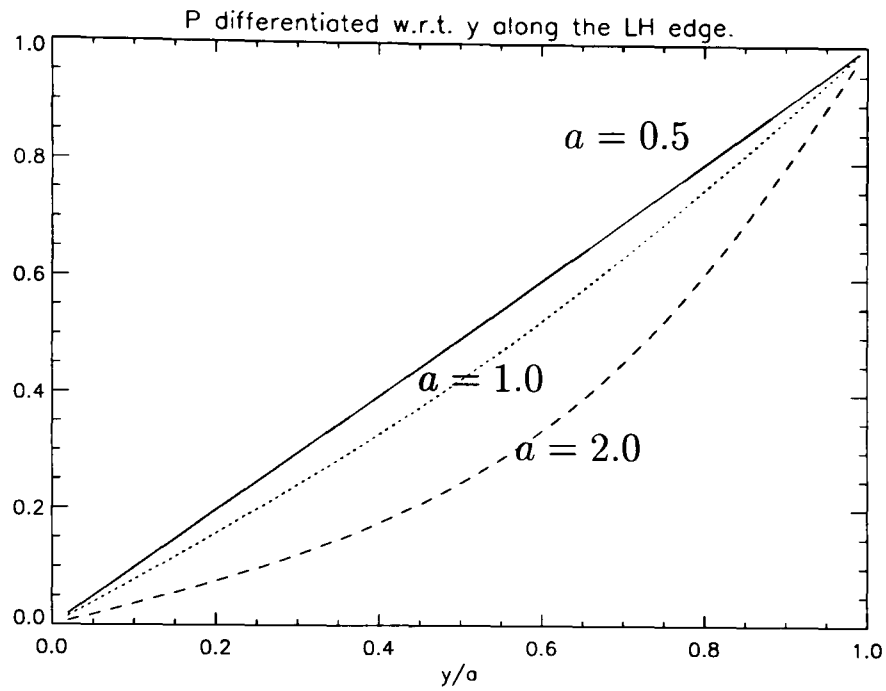
Figure 3.15: $\frac{\partial P}{\partial y}$ along the left hand wall.
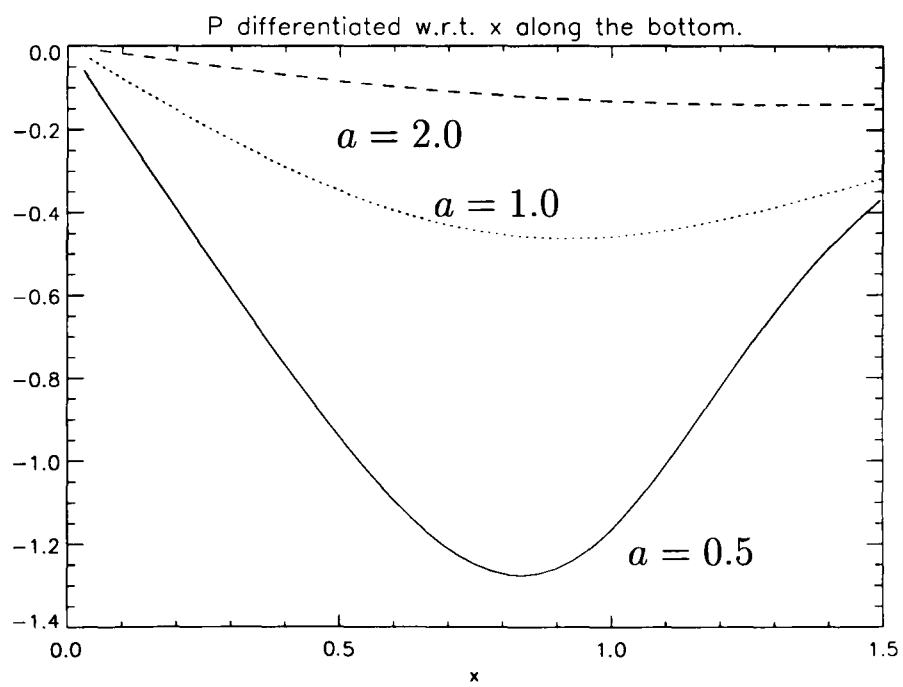
Figure 3.16: $\frac{\partial P}{\partial x}$ along the bottom.

102

Consideration of the gradient of pressure impulse near the edge of the deck shows alarmingly high values because the mathematical solution has a singularity at the edge of the deck. Clearly a better approximation is needed there. One simple way of obtaining more realistic values is to consider how the solution is obtained for the infinite-depth case, $a = \infty$. There, the solution for the flow past a plate is used. This solution is a limit of flow past an ellipse. Thus a somewhat better solution could be obtained from the flow past a slender ellipse. In any case, it seems reasonable to conclude that attachments beneath a deck are vulnerable to especially large impact forces if they are near the edge of the deck, or the edge of the impact zone.

3.8 Estimation of velocity of impact.

We note that throughout this account we have taken the vertical velocity of impact to be uniform and of magnitude one. In this section we make a more realistic approximation for the magnitude and distribution of the impact velocity and also for the impact width. As a standing wave evolves in time a peak in the free surface evolves. It is therefore a reasonable approximation to consider the evolution of a standing wave, and estimate the pressure impulse involved in the impact of the standing wave under a deck. We make an estimate of the vertical velocity of the standing wave and the approximate width of the wave which undergoes impact with the deck. So, we can then feed these parameters into the general impact on a deck model to calculate the appropriate pressure impulse. We need the width and velocity of the standing wave at still water level because, in the deck impact model, we assume that impact occurs at water level.

Many studies have been carried out on the approximation of standing wave profiles, for example Mercer and Roberts (1992, 1994) and Tsai and Jeng (1994). From Mercer and Roberts (Private communication) we obtain a profile for a standing wave on finite depth. The profile used in this section has initial acceleration -0.85, depth 1.0, 64 surface points, period 7.275, and steepness 0.167, in units with $g = 1$.

The initial wave profile and velocity profile are shown in figure 3.17.
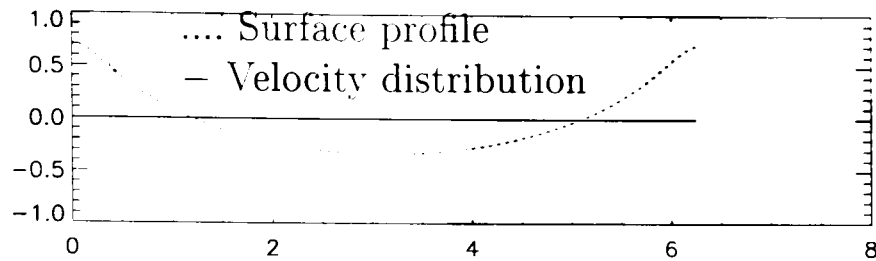
Figure 3.17: Initial surface and velocity profiles for a standing wave: depth 1.0, Initial acc. -0.85, period 7.275, steepness 0.167.(Mercer and Roberts (Private communication))

We then use a periodic version of a numerical boundary-integral method (described very briefly here, see Dold (1992), Dold and Peregrine (1986), Cooker (1990) for further details) to calculate the surface profiles and vertical velocity as the wave evolves. Let $(x, y) = (X(s,t), Y(s,t))$ be a point on the free surface, where t is time, and s is a time independent parameter. The fluid is incompressible and irrotational so there is a velocity potential, ϕ, which satisfies Laplace's equation:

$$\nabla^2 \phi = 0. \tag{3.9}$$

On the impermeable bed we require:

$$\frac{\partial \phi}{\partial n} = 0, \tag{3.10}$$

where n is normal to the bed. We also need to impose the free surface kinematic and dynamic boundary conditions:

$$\nabla \phi = \left(\frac{\partial X}{\partial t}, \frac{\partial Y}{\partial t} \right) \tag{3.11}$$

and

$$\frac{\partial \phi}{\partial t} + \frac{1}{2} \left[\left(\frac{\partial \phi}{\partial x} \right)^2 + \left(\frac{\partial \phi}{\partial y} \right)^2 \right] + gY = 0. \tag{3.12}$$

We use a periodic version of the boundary integral method, which solves Laplace's equation subject to the above boundary conditions, but also keeps the flux of the fluid going in and out of the fluid region as a constant.

We need to find the velocity distribution of the wave when the surface profile is almost flat at water level. This is achieved at time 0.067 as shown in figure 3.18.
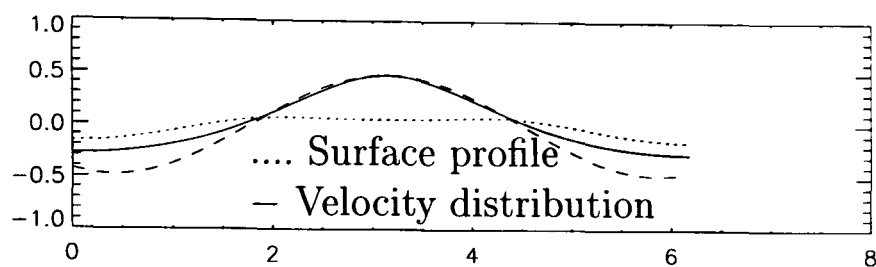
Figure 3.18: Surface and velocity profiles for a standing wave at time t=0.067 : depth 1.0, Initial acc. -0.85, period 7.275, steepness 0.167, evolved using a boundary integral method program.

The plot is obviously symmetric about π so we take this to be the position of the wall, and take the length of the deck to be half the length of the 'flat' part of the surface profile: 1.46. On examination of figure 3.18, we see that the velocity profile is approximately sinusoidal over the region where the impact would occur. If we feed in this velocity profile ($V = 0.48\cos(1.15x)$), and the length of the deck into the general deck impact program we can obtain the pressure impulse contours shown in figure 3.19. The dashed line in figure 3.18 shows the cosine velocity distribution used for figure 3.19.
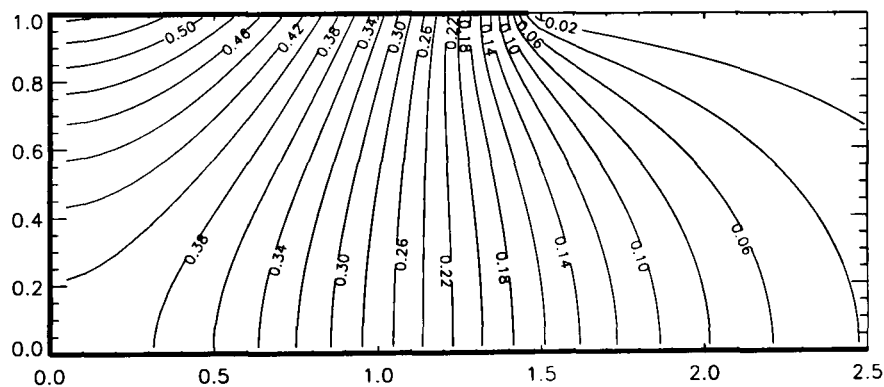
Figure 3.19: Dimensional pressure-impulse $/\rho$ contours for a deck of length 1.46. and velocity profile from a standing wave.

Hence the contours plotted in figure 3.19 give more realistic pressure-impulse

contours. It may be more appropriate to choose the contour of 0.02 as the free-surface, hence we would subtract 0.02 from the pressure-impulse values in the figure.

3.9 Three-dimensional effects.

All the above work assumes uniformity perpendicular to the (x, y) plane, or some rigid boundaries parallel to that plane. In practice this is unlikely, and three-dimensional effects may be important. That is the impact area on the deck, rather than being a long strip of finite width L, should be taken as a finite area of an appropriate shape. A simple approach to looking at a more three-dimensional solution is to examine infinite depth solutions. A solution for impact on an elliptic area can be found from the potential flow round an ellipsoid.

3.10 Impact of an elliptic plate on infinite depth of water.

If we consider the impact of an elliptic plate on infinite depth of water, this is equivalent to elliptic impact on a deck. Consider as in Lamb (1995, section 114) and Milne-Thompson (1963, section 16.50) an ellipsoid given by equation (3.13), where a, b and c are the lengths of the semi-axes. We take our length scale L to be semi axis b, which we set to be 1.

$$\frac{x^2}{a^2} + y^2 + \frac{z^2}{c^2} = 1 \tag{3.13}$$

The velocity potential for the motion of a fluid at rest with a solid ellipsoid passing through it with velocity $U(= 1)$ in the x direction is given by:

$$\phi = Cx \int_\lambda^\infty \frac{d\lambda}{(a^2 + \lambda)\Delta}, \tag{3.14}$$

where,

$$C = \frac{ac}{2 - \alpha_0} \tag{3.15}$$

and α_0 and Δ are given by:

$$\alpha_0 = ac \int_0^\infty \frac{d\lambda}{(a^2 + \lambda)\Delta}. \tag{3.16}$$

106

$$\Delta = \left[(a^2 + \lambda)(1 + \lambda)(c^2 + \lambda)\right]^{\frac{1}{2}}. \tag{3.17}$$

λ is given by the positive root of the following cubic equation:

$$x^2(1+\lambda)(c^2+\lambda) + y^2(c^2+\lambda)(a^2+\lambda) + z^2(a^2+\lambda)(1+\lambda) - (a^2+\lambda)(1+\lambda)(c^2+\lambda) = 0, \tag{3.18}$$

where the positive root is taken, as then $\lambda = $ constant corresponds to ellipsoids. NAG routine C02AEF was used to solve the cubic for λ.

To obtain the velocity potential for an elliptic plate moving through the liquid we need to take $a \to 0$. However if we take $a \to 0$ directly then the integral, α_0, becomes singular, so we begin by making a change of variables $u = \lambda + a^2$.

$$\phi = Cx \int_{\lambda+a^2}^{\infty} \frac{du}{u^{\frac{3}{2}}(u+1-a^2)^{\frac{1}{2}}(u+c^2-a^2)^{\frac{1}{2}}} \tag{3.19}$$

We denote the integral (or ϕ/Cx) as J. Hence,

$$J = -2 \int_{\lambda+a^2}^{\infty} \frac{d(1/u^{\frac{1}{2}})}{(u+1-a^2)^{\frac{1}{2}}(u+c^2-a^2)^{\frac{1}{2}}}. \tag{3.20}$$

Integration by parts gives:

$$J = \frac{2}{\left[(\lambda+a^2)(\lambda+1)(\lambda+c^2)\right]^{\frac{1}{2}}} \tag{3.21}$$
$$+2 \int_{\lambda+a^2}^{\infty} \frac{-1}{u^{\frac{1}{2}}} \left[\frac{1}{2(u+1-a^2)^{\frac{3}{2}}(u+c^2-a^2)^{\frac{1}{2}}} + \frac{1}{2(u+1-a^2)^{\frac{1}{2}}(u+c^2-a^2)^{\frac{3}{2}}} \right] du.$$

With some rearrangement and taking $\lambda \to 0$ we have:

$$J(\lambda=0) = \frac{2}{ac} - \int_{a^2}^{\infty} \frac{2u+1+c^2-2a^2}{u^{\frac{1}{2}}(u+1-a^2)^{\frac{3}{2}}(u+c^2-a^2)^{\frac{3}{2}}} du. \tag{3.22}$$

From equation (3.16) and (3.22), we get an expression for α_0 as $a \to 0$:

$$\alpha_0 = 2 - a\left[c \int_0^{\infty} \frac{2u+1+c^2}{u^{\frac{1}{2}}(u+1)^{\frac{3}{2}}(u+c^2)^{\frac{3}{2}}} du\right] + O(a^2). \tag{3.23}$$

Hence C is given by:

$$C = 1 / \int_0^{\infty} \frac{2u+1+c^2}{u^{\frac{1}{2}}(u+1)^{\frac{3}{2}}(u+c^2)^{\frac{3}{2}}} du, \tag{3.24}$$

when $a = 0$. So, from equations (3.14) and (3.24), with $a = 0$ in equation (3.14), we can find values for ϕ for an elliptic plate moving with velocity 1 in a stationary liquid. ϕ satisfies the same conditions we require P to satisfy. Hence we can get plots for the pressure impulse for an elliptic plate dropping onto an infinite body of liquid. Integration is carried out using NAG routine D01AMF. Figure 3.20 shows the pressure-impulse contours when $c = 100.0$. Here the ellipse is so long that it is the same as the infinite depth solution shown in figure 3.2. Figure 3.21 shows the
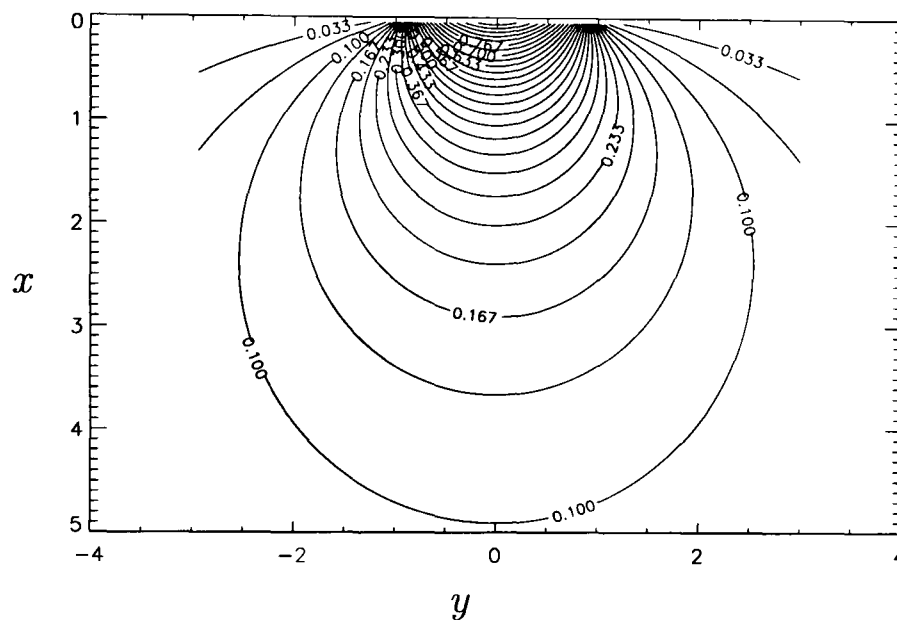
Figure 3.20: Pressure impulse for impact of an elliptic plate on an infinite body of water. $c = 100.0$ and $z = 0$. Maximum P is 0.99973.

pressure-impulse distribution below a circular plate of radius 1. Figures 3.22 and 3.23 show two more examples of elliptic plate impact. Figure 3.24 shows a plot of pressure impulse down the line from the centre of the ellipse perpendicular to the plate.

Near the plate the pressure impulse is at its largest for the larger values of c. The larger the value of c the deeper the impact penetrates the liquid.

Care must be taken in evaluating pressure impulse on the plate itself. In particular in evaluating the integral (3.19). From equation (3.18), we obtain on the plate:

$$a^2 + \lambda = \frac{x^2}{1 - y^2 - z^2/c^2}.$$

(3.25)

108
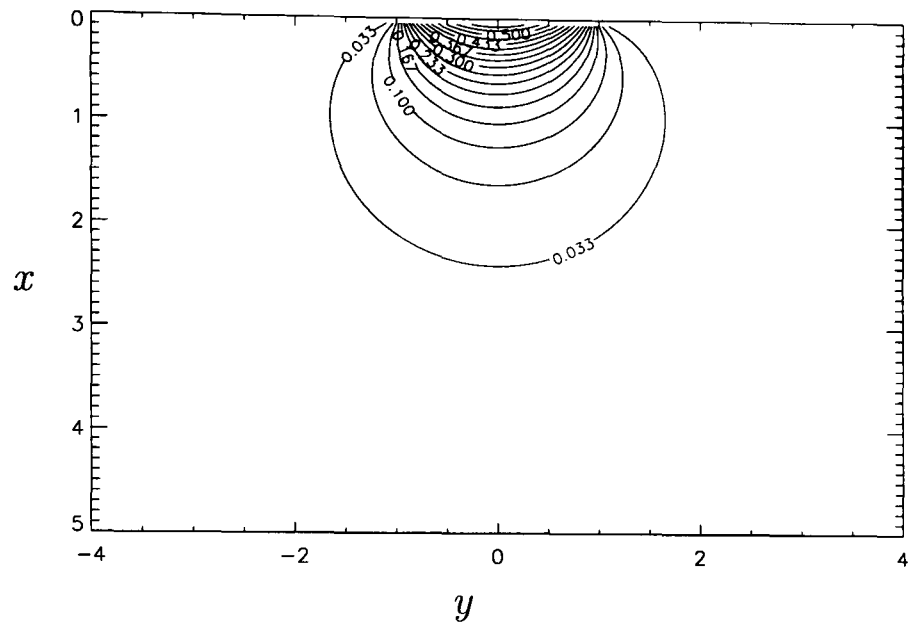
Figure 3.21: Pressure impulse for impact of a circular plate on an infinite body of water. $c = 1.0$ and $z = 0$. Maximum P is 0.63662.
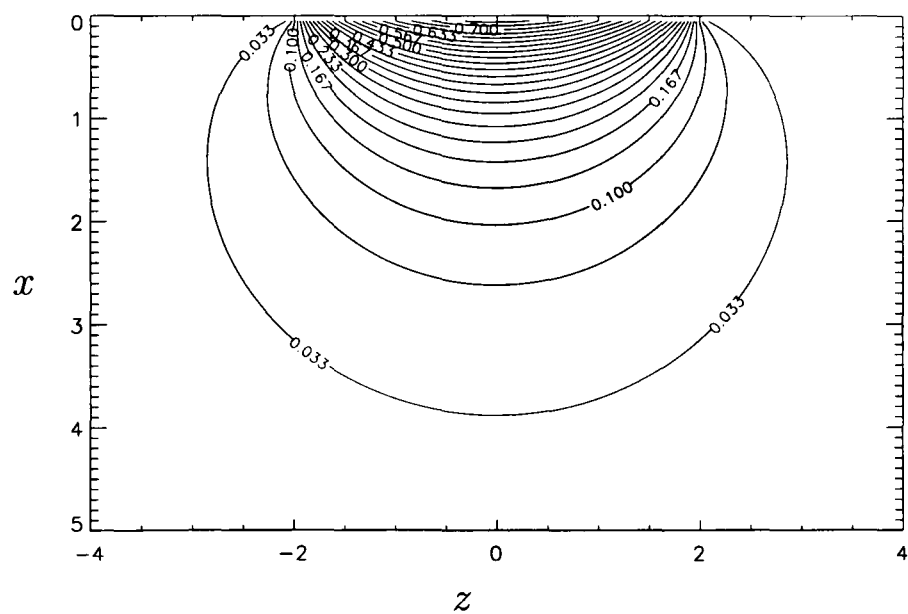
Figure 3.22: Pressure impulse for impact of an elliptic plate on an infinite body of water. $c = 2.0$ and $y = 0$. Maximum P is 0.82573.
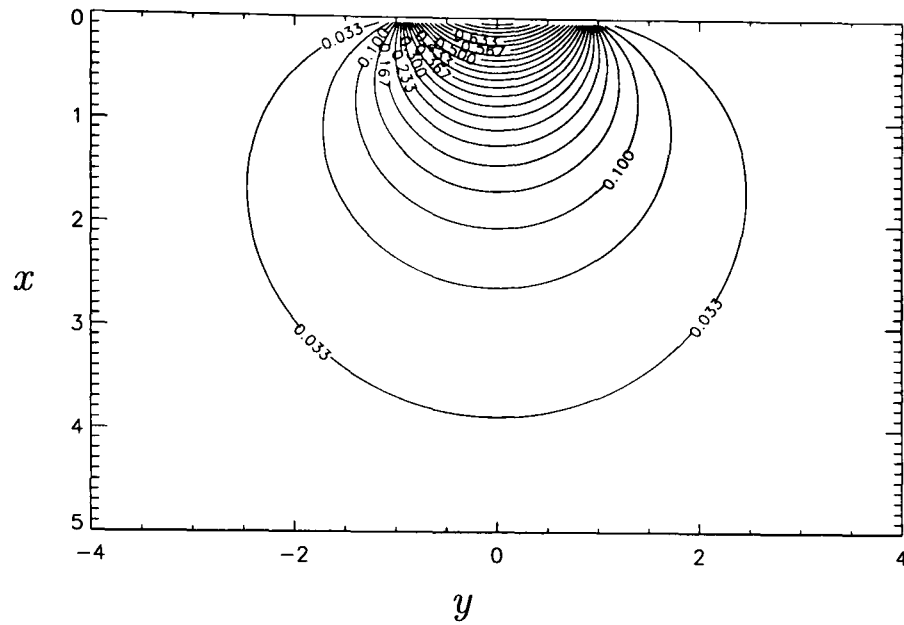
Figure 3.23: Pressure impulse for impact of an elliptic plate on an infinite body of water. $c = 2.0$ and $z = 0$. Maximum P is 0.82573.
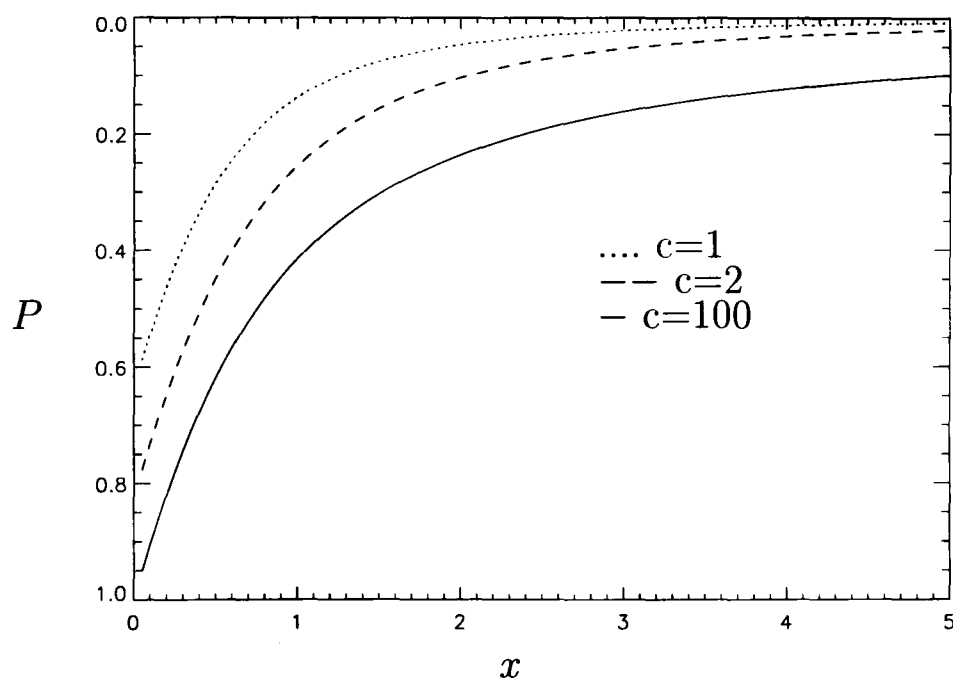
Figure 3.24: Pressure impulse for impact of an elliptic plate. Plots are down the line from the centre of the ellipse, perpendicular to the plate.

110

we also note that:

$$\int \frac{du}{u^{\frac{3}{2}}} \sim -\frac{2}{3u^{\frac{1}{2}}}, \tag{3.26}$$

near the origin. Hence the integral in equation (3.19) is dominated by $2/[3c(a^2 + \lambda)^{\frac{1}{2}}]$, as $a \to 0$, which equals: $2(1-y^2-z^2/c^2)^{\frac{1}{2}}/cx$. Hence the x in equation (3.19) cancels with the x from the approximation of the integral, and we can evaluate P on the plate using:

$$P = \frac{2C(1 - y^2 - z^2/c^2)^{\frac{1}{2}}}{c}, \tag{3.27}$$

where C is still given by equation (3.24). Figure 3.25 shows a plot of pressure-impulse contours on the plate for an elliptic plate, $c = 2$. We note that the total impulse is given by $4\pi C/3$. Note the closeness of the contours towards the edge of the plate. This high pressure-impulse gradient again indicates that attachments at the edges of the impact region, i.e. the edges of the ellipse, would be subject to alarmingly high velocity components. Finally, we examine how C varies with $1/c$,
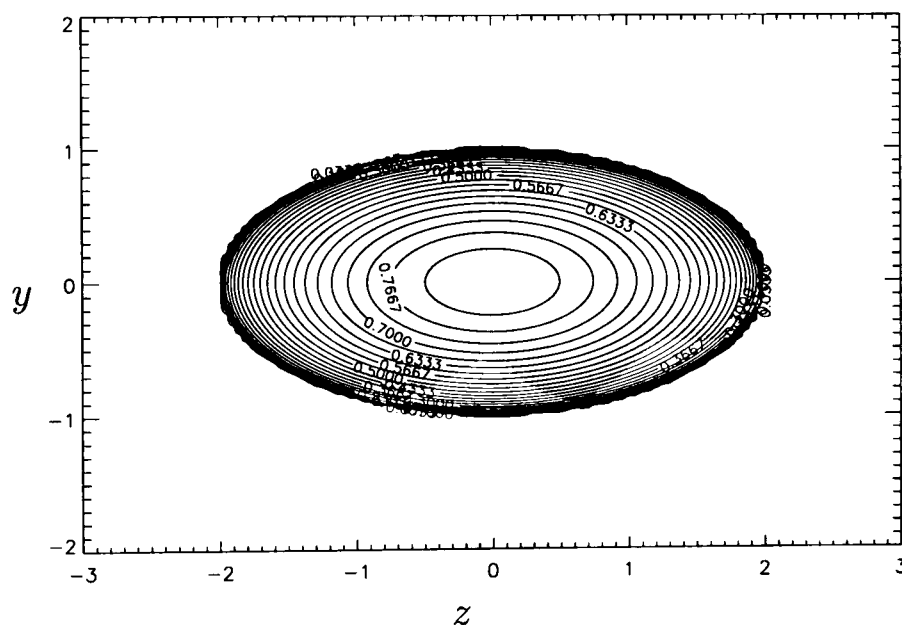
Figure 3.25: Pressure impulse for impact of an elliptic plate, $c = 2$, with contours on the plate.

which is plotted in figure 3.26. We see that as $1/c$ increases C increases linearly. If we look at figure 3.27 which is a plot of Cc, we see that C divided by the aspect ratio of the ellipse tends to 0.5 as $1/c$ becomes very large. The significance of this is unclear. This is what we would expect from the infinite depth solution.

111
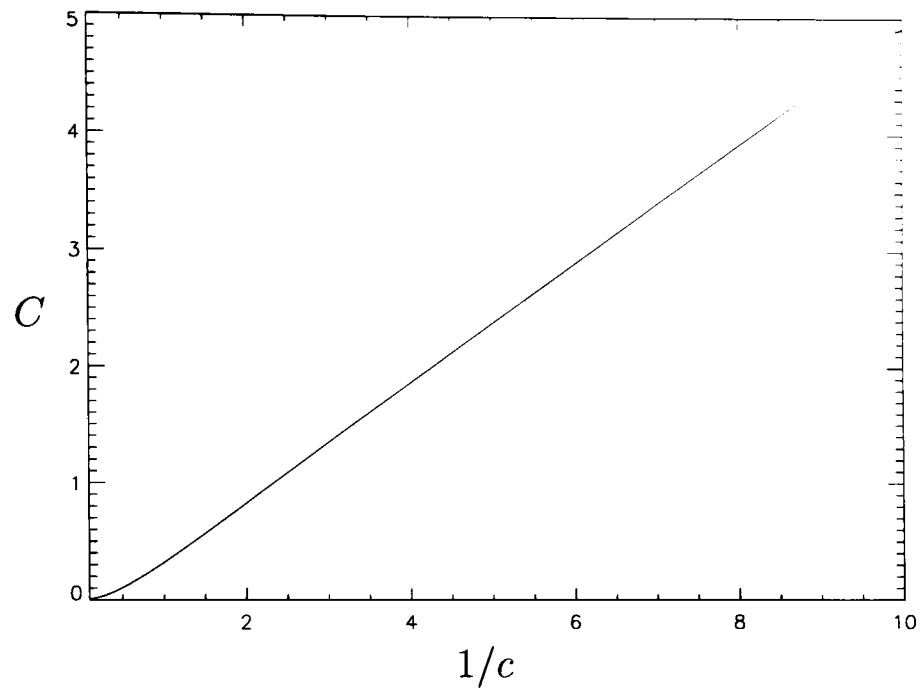
Figure 3.26: C against $1/c$, for impact of an elliptic patch.
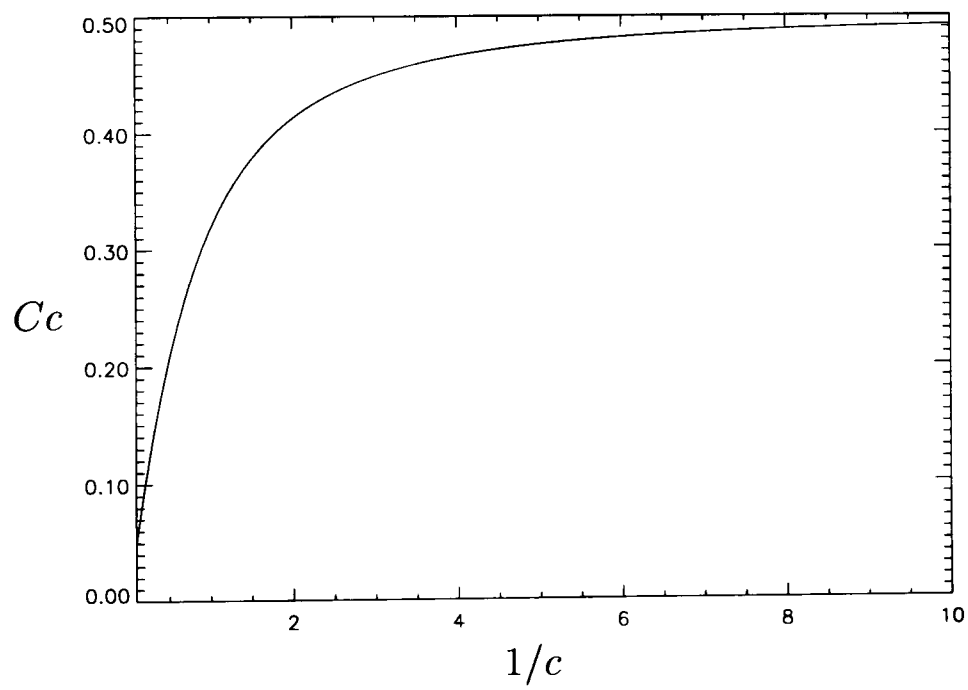
Figure 3.27: Cc against $1/c$, for impact of an elliptic patch.

3.11 Method of solution.

Whilst the method used in this thesis for this problem is complex maps and Fourier series there are many other methods which could have been used. Other methods include: 1) Boundary-integral method and 2) Finite element or differences. Both of these methods would work well for the problems in both this and the previous chapter. Both methods are more easily adapted to different geometries than the method in this chapter. The second method would be more appropriate for extensions to three-dimensional models. However for both of these methods rather complex computations are required. The advantage of the methods used in this and the preceding chapter is the very simple formulae which arise. In addition as we are only evaluating a Fourier series each time, most of the problems take very short periods of time on a computer to evaluate.

3.12 Conclusions.

A readily evaluated 2D solution is presented for the pressure impulse from waves hitting a deck from below. It is found that, for a fixed impact velocity, the impulse is greater if the water is shallower. The same results may be useful for estimating the effects of upward impact by liquid confined within a container.

If we consider the problem in terms of keeping the depth of water constant and varying the length of deck we find that the maximum pressure impulse, the total impulse, total moment along the left hand wall, and the total impulse along the deck all increase, as we would expect, with increase of the length of deck.

It is also important to notice that there is a downward impulse away from the deck, hence anything attached beneath it, such as a pipe, experiences a downwards force which may be substantial enough to pull it away from the main deck.

A three-dimensional solution for impact on an elliptic deck is also given. Again there is a high pressure-impulse gradient at the edge of a deck. Physically a splash may occur at the edge of the plate.

Chapter 4

Impinging jets.

4.1 Introduction.

A wave begins to break when the wave crest begins to overturn. However, the specific way a wave breaks can vary greatly from one wave to the next. Classification of waves is largely dependent on the form of the front of the wave. Peregrine (1991) gave a review of wave breaking, and described these classifications. Breaking waves can be grouped into two categories: plunging and spilling breakers. When a wave begins to break a well-defined jet of water may plunge forward from the front of the wave (a plunging breaker), or alternatively the water at the top of the wave crest may come 'spilling' down the front of the wave (a spilling breaker). Of course in practice it is not so easy to classify waves into clearly defined categories, as often the waves are somewhere in between these two categories. In addition, if the wave is breaking on a beach, instead of just the crest of the wave being involved in the breaking process, it may be that a high proportion of the wave front collapses leading to another category of 'collapsing' or 'surging' breakers.

In this chapter we look in particular at the case of a plunging breaker. In the case of a well developed plunging breaker a well developed jet of water is projected from the front of the wave. Many studies have been carried out to examine the plunging breaker motion. However, even in the cases where the model is capable of computing the evolution of the jet, the modelling terminates once the jet impacts on the undisturbed water in front of the wave. When the jet impacts on the surface

111

a splash occurs, and it is this 'splashing' that we attempt to model later in this chapter. The jet impacting on the undisturbed surface is similar to a jet impacting on an infinitely wide jet. To make a start we investigate steady flow problems. For a thin jet there may be value in this since jet properties may change little while a water particle passes into the splash. Two methods are examined. First we model two finite jets impacting, and taking the limit as one jet becomes infinitely wide (an extension of a model described in Milne-Thompson (1962)). Secondly we assume that one jet is infinitely thick from the start of the calculation.

4.2   Evolution of the jet from a plunging breaker.

It is difficult to compute wave breaking. The first numerical models of the evolution of a plunging wave broke down when the wave began to overturn. Longuet-Higgins and Cokelet (1976) was the first numerical study which could accurately continue the calculation even after the wave had begun to break. They used a boundary-integral technique to compute breaking waves in deep water which nicely showed the formation of the jet during the plunging motion. However, once the curvature of the wave near the jet tip becomes too high the model of the jet is no longer reliable. That paper looked largely at the surface profile of the wave, however, Cokelet (1979) extended the method and reported the fluid velocities and accelerations below the surface. These values were calculated using Cauchy's theorem which meant only the values at the free surface needed to be known. This method was used by Peregrine, Cokelet and McIver (1980), to look again at the velocities and accelerations below the wave. They identified a region of high particle acceleration at the front of the wave, and a region of low acceleration at the rear of the wave. It was suggested that this area of low acceleration gave support to the high pressure gradients at the front of the wave which were required to accelerate the fluid particles into the jet.

Peregrine (1983) gave a review of wave breaking which in particular described the background to classification of waves, their instabilities, the mechanism of over-

turning and the evolution of a plunging breaker. He also gave some description (and photographs) of what occurs when the jet of water from the plunging breaker impacts on the free surface in front of the wave. (see later)

New, McIver and Peregrine (1985) extended the work of Longuet-Higgins and Cokelet (1976) to account for finite uniform depth. This was done by adjusting the Green's function in the boundary-integral method to plot breaking waves on a finite depth of water. This study included a look at the projection of a small-scale jet at the wave crest, and presents calculations of the evolution of the jet up to the time the jet almost reaches the water surface again.

As an alternative to these numerical methods more analytical methods were also developed. Longuet-Higgins (1982) looked in particular at the forward face of the wave. He did this by examining a series of time-dependent flows given in parametric form. In particular he examined the flow of a decelerating liquid flowing upwards with a surface of zero pressure above it. This particular flow could be solved using these parametric methods, and was found to be part of a family of complementary solutions. One of this family of curves was found to have many similarities to the flow at the forward face of a plunging breaker. The paper also included some good photographs of plunging jets impacting on water.

New (1983) examined the profile of a wave with a plunging jet in front, concentrating on the loop below the jet. By noticing that the shape below the jet was often an ellipse he obtained some exact solutions for the free-surface under the jet. In particular these solutions continued to give reasonable approximations to 'real life' even after the jet had hit the free surface in front. However, no model of the actual impact of the jet was put forward.

New's solution was for the loop under the jet, whereas Longuet-Higgins' model was for the forward face of the plunging wave. Greenhow (1983) noted that they were both in fact complementary solutions of the same equation. By examining this equation further he combined and extended the two solutions to give an approximate

116

solution which predicts the profile of the forward face, loop and rear of the wave all in one model.

Another approach was to look at the vortex motion which occurs during wave breaking. Basco (1985) has both descriptions and some photographs of the jets from the plunging breakers impacting on water and concentrated on the vortex motion involved in the splash process. He commented that there are two vortex motions, one caused by the jet 'splashing up' and another surface vortex (a similar mechanism to that involved in a hydraulic jump). A similar approach was taken in Tallent, Yamashita, & Tsuchiya (1990), where the importance of the vortex motion in the impact of the jet of water from a plunging breaker was investigated. He comments that when the jet first impacts down, the high acceleration of the fluid, which accelerates the fluid particles towards the wave crest, causes the liquid in the jet to be swept towards the wave crest. However, as the wave continues to propagate a 'splash-up' occurs. Tallent, Yamashita, & Tsuchiya (1990) note that the splash up occurs in almost the vertical direction with a slight tendency to splash backwards on to the incoming plunging jet.

Dommermuth, Yue, Lin, Rapp, Chan and Melville (1988) also developed a model by using potential flow theory for steep gravity waves. Their model, which used a mixed Eulerian-Lagrangian method, gave good predictions of plunging wave profiles which compared well with experiment.

Peregrine (1991) gave a general discussion of the position of breaking wave research. He summarized the current thinking on the mechanism behind breaking waves and their instabilities.

A recent study, Jenkins (1994), uses a reference frame moving with the wave crest to represent the flow in a breaking-wave crest by a complex velocity potential on a Riemann surface. The interaction of the jet with the rest of the fluid is neglected. A conformal transformation is used and the Bernouilli condition is forced to hold on the boundary, and the resulting equations are solved numerically. Plots of jets

117

from the breaking wave crests are shown, falling past the free surface on a different sheet of the Riemann surface. In this chapter we similarly choose a reference frame moving with the impact, and seek a steady solution. We also use one of the plots in Jenkins (1994) to obtain a feasible breaking wave jet angle to feed into our model.

4.3   Jets and splashes.

We now look at the plunging wave jet impacting on a body of water as an extreme case of two impinging jets. In the 18th and 19th century Borda, Helmholz and Kirchoff all examined flows of jets, in particular the flow of a jet from an orifice. The use of complex analysis to study these types of free-streamline flows was developed. Milne-Thompson (1962) used these methods, which we will extend, in his discussion of two jets impacting. This model is also given in Gurevich (1965), which also refers back to many old sources, including Zhukovskii (1890), Voight (1886) and Cisotti (1921). An important assumption is that we have steady flow and hence a stagnation point. Milne-Thompson's conclusion is that if we just state the width and angle of the incoming jets, in general, a unique solution is not possible. However, in the case of symmetric jets, or where another piece of information is given, the solution may be forced to be unique.

More recently the importance of studying jet impact to aid understanding of wave breaking has been recognized. Peregrine (1983) described how when a plunging breaker impacts on water a 'splash-up' occurs. He included some photographs showing the occurrence of the splash. He asked where does the water in the splash-up comes from? Among other possibilities he concluded that the splash-up, or outgoing jet, may consist partly of water from the incoming jet and partly of the fluid from the undisturbed water. He noted that this process of splashing can be repeated several times, where the outgoing jet (or splash) next becomes the incoming jet and the splashing continues in a cycle. However, other effects become important soon after impact, such as air, surface tension, drops, bubbles and vorticity. Basco (1985)

mentioned this splash up, and discussed the vortex which is produced beneath the jet. Peregrine (1981) carried out analysis for a 'splash' on very shallow water. Using the Bernoulli equation, and conservation of mass and momentum a simple model for the 'splash' was found.

Impact of jets was further investigated by Keller (1990) and Frankel and Weihs (1990). Keller extended Milne-Thompson's theory by introducing a parameter for the lateral offset positions of the two jets in the far-field. Providing this piece of information is enough to provide a unique solution to the problem. Keller showed many plots of jets impacting. Frankel and Weiss looked at glancing impact of two jets. They considered a change in reference frame for the glancing impact case which then allowed them to consider the impact as impinging jets. They too extended Milne-Thompson's method, but as they assume that one jet is infinite in depth they do not require Keller's fourth condition. Hence, a solution to the impinging jet problem where one jet is infinite is given, however it is an asymptotic solution, and is only used as a way to examine glancing impact and it not investigated further.

Work on splashes in general is very closely linked with the impact of the plunging breaker. Dias and Christodoulides (1991) examined a two-dimensional jet emerging from a nozzle using the Bernoulli equation and complex analysis. In particular they examined the case of the bow splash which was found to involve similar mathematics. Here the water on the bow of a ship splashes back on itself, however the calculation stops when the jet impacts on the water, unless it is taken to be on another Riemann surface.

4.4   Milne-Thompson model.

4.4.1   General model.

Consider a plunging breaker, where the jet is well developed. Eventually the jet will impact with the undisturbed water in front of the wave. Figure 4.1 shows a sketch of a possible plunging breaker with a well developed jet impacting on undisturbed

119

water in front of the wave. The dotted lines shows where the 'splash up' may occur.
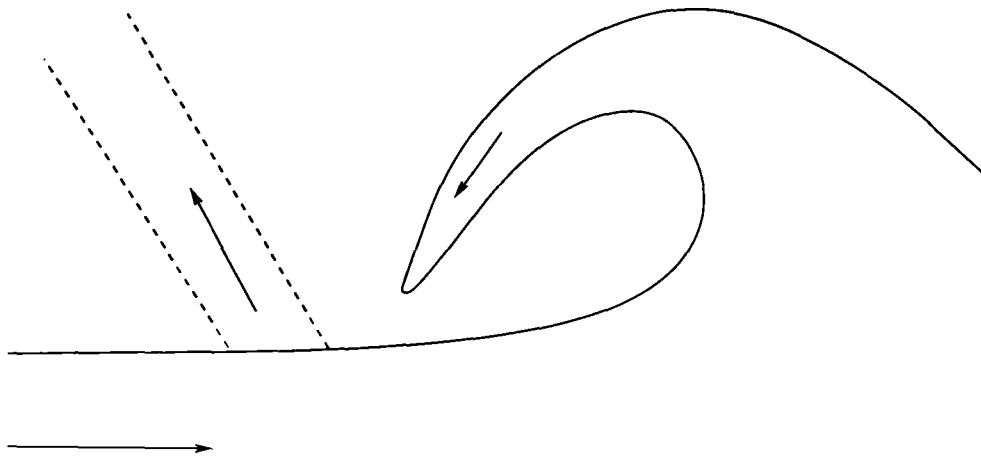
Figure 4.1: Plunging breaker with a well developed jet impacting on undisturbed water in front of the wave. The dotted lines shows where the 'splash up' may occur.

Where the jet from the breaker impacts on the undisturbed water it is very similar to a jet of water impacting on an infinitely thick jet of water. We choose a reference frame moving with the impact. Milne-Thompson (1962) examined the case of two finite impinging jets. We follow this analysis at first and extend it by looking at what occurs if one of the jets is infinitely thick. We aim to consider two impinging jets which undergo steady motion, as shown in figure 4.2. We note that this model is the simplest possible where we ignore any vortex sheets which are generated and assume steady motion. We assume inviscid, two-dimensional motion and that the splash is so quick we can neglect gravity.

On a free streamline ψ (the streamfunction), speed, and pressure are constants. If at ∞ one of the incoming jets has speed U, then as the edges of the jets are free streamlines, and so have constant speed, all four jets must have speed U at ∞. Without loss of generality U can be chosen to be 1. The four jets are assumed to undergo steady motion, and hence where the jets meet a stagnation point is likely (and is assumed) to exist, and continues to exist throughout the motion. The origin is taken to be at the stagnation point. Axes are as shown in figure 4.2. The two incoming jets are of width h_1 and h_2, and the two outgoing jets are of width k_1
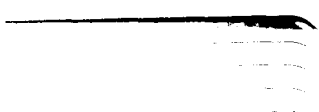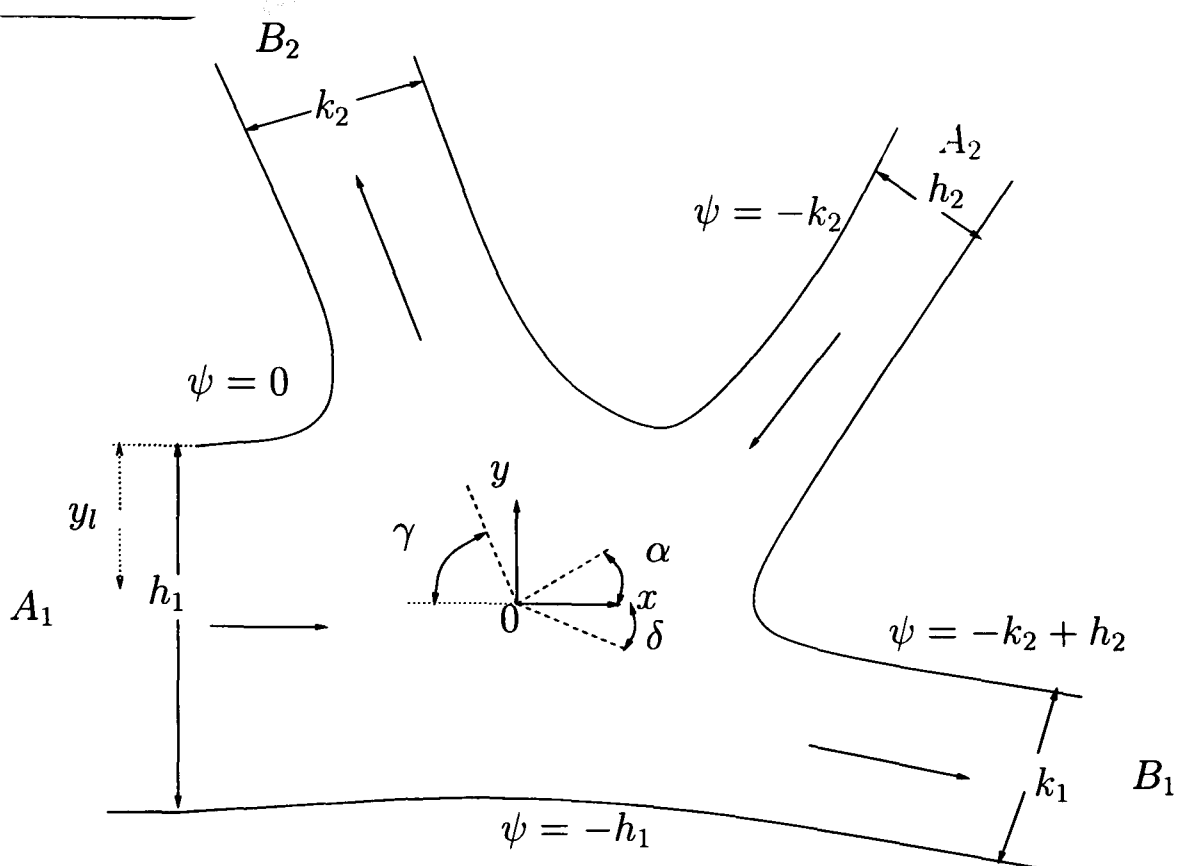
Figure 4.2: Two finite impinging jets undergoing steady motion

and k_2. Values of h_1, h_2, and the angle at which the jet of width h_2 impinges, are assumed to be given. Note that the angles are defined to be between $-\pi$ and π, this is because it it easier to envisage angles of impact which are less than π in magnitude.

Next, let us consider a jet of width h. In time δt, the mass of flow in from this jet is, $h\delta x\rho$, where δx is the distance a portion of fluid has travelled in δt. Therefore in unit time, the mass flowing in from this jet is $h(\delta x/\delta t)\rho = h\rho$ (as $\delta x/\delta t = U = 1$ at ∞). The mass of fluid entering the system must be the same as that leaving it, therefore, using the notation shown in figure 4.2 (and dividing by ρ):

$$h_1 + h_2 = k_1 + k_2 \tag{4.1}$$

The components of momentum are conserved in the x and y directions. Momentum = mass $\times$ velocity. Mass flux= $h\rho$. Therefore flux of momentum= $h\rho$ in the direction of flow. (velocity taken to be one.) Conservation of momentum flux

121

in the x direction (after dividing by ρ) gives:

$$h_1 - h_2 \cos\alpha = k_1 \cos\delta - k_2 \cos\gamma \qquad (4.2)$$

Conservation of momentum flux in the y direction (after dividing by ρ) gives:

$$-h_2 \sin\alpha = -k_1 \sin\delta + k_2 \sin\gamma \qquad (4.3)$$

These equations (4.1-4.3), are three equations for the four unknowns. Now consider the complex velocity, w, which can be written as $w = qe^{-i\theta}$, where θ is the angle of the velocity to the positive x-axis, and q is the speed. To be consistent with Milne-Thompson we take θ to be between -2π and 0. Hence the values for θ (the direction of the velocity), at positions A_1, B_1, A_2, and B_2 are 0, $-\delta$, $-\pi + \alpha$ and $-\pi - \gamma$ respectively. Figure 4.3 shows a plot of $qe^{-i\theta}$. Note that the angles shown are $-\theta$.
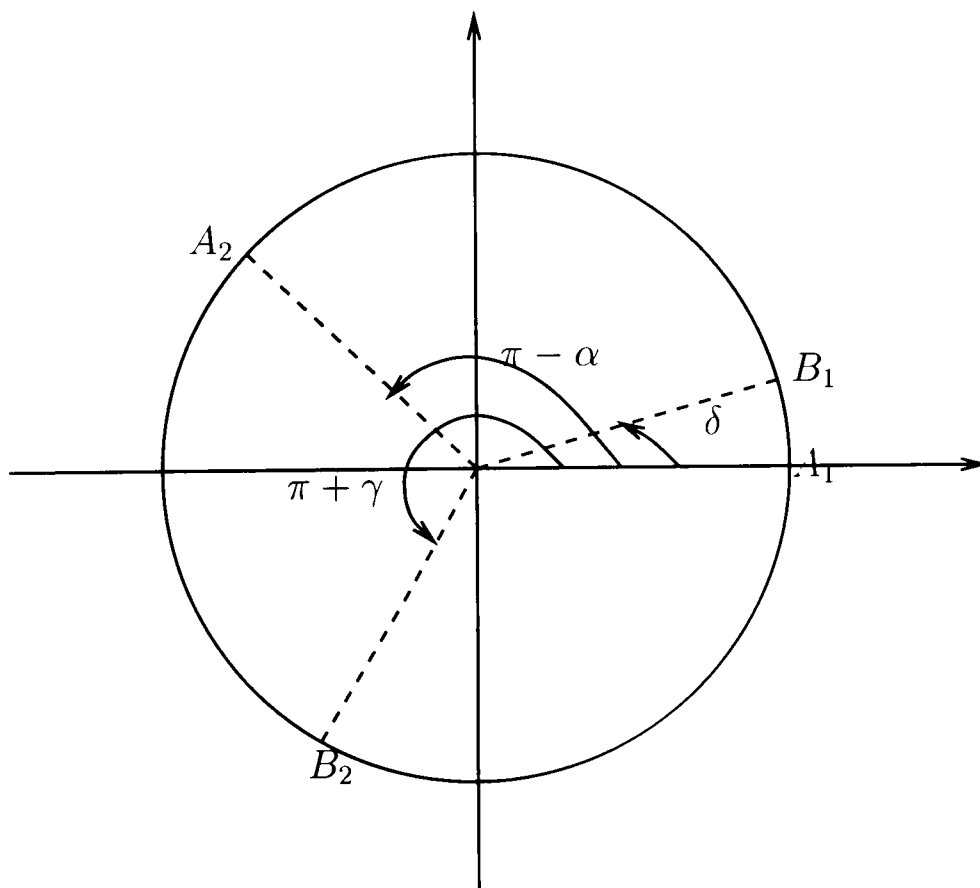
Figure 4.3: The w plane, angles of $-\theta$ are marked.

On the free streamlines, q is a constant, 1, and so $w = e^{-i\theta}$, where $-\theta$ lies

between values which may be deduced from figure 4.3. The flux at ∞ of each of the four jets is h_1, k_1, h_2 and k_2. One can choose a position for $\psi = 0$ arbitrarily. and so we choose $\psi = 0$ on the upper surface of the incoming left hand jet. Flux of fluid crossing a line from $\mathbf{x_0}$ to $\mathbf{x_1}$ is $\psi(\mathbf{x_0}) - \psi(\mathbf{x_1})$. ψ therefore has the values shown in figure 4.2. We use the fact that ψ is the imaginary part of f to find f (the complex potential).

We now need to use the formula of Schwarz as given in Milne-Thompson: Given a circle, centre $z = 0$, radius R, the function $g(z)$, which is holomorphic within the circle and whose real part takes the value $\phi(\theta)$ on the circumference, is given, save for an imaginary constant, by

$$2\pi g(z) = \int_0^{2\pi} \phi(\theta) \frac{Re^{i\theta} + z}{Re^{i\theta} - z} d\theta \qquad (4.4)$$

We know that $\psi = -Re(if)$. So in equation 4.4 we take 'g' as $-if$, and so 'ϕ' takes the values of ψ on the free-streamlines. Integrating around the free streamline, in the w plane, consisting of a circle of radius U=1, gives:

$$2\pi i f = \int_0^\delta h_1 \frac{e^{i\theta} + w}{e^{i\theta} - w} d\theta + \int_\delta^{\pi-\alpha} (k_2 - h_2) \frac{e^{i\theta} + w}{e^{i\theta} - w} d\theta + \int_{\pi-\alpha}^{\pi+\gamma} k_2 \frac{e^{i\theta} + w}{e^{i\theta} - w} d\theta \qquad (4.5)$$

However, we know that:

$$\int \frac{e^{i\theta} + w}{e^{i\theta} - w} d\theta = \theta - 2i \log\left(1 - \frac{w}{e^{i\theta}}\right), \qquad (4.6)$$

and so using this and equation (4.1) we have:

$$\pi f = h_2 \log\left(1 - \frac{w}{e^{i(\pi-\alpha)}}\right) - k_1 \log\left(1 - \frac{w}{e^{i\delta}}\right) - k_2 \log\left(1 - \frac{w}{e^{i(\gamma+\pi)}}\right) + h_1 \log(1 - w) \qquad (4.7)$$

We know that $w = df/dz$, so we also know that $wdz = (df/dw)dw$. Hence, differentiating equation (4.7), and simplifying using the conservation of momentum equations, (4.2) and (4.3), we obtain:

$$dz = \frac{1}{\pi}\left[\frac{k_1}{e^{i\delta}}\frac{1}{e^{i\delta} - w} + \frac{k_2}{e^{i\gamma}}\frac{1}{e^{i\gamma} + w} - \frac{h_1}{1 - w} - \frac{h_2}{e^{-i\alpha}}\frac{1}{e^{-i\alpha} + w}\right] dw \qquad (4.8)$$

From integration and using $z = 0$ when $w = 0$, we get an expression for the position of the streamlines:

$$z = \frac{1}{\pi}\left[h_1 \log(1-w) - \frac{h_2}{e^{-i\alpha}}\log\left(1 + \frac{w}{e^{-i\alpha}}\right) - \frac{k_1}{e^{i\delta}}\log\left(1 - \frac{w}{e^{i\delta}}\right) + \frac{k_2}{e^{i\gamma}}\log\left(1 + \frac{w}{e^{i\gamma}}\right) \right]$$

(4.9)

It is important to remember that when we evaluate the log terms, a suitable cut must be chosen. As the angles in the original problem in figure 4.2 range from $-\pi$ to π, the imaginary part of the complex log evaluation was chosen to also lie between $-\pi$ and π to be consistent.

As Milne-Thompson commented, we now have an equation for the streamlines, however we have four unknowns: k_1, k_2, δ and γ and yet we have only three equations to solve for these: (4.1-4.3). So we need to specify another piece of information. Keller (1990) introduces y_l, where y_l is the vertical offset from the stagnation point to the asymptote of the upper surface of the jet coming in from the left (as shown in figure 4.2). Provided this fourth quantity is given the equations can in theory be solved. A fourth equation in terms of y_l is obtained from taking the imaginary part of equation (4.9) as $\theta \to -2\pi$ from above. The equation in Keller (1990) for y_l, using the angle notation in this thesis, is:

$$\pi y_l = -h_2 \sin\alpha \log\cos\frac{\alpha}{2} + k_1 \sin\delta \log\sin\frac{\delta}{2} - k_2 \sin\gamma \log\cos\frac{\gamma}{2}$$
$$+ \frac{1}{2}[h_2(\pi - \alpha)\cos\alpha + k_1\delta\cos\delta - k_2(\pi + \gamma)\cos\gamma]$$

(4.10)

Hence if we give a value for y_l then we have four equations in four unknowns. However, at this stage we still have finite widths of jets.

4.4.2 Approximations.

For the case of a plunging breaker jet we need to consider making h_1 large compared with h_2. So we let $h_2/h_1 = \eta$, where η is small. We also make the assumption that the large jet is not deflected very much from the horizontal, i.e. δ is assumed

Dividing equation (4.1) by h_1 gives the following equation:

$$1 + \eta = \frac{k_1}{h_1} + \frac{k_2}{h_1} \tag{4.11}$$

Dividing equation (4.2) by h_1, and using equation (4.11) gives:

$$1 - \eta \cos \alpha = (1 + \eta - \frac{k_2}{h_1}) \cos \delta - \frac{k_2}{h_1} \cos \gamma \tag{4.12}$$

Now let k_2/h_1 be denoted by λ. So we have now effectively taken the width of the large ingoing jet as our length scale. Using the fact that δ is small to make the approximation $\cos \delta \approx 1 - \frac{1}{2}\delta^2$ gives:

$$1 - \eta \cos \alpha = (1 + \eta - \lambda)(1 - \frac{1}{2}\delta^2) - \lambda \cos \gamma \tag{4.13}$$

Next we rearrange this equation, and neglect small terms to obtain an expression for λ:

$$\lambda = \frac{\eta(\cos \alpha + 1) - \frac{1}{2}\delta^2}{1 - \frac{1}{2}\delta^2 + \cos \gamma} \tag{4.14}$$

Dividing equation (4.3) by h_1, and using equation (4.11) gives:

$$-\eta \sin \alpha = -(1 + \eta - \lambda)\delta + \lambda \sin \gamma \tag{4.15}$$

Rearranging this equation we obtain another expression for λ:

$$\lambda = \frac{-\eta(\sin \alpha - \delta) + \delta}{\sin \gamma + \delta} \tag{4.16}$$

Equating the two expressions for λ ((4.14) and (4.16)), rearranging, and neglecting terms smaller than η and δ^2 we obtain:

$$\eta = \frac{\delta(1 + \cos \gamma + \frac{1}{2}\delta \sin \gamma)}{\cos \alpha \sin \gamma + \sin \gamma + \sin \alpha + \sin \alpha \cos \gamma} \tag{4.17}$$

From this equation we can see that $\eta \sim \delta$, so we can neglect the δ^2 terms for a first approximation, which transforms equation (4.14) to:

$$\lambda = \frac{\eta(\cos \alpha + 1)}{1 + \cos \gamma} \tag{4.18}$$

125

Now let $K = (\cos \alpha + 1)/(\cos \gamma + 1)$. Using equations (4.15) and (4.18) gives:

$$\eta = \frac{\delta}{\sin \alpha + K \sin \gamma} \tag{4.19}$$

We now have four equations (4.10, 4.11, 4.18 and 4.19) for the four unknowns. However, given a value for y_l it is difficult to use equation (4.10) to solve for the other parameters. So, instead we provide values of η, α and γ. We then calculate δ using equation (4.19) and then obtain λ and k_1 from equations (4.18) and (4.11) respectively, and finally y_l from equation (4.10).

Figures 4.4, 4.5 and 4.6 are examples of the free-streamlines obtained by using this method.
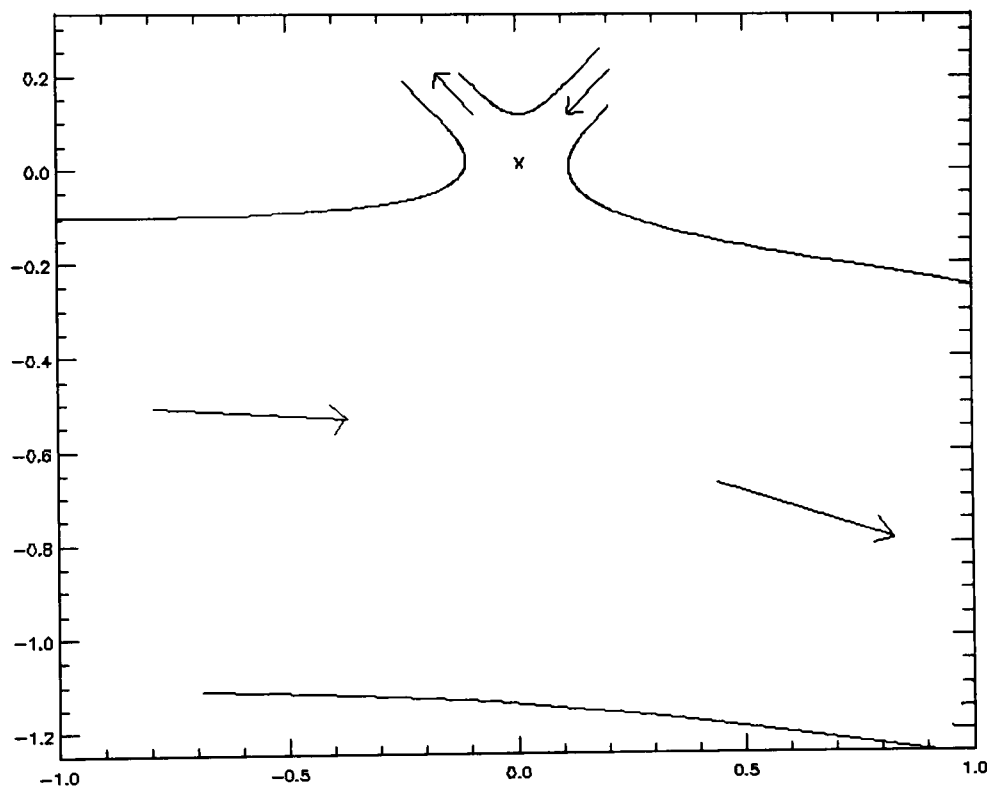
Figure 4.4: Free-streamlines using the extension of the Milne-Thompson/Keller method, for $\alpha = 45^o$, $\gamma = 45^o$ and $\eta = 0.1$, giving $\delta = 8.1^o$, $k_1 = 1$, $k_2 = 0.1$ and $y_l = -0.13$.

However, this method is unsatisfactory as it is difficult when given values for α and η to choose a realistic value for γ.
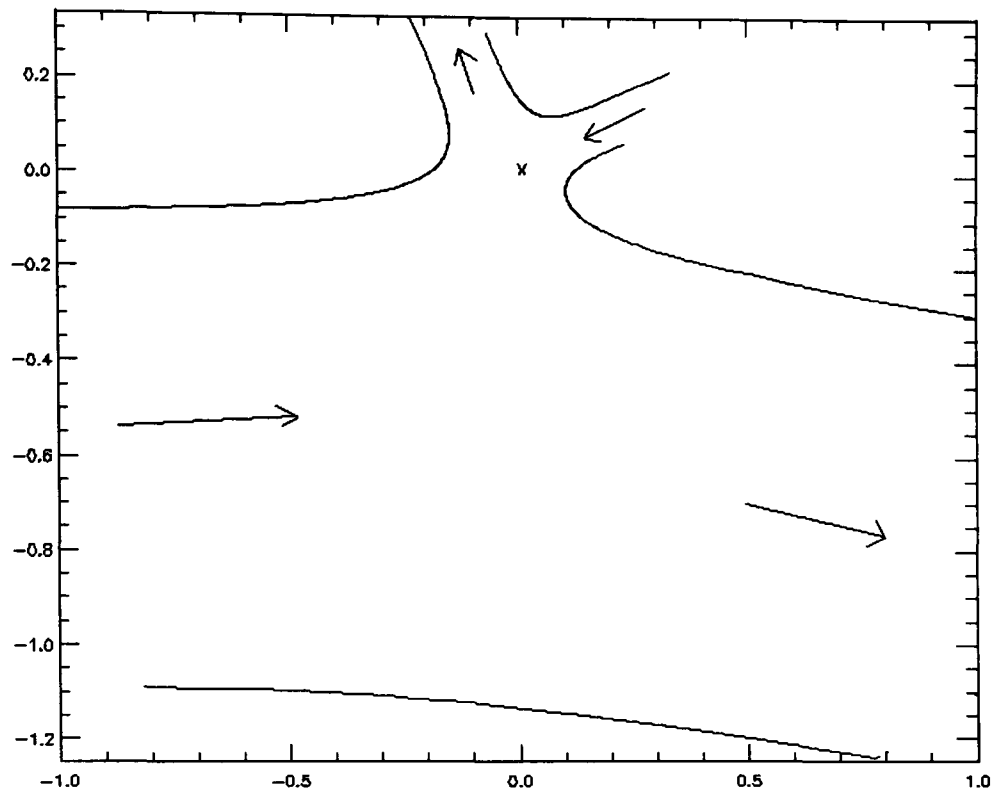
Figure 4.5: Free-streamlines using the extension of the Milne-Thompson/Keller method, for $\alpha = 22.5^o$, $\gamma = 67.5^o$ and $\eta = 0.1$, giving $\delta = 9.6^o$, $k_1 = 0.961$, $k_2 = 0.139$ and $y_l = -0.110$.
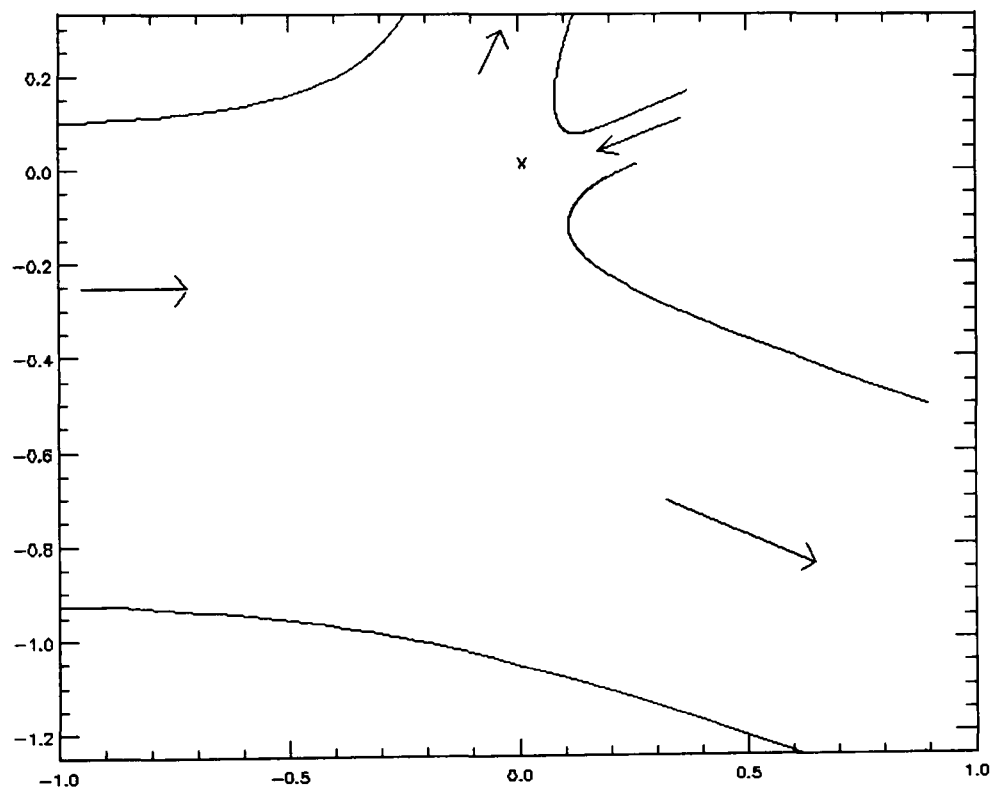
Figure 4.6: Free-streamlines using the extension of the Milne-Thompson/Keller method, for $\alpha = 22.5^o$, $\gamma = 112.5^o$ and $\eta = 0.1$, giving $\delta = 18.7^o$, $k_1 = 0.789$, $k_2 = 0.311$ and $y_l = 0.058$.

We next reconsider the model and assume that one of the incoming jets is of infinite depth from the start of the calculation. This is equivalent to having the streamline A_1B_1 (in figure 4.2) down at $y = -\infty$. The new problem we are solving is shown in figure 4.7. Note again that the angles are originally defined as between $-\pi$ and π. We begin as in section 4.4.1, by mapping to the w plane, where $w = qe^{-i\theta}$, with
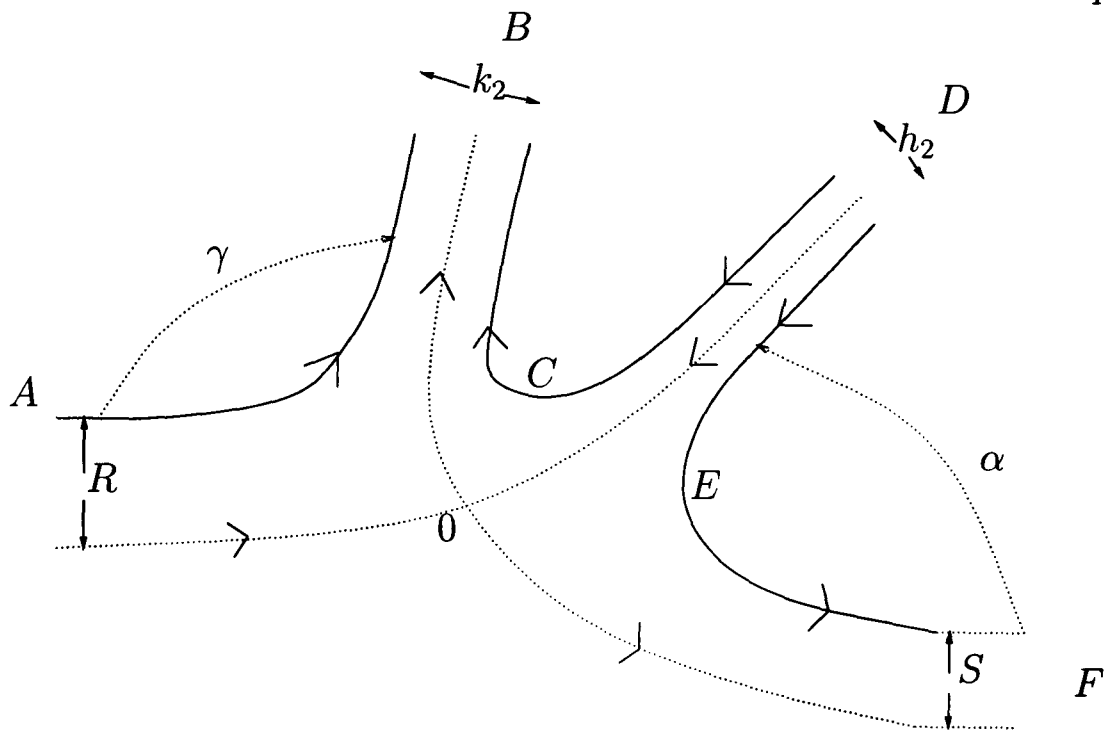
Figure 4.7: Two impinging jets, one of which has infinite width, undergoing steady motion. x is horizontal, and y vertical.

q and θ as the magnitude and angle of the velocity respectively. To be consistent with Milne-Thompson, we now use angles such that θ is between -2π and 0. Hence θ, the angles of the velocity, at A, B, C, D, E and F are given by -2π, $-\pi - \gamma$, $-\pi$, $-\pi + \alpha$, $-\pi/2$, and 0 respectively. Figure 4.8 shows a plot of the w plane. Note again that as we plot $qe^{-i\theta}$ values of $-\theta$ are shown in brackets. The circle corresponds to the free streamlines, and the other lines are some of the other streamlines. The arrows mark the direction of the streamlines.

We next map to a half plane, the ξ plane, using the following map:

$$\xi = ti\frac{1 + w}{1 - w}, \tag{4.20}$$

128
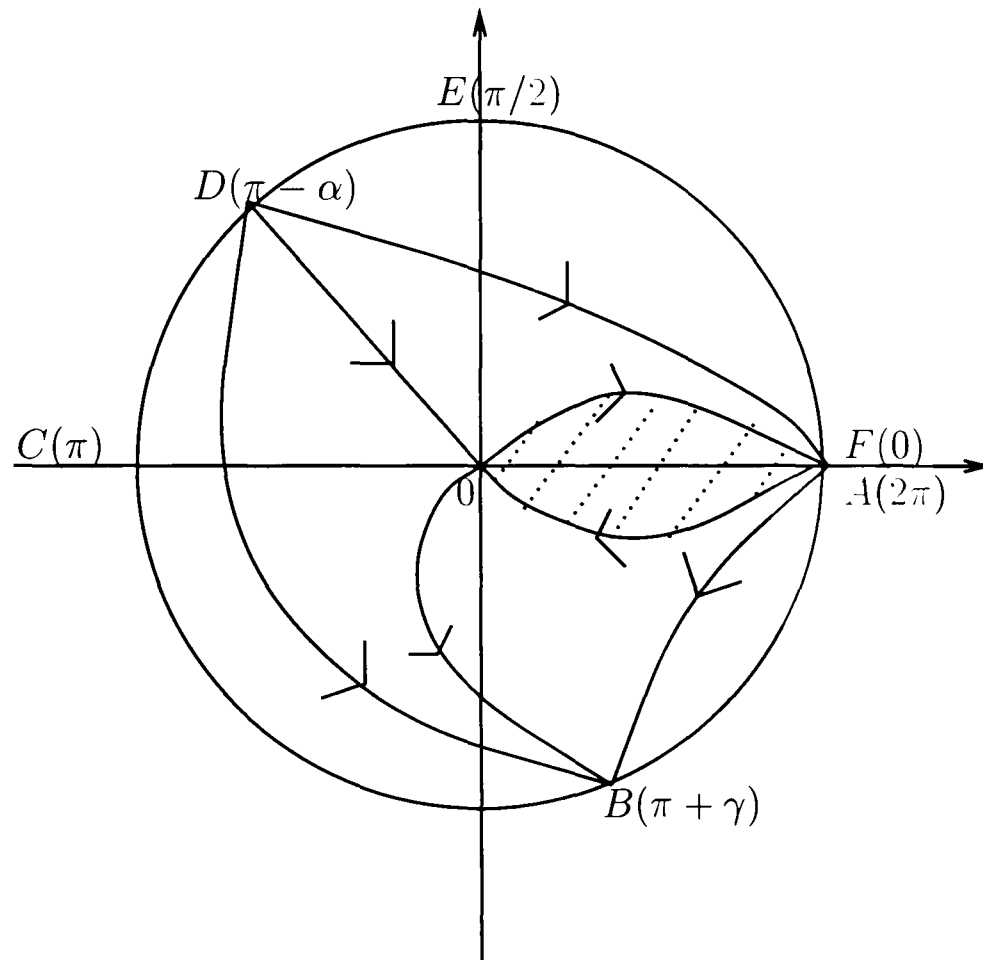
Figure 4.8: The w plane. $-\theta$ is given in brackets. The shaded region is fluid below AOF in Figure 4.7.

where t is a constant.
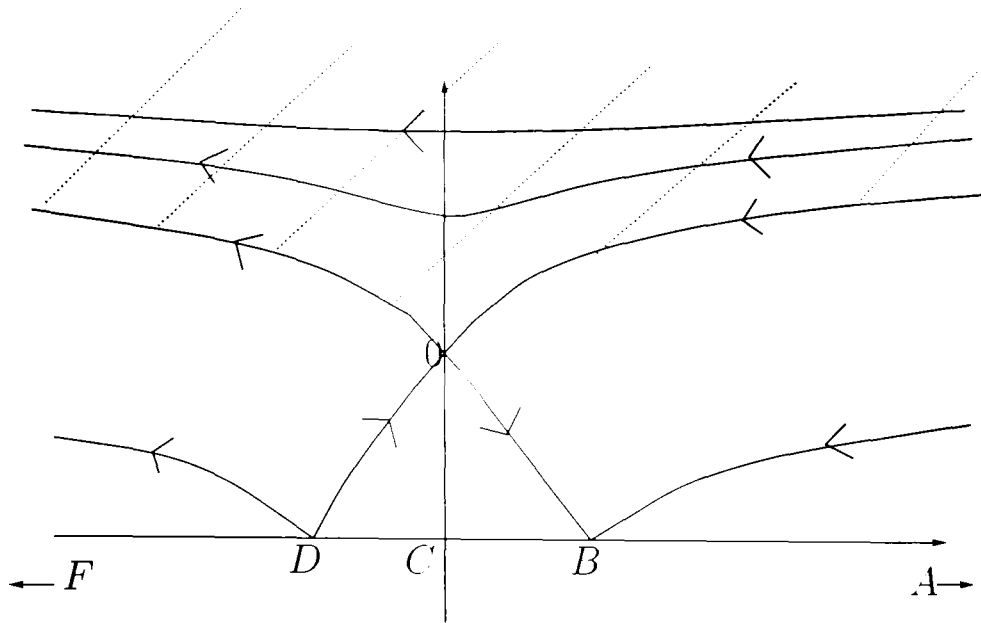
Figure 4.9: The ξ plane. The shaded region is fluid below AOF in Figure 4.7.

Figure 4.9 shows the stream-lines in the ξ plane. The stagnation point in the w plane is mapped to ti in the ξ plane. Enforcing the stagnation point to be along the imaginary axis provides one of the equations to be solved later.

The points on the circle $w = e^{-i\theta}$ are mapped to $\xi = t\cot(\theta/2)$. Hence, the position of B is $b = t\tan(\gamma/2)$, and D is $d = -t\tan(\alpha/2)$. As $\theta \to 0$ ξ tends to $\pm\infty$, depending on whether 0 is approached from above or below. This shows that A is mapped to ∞ and F is mapped to $-\infty$.

Conservation of momentum in the horizontal direction gives from figure 4.7:

$$R - h_2 \cos\alpha = S + k_2 \cos(\pi - \gamma), \qquad (4.21)$$

but we know from conservation of mass that

$$R = k_2 - h_2 + S \qquad (4.22)$$

Combining equations (4.21) and (4.22), and rearranging we get:

$$k_2(1 + \cos\gamma) = h_2(1 + \cos\alpha) \qquad (4.23)$$

130

Note that S has cancelled out. By extending figure 4.9, by a reflection in the horizontal axis, we can make B a sink and D a source. We also have negative uniform flow at ∞. Let m_1 and m_2 be the total outward/inward flux of fluid volume across any closed contour surrounding the point of the source/sink respectively. Considering the flux of fluid volume we obtain (in the top half plane only):

$$m_1 = \frac{h_2}{\pi} \quad \text{and} \quad m_2 = \frac{k_2}{\pi} \tag{4.24}$$

Hence we can write down the complex potential, using the standard expressions for a source, sink and uniform flow:

$$f = -\xi + m_1 \log(\xi - d) - m_2 \log(\xi - b) \tag{4.25}$$

Note that the velocity of the flow at ∞ in the ξ plane is -1, because the velocity in the original plane at $-\infty$ is 1.

We now need to enforce the condition that there is a stagnation point at $\xi = ti$. So we need $df/d\xi|_{\xi=ti} = 0$. So,

$$\left.\frac{df}{d\xi}\right|_{\xi=ti} = -1 + \frac{m_1}{it - d} - \frac{m_2}{it - b} = 0 \tag{4.26}$$

Taking the imaginary part of equation (4.26):

$$\frac{m_1}{t^2 + d^2} - \frac{m_2}{t^2 + b^2} = 0, \tag{4.27}$$

substituting for b and d gives:

$$h_2(1 + \cos\alpha) - k_2(1 + \cos\gamma) = 0 \tag{4.28}$$

which is already satisfied by conservation of momentum. Now we look at the real part of equation (4.26):

$$1 + \frac{m_1 d}{t^2 + d^2} - \frac{m_2 b}{t^2 + b^2} = 0 \tag{4.29}$$

If we substitute for b and d we obtain an equation relating α, γ and h_2:

$$\tan\frac{\gamma}{2} = \frac{2\pi t}{h_2(1 + \cos\alpha)} - \tan\frac{\alpha}{2} \tag{4.30}$$

131

Hence if we specify h_2 and α we can calculate γ and k_2 from equations (4.30) and (4.28) respectively.

t is now seen to be intrinsically linked with the length scales of the problem. Since it does not appear to have a simple interpretation, we choose to set $t = 1$, for simplicity. This choice has the advantage that only the lengths of interest appear in the diagrams and discussions. In section 4.4 we did not have this length, instead we had the apparently irrelevant thickness of the main jet (infinitely thick incoming jet). Other choices for this unit of length are possible, though less simple. e.g. the width of the incoming jet could be chosen to be unity. The solutions could then be, in principle, treated as functions of two parameters: (α, t) is the most convenient pair, $(\alpha, \Delta h)$ is a pair that is easier to interpret. (where $\Delta h = k_2 - h_2$ is the difference in height of the main jet at $x = \pm\infty$)

Next we need an expression for z, so use:

$$\frac{1}{w}\frac{df}{dw} = \frac{dz}{dw} \tag{4.31}$$

and so, by use of the chain rule (and cancelling $d\xi/dw$):

$$\frac{1}{w}\frac{df}{d\xi} = \frac{dz}{d\xi} \tag{4.32}$$

Differentiating equation (4.25) we obtain:

$$\frac{df}{d\xi} = -1 + \frac{m_1}{\xi - d} - \frac{m_2}{\xi - b} \tag{4.33}$$

Combining equations (4.32) and (4.33), and writing w in terms of ξ we get:

$$\frac{dz}{d\xi} = \frac{1 - i\xi}{1 + i\xi}\left[1 - \frac{m_1}{\xi - d} + \frac{m_2}{\xi - b}\right] \tag{4.34}$$

Rearrangement gives:

$$\frac{dz}{d\xi} = -1 + \frac{2}{1 + i\xi}\left[1 + \frac{m_1 i}{1 + id} - \frac{m_2 i}{1 + ib}\right] + \frac{m_1(id - 1)}{(1 + id)(\xi - d)} - \frac{m_2(ib - 1)}{(1 + ib)(\xi - b)} \tag{4.35}$$

However, the term in the square brackets in equation 4.35 is from equation 4.26.

To find an equation for z we now integrate equation (4.35).

$$z = -\xi + m_1\frac{id - 1}{1 + id}\log(\xi - d) - m_2\frac{ib - 1}{1 + ib}\log(\xi - b) - K. \tag{4.36}$$

132

K is given by using $z = 0$ at $\xi = i$, so

$$z = -\xi + i - m_1 \frac{id - 1}{1 + id} \log \left(\frac{i - d}{\xi - d} \right) + m_2 \frac{ib - 1}{1 + ib} \log \left(\frac{i - b}{\xi - b} \right). \qquad (4.37)$$

To plot the free-streamlines we take real $\xi \in (-\infty, \infty)$ and find the values for z from the above equation. When we evaluate z, the argument of z is chosen to be between $-\pi$ and π so we must choose the branch cut for log appropriately. We now know how to calculate all the unknowns and we have an expression for the free streamlines, which we can now plot. Figures 4.10, 4.11, 4.12 and 4.13 give examples of impinging jets, using this method, with $\alpha = \pi/4$ fixed, and increasing values for h_2. As h_2 increases in width the outgoing jet becomes smaller in width, and gamma increases. We write equation (4.30), in terms of half angles:

$$\tan \frac{\gamma}{2} = \frac{\pi}{h_2 \cos^2 \left(\frac{\alpha}{2} \right)} - \tan \frac{\alpha}{2} \qquad (4.38)$$

If h_2 is substantially smaller than π, as in figures 4.10 and 4.11, then the incoming jet is smaller than order one and hence 'peels' off a large section of water from the infinitely large jet.i.e. that the so called 'small' outgoing jet (of width k_2) is actually quite large and γ is larger than $\pi/2$. As h_2 increases to approximately π or larger, the jet of width k_2 has an angle of less than $\pi/2$ and a width comparable to h_2.

Figures 4.14, 4.15, 4.16, 4.17 and 4.18 are also plots of the impinging jets, but this time keeping the width constant ($h_2 = \pi/2$), and increasing values of α. As α increases γ and k_2 both show either a decrease then an increase or a continual decrease.

Note that we can find R and S if required by the following process. We could find the value of the streamfunction of the streamline which passes through the stagnation point, b and d, using equation (4.25). We then look at this streamline as the real part of ξ tends to $\pm\infty$, to find the imaginary part of ξ on this streamline at these limits. As the maps used in this analysis are all conformal these two values will give the values for R and S.

Figure 4.19 is a plot of γ against α, for fixed h_2. We consider only $\alpha < \pi/2$, as these are the values consistent with our geometry as shown in figure 4.7 (the

133

Figure 4.10: Impact of two jets, one of which is infinite. $\alpha = 45^o, \gamma = 168.7^o, h_2 = 0.351, k_2 = 30.691$. The height of the surface of the main jet at $x = \pm\infty$ are -9.485 and 20.889.
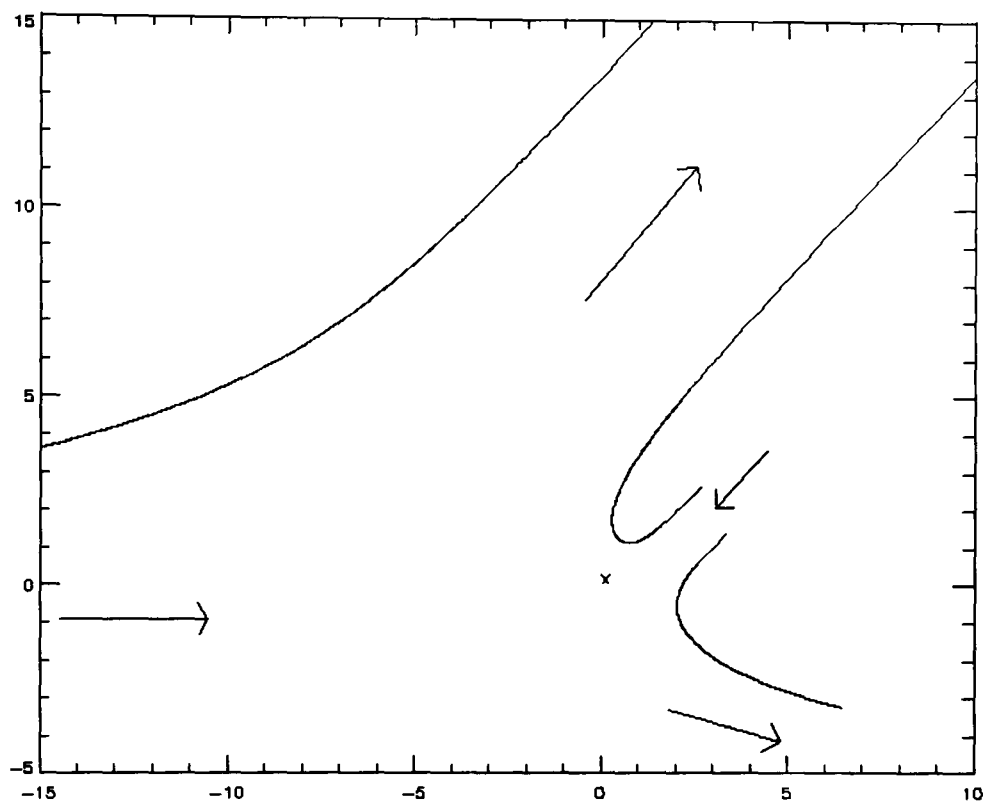
Figure 4.11: Impact of two jets, one of which is infinite. $\alpha = 45^o, \gamma = 133.0^o, h_2 = 1.357, k_2 = 7.275$. The height of the surface of the main jet at $x = \pm\infty$ are -12.486 and -6.600.

135

Figure 4.12: Impact of two jets, one of which is infinite. $\alpha = 45^o, \gamma = 89.7^o, h_2 = 2.613, k_2 = 4.436$. The height of the surface of the main jet at $x = \pm\infty$ are -13.433 and -11.608.

136
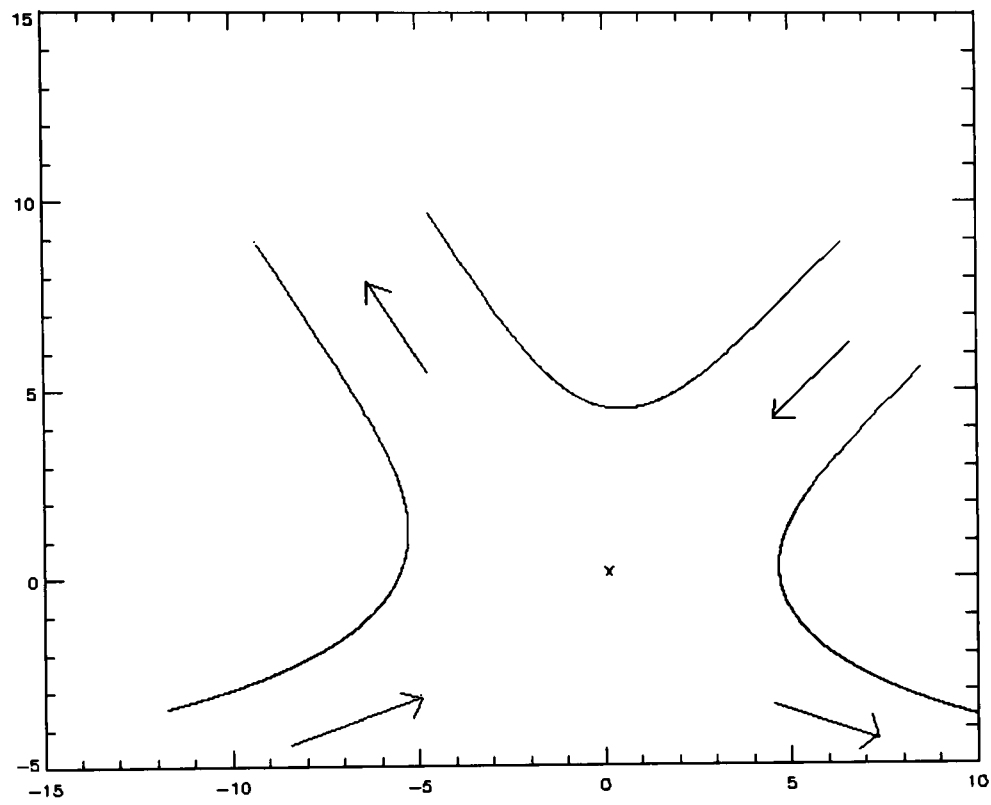
Figure 4.13: Impact of two jets, one of which is infinite. $\alpha = 45^o, \gamma = 56.4^o, h_2 = 3.870, k_2 = 4.256$. The height of the surface of the main jet at $x = \pm\infty$ are -13.508 and -13.121.

Figure 4.14: Impact of two jets, one of which is infinite. $\alpha = 8.1^o, \gamma = 125.4^o, h_2 = \pi/2, k_2 = 7.439$. The height of the surface of the main jet at $x = \pm\infty$ are -12.780 and -6.905.

138

Figure 4.15: Impact of two jets, one of which is infinite. $\alpha = 15.5^o, \gamma = 124.5^o, h_2 = \pi/2, k_2 = 7.1165$. The height of the surface of the main jet at $x = \pm\infty$ are -12.834 and -7.281.
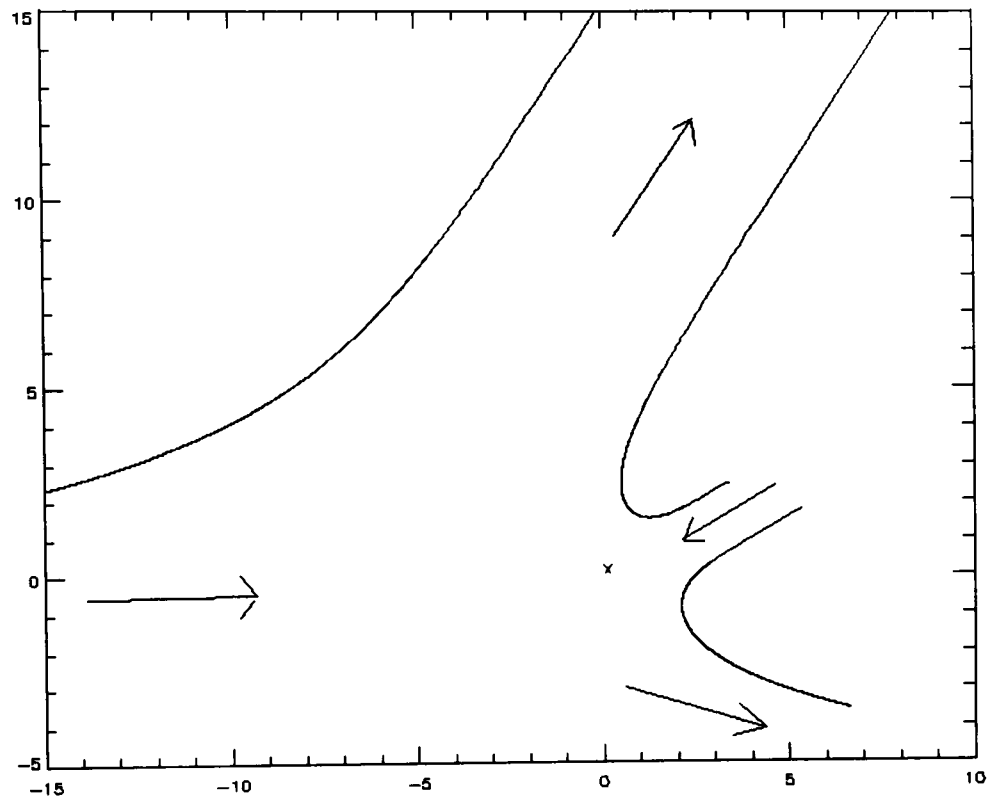
Figure 4.16: Impact of two jets, one of which is infinite. $\alpha = 30.1^{o}, \gamma = 123.9^{o}, h_2 = \pi/2, k_2 = 6.619$. The height of the surface of the main jet at $x = \pm\infty$ are -12.859 and -7.804.

140

Figure 4.17: Impact of two jets, one of which is infinite. $\alpha = 42.2^o, \gamma = 124.8^o, h_2 = \pi/2, k_2 = 6.365$. The height of the surface of the main jet at $x = \pm\infty$ are -12.791 and -7.990.
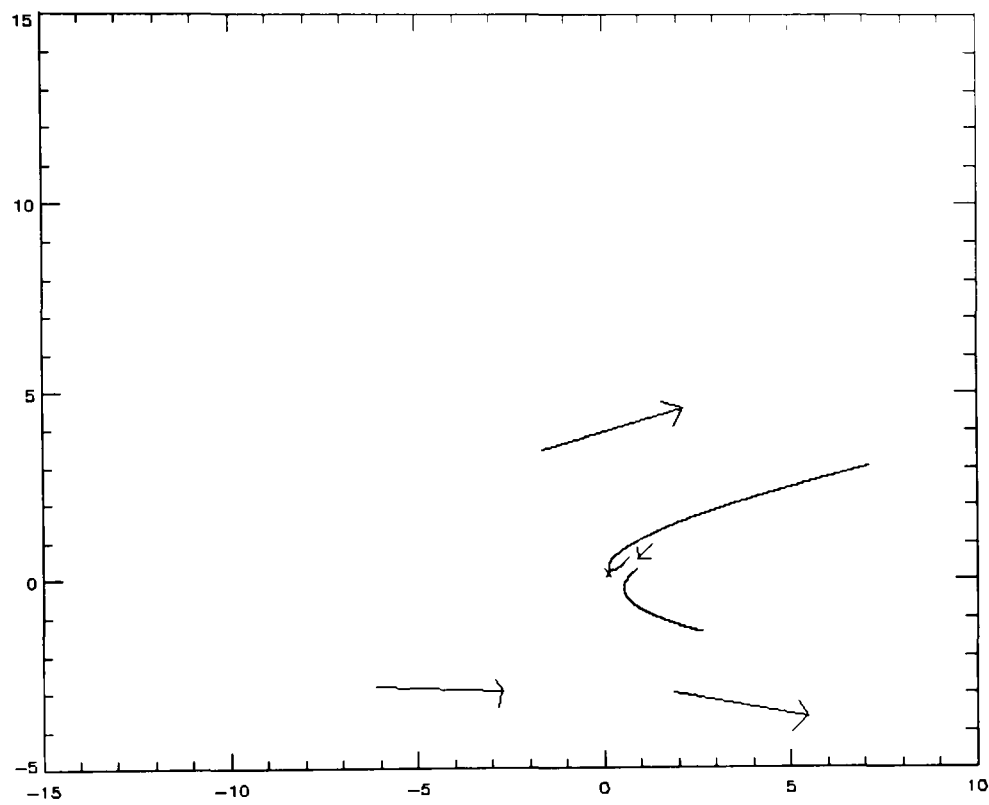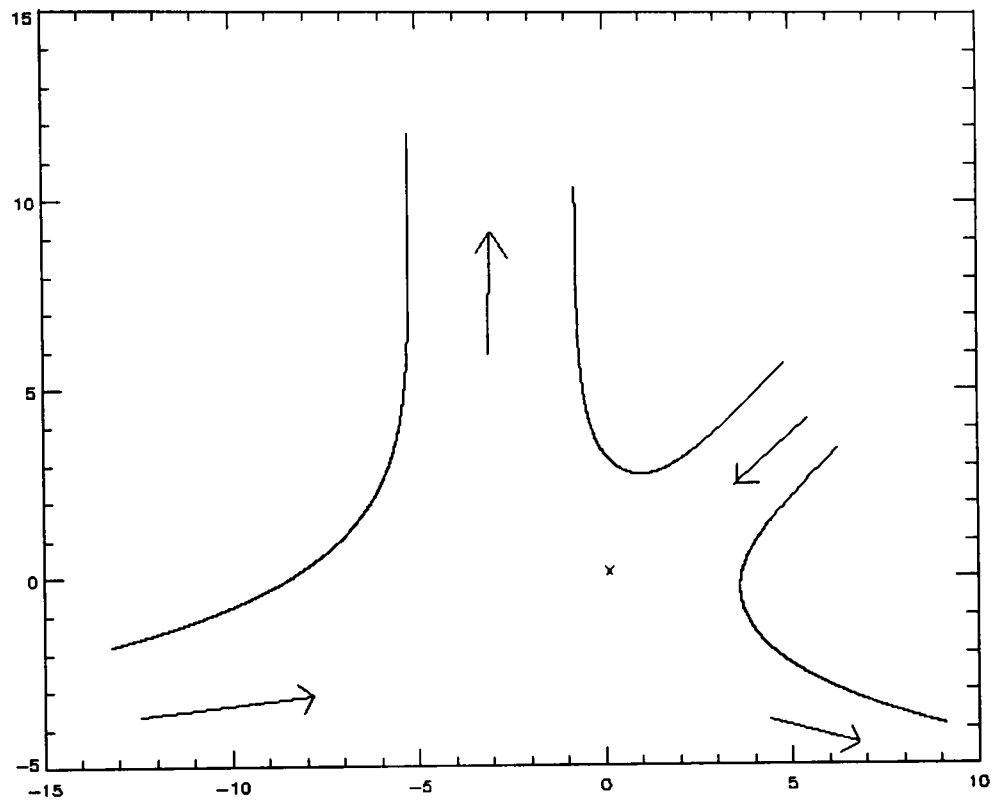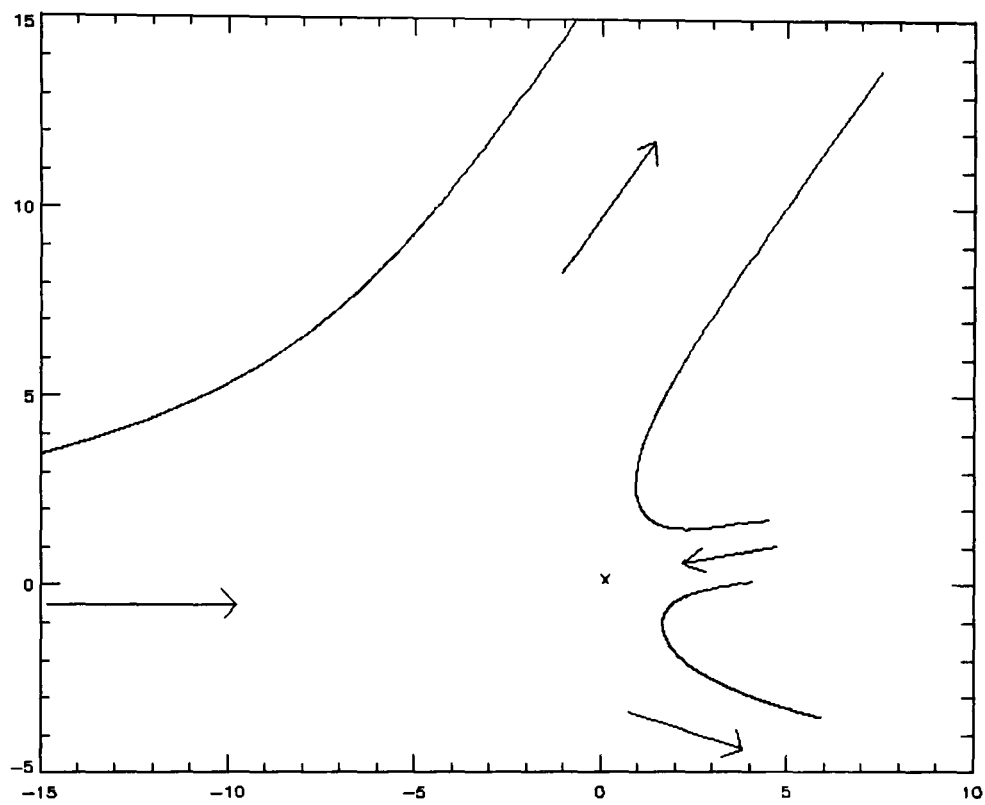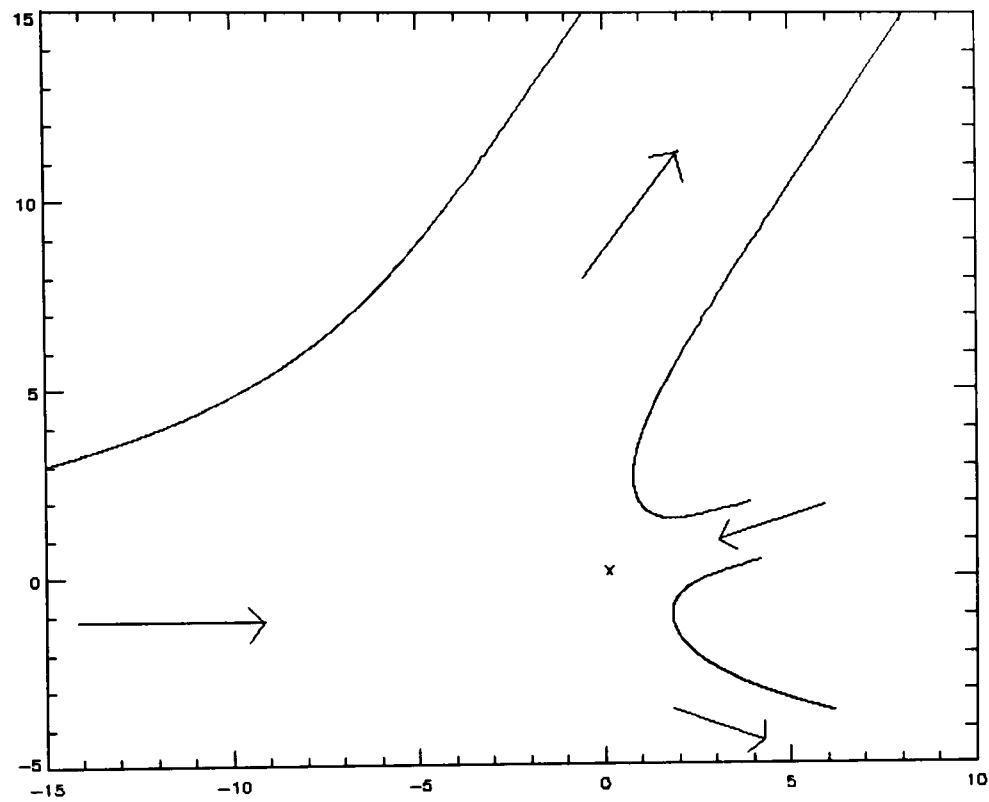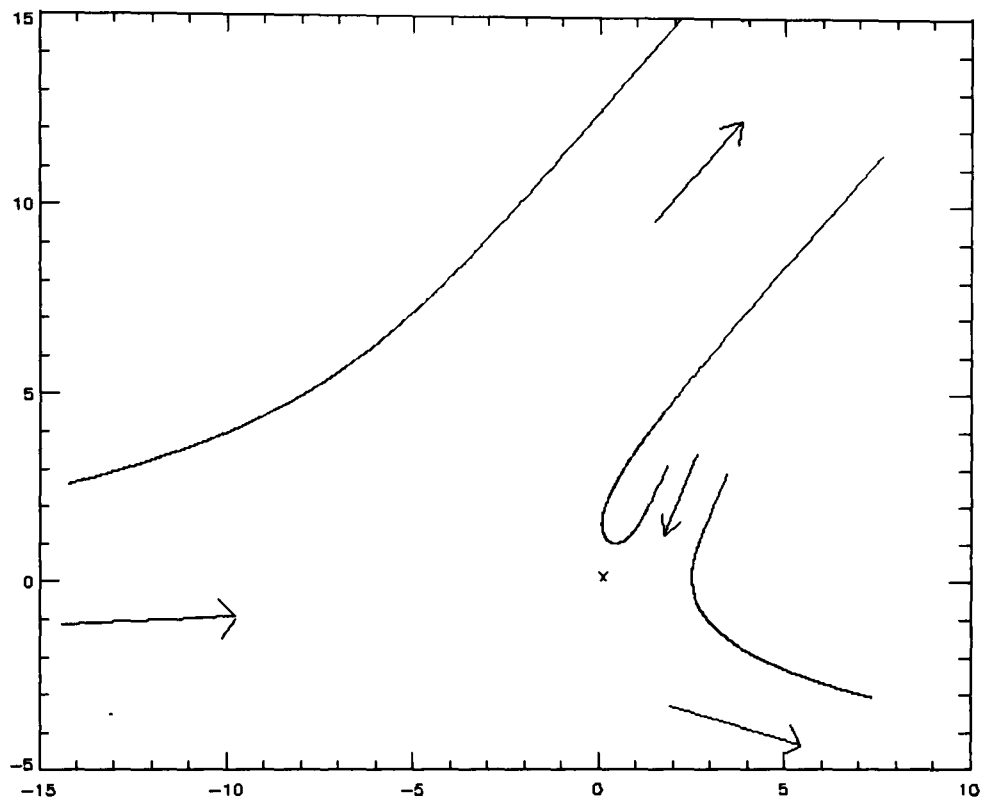
Figure 4.18: Impact of two jets, one of which is infinite. $\alpha = 66.5^o, \gamma = 131.2^o, h_2 = \pi/2, k_2 = 6.434$. The height of the surface of the main jet at $x = \pm\infty$ are -12.379 and -7.509.

142

two incoming jets come from opposing directions). The parameter range where we have a self-intersecting jet surface is marked. If h_2 is greater than π then γ is less than $\pi/2$ regardless of the choice of α. If h_2 is smaller than π then there is a restriction on suitable α to avoid self intersection. If h_2 is smaller than $3\pi/4$ then γ is always greater than $\pi/2$. Increasing h_2 increases γ. Figure 4.20 is a plot of k_2 against α, for fixed h_2. For $h_2 = \pi/2$ the value of k_2 decreases then increases, as α increases. When $h_2 = \pi$ or $3\pi/2$, as α increases k_2 decreases.

Figure 4.21 is a plot of the parameter space showing which values of h_2 and α produce a jet which deflects the infinite depth jet in a forwards or ongoing splash, or alternatively splashes back in the same direction from which it came producing a backwards splash. Figure 4.22 shows a plot of the parameter space, but this time showing when k_2, the width of the smaller outgoing jet, is larger or smaller than the incoming jet of width h_2.

4.5.1 Choice of α.

Jenkins (1994) looks at a potential-flow approximation to breaking waves, in particular he looks at the evolution of the jet from the wave crest. He gives an example of a jet in figure 3, where the angle that the jet hits the free surface is 40°. This suggests that a reasonable choice of α would be 40°. It is not clear what value of h_2 would be suitable, so an example for $h_2 = 3\pi/4$ is shown in figure 4.23. We note that a different orientation of the x axis relative to the rest of the free-surface may give a more realistic breaking wave splash profile.

4.5.2 Conclusions.

As α increases, for a given h_2, gamma first decreases then increases. The larger the value of h_2 the smaller the value of γ. If we take h_2 to be less than $3\pi/4$ then the small incoming jet 'peels' off part of the larger jet. This means that the jets of width h_2 and k_2 lie within the same quarter plane that it came in from. The results of Tallent, Yamashita, & Tsuchiya (1990) suggest that for a plunging

143
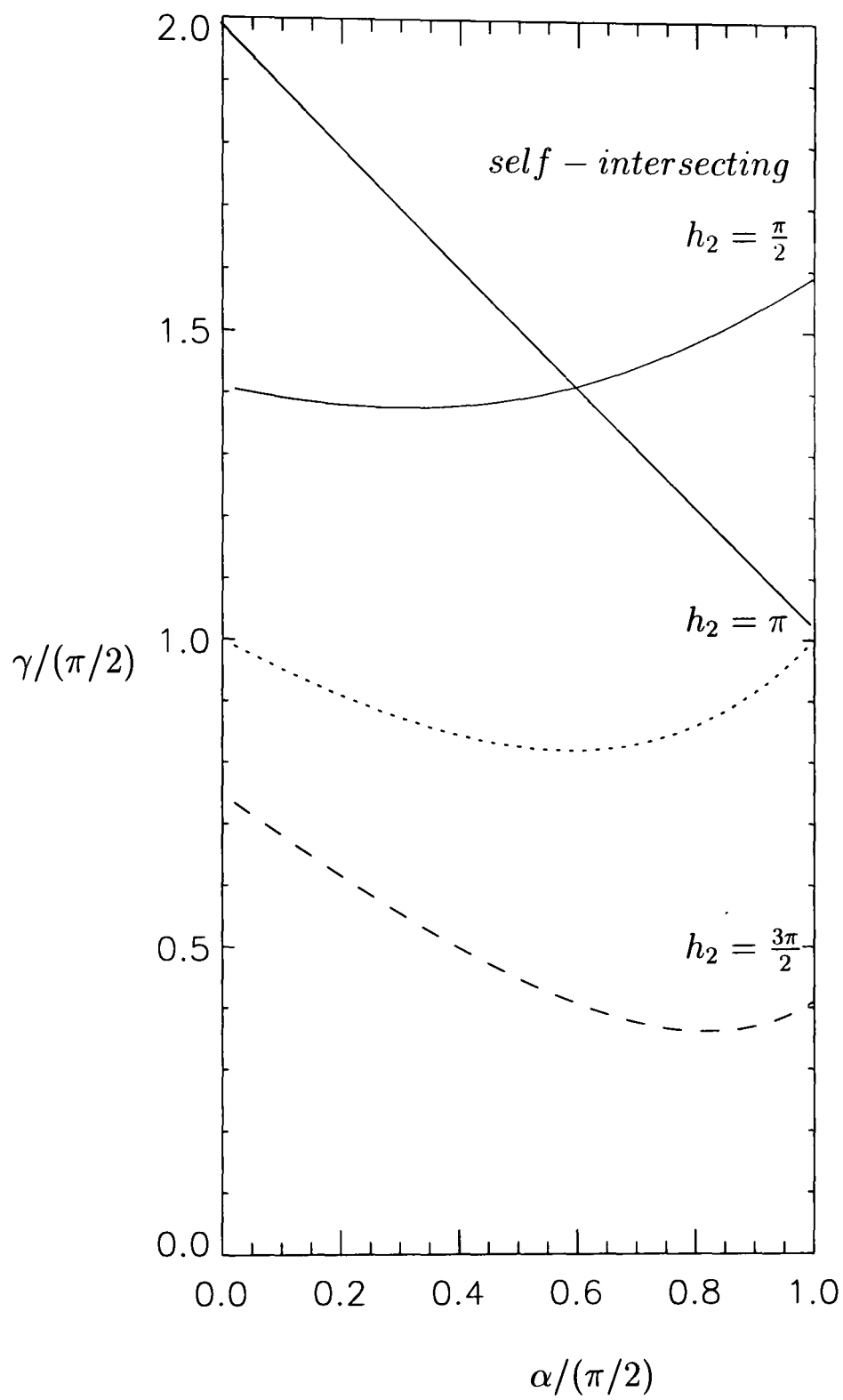
Figure 4.19: Impact of two jets, one of which is infinite. Graph showing change in γ with α for a given h_2. Above the diagonal line is where there is self-intersecting of the jet surface. Angles in radians.

144
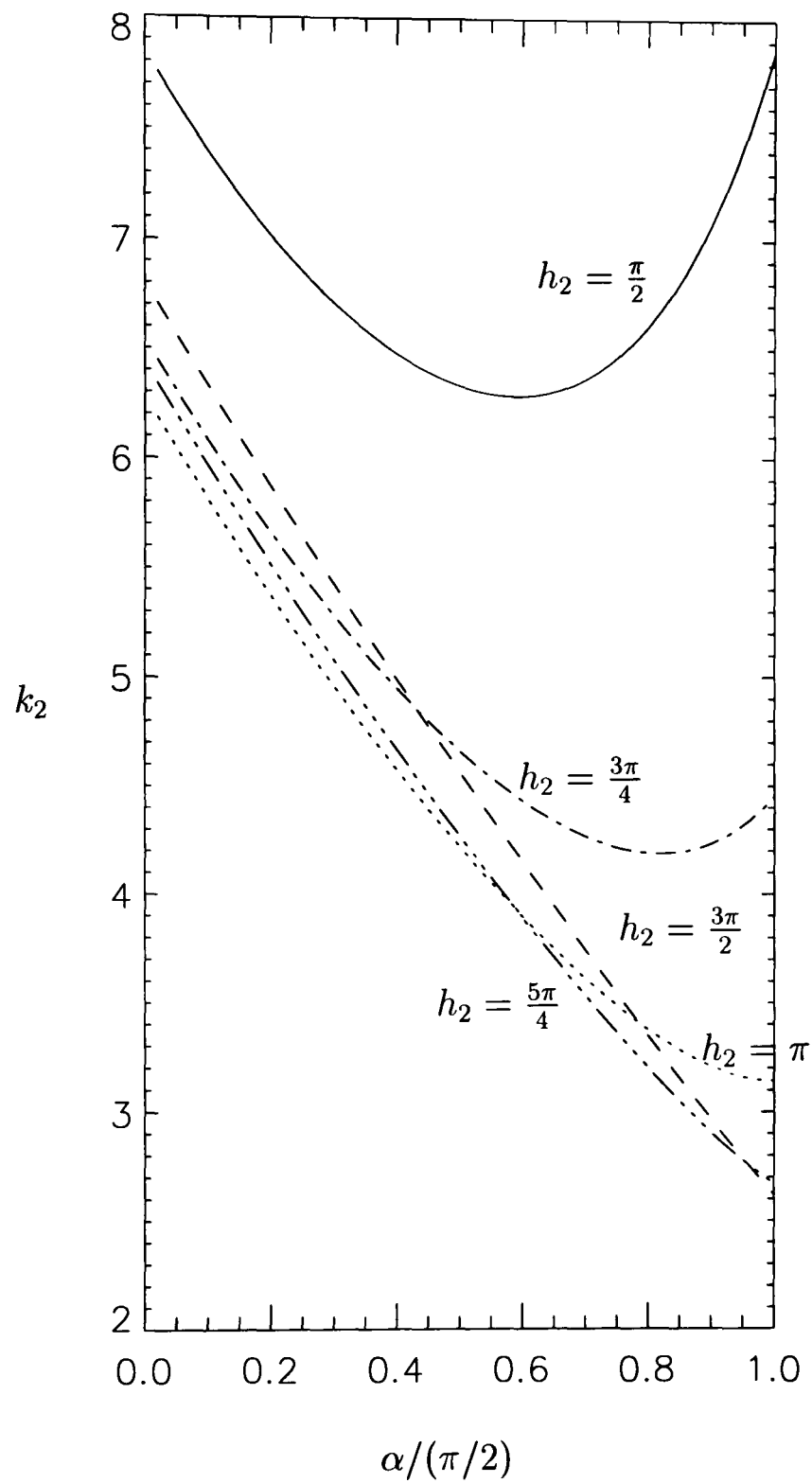
Figure 4.20: Impact of two jets, one of which is infinite. Graph showing change in k_2 with α for a given h_2. Angles in radians.

Forwards/Ongoing splash

h_2

Backwards splash

$\alpha/(\pi/2)$
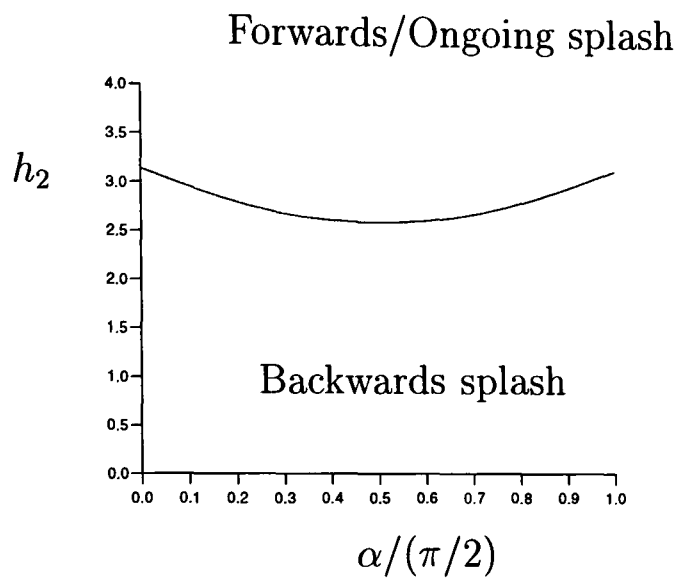
Figure 4.21: Impact of two jets, one of which is infinite. Graph show forwards/backwards splash. Angles in radians.

h_2

$k_2 < h_2$

$h_2 < k_2$

$\alpha/(\pi/2)$

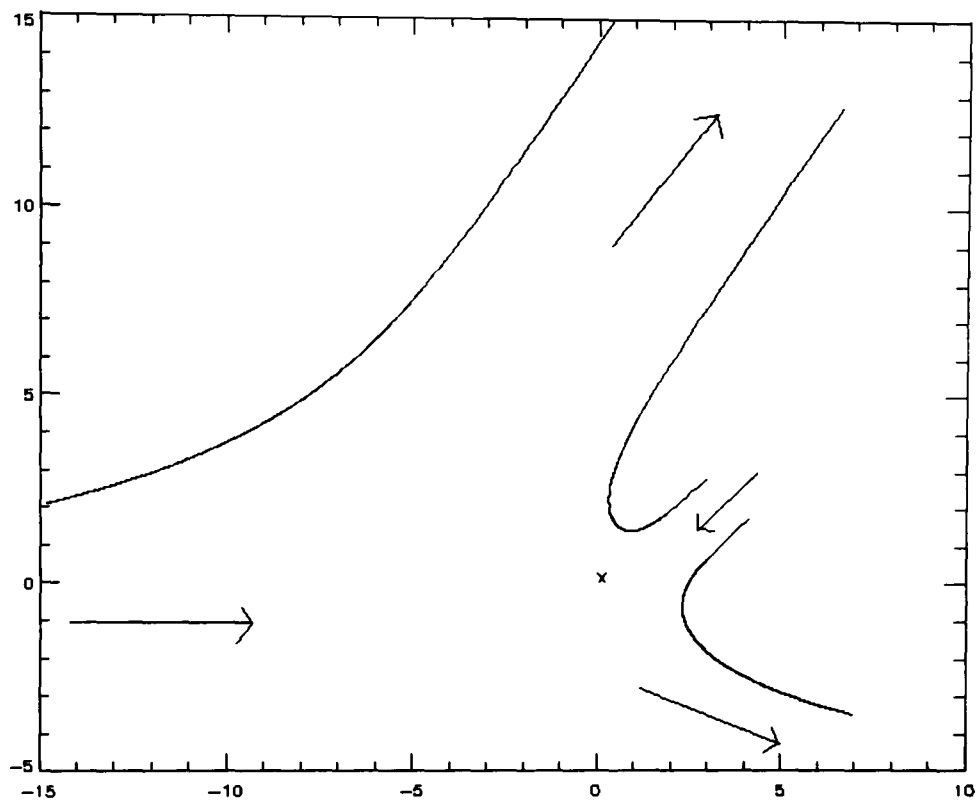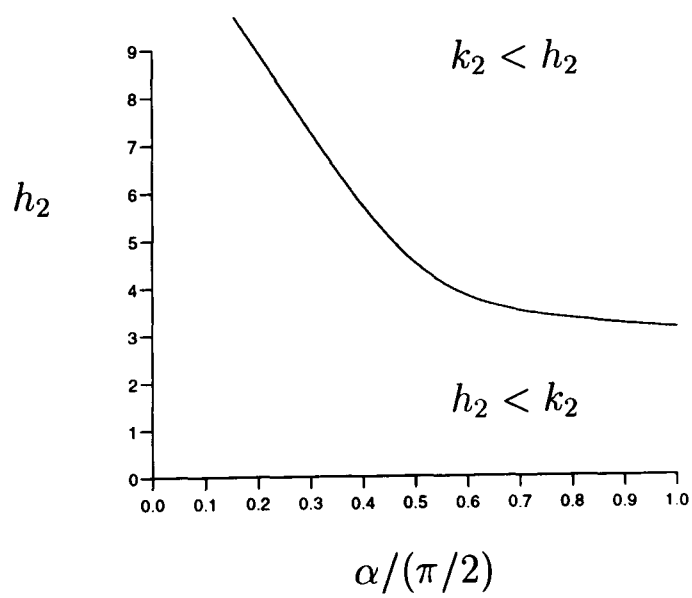Figure 4.22: Impact of two jets, one of which is infinite. Graph to show where k_2 is greater than h_2. Angles in radians.
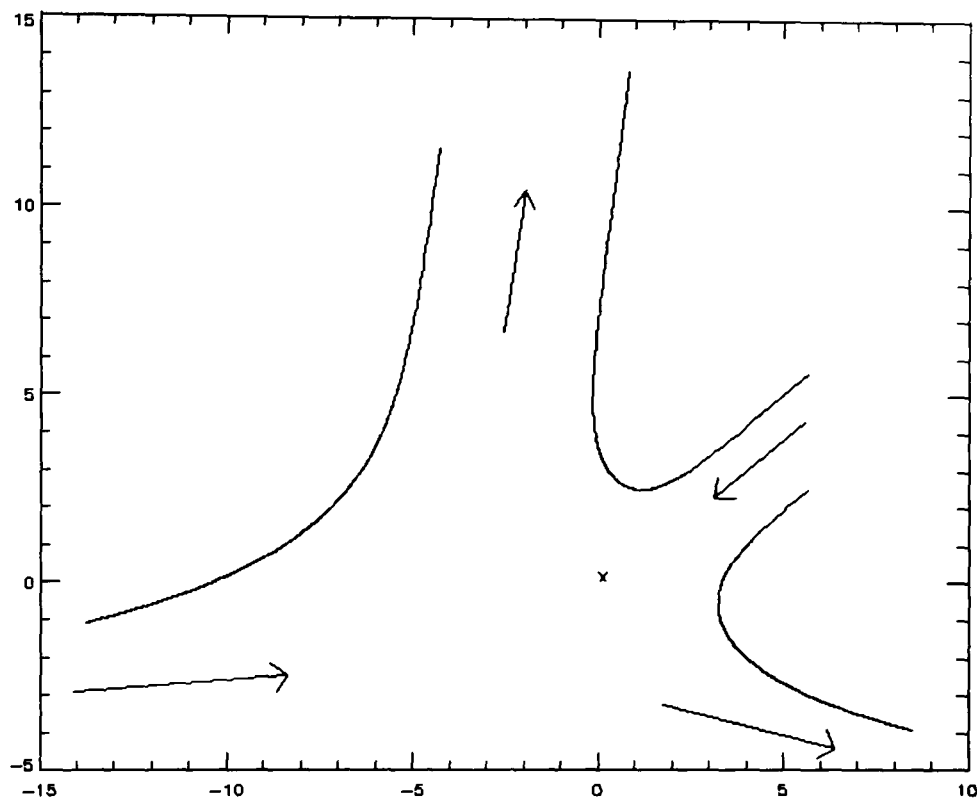
Figure 4.23: Impact of two jets, one of which is infinite. $\alpha = 40^o, \gamma = 97.4^o, h_2 = 3\pi/4, k_2 = 4.8$. The height of the surface of the main jet at $x = \pm\infty$ are -13.401 and -10.994.

breaker 'splash' the 'peeling' off is quite realistic.

The method in section 4.5 is better than both the methods in section 4.4 and Frankel and Weihs (1990) as it is an exact solution to the steady flow approximation, and does not involve any asymptotics. However it is difficult to draw any further conclusions without having more detailed experimental data for splashes.

Chapter 5

Conclusion.

5.1 Impacts on vertical structures.

The Cooker and Peregrine (1990 b, 1992) model for impact on a wall was reviewed in chapter 2. It was found that when the impact is on the top of the depth of water, with infinite depth of water below the impact, the total impulse evaluated using this model tends to infinity. This particular case is important when considering wave impact on a breakwater in deep water, so we considered ways in which the model could be improved. The Cooker and Peregrine model assumed two-dimensional impact and took no account of the effect of trapped air. When a wave impacts on a wall, especially in the field, the impact is often just on a patch of the wall. It was thought that having impact on just a patch of the wall rather than along the whole width of the wall would lead to a reduction in the total impulse. Chapter 2 extended the two-dimensional model to the impact of a wave on a patch of the wall and a reduction in the pressure impulse was found. The reduction is enough that it keeps the total impulse finite even when the water becomes infinitely deep.

We then sought to examine how wide the patch needed to be before we could assume that the pressure impulse at the centre of the patch could be accurately predicted by the two-dimensional model. To do this it was useful to consider the impact of a wave on a semi-infinite patch of a wall. The advantage of this model was that the patch had only one edge, and so the depth of penetration of the effect of just one edge of the patch could be found. The penetration length was found

to be about twice that of the height of the water at the wall. Interestingly this 'penetration' distance was little affected by the percentage of the depth of the water on which impact occurred.

Two more areas which were investigated, were the effect on the impact of having a berm in front of the breakwater, and secondly the effect of having a pocket of air which 'bounces back' when the wave impacts on the wall.

For a porous berm in front of the wall the pressure-impulse contours are kinked at the boundary between the porous mound below and the water above. This is due to a difference in pressure-impulse gradient between the mound and the water. An increase in porosity is associated with an increase in the fraction of the interface between the two regions with holes. An increase in the porosity of the berm leads to a reduction in the pressure impulse in the region above the berm. The effect of increasing the porosity was found to be greatest at the wall, and the larger the proportion of wall struck by the wave the greater the effect of any change in porosity. In the case of deep water below the impact region the effect of having a porous berm in front of the wall was found to be negligible.

When a wave impacts on a structure often an air bubble becomes trapped. This bubble first contracts then expands and in doing this pushes the water behind it backwards. We call this effect 'bounce back' and adapt the Cooker and Peregrine impact on a wall model to allow for this effect. The simplest model was to allow the velocity of the fluid behind the bubble to undergo a change in sign at impact. The 'bounce-back' model was compared with experimental data (Hattori and Arami (1992 and private communication)) in section 2.5.3, and although the pressure-impulse distribution down the wall was not well predicted, the total impulse on the wall was predicted quite accurately. Two reasons were put forward for the discrepancy in the prediction of the pressure-impulse distribution. Firstly we assumed the bounce-back velocity was of the same magnitude as the incoming velocity of the wave. This meant that the model did not take into account the shape

150

of the bubble. The second reason for the discrepancies was thought to be that the crude method of calculating the pressure impulse, from the experimental data, was inadequate.

The 'bounce-back' model was then adapted by allowing the velocity of the wave at the bubble after impact to have a cosine distribution. This meant that at the edges of the bubble no 'bounce back' occurred whereas at the centre of the bubble the 'bounce-back' velocity is equal to, but opposite in sign, to the ingoing velocity. This was equivalent to considering the bubble to be cylindrical and the velocity of bounce back to be perpendicular to the cylinder's surface. Hence by using a cosine distribution we have taken the horizontal component of the velocity at the surface of the bubble. A comparison in section 2.5.4 with PIV experiments carried out at Edinburgh University gave good results. A method for calculation of the pressure impulse from experimental data was discussed, and it was found that the subtraction of a 'background' reflective pressure was required. The prediction of the pressure impulse down the wall and on the berm was found to be quite good. The prediction was within about 40% which, as few theoretical models for this type of impact exist, was a significant step forward. From the work with the porous berm, the effect of changing the porosity was found to be small, so even though the 'bounce-back' model assumed an impermeable berm, predictions of pressure-impulse distribution along the berm (even for a permeable berm) should be possible using this model. The bounce-back effect influences the peak pressures more than the porosity of the berm.

Finally, three-dimensional effects are very important to consider when the wave impact is not on a flat wall. In this chapter we considered the impact of a wave on a cylindrical structure, which has importance when considering impact of waves onto oil-rig legs and circular heads of breakwaters. Two models were considered, firstly that of impact on a cylinder on a patch just below water level, and secondly the impact of a wedge of water on a cylinder. If we compare the impact on a patch of a cylinder and a flat vertical wall (both impacts on the top 10% of the water depth)

here is a reduction of approximately 23% of the maximum pressure impulse. This shows that the three-dimensional convex nature of the cylinder has a very strong effect on the pressure impulse distribution. The impact of a wedge of water on a cylinder led to a further reduction in the predicted pressure impulse. The reduction of the pressure impulse between the two cylinder models was most noticeable at the base of the cylinder. For the impact on the cylinder on the patch below water level, negative pressures were calculated on the side of the cylinder opposite to the impact region. These negative pressures could be due to not taking enough terms in the Fourier series, or due to the particular mathematical model used for the impact.

5.2 Impact under a deck.

Chapter 3 examines pressure impulse for a wave impacting upwards on a deck. The two extreme cases of infinite depth and infinite length of deck are examined first, and then a more general solution is found. The problem of a square root singularity in the mathematical model of the impact is eliminated by using a sequence of conformal maps, which implicitly contain the singularity, and so the problem can be solved in the final complex plane using standard solution methods.

Contours of constant pressure impulse are plotted. We confirmed that increasing the length of deck (with fixed depth of water) increases the pressure impulse and total impulse. It is clear that increasing the length of the deck makes the fluid motion more constrained, and hence the impulse involved is much larger. Similar results were found in Cooker and Peregrine (1995) and Topliss (1994). Whilst the original free-surface is horizontal it is noted that any of the pressure-impulse contours, $P = P_0$ can be taken as a free-surface, by subtracting off P_0 from P, which can lead to more realistic wave-like free-surfaces. High gradients of pressure impulse directed away from the deck mean that any body attached to the underside of the deck is subject to high forces pulling it away from the deck. This may be highly dangerous for example, an oil pipe beneath the deck could be pulled away by this impulsive

152

orce. The elliptic patch impact model also had these high gradients of pressure mpulse directed away from the edges of the patch.

5.3 Wave breaking and impinging jets.

Two methods are put forward for a simple model of a splash on undisturbed water from the plunging jet of a breaking wave.

The first method is an asymptotic extension of the impact of two finite jets, where the width of one of the jets tends to infinity. However, this method requires the feeding in of both the ingoing and outgoing jet angles. Giving the widths of the ingoing jets, and the angles of the ingoing and outgoing jets, enables plots of the free streamlines.

The second method is by far the most superior of the two methods given in chapter 4. It involves a map to the hodograph plane followed by a conformal map. The complex potential for the flow in the final plane can be written down as that of the sum of a source, sink and uniform flow at infinity. An equation for the free-streamlines can be obtained from this combined with conservation of horizontal momentum and mass.

Plots for the free-streamlines of the jets were found and many examples are given in chapter 4. It is noted that the most realistic free-surface profiles are obtained when the width for the incoming jet h_2 is taken to be just less than π. This leads to a geometry where the small jet 'peels off' or divides the infinite jet. Here the jets of width h_2 and k_2 lie within the same quarter plane. Unless the incoming jet of width h_2 is very much smaller than $\pi/2$, the outgoing jet turns to a near vertical direction as described by Tallent, Yamashita & Tsuchiya (1990).

5.4 Future work.

In chapter 2, for waves impacting on a wall, it was shown that the 'bounce-back' model can be used to predict pressure-impulse distributions both down the wall and

along the berm. The way in which pressure impulse should be calculated from experimental data needs much more investigation. In particular the lack of dependence on the porosity of the berm means that these models could be used in future to aid in the prediction of pressure-impulse distribution, in particular to predict the distance along the berm which the pressure impulse penetrates. Further investigation on the boundary conditions used in both the 'bounce-back' and berm models would bring about great improvements to the models. Specifically the shape of the bubble in the 'bounce-back' method should be better accounted for, and investigation of the appropriateness of the continuity conditions used in the berm model.

It is also hoped that the 'patch' model impact could be used to compare with experimental analysis of the spread of wave impact. In particular three-dimensional wave impact tests are being carried out in connection with the PROVERBS project. Similarly experimental comparisons with the cylinder problem would be beneficial.

Impact under a deck was primarily a two-dimensional study, with a brief look at the impact of an elliptic plate for infinite depth of water. An extension of this would be to investigate more three-dimensional impacts, such as impact on just a small region of a deck. It would be interesting to also include the effect of the air trapped beneath the deck.

Experimental comparison of the impact of the plunging jet impact would be advantageous in analysing the usefulness of this model. It would also be of interest to investigate a solution which does not assume steady motion, and make comparisons.

References

- APELT, C.J. & PIOREWICZ, J. (1987). Laboratory studies of breaking wave forces acting on vertical cylinders in shallow water. *Coastal Engng* **11** 263-282.

- BAGNOLD, R.A. (1939). Interim report on wave-pressure research. *J. Inst. Civil Engrs* **12**, 202-226.

- BASCO, D.R. (1985). A qualitative description of wave breaking. *J. Water-way, Port, Coastal and Ocean Engng. Div., Proc. ASCE* **111** 171-188.

- BATCHELOR, G.K. (1967). *An Introduction to Fluid Dynamics* Cambridge University Press.

- BLACKMORE, P.A., & HEWSON, P.J. (1984). Experiments on full-scale wave impact pressures. *Coastal Engng.* **8**, 331-346.

- CHAN, E.S. & MELVILLE, W.K. (1988). Deep-water plunging wave pressures on a vertical plane wall. *Proc. Roy. Soc. Lond. A* **417** 95-131.

- CHAN, E.S. (1994). Mechanics of deep water plunging-wave impacts on vertical structures. *Coastal Engng.* **22**, 115-133.

- CHAPLIN, J.R., GREATED, C.A., FLINTHAM, T.P. & SKYNER, D.J. (1992). Breaking wave forces on a vertical cylinder. *U.K. Dept. of Energy Report OTH-90-324.*

- CISOTTI, U. (1921). *Idromeccanica piana,* Milano, **1**.

- COINTE, R. & ARMAND, J.-L. (1987). Hydrodynamic impact analysis of a cylinder. *J. Offshore Mechanics and Arctic Engng.* **109** 237-243.

- COINTE, R. (1989). Two-dimensional water-solid impact. *J. Offshore Mechanics and Arctic Engng.* **111** 109-114.

- COKELET, E.D. (1979). Breaking waves-the plunging jet and interior flow-field. *Mechanics of Wave-induced Forces on Cylinders.* (ed. T.L. Shaw) Bristol, Pitman. 287-301.

- COOKER, M.J. (1990). The interaction between steep waves and coastal structures. Ph.D. dissertation, University of Bristol. 209pp.

- COOKER, M.J. & PEREGRINE, D.H. (1990a). Violent water motion at breaking wave impact. *Proc. 22nd Internat. Conf. Coast. Engng., ASCE*, vol 1, 164-176.

- COOKER, M.J. & PEREGRINE, D.H. (1990b). A model for breaking wave impact pressures. *Proc. 22nd Internat. Conf. Coast. Engng., ASCE*, vol 1, 1473-1486.

- COOKER, M.J. & PEREGRINE, D.H. (1992). Wave impact pressure and its effect upon bodies lying on the sea bed. *Coastal Engng.* **18** 205-229.

- COOKER, M.J. & PEREGRINE, D.H. (1995). Pressure-impulse theory for liquid impact problems. *J. Fluid Mech.* **297** 193-214.

- CUMBERBATCH, E. (1960). The impact of a water wedge on a wall. *J. Fluid Mech.***7** part 3, 353-374.

- DALTON, C. & NASH, J.M. (1976). Wave slam on horizontal members of an offshore platform. *Eighth Annual Offshore Technology Conference, Dallas, Texas, 1976* 769-780.

- DIAS, F. & CHRISTODOULIDES, P. (1991). Ideal jets falling under gravity. *Phys. Fluids A***3**, No. 7, 1711-1717.

- DENNY, D.F. (1951). Further experiments on wave pressures. *J. Inst. Civ. Engs.* **35** 330-345.

- DOLD, J.W. (1992). An efficient surface-integral algorithm applied to unsteady gravity waves. *J. Computational Physics* **103**, 90-115.

- DOLD, J.W. & PEREGRINE, D.H. (1986). An efficient boundary-integral method for steep unsteady water waves. *Numerical Methods for Fluid Dynamics II*, (ed. K.W.Morton & M.J.Baines), 671-679.

- DOMMERMUTH, D.G., YUE, D.K.P., LIN, W.M., RAPP, R.J., CHAN, F.S., & MELVILLE, W.K. (1988). Deep-water plunging breaking: a comparison between potential theory and experiments. *J. Fluid Mech.* **189** 423-442.

- FRANKEL, I., & WEIHS, D. (1990). Hydrodynamic theory of glancing impact. *J. Fluid Mech.* **216** 213-229.

- FRENCH, J.A. (1969). Wave uplift pressures on horizontal platforms. W. M. Keck Laboratory of Hydraulics and Water Resources, California Institute of Technology Report KH-R-19.

- FURUDOI, T. & MUROTA, A. (1966). Wave-induced up-lift forces acting on quay-aprons. Reprinted from *Technology Reports of the Osaka University* **16** No. 734, 605-616.

- GODA, Y. (1985). *Random Seas and Design of Maritime Structures.* University of Tokyo Press.

- GREENHOW, M. (1983). Free-surface flows related to breaking waves. *J. Fluid Mech.* **134** 259-275.

- GUREVICH, M.I. (1965). Theory of jets in ideal fluids. Academic Press Inc. New York and London.

- HAMMING, R.W. (1973). *Numerical Methods for Scientists and Engineers*, 2nd Edition, McGraw-Hill, 532-536.

- HATTORI, M. & ARAMI, A. (1992). Impact breaking wave pressures on vertical walls. *Proc. 23nd Internat. Conf. Coast. Engng.. ASCE*, vol2. 1785-1798.

- HATTORI, M., ARAMI, A. & YUI, T. (1994). Wave impact pressure on vertical walls under breaking waves of various types. *Coastal Engng.* **22** 79-114.

- HAYASHI, T. & HATTORI, M. (1958). Pressure of the breaker against a vertical wall. *Coastal Engng. in Japan, JSCE* **1** 25-37.

- HIROI, I. (1920). The force and power of waves. *The Engineer* vol 2, Aug. 1920,184-185.

- HONDA, T. & MITSUYASU, H. (1974). Experimental study of breaking wave force on a vertical circular cylinder. *Coastal Engng. in Japan, JSCE* **17** 59-70.

- HOWISON, S.D., OCKENDON, J.R. & WILSON, S.K. (1991). Incompressible water-entry problems at small deadrise angles. *J. Fluid Mech.* **222** 215-230.

- JENKINS, A.D. (1994). A stationary potential-flow approximation for a breaking-wave crest. *J. Fluid Mech.* **280** 335-347.

- KELDYSH, M.V. (1935). Plate impact on water of finite depth. *Tr. Tsentr. Aerogidrodin Inst.* **152** 13-20.

- KELLER, J.B. (1990). On unsymmetrically impinging jets. *J. Fluid Mech.* **211** 653-655.

- KIRKGÖZ, M.S. (1991). Impact pressure of breaking waves on vertical and sloping walls. Ocean Engng.**18** no.1/2 45-49.

- KOROBKIN, A.A. & PUKHNACHOV, V.V. (1988). Initial stage of water impact. *Ann. Rev. Fluid Mech* **20** 159-185.

- LAI, C.P. & LEE, J-J. (1989). Interaction of finite amplitude waves with platforms and docks. *J. waterway, Port, Coastal and Ocean Engng. ASCE* **115** 19-39.

- LAMB, H. (1995). *Hydrodynamics.* 6th Edn. Cambridge University Press.

- LONGUET-HIGGINS, M.S. & COKELET, E.D. (1976). The deformation of steep surface waves on water I. *Proc. Roy. Soc. Lond. A* **371** 1-26.

- LONGUET-HIGGINS, M.S. (1982). Parametric solutions for breaking waves. *J. Fluid Mech.* **121** 403-424.

- LOSADA, M.A., MARTIN, F.L. & MEDINA, R. (1995). Wave kinematics and dynamics in front of reflective structures. *Wave forces on inclined and vertical wall structures. ASCE* editors N. Kobayashi & Z. Demirbilek 282-310.

- LUNDGREN, H. (1969). Wave shock forces: An analysis of deformations and forces in the wave and in the foundation. *Research on wave action. Symposium. Proc. Delft 1969* Vol 2, 153-174.

- LUNDGREN, H. (1991). Perspectives of structural breakwater technology. *Proc. 1st Workshop on Wave Impact Loading of Vertical Structures, Hannover, MAST contract 0032-M(JR).*

- MASSEL, S.R., OLESZKIEWICZ, M. & TRAPP, W. (1978). Impact wave forces on vertical and horizontal plate. *Proc. 16th Internat. Conf. Coast. Engng., ASCE*, vol 3, 2340-2359.

- MERCER, G.N., & ROBERTS, A.J. (1992). Standing waves in deep water: Their stability and extreme form. *Phys. Fluids A* **4**, No. 2, 259-269.

- MERCER, G.N., & ROBERTS, A.J. (1994). The form of standing waves on finite depth water. *Wave Motion* **19**, 233-244.

- MILNE-THOMPSON, L.M. (1962). *Theoretical Hydrodynamics.* Macmillan.

- MITSUYASU, H. (1966). Shock pressures of breaking wave. *Proc. 10th Internat. Conf. Coast. Engng., ASCE*, vol 1, 268-283.

- MOLITOR, D.A. (1935). Wave pressures on sea-walls and breakwaters. *Trans. ASCE 1935* **100** 984-1002 +15pp discussion.

- NAGAI, S. (1960). Shock pressures exerted by breaking waves on breakwaters. *J. WW. H. Div., Proc. ASCE* **86** WW2, 1-38.

- NEW, A.L. (1983). A class of elliptical free-surface flows. *J. Fluid Mech.* **130** 219-239.

- NEW, A.L., MCIVER, P. & PEREGRINE, D.H. (1985). Computations of overturning waves. *J. Fluid Mech.* **150** 223-251.

- OUMERACI, H. & PARTENSCKY, H.-W. (1991). Breaking wave impact loading of caisson breakwaters - Effect of entrapped air on structural response. *Proceedings 1st Workshop on Wave Impact Loading of Vertical Structures.* Hannover, MAST contract 0032-M (JR)

- OUMERACI, H., BRUCE, T., KLAMMER, P. & EASSON, W.J. (1995). Breaking wave kinematics and impact loading of caisson breakwaters. *Proceedings Internat. Conference on Coastal and Port Engng. in Developing Countries (COPEDEC), Rio de Janeiro, Brazil* Vol. 4, Part 3, 2394-2410.

- OUMERACI, H., PARTENSCKY, H.-W., KLAMMER, P. & KORTENHAUS, A. (1997). Entwicklung von Bemessungsgrundlagen fuer monolithische wellenbrecker. *Abschlussbericht zum forschungsvorhaben, Braunschweig, Germany* 49pp, 5 Annexes. Unpublished. In German.

- PARTENSCKY, H.W. (1988). Dynamic forces due to waves breaking at vertical coastal structures. *Proc. 21st Internat. Conf. Coast. Engng., ASCE.* vol 3, 2504-2518.

- PEREGRINE, D.H., COKELET, E.D. & MCIVER. P. (1980). The fluid mechanics of waves approaching breaking. *Proc. 17th Internat. Conf. Coast. Engng., ASCE*, 512-528.

- PEREGRINE, D.H. (1983). Breaking waves on beaches. *Ann. Rev. Fluid Mech.* **15** 149-178.

- PEREGRINE, D.H. (1991). Breaking water waves. *Nonlinear Topics in Ocean Physics*, ed. Osborne, A.R., Course 109, Italian Phys. Soc.. Internat. Sch. of Physics, North Holland. 499-526.

- PEREGRINE, D.H. (1994). Pressure on breakwaters: a forward look. *Internat. Workshop on Wave Barriers in Deep Waters*, Port and Harbour Research Institute, Japan, ed. T. Takayama, 553-573.

- PEREGRINE, D.H. & KALLIADASIS, S. (1996). Filling flows, coastal erosion and cleaning flows. *J. Fluid Mech.* **310** 365-374.

- PEREGRINE, D.H. & THAIS, L. (1996). The effect of entrained air in violent water wave impacts. *J. Fluid Mech.* **325** 377-397.

- RAMKEMA, C. (1978). A model law for wave impacts on coastal structures. *Proc. 16th Internat. Conf. Coast. Engng., ASCE*, vol 3, 2308-2327.

- RICHERT, G. (1968). Experimental investigation of shock pressures against breakwaters. *Proc. 11th Internat. Conf. Coast. Engng., ASCE* 954-973.

- SAINFLOU, M. (1928). Essai sur les digues maritimes verticales. *Annales des Ponts et Chauss*ées. **98** No. 4, 5-48.

- SCHMIDT, R., OUMERACI, H. & PARTENSCKY, H.-W. (1992). Impact loads induced by plunging breakers on vertical structures. *Proc. 23st Internat. Conf. Coast. Engng., ASCE* vol 2, 1545-1558.

- SHIH, R.W.K. & ANASTASIOU, K. (1992). A laboratory study of the wave-induced vertical loading on platform decks. *Proc. Instn Civ. Engrs Wat., Marit. & Energy* **96** 19-33.

- SMITH, N.J. & STANSBY, P.K. (1997). The slam force on a flat plate in free flight due to impact on water waves. pre-print

- STEVENSON, T. (1886). *Design and construction of harbours.* 3rd Edition. Black.

- TAKAHASHI, S., TANIMOTO, K., & SHIMOSAKO, K. (1994). Dynamic response and sliding of breakwater caissons against impulsive breaking wave forces. *Internat. Workshop on Wave Barriers in Deep Water, Port and Harbour Research Institute, Japan,* ed. T. Takayama, 362-401.

- TAKAHASHI, S. (1996). Design of vertical breakwaters. *Coastal Structures (ICCE 1996 Short Course), Orlando, Florida* 85pp.

- TAKAGI, K. (1997). Three-dimensional slamming of a distorted plate. *Proc. 7th Internat. Offshore and Polar Engng. Conference, Honolulu, USA, The International Society of Offshore and Polar Engineers.* 237-244.

- TALLENT, J.R., YAMASHITA, T. & TSUCHIYA, Y. (1990). Transformation characteristics of breaking water waves. *Water Wave Kinematics* (ed. Tørum, A. & Gudmestad, O.T., Kluwer Academic, Amsterdam) 509-523.

- TOPLISS, M.E. (1994). *Water wave impact on structures.* Ph.D. dissertation, University of Bristol.

- TSAI, C.-P., JENG, D.-S. (1994). Numerical fourier solutions of standing waves in finite water depth. *Applied Ocean Research* **16**, 185-193.

- VEKLICH, N.A. & MALYKH. B.M. (1984). Plane problem of impact on liquid layer. *Interaction of plates and shells with liquid and gas* (ed. A.G. Gorshkov) Moscow University. Institute of Mechanics. 99-121.

162

- VERHAGEN, J.H.G. (1967). The impact of a flat plate on a water surface. *J. Ship Research* **11** No. 4, 211-223.

- VOIGHT, (1886). *Math. Annal.* **28**.

- VON KARMAN, T. (1929). The impact on seaplane floats during landing. *NACA T.N. 321.*

- WAGNER, H. (1932). Über Stoß-und Gleitvorgänge an der Oberfläche von Flüssigkeiten. *ZAMM* Band 12, Heft 4.

- WALKDEN, M.J.A., HEWSON, P.J., & BULLOCK, G.N. (1997). Scaling. *Proc. Task 1 Technical Workshop on Probabilistic Design Tools for Vertical Breakwaters*, Edinburgh, MAST contract MAS3-CT95-0041.

- WEGGEL, J.R. & MAXWELL, W.H.C. (1970). Numerical model for wave pressure distributions. *J. WW. H. C. Engng. Div., Proc. ASCE* **96** 623-642.

- WHITMAM, A. M. & PANCIONE, M.C. (1973). A similitude relation for flat-plate hydrodynamic impact. *J. Ship Research* **17** No. 1, 38-42.

- WIEGEL, R.L. (1982). Forces induced by breakers on piles. *Proc. 18th Internat. Conf. Coast. Engng., ASCE* 1699-1715.

- WITTE, H.H. (1988). Wave-induced impact loading in deterministic and stochastic reflection. *Mitteilungen, Leichtweiss Institut für Wasserbau, Tech. University Braunschweig* **102** 1-227.

- ZHANG, S., YUE, D. K. P., & TANIZAWA, K. (1996). Simulation of plunging wave impact on a vertical wall. *J. Fluid Mech.* **327** 221-254.

- ZHOU, D., CHAN, E.S., & MELVILLE, W.K. (1991). Wave impact pressures on vertical cylinders. *Applied Ocean Research* **13** 220-234.

- ZHUKOVSKII, N.E. (1890). *Math. Coll.* **15**

163